

Tissue cell polarity throughout leaf development in *Arabidopsis thaliana*

Catherine A. Mansfield

Thesis submitted for the Degree of Doctor of Philosophy

University of East Anglia

John Innes Centre

Submitted September 2018

© This copy of the thesis has been supplied on the condition that anyone who consults it is understood to recognise that its copyright rests with the author and that use of any information derived there from must be in accordance with current UK Copyright Law. In addition, any quotation or extract must include full attribution.

Abstract

Polarity is a property of many cell types across a multitude of organisms. In multicellular organisms, cell polarity can be coordinated forming tissue-wide polarity fields. Coordinated polarity fields have been described in planar organs in animals, such as the *Drosophila* wing, and are implicated in transport, growth and differentiation. In plants, coordinated polarity fields have been described across the leaf primordia, and in specific developmental contexts, using PIN proteins. Polarity fields have also been identified in subgroups of leaf epidermal cells later in development, such as in trichomes and the stomatal lineage. However, it is unclear whether coordinated polarity is an underlying feature of planar plant organs. Despite this, predictions have been made that suggest polarity may provide the axial information to guide growth in plants. In this work, I use ectopic expression of the stomatal protein BREAKING OF ASYMMETRY IN THE STOMATAL LINEAGE (BASL) to reveal a coordinated tissue-wide polarity field that exists throughout *Arabidopsis thaliana* leaf development. Ectopic BASL localises towards the proximal end of cells and the polarity field revealed diverges in lateral parts of the lamina at later stages of development, suggesting it may be deformed during growth. I show that this polarity field is independent of the stomatal lineage and that cell shape anisotropy is not required for orienting polarity. In addition, I explore mechanisms involved in polarity coordination, and analyse ectopic BASL polarity in relation to PIN polarity at serrations. I show that ectopic BASL polarity mirrors epidermal PIN patterns which suggests a possible common underlying polarity system. Finally, I use a biochemical approach to identify potential novel factors involved in polarity formation in plants. This work provides evidence for tissue-wide polarity in leaves that, like in animals, may provide a general cellular mechanism for guiding growth and differentiation.

Contents

Abstract	3
Contents	4
List of tables	13
List of figures	14
Author contributions	19
Acknowledgments	20
1 General introduction	23
1.1 The existence of polarity	23
1.1.1 Defining polarity.....	23
1.1.2 Polarity in single-celled organisms.....	25
1.1.3 Polarity in multicellular organisms.....	25
1.1.3.1 Polarity in animals.....	26
1.1.3.2 Polarity in plants	27
1.1.3.2.1 Physical markers of polarity in plants.....	28
1.1.3.2.2 Molecular markers of polarity in plants	29
1.2 The role of polarity systems	31
1.2.1 The role of polarity in animal tissues.....	31
1.2.2 The role of polarity in plant tissues.....	32
1.2.2.1 The growth of plants	33
1.2.2.2 The role of polarity in the growth of plant tissues	36
1.2.2.3 Growth without polarity	37
1.2.2.4 Distinguishing between models.....	38
1.3 The leaf as a model for studying polarity	38
1.4 Establishment and coordination of polarity in plants	40
1.4.1 Models for polarity establishment and coordination in plants	41
1.4.2 Polarity coordination in the stomatal lineage	42

1.4.3	The need for polarity markers in plants.....	42
1.5	Aims of this work.....	43
2	Evidence for a tissue-wide polarity field in leaves	45
2.1	Polarity in planar plant organs.....	45
2.1.1	PIN as a marker of polarity.....	45
2.1.2	Polarity at later stages of development.....	46
2.1.3	BASL localisation in stomatal lineage cells.....	48
2.2	Aims of this work.....	50
2.3	Ectopic BASL expression in a wild-type background	51
2.3.1	Ectopic BASL expression in sectors	52
2.3.2	Ectopic BASL expression across the lamina	53
2.3.3	Ectopic BASL expression at later stages of development	55
2.4	Quantifying the polarity pattern revealed by BASL	58
2.4.1	BASL vectors indicate cell polarity	58
2.4.2	Automated polarity vectors	58
2.4.3	Semi-automated polarity vectors	61
2.4.4	Visualising the BASL vectors.....	64
2.4.5	Testing the software using randomly generated tensors	64
2.5	BASL vectors in wild type	65
2.5.1	<i>35S::GFP-BASL</i> is coordinated across a tissue indicating a polarity pattern..	65
2.5.2	Down-sampling allows tissue-level patterns to be visualised	68
2.5.3	Higher-order leaves suggest a divergence of BASL vectors towards serrations	70
2.6	Size of BASL crescent.....	71
2.7	BASL crescent appears as a distinct domain after heat-shock	72
2.8	Ectopic BASL polarity is more coordinated in the midvein, and less coordinated at the tip	74
2.8.1	Local variation in BASL polarity differs across the lamina	74

2.8.2	Local variation in BASL vector could be due to stomatal lineage cells	76
2.9	Ectopic BASL reveals a polarity field independent of stomatal lineages	78
2.10	Endogenous BASL	82
2.11	Discussion	86
2.11.1	Characterising the ectopic BASL polarity pattern	86
2.11.1.1	Ectopic BASL reveals a coordinated polarity field throughout development	86
2.11.1.2	The ectopic BASL polarity pattern is independent of the stomatal lineage ..	88
2.11.2	Development of software to quantify the polarity field.....	89
2.11.3	Concluding remarks and future work	90
3	Testing predictions of a tissue-wide polarity field	93
3.1	The role of a tissue polarity field	93
3.1.1	Polarity at the tissue level.....	93
3.1.2	Polarity at the cell level.....	94
3.1.3	Continuous versus discrete polarity.....	94
3.2	Ectopic BASL polarity in relation to PIN polarity.....	95
3.2.1	Testing of a polarity field in developmental contexts	96
3.3	Mechanisms underlying the establishment and maintenance of polarity	96
3.3.1	Establishment of polarity	96
3.3.2	Maintenance and coordination of polarity.....	97
3.4	Aims of this work.....	97
3.5	Polarity and cell shape	98
3.5.1	Artefact of cell anisotropy and polarity	99
3.5.2	Ectopic BASL polarity is correlated with cell shape anisotropy	100
3.5.3	Isotropic cells allow uncoupling of cell shape and polarity	105
3.5.3.1	Cell eccentricity can be used as a proxy for cell shape anisotropy.....	105
3.5.3.2	BASL in isotropic cells shows a divergent pattern	106
3.6	Uncoupling polarity and cell long axis orientation	111

3.6.1	Cells not in line with proximodistal axis also allow separation of cell shape and polarity	111
3.6.2	<i>gap1gap2</i> mutant allows uncoupling of polarity and cell geometry.....	115
3.7	Relationship to PIN polarity	121
3.7.1	BASL and PIN in early leaf	122
3.7.2	BASL in serrations	125
3.7.3	Ectopic BASL in <i>kanadi1kanadi2</i> outgrowths.....	130
3.7.4	BASL and PIN in roots.....	135
3.8	Coordinating polarity across a tissue.....	137
3.8.1	Ectopic BASL and inhibiting auxin transport with NPA.....	137
3.8.2	Ectopic BASL and microtubules.....	140
3.8.3	Coordination of ectopic BASL in leaves with closed plasmodesmata.....	142
3.9	BASL and response to mechanical stress.....	144
3.10	Testing polarity outside of a tissue context using BY-2 cells	147
3.11	Discussion	153
3.11.1	Relationship between cell anisotropy, cell orientation and polarity.....	153
3.11.2	BASL in relation to the ROP pathway and the cytoskeleton.....	154
3.11.3	Relationship of ectopic BASL polarity field and PIN.....	155
3.11.4	Role of plasmodesmata in polarity coordination.....	157
3.11.5	Mechanics and polarity.....	158
3.11.6	BASL in BY-2 cells	159
3.11.7	Concluding remarks and future work	161
4	Exploring mechanisms of polarity coordination	163
4.1	Interactors of BASL.....	163
4.1.1	Using the Membrane-linked Interactome Database	163
4.1.2	Using a biochemical approach to identify BASL interactors	164
4.2	Aims of this work.....	164
4.3	Membrane-linked Interactome Database candidates	165

4.3.1	Testing putative BASL interactors in <i>N. benthamiana</i>	167
4.3.2	Testing putative BASL interactors in <i>A. thaliana</i>	170
4.4	Protein extraction looking for BASL interactors	173
4.4.1	Total protein extraction in <i>A. thaliana</i>	173
4.4.2	Total protein extraction in <i>N. benthamiana</i>	176
4.4.2.1	Ectopic BASL expression in <i>N. benthamiana</i>	176
4.4.2.2	Optimising protein extraction in <i>N. benthamiana</i>	177
4.4.2.3	Total protein extraction using eGFP (GFP-2)	178
4.4.3	Immunoprecipitation in <i>N. benthamiana</i>	183
4.4.4	Immunoprecipitation in <i>A. thaliana</i>	185
4.4.4.1	IP in collaboration with Weijers lab, Wageningen University	185
4.4.4.2	Immunoprecipitation in <i>A. thaliana</i> using previously tested conditions ..	188
4.4.5	Testing GFP sequence differences in <i>N. benthamiana</i>	189
4.4.5.1	Immunoprecipitation with mass-spec analysis.....	191
4.5	Discussion	193
4.5.1	Putative BASL interactors from mb-SUS screen.....	193
4.5.2	Protein extraction and co-immunoprecipitation to identify BASL interactors..	194
4.5.3	Concluding remarks and future work	196
5	Main discussion	197
5.1	Summary of this work	197
5.2	Evidence for a polarity field in leaves present throughout development and independent of the stomatal lineage	198
5.3	Polarity and growth	199
5.4	Mechanisms underlying polarity establishment and coordination	201
5.4.1	Maintenance of polarity systems.....	201
5.4.2	Establishment of polarity systems	202
5.5	Evolution of a polarity field	204
5.5.1	The role of polarity in patterning the leaf epidermis.....	204

5.5.2	BASL polarity in other contexts.....	205
5.5.3	Polarity in single-celled organisms and multicellularity	206
5.6	Tools for understanding polarity	206
5.6.1	Development of software	206
5.6.2	Development of a polarity marker.....	207
5.6.3	Development of a biochemical assay for identifying potential polarity factors	208
5.7	Future directions	208
5.7.1	Understanding the relationship between polarity and growth.....	208
5.7.2	Understanding the establishment of polarity.....	209
5.7.3	Understanding the polarity coordination mechanisms	210
5.7.4	Exploring polarity in other systems	210
5.8	Concluding remarks.....	211
6	Materials and methods	213
6.1	Plant materials and growth conditions	213
6.1.1	<i>Arabidopsis thaliana</i> growth conditions	213
6.1.2	Seed sterilisation.....	213
6.1.3	<i>Nicotiana bethamiana</i> growth conditions	213
6.1.4	Existing plant material used.....	214
6.1.4.1	Mutants and fluorescent markers	214
6.1.4.2	Generation of inducible 35S::GFP-BASL.....	214
6.1.5	Crossing.....	216
6.1.6	Generation of new plant lines.....	216
6.2	Cloning and <i>A. thaliana</i> transformation.....	217
6.2.1	Golden gate cloning	217
6.2.1.1	General Golden Gate protocols	217
6.2.1.2	Generation of mCherry-tagged putative BASL interactors.....	218
6.2.1.3	Generation of 35S::GFP-BASL constructs.....	220

6.2.1.4	Generation of inducible 35S:mCherry-BASL construct	220
6.2.2	Transformation of <i>E. coli</i>	223
6.2.3	Plasmid preparation	223
6.2.4	Sequencing	223
6.2.5	Copy number analysis	224
6.2.6	Electroporation transformation of <i>Agrobacterium tumefaciens</i>	225
6.2.7	Stable transformation of <i>A. thaliana</i> by floral dipping	225
6.2.7.1	Dipping into kanadi1kanadi2 mutants	225
6.3	Heat-shock and imaging	226
6.3.1	Heat-shock of inducible transgenic lines	226
6.3.2	Propidium iodide staining	226
6.3.3	Confocal imaging	226
6.3.3.1	Using the growth chamber/time lapse imaging	226
6.3.3.2	Time lapse imaging of BASL following induction	227
6.4	Drug treatments	227
6.4.1	Oryzalin treatment	227
6.4.2	NPA treatment	227
6.5	Leaf stretching	227
6.5.1	Developing leaf stretching device	227
6.5.2	Leaf stretching and imaging	228
6.6	Software development	228
6.6.1	Developing software for assigning BASL vectors	228
6.6.1.1	Cells-from-leaves and cells-from-leaves-tagger software	228
6.6.1.2	MATLAB scripts to quantify the BASL vector field	229
6.6.1.2.1	SampleArrows8 software	229
6.6.1.2.2	CellLongAxisCorr7 software	230
6.7	Image analysis and statistics	230
6.7.1	BASL crescent and perimeter measurements	230

6.7.2	Isotropic cell selection	230
6.7.3	Statistics comparing coordination of vectors	231
6.7.4	Figure preparation	231
6.8	BY-2 cells	231
6.8.1	Stable transformation of BY-2 cells.....	231
6.8.2	Maintenance of BY-2 cell lines	232
6.8.3	Protoplasting of BY-2 cells	232
6.8.4	Regeneration of protoplasts	232
6.8.5	Imaging of BY-2 cells	232
6.9	Biochemistry	233
6.9.1	<i>N. benthamiana</i> infiltration	233
6.9.2	Sample preparation	233
6.9.2.1	Sample preparation for protein extraction using <i>N. benthamiana</i>	233
6.9.2.2	Sample preparation for protein extraction using <i>A. thaliana</i>	233
6.9.3	Total protein extraction	234
6.9.3.1	Extraction buffer 1	234
6.9.3.2	High salt extraction buffer	234
6.9.3.3	Acetone precipitation	234
6.9.3.4	Extraction buffer 2	234
6.9.4	Protein extraction for co-immunoprecipitation	235
6.9.5	Immunoprecipitation	235
6.9.5.1	Co-Immunoprecipitation with mass-spectrometry (Wageningen collaboration).....	235
6.9.5.1.1	Immunoprecipitation with magnetic monoclonal anti-GFP beads (Miltenyi Biotec).....	235
6.9.5.1.2	Preparation of Immunoprecipitation samples for Mass Spectrometry	236
6.9.5.2	Co-Immunoprecipitation with mass-spectrometry (<i>N. benthamiana</i> , JIC)....	236

6.9.6	Analysis of mass-spectrometry data.....	238
6.9.7	SDS-page gel.....	238
6.9.8	Western blotting	239
6.9.8.1	Testing antibodies in <i>A. thaliana</i> total protein extraction	239
7	Appendices.....	241
7.1	Appendix A: Constructs generated using Golden Gate.....	241
7.2	Appendix B: Membrane-linked Interactome Database results for BASL	247
7.3	Appendix C: Wageningen IP-MS results	248
7.4	Appendix D: <i>N. benthamiana</i> IP-MS results.....	250
7.5	Appendix E: Manuscript.....	253
8	Abbreviations.....	267
9	References	269

List of tables

Table 2.1 Two-way chi-squared tests for comparing BASL vector orientation across genotypes.....	85
Table 3.1 Average vectors from isotropic cells in regions of additional subdivided leaves.	110
Table 4.1 Six candidates from Jones et al. (2014) were the best putative BASL interactors.	166
Table 4.2 Short-list of five protein candidates, including BASL, identified by IP-MS.	193
Table 6.1 Mutant and reporter lines used from previously published sources.	214
Table 6.2 Primers and vectors used in the generation of the heat-shock inducible BASL line.	215
Table 6.3 Primers used for confirming sequences during Golden Gate cloning.	224
Table 7.1 Result of membrane interactome screen by Jones et al. (2014) using BASL as a bait.	247
Table 7.2 Wageningen IP-MS results (filtered).....	248
Table 7.3 Candidates identified from IP-MS in <i>N. benthamiana</i> (filtered).....	250

List of figures

Figure 1.1 Polarity can be coordinated to different extents in multicellular tissues.	24
Figure 1.2 Physical and molecular markers of polarity exist in both plant and animal tissues.	27
Figure 1.3 Key concepts in describing growth across a tissue.	34
Figure 2.1 <i>PIN1::PIN1-GFP</i> expression is visible at early stages of leaf development.	46
Figure 2.2 Modelling predicts a polarity field throughout <i>A. thaliana</i> leaf development.	47
Figure 2.3 <i>BASL::GFP-BASL</i> in meristemoid mother cells localises opposite new cell walls.	49
Figure 2.4 A Cre-lox based system was used for inducing <i>BASL</i> expression.	51
Figure 2.5 <i>35S::GFP-BASL</i> localises proximally in sectors in a wild-type background.	53
Figure 2.6 <i>35S::GFP-BASL</i> exhibits proximal bias across the leaf at different stages of development.	55
Figure 2.7 <i>35S::GFP-BASL</i> localisation is proximal at later stages of development.	56
Figure 2.8 Three-way junctions and cytoplasm bleeding allow allocation of <i>BASL</i> signal to a cell.	57
Figure 2.9 Fully automated software could not accurately assign <i>BASL</i> vectors.	60
Figure 2.10 Semi-automated image analysis (part 1) creates a surface and segments cells.	62
Figure 2.11 Semi-automated image analysis (part 2) rotates cells and allows vectors to be assigned.	63
Figure 2.12 <i>BASL</i> vectors are assigned from the <i>BASL</i> crescent to the cell centroid.	64
Figure 2.13 Testing re-rotation of semi-automated software.	65
Figure 2.14 Analysis of the vector field shows a coordinated pattern across the leaf at different stages.	67
Figure 2.15 Additional wild-type leaves with <i>35S::GFP-BASL</i> vectors confirm a proximodistal polarity field.	68
Figure 2.16 Down-sampling allows tissue-wide patterns to be visualised.	69
Figure 2.17 Larger, higher order leaves show a proximodistal polarity field and divergence towards serrations.	71
Figure 2.18 <i>BASL</i> crescent increases in size but does not maintain a constant proportion of the cell perimeter.	72
Figure 2.19 Time lapse imaging after <i>35S::GFP-BASL</i> induction shows gradual increase in signal intensity.	73

Figure 2.20 Ectopic BASL vectors are locally coordinated, particularly in the midvein region.	75
Figure 2.21 <i>35S::GFP-BASL</i> in meristemoids shows a spiral polarity pattern.....	77
Figure 2.22 Proximodistal patterning of ectopic BASL may be disrupted by stomata.	78
Figure 2.23 Inducible <i>35S::GFP-BASL</i> in <i>speechless</i> leaves localises proximally.....	80
Figure 2.24 Analysis of the ectopic BASL vector field in <i>speechless</i> shows a coordinated pattern across the leaf at different stages.....	81
Figure 2.25 Additional <i>speechless</i> leaves with <i>35::GFP-BASL</i> vectors confirm a proximodistal polarity field.....	82
Figure 2.26 <i>BASL::GFP-BASL</i> reveals proximodistal coordination in the stomatal lineage. .	83
Figure 2.27 Quantification of <i>BASL::GFP-BASL</i> vectors indicates coordination.....	84
Figure 2.28 <i>35S::GFP-BASL</i> in a wild-type background shows intermediate coordination between <i>spch</i> and native BASL.	85
Figure 3.1 The downsampled ectopic BASL polarity pattern resembles the predicted polarity of the deforming organiser-based model from Kuchen et al. (2012).	98
Figure 3.2 Polarity and long axis information is correlated in anisotropic cells.	100
Figure 3.3 Cell long axes across the leaf are similar to proximodistal polarity orientations.	102
Figure 3.4 Angles between the cell long axis and BASL vector can be calculated.....	103
Figure 3.5 The ectopic BASL vectors correlate with the cell long axis.....	104
Figure 3.6 A two-way relationship exists between polarity and growth/cell anisotropy. .	105
Figure 3.7 Eccentricity can be used as a measure of cell shape.	106
Figure 3.8 Cells with eccentricity of below 0.6 were considered near isotropic.	106
Figure 3.9 Near-isotropic cells show no predominant orientation of cell long axis.	107
Figure 3.10 Ectopic BASL vectors in near-isotropic cells of large leaves were predominantly proximodistal.	108
Figure 3.11 Quantification of ectopic BASL vectors in near isotropic cells showed preferential proximodistal orientation.	109
Figure 3.12 Average BASL vector angles from isotropic cells in subdivided regions show a divergent proximodistal pattern.....	110
Figure 3.13 BASL localisation in anisotropic cells oriented more than 50° from the leaf proximodistal axis was variable.	113
Figure 3.14 Ectopic BASL localises to a proximal lobe in more than 50% of anisotropic cells aligned approximately with the mediolateral axis in a wild-type leaf.....	115

Figure 3.15 Cells in <i>gap1gap2</i> in which the long axis is not aligned with the proximodistal axis of the leaf allow uncoupling of polarity and cell orientation.	116
Figure 3.16 <i>gap1gap2</i> mutant has multiple cells in which the long axis is not proximodistally aligned.....	117
Figure 3.17 <i>gap1gap2</i> cotyledons have an elongated cotyledon shape compared to wild type.	118
Figure 3.18 <i>35S::GFP-BASL</i> in a <i>gap1gap2</i> cotyledon is typically proximally localised.	119
Figure 3.19 <i>35S::GFP-BASL</i> in <i>gap1gap2</i> cotyledons, stained with PI.	120
Figure 3.20 PIN and BASL vectors are assigned differently.	122
Figure 3.21 <i>35S::GFP-BASL</i> localised at the opposite end of cells to PIN1 in primordia. ...	123
Figure 3.22 Ectopic BASL and PIN1 localised to the opposite ends of individual cells.	124
Figure 3.23 Two hypotheses illustrate possible BASL behaviour at serrations.	126
Figure 3.24 Ectopic <i>35S::mCherry-BASL</i> mirrors PIN1 convergence and divergence points at serrations.	128
Figure 3.25 Regions of reversed BASL polarity can be seen in the distal region of serrations.	129
Figure 3.26 PIN1 forms ectopic convergence points at the tip of <i>kanadi1 kanadi2</i> outgrowths, preceding outgrowth formation.	130
Figure 3.27 Two hypotheses could account for ectopic BASL behaviour at <i>kan1kan2</i> outgrowths.....	131
Figure 3.28 No reorientation of ectopic BASL was seen during time-lapse imaging of <i>kan1kan2</i> outgrowths.	133
Figure 3.29 Ectopic BASL remains proximal in cells in some <i>kan1kan2</i> leaves.	134
Figure 3.30 Ectopic BASL reorients in some cells around some <i>kan1kan2</i> outgrowths.....	135
Figure 3.31 <i>PIN1::PIN1-GFP</i> and <i>35S::mCherry-BASL</i> may both localise proximally in root cells.	137
Figure 3.32 Ectopic BASL remains polarised in leaves following treatment with NPA.....	139
Figure 3.33 Ectopic BASL is able to localise polarly in leaves germinated on NPA.....	140
Figure 3.34 <i>35S::GFP-BASL</i> localisation remains proximal in cells treated with oryzalin. ...	142
Figure 3.35 Ectopic BASL localises to the proximal end of cells when induced in leaves and cotyledons with constitutively closed plasmodesmata.	143
Figure 3.36 A small stretching device allowed seedlings to be imaged whilst being stretched.....	145

Figure 3.37 Mechanical stretching of a cotyledon showed no ectopic BASL reorientation.	146
Figure 3.38 <i>35S::GFP-BASL</i> in BY-2 cells is polarly localised.	148
Figure 3.39 Ectopic BASL can be polarised in individual BY-2 protoplasts.	149
Figure 3.40 BASL remains polarised in protoplasts resuspended in regeneration media overnight.	151
Figure 3.41 BASL localises to the end of outgrowths in regenerating protoplasts.	152
Figure 3.42 Possible hypotheses for BASL polarity being inherited at cell division.	160
Figure 4.1 The mb-SUS screen was used to identify interactions with membrane proteins.	165
Figure 4.2 Putative BASL interactors showed differing subcellular localisations in <i>N. benthamiana</i>	169
Figure 4.3 Multiple putative BASL interactors were plasma membrane localised in <i>A. thaliana</i>	172
Figure 4.4 Total protein extraction in <i>A. thaliana</i> did not extract GFP-BASL.	175
Figure 4.5 <i>35S::LYK5-eGFP</i> and <i>35S::GFP-BASL</i> transiently expressed in <i>N. benthamiana</i> provide a system for optimising protein extraction conditions.	177
Figure 4.6 <i>N. benthamiana</i> total protein extraction did not extract GFP-BASL.	178
Figure 4.7 The GFP-1 variant differs from standard eGFP (GFP-2) at multiple residues. ...	179
Figure 4.8 BASL tagged with GFP-2 localised to the lobes of pavement cells.	181
Figure 4.9 An alternative GFP variant and different reducing agents were tested in total protein extraction in <i>N. benthamiana</i>	182
Figure 4.10 Gel and blots of immunoprecipitation in <i>N. benthamiana</i> indicated possible BASL extraction.	184
Figure 4.11 GFP localisations were confirmed in <i>A. thaliana</i> leaves before harvesting for co- IP.	186
Figure 4.12 BASL-interacting partners were not identified from the IP-MS analysis in Wageningen.	187
Figure 4.13 IP with inducible BASL in <i>A. thaliana</i> did not successfully extract GFP-BASL. .	189
Figure 4.14 IP in <i>N. benthamiana</i> using GFP-2 indicated GFP-BASL extraction.	190
Figure 4.15 BASL was identified as a unique peptide with good coverage and fragmentation.	192
Figure 6.1 MIND gene construct outlines generated using Golden Gate cloning.	219

Figure 6.2 The heat-shock inducible *35S::mCherry-BASL* construct was generated using Golden Gate cloning..... 222

Author contributions

Much of the work presented in Chapter 2 and Chapter 3 of this thesis contributed to the following publication:

Mansfield, C., Newman, J. L., Olsson, T. S. G., Hartley, M., Chan, J and Coen, E. (2018). Ectopic BASL Reveals Tissue Cell Polarity throughout Leaf Development in *Arabidopsis thaliana*. *Current Biology* 28, 2638–2646.

A copy of the manuscript is included in Appendix E of this thesis and is available online at [https://www.cell.com/current-biology/fulltext/S0960-9822\(18\)30810-8](https://www.cell.com/current-biology/fulltext/S0960-9822(18)30810-8).

Enrico Coen and I wrote the manuscript. Jake Newman, Tjelvar Olsson and Matthew Hartley developed software for data analysis and Jordi Chan developed resources. These contributions are outlined in the publication, and individual contributions are highlighted in the relevant sections of this thesis.

In addition, I was involved in supervising an undergraduate student (Jamie Spooner) whose contributions to this work are also highlighted (Chapter 3.9).

Acknowledgements

Thanks to Enrico Coen for his supervision and support during my PhD. In particular, for all the words of wisdom regarding communication and presentation skills that I hope I'll take with me in my future endeavours. A particular thanks to Jordi Chan for paving the way for this work; none of the work in this thesis would exist without his initial work and supervision throughout. Thanks for letting me make this project my own.

Thanks to members of the Coen lab past and present for making the lab a lovely environment to work in. In particular, thanks to Chris Whitewoods and Beatriz Gonçalves for the ideas and help throughout my PhD and for reading chapters of this thesis, and Annabel Whibley for all the support and friendship over the last few years. Thanks to Des Bradley for seemingly always having the right answer and for asking the difficult questions, and to Karen Lee, Lucy Copesey, Matt Couchman, Rebecca Horn, Robert Bellow and Man Yu for lots of laughs and fun over the last four years. Thanks to Samantha Fox and Xana Rebocho for their guidance whilst I was finding my feet in the Coen lab. Also, thanks to Mabon Ellis, Claire Bushell and Annis Richardson, fellow Coen lab PhD students, with whom I shared many ups and downs, and who shared their guidance with me. Thanks to Jamie Spooner and Noemi Svolacchia for their time and contributions as undergraduate students spent working on projects related to this, and to future students and lab members who work on this project...enjoy it!

A particularly big thank you to Christine Faulkner (the world's best secondary supervisor) who has given me hours of her time, scientific advice, and moral support when I needed it most. Thanks for having confidence in me and encouraging me to persevere with the biochemistry.

Thanks to Jake Newman for his Matlab expertise and being a great collaborator, and to Tjelvar Olsson and Matthew Hartley who spent hours of their time helping with software development and analysis that made the paper possible.

To Steph Bornemann and Nick Brewin who made my rotation year run smoothly and to Steph, particularly, who has provided invaluable support throughout the rest of my PhD. Thanks to my rotation supervisors, their labs and, importantly, to the John Innes Foundation for funding my PhD.

Thanks to Gerhard Saalbach, Paul Derbyshire, Maritza van Dop and Dolf Weijers for their assistance (and patience) with all aspects of the proteomics work. Thanks to Dominique

Bergmann for helpful discussions, and to Joe Cammarata for sharing his BASL-related insights. Thanks also the JIC Horticultural Services team, particularly Tim Wells who has kept my plants alive, and to the JIC lab support team. Thanks to JIC Bioimaging, especially Grant Calder, who has taught me so much and has put up with many of my badly timed pleas for help and advice.

I would also like to thank my friends and housemates who have made my four years in Norwich very enjoyable. In particular, Catherine Gardener for lots of laughs and tea and Eleri Tudor for sharing all the ups and downs, keeping me sane and exploring the eating and drinking establishments of Norwich with me.

To my family, sisters and parents for being supportive throughout and always at the end of the phone (even if you don't understand what I'm talking about). I also want to acknowledge my granny, who always took a keen interest in what I was doing and who would have been very proud of this achievement. Thanks to Fiona for signing me up for the Great North Run. And to Rob, an excellent proof-reader, whose unwavering support and confidence in me has made this undertaking possible. Thank you for exploring East Anglia with me, and I'm very excited for our future adventures together.

“Weeds are flowers too,
once you get to know them.”

A. A. Milne

1 General introduction

1.1 The existence of polarity

“...to construct a part of London, or to find one’s way in a desert, plans or maps are not enough; one needs a compass or the sun for orientation. Likewise, to build a limb, individual cells need vectors to tell them in which direction to move, to divide as well as how to orient extensions, such as cilia, bristles or axons. Multicellular organisms could not be built without vectors.” (Lawrence et al., 2007)

The statement above alludes to the importance of coordinated vector information (or polarity) in multicellular organisms. From the coordinated direction of hairs on your arm, to the cilia on the mouse eye and the trichomes on a *Drosophila* wing, coordination of polarity is observable in many multicellular organisms. Some organisms also exhibit a clear polarity across their body axis: for example, the typical plant is polarised with a root at one end and a shoot at the other. Polarity is also a property of many single-celled organisms. To explore the existence and function of polarity, it is first necessary to define this term.

1.1.1 Defining polarity

The term polarity, at its most basic level, refers to an asymmetry to which a vector could be assigned. Cell polarity therefore refers to an asymmetry within a cell. This definition can be applied to physical structures, for example the flagella of a bacteria, or molecular asymmetries, for example proteins localised to one end of a cell. For a single cell, the definition of polarity is relatively straightforward, but this becomes substantially more complex when considering multicellular tissues or organisms.

In a multicellular, and often 3D, tissue, individual cell polarities can be coordinated which raises the issue of defining a polarity field (Figure 1.1). Mathematically, a polarity field is equivalent to a vector field, where each point has a vector associated with it (Lawrence et al., 2007). In biological terms, this is often understood as each cell having an individual polarity. However, the discrete nature of polarity in cells is notably different from the mathematical definition in which polarity is a continuous phenomenon. Indeed, it has been argued that there is no universally accepted satisfactory mathematical definition of polarity for biological use (Axelrod and Bergmann, 2014).

General introduction

In a tissue, cell polarity can be coordinated (or not) between neighbouring cells in cell files, between cell files, and with a tissue axis (Figure 1.1). Arguably all these situations involve a polarity field. A tissue in which at least some cells are polarised (i.e. possess cell polarity) could be described as possessing an overall polarity field which could vary from random to highly coordinated (Figure 1.1 A-D). A situation in which not every cell has a polarity could be termed a partial polarity field, contrasting with a system in which every cell presents a polarity (although in biological tissues this tends not to be the case and therefore this distinction is probably unnecessary). Polarity may be uncoordinated (Figure 1.1 A), coordinated within but not between cell files (Figure 1.1 B), within and between cell files (Figure 1.1 C), and even in three dimensions between the cell layers of a tissue (Figure 1.1 D).

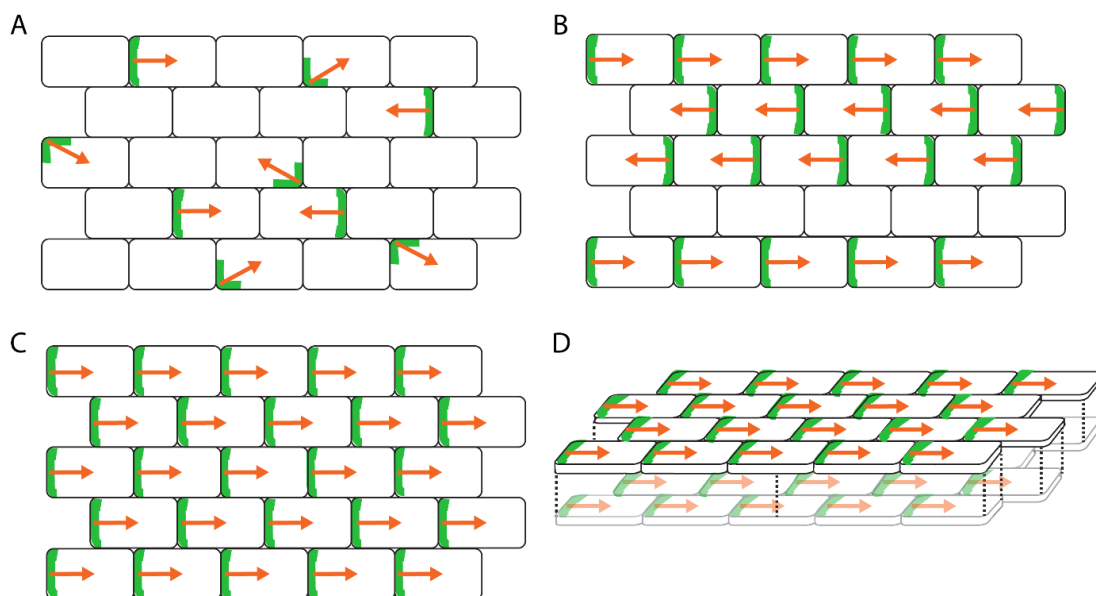


Figure 1.1 Polarity can be coordinated to different extents in multicellular tissues.

(A) Some cells in a tissue may possess polarity (indicated by a green line representing a polarity marker and orange arrow representing a polarity vector) which may not be clearly coordinated across the tissue. (B) Polarity may be coordinated within but not always between cell files, or (C) polarity may be coordinated within and between cell files. (D) In 3-dimensional tissue, polarity may also be coordinated between cell layers.

The terms tissue cell polarity (Abley et al., 2013) and planar cell polarity (Goodrich and Strutt, 2011; Jones and Chen, 2007) are often used to refer to a cell-based coordinated polarity field across a planar tissue (i.e. the situation pictured in Figure 1.1 C or D). Planar cell polarity is often referred to in animal systems and refers to the polarisation of a field of cells within the plane of a cell sheet (Jones and Chen, 2007). Tissue cell polarity refers to a vector field across

a tissue. This is distinct from regional polarity which is a scalar field (Lawrence et al., 2007; Richardson et al., 2016). The term regional polarity refers to spatial variation in regional identities (Richardson et al., 2016), such as spatially different gene expression levels across a tissue. A well-studied example of regional polarity is the polarity of the abaxial and adaxial side of a leaf, where regional differences in the expression of *KANADI* and *HD-ZIP* genes, amongst others, leads to the development of a leaf with two distinct surfaces (Byrne, 2012).

In this work, I will refer to the coordination of cell polarity across a tissue as 'tissue cell polarity' or simply a polarity field. This does not require every cell to possess polarity or that polarity is coordinated in every cell and cell layer, but that it is broadly coordinated across a tissue. This is also distinctly different from regional polarity used to describe the asymmetry across the leaf, rather than polarity at a cellular level.

1.1.2 Polarity in single-celled organisms

Cell polarity is an important feature of single celled organisms as it allows directional responses such as asymmetric cell division, chemotaxis, and cell migration (Etienne-Manneville, 2008; Macara and Mili, 2008). In rod-shaped bacteria, for example, the existence of a flagella at one end of the cell provides evidence for a physical marker of polarity that is vital for cell motility. In single celled organisms, polarity is often established in response to an external cue, for example in *Dictyostelium discoideum* where polarised cell migration occurs in response to a gradient of chemoattractants (Devreotes and Zigmond, 1988). In budding yeast, the bud scar from previous divisions provides a polarity cue for further budding to occur allowing division to take place at the optimum position relative to previous divisions (Chant and Herskowitz, 1991; Wedlich-Soldner and Li, 2003). The zygote of the brown algae *Fucus* polarises in response to external factors (Goodner and Quatrano, 1993; Jaffe, 1956; Torode et al., 2016). In these cases, asymmetric localisation of proteins, membrane domains or cellular machinery must underlie the physical cell asymmetries described.

1.1.3 Polarity in multicellular organisms

In multicellular organisms of both the plant and animal kingdoms, examples of polarity can be observed which are thought to play an important role at the level of individual cells, for instance allowing asymmetric responses such as endomembrane trafficking (Li et al., 2016). However, multicellularity also allows cell polarity to be coordinated to produce tissue level coordination, allowing communication and transport across a tissue (Meinhardt, 2007).

1.1.3.1 Polarity in animals

In animals, the best studied example of tissue cell polarity is in *Drosophila melanogaster*, where many molecular components involved in establishing cell polarity have been elucidated (Strutt and Strutt, 2009). In the *Drosophila* wing, a hair forms at the distal end of each cell. The hairs all point distally producing a coordinated proximodistal pattern across the wing (Figure 1.2 A). Coordinated asymmetrical localisation of protein complexes in cells during wing development underlies the coordinated hair patterns produced.

In *Drosophila*, two main systems govern the coordinated polarity in the wing: the 'core' planar polarity pathway (involving the proteins Vangl, Celsr, Frizzled, Dishevelled and Prickle amongst others (Henderson et al., 2018)) and the Fat/Dachsous (Ft/Ds) system (Goodrich and Strutt, 2011). The core planar polarity pathway of the *Drosophila* wing involves the Wnt ligand binding to a Frizzled receptor at the cell surface. This triggers recruitment of Dishevelled to the cell membrane (Wang et al., 2016). Unlike members of the core pathway, the Ft/Ds proteins do not appear to be clearly polarised in cells, but their important role in establishing polarity is apparent in the *ds* mutant which has an unusual swirled pattern of hairs on the wing (Thomas and Strutt, 2012). It remains unclear how the core system and the Ft/Ds are linked in establishing polarity (Thomas and Strutt, 2012).

Similarly, in the ependymal brain cells of mice, basal bodies consistently localise to one side of the hexagonal cells creating coordinated polarity across the tissue and providing further examples for the molecular basis of polarity in animal tissues (Figure 1.2 C) (Goodrich and Strutt, 2011).

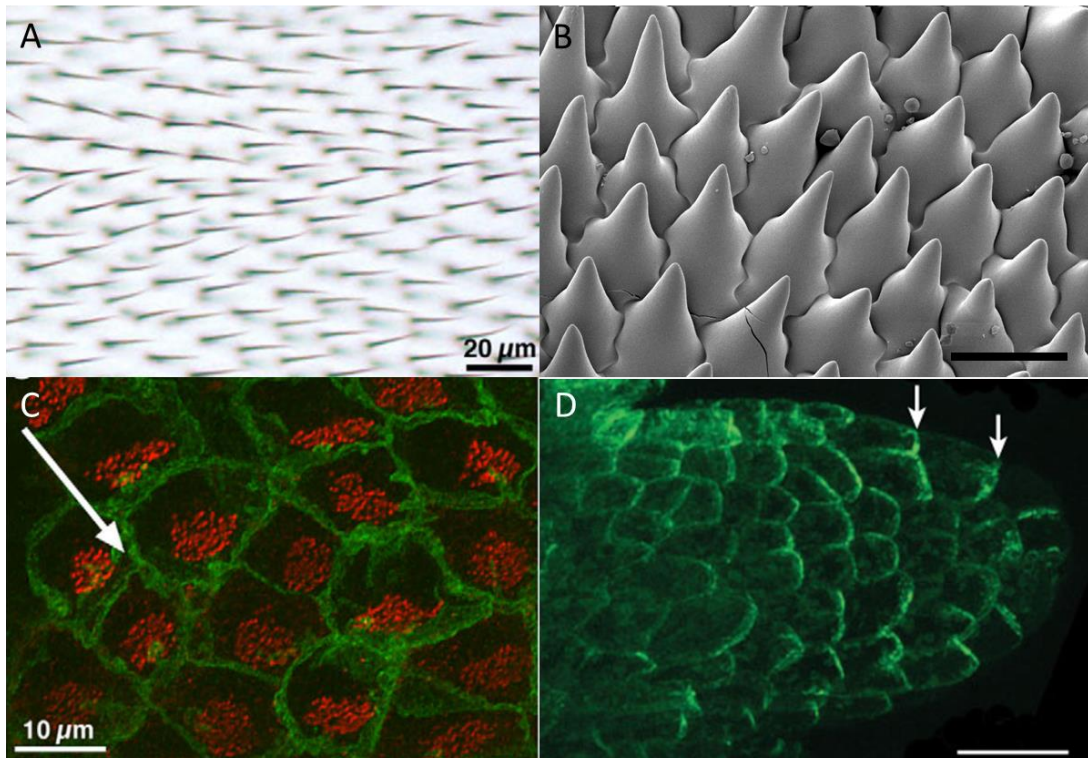


Figure 1.2 Physical and molecular markers of polarity exist in both plant and animal tissues.

(A) Hairs on a *Drosophila* wing point from proximal to distal positions in a coordinated manner. Scale bar 20 μm . (B) Cells on the ventral petal of *Mimulus* exhibit coordinated tissue cell polarity, image from Xana Rebocho (unpublished). Scale bar 50 μm . (C) Confocal image of mouse brain endymal cells, with cell membranes stained for β -catenin (green) and cilia basal bodies for γ -tubulin (red). In each cell, basal bodies are displaced towards one side (white arrow) in a coordinated manner. (D) *PIN1::PIN1-GFP* expression in the primordia of *A. thaliana*. PIN1 localises to the apical end of cells. Image taken by Erika Kuchen. A and C are adapted with permission from Goodrich and Strutt (2011), C is adapted with permission from Abley et al. (2013).

1.1.3.2 Polarity in plants

As mentioned above, plants as whole organisms typically appear polarised, with a root at one end and a shoot at the other. Individual organs also possess regional polarity, such as the axes of the leaf. As in animals, physical markers of polarity are present in plants, some cell types also appear polarised, and some molecular markers of polarity have been characterised. Whilst in some cases molecular polarity markers do underlie the formation of physical polarised structures, in many examples in the plant kingdom the molecular foundations have not been elucidated. In general, the molecular mechanisms underlying polarity in plants are less well understood than in animal systems.

1.1.3.2.1 Physical markers of polarity in plants

Physical markers of polarity exist in the plant kingdom across different organs. In *Arabidopsis thaliana* leaves, trichome development appears to require cell polarity as the divisions in trichome development are closely correlated with the leaf axis. The first trichome division takes place along the proximodistal leaf axis, and the second only occurs in the distal branch resulting in one branch of the trichome pointing proximally and two pointing distally (Bouyer et al., 2001; Hülskamp et al., 1994). Mutants in trichome development can produce misaligned trichomes with aberrant divisions (Bouyer et al., 2001; Hülskamp et al., 1994).

The bladder of the carnivorous bladderwort *Utricularia gibba* also has physical markers of polarity in four-pronged quadrifid glands found on the inside surface of the bladder (Bushell, 2016). Quadrifid glands are not symmetrical and can be assigned a polarity based on the angles between the cross-shaped terminal cells of the glands. Across the bladder, these glands show a coordinated polarity, from the stalk region of the bladder to the mouth of the trap (Bushell, 2016). Notably, in the case of both trichomes in *A. thaliana* and quadrifid glands in *U. gibba*, the polarity is not coordinated across every cell as not every leaf epidermal cell produces a trichome and not every bladder cell produces a quadrifid gland (representing a situation between that shown in Figure 1.1 A and C). Furthermore, the molecular mechanisms underlying trichome and quadrifid patterning and coordination are not well understood.

Another physical example of polarity apparent in some plant tissues is petal conical cell shape. Petal cells can be asymmetric in their shape and coordinated across a tissue, such as in *Mimulus* where the tips of cells in the ventral petal are coordinated (Figure 1.2 B). This is one of very few examples of physical markers of polarity coordinated across every cell in a plant organ, but it has not been characterised in detail, or studied at the molecular level. Other species have been reported to show a similar phenomenon and this may play a role in how insects interact with petals (Whitney et al., 2009). For example, in *Arisaema jacquemontii*, modified polarised conical cells exist that form a coordinated pattern across the petal, pointing down into the trap of this flower (Whitney et al., 2009). Some carnivorous plant traps also possess these polarised cells that are hypothesised to aid insect capture by making it easy for insects to slide into a trap but difficult to escape (Juniper et al., 1989; Vogel and Martens, 2000).

In roots, the root hair consistently protrudes from the basal end of root hair cells (Masucci and Schiefelbein, 1994). This patterning in roots is known to involve auxin signalling (Grebe et al., 2002) and provides further evidence that different plant cell types possess coordinated polarity. However, roots are cylindrical and therefore do not display planar cell polarity across a 2D sheet of tissue in the same way as planar organs such as leaves, which I focus on here.

1.1.3.2.2 Molecular markers of polarity in plants

Members of the auxin efflux carrier PIN-FORMED (PIN) protein family are commonly used as markers of polarity in plants and have formed the basis of multiple models of polarity formation (see section 1.4) (Abley et al., 2013; Jonsson et al., 2006; Rolland-Lagan and Prusinkiewicz, 2005; Stoma et al., 2008).

The eight PIN genes in *A. thaliana* can be broadly divided into two subfamilies: the 'long' PINs, which includes all those defined as auxin efflux carriers localised at the plasma membrane (PIN1-4, PIN7 and usually PIN6), and the other subfamily composed of PIN5 and PIN8 which mediate internal auxin homeostasis (Křeček et al., 2009). The tissue context and specific sequence of PIN proteins controls their polarity (O'Connor et al., 2014; Wisniewska et al., 2006), with members of the 'long' family often, but not always, polarly localised in different developmental contexts (Křeček et al., 2009). PIN1, for example, is upregulated in outgrowth formation and is expressed in the *A. thaliana* meristem (Reinhardt et al., 2003) and is distally localised in cells of the primordia (Guenot et al., 2012; Scarpella et al., 2006) (Figure 1.2 D). Polarised PIN1 expression is also observed in serrations (Bilsborough et al., 2011; Hay et al., 2006) and ectopic outgrowths (Abley et al., 2016).

In addition to PIN proteins, few other molecular markers of coordinated tissue cell polarity are known to exist in plant tissues. Members of the NODULIN26-LIKE INTRINSIC PROTEINS (NIPs) and BORON TRANSPORTERS (BOR1) are polarly localised in a coordinated manner in roots (Shimotohno et al., 2015; Takano et al., 2010). OCTOPUS, a protein involved in phloem differentiation, also has a coordinated polar localisation that has also been largely characterised in roots (Truernit et al., 2012). Likewise, the recently identified SOSEKI (SOK) protein family are found to be polarly localised in roots; interestingly different members of this protein family localise to different corners of root cells (Yoshida et al., 2019). The SOK proteins are reported to possess a DIX domain (Yoshida et al., 2019), which is a motif involved in polarity establishment in animals (Schwarz-Romond et al., 2007) which might suggest novel links between the polarity systems of plants and animals. However, examples of

General introduction

coordinated tissue-wide polarity markers in plants are largely confined to the roots, with the exception of PIN proteins.

Markers of coordinated polarity in leaves (beyond the primordia stage) are lacking. The pavement cells that make up much of the epidermis of *A. thaliana* leaves are often referred to as being polarised (Yang, 2008). However, pavement cells appear to possess multiple polarities (and may be referred to as multi-polar cells), rather than possessing a single cell polarity. At the molecular level, the interdigitation of pavement cells involves the asymmetric localisation of proteins including Rho of plants 2 (ROP2), which localises to the lobes of pavement cells (Fu et al., 2002; Fu et al., 2005). The multi-polar interdigitation of pavement cells is also reported to be regulated by auxin (Chen et al., 2015; Yang, 2008).

A number of proteins that localise preferentially to one end of the cell have been described (i.e. markers of cell polarity rather than necessarily tissue cell polarity) within the stomatal lineage of *A. thaliana*. BREAKING OF ASYMMETRY IN THE STOMATAL LINEAGE (BASL) is one such protein which is involved in asymmetric divisions in the stomatal lineage and localises in a polar crescent at the cell periphery before an asymmetric division (Dong et al., 2009; Robinson et al., 2011). Other proteins specific to the stomatal lineage, such as POLAR (Pillitteri et al., 2011) and the BASL-interactor BREVIS RADIX LIKE 2 (BRXL2) (Rowe, 2013), are polarised in the stomatal lineage, though not in every cell of the lamina (Bringmann and Bergmann, 2017). Recent work has shown that there is some tissue-level coordination of BRXL2 polarity in the stomatal lineage with this protein preferentially localising at the proximal end of meristemoid mother cells (Bringmann and Bergmann, 2017). Polarity in the stomatal lineage may represent a situation like that shown in Figure 1.1 A, while PIN polarity may be more similar to the coordinated polarity shown in Figure 1.1 B or C. Thus, the stomatal lineage provides an indication that some individual cell types are polarised throughout development, and the coordination of PIN proteins and physical polarity markers in plants, as described above, suggests coordinated tissue cell polarity exists in at least some plant tissues. However, it remains unclear whether tissue cell polarity is an underlying feature of planar plant organs.

1.2 The role of polarity systems

The existence of coordinated polarity across organs raises the question of what its purpose or function is in tissues. Multicellularity requires coordinated signalling and transport between cells. Indeed, it is difficult to imagine how directional transport across a tissue could occur without polarity. Polarity may also play a role in the patterning and differentiation of tissues.

Here I will consider the role of polarity in multicellular plant and animals tissues, but it is also worth noting the importance of polarity in single-celled organisms. In the amoeba *D. discoideum*, for example, the absence of an external gradient of chemoattractants prevents chemotaxis. However, the cells still polarise and move in random orientations (Devreotes and Zigmond, 1988). In yeast, if the bud scar from the previous division (normally required as a polarity cue) is removed, the cells can still divide, but only randomly (Chant and Herskowitz, 1991; Wedlich-Soldner and Li, 2003). Polarisation can also occur in *Xenopus laevis* eggs in the absence of the polarity cues that normally direct this process: cortical rotation occurs in random directions upon egg activation, independent of a sperm entry site that normally polarises this process (Gerhart et al., 1989). These examples suggest that polarity forming mechanisms are intrinsic and important, at least in single-celled organisms.

1.2.1 The role of polarity in animal tissues

In *Drosophila*, where tissue cell polarity has been intensively studied, it is known to play a role in regulating hair orientation in the wing and eye development (Chen et al., 2015; Goodrich and Strutt, 2011). More generally in animals, polarity is known to play a role in morphogenesis and the intercalation of cells in a process called convergent extension during neurulation and gastrulation in the early embryo (Sebbagh and Borg, 2014; Singh and Mlodzik, 2012). Disrupted tissue cell polarity can lead to substantial morphological defects, suggesting it has a crucial role. In humans, for example, neural tube defects (Lei et al., 2010) leading to malformations such as cleft palate and spina bifida (Kibar et al., 2007; Yang et al., 2014) can arise when polarity is disrupted.

1.2.2 The role of polarity in plant tissues

In plant tissues, polarity has been predicted to play a role in patterning and morphogenesis. However, the lack of evidence for tissue-wide polarity through plant tissues means that its function is not fully understood.

Work in the stomatal lineage has shown that polarity has a role in patterning and differentiation. BASL dynamics in stomatal divisions indicate a polarity switching mechanism that allow the correct and efficient spacing of stomata across the lamina (Robinson et al., 2011). The *basl* mutant has excessive numbers of small epidermal cells and incorrectly spaced stomata that form in clusters (Dong et al., 2009). Whilst this indicates that cell polarity is important in patterning this lineage, the function of tissue-wide proximodistal coordination across the stomatal lineage, as revealed by native BRXL2 expression (Bringmann and Bergmann, 2017), remains unclear.

PIN polarity also plays an important role in plant tissues. Single mutants of most of the PIN protein family do not display obvious shoot phenotypes under normal conditions (Guenot et al., 2012). *pin1* mutants, however, do have significant developmental phenotypes, indicating that PIN1 plays a crucial role in the initiation of organs. The *pin1* mutant has an impaired inflorescence meristem which gives rise to naked inflorescences with few or no flowers (Galweiler et al., 1998; Okada et al., 1991). Treatment of seedlings with polar auxin transport inhibitors, such as N-1-Naphthylphthalamic Acid (NPA), leads to a similar phenotype to a *pin1* mutant, indicating that it is the polarity of PIN1 that is implicated in organogenesis (Okada et al., 1991). However, *pin1* mutants are still able to produce leaves and, in some weaker alleles, flowers (Okada et al., 1991), which makes the role of PIN polarity in development unclear and could indicate that polarity is not critical for leaf development.

In the leaves of a *pin1* mutant, however, serration formation is abolished and a smoother margin (compared to wild-type) is observed in NPA treated leaves (Hay et al., 2006). In NPA-treated leaves, PIN1 is reported to localise in a more apolar manner (Hay et al., 2006) indicating that PIN polarity does play a role in outgrowth formation. Given that auxin, which is transported by PIN proteins, has multiple crucial functions in plant development, it is challenging to experimentally or theoretically separate auxin and PIN activity from the polar element of PIN proteins.

Whilst experimentally testing the function of polarity in plant tissues is challenging, polarity has been implicated in morphogenesis using theoretical and modelling approaches. In order

to further discuss the potential role for polarity in guiding growth, it is necessary to first define and explore the growth of plant tissues.

1.2.2.1 *The growth of plants*

Planar plant organs, such as leaves and petals, form from a primordium. Even in the case of complex final organ shapes, such as complex leaf shapes, petal shapes, or other organs such as the traps of carnivorous plants, the primordia are initially relatively simple in shape. Through the process of growth, the organ reaches its final shape which, unlike the primordia, can be complex and vary widely between species. Growth, even of a simple 2D planar organ, is a complex process with areas of the tissue growing at different rates and in different directions.

Growth can be defined as an ‘irreversible increase in size’ (Whitewoods et al., 2017), a definition that spans both tissue and cell growth. Mathematically, growth is a tensor (Hejnowicz and Romberger, 1984) (Figure 1.3 A). By definition, it therefore has a magnitude (in 2D or 3D), an axis (also in 2D or 3D) and may have a rotational aspect (Coen et al., 2017; Hejnowicz and Romberger, 1984). Growth does not have a direction (i.e. no arrowhead can be assigned to a growth tensor). In development, each aspect of growth may vary across a tissue (Figure 1.3 B-D). For example, growth rates (a scalar, Figure 1.3 A) could change across a tissue, and therefore a field of scalars would be required to describe growth rates across a tissue. Growth can be isotropic (i.e. the same in all directions) or anisotropic (i.e. not the same in all directions). Whilst some tissues or parts of tissues are thought to grow more isotropically (Solly et al., 2017), most are known to require anisotropic growth. This has been demonstrated by measuring growth rates and orientations. The importance of understanding growth rates and directions in order to study growth has been apparent for many years, and was recognised by D’Arcy Thompson (Thompson, 1942).

If growth is isotropic across a tissue, then the mathematical description of growth is relatively simple as the magnitude of growth in different directions is the same (Figure 1.3 B). However, for anisotropic growth the magnitude of growth in different directions can vary (Whitewoods and Coen, 2017). In addition, anisotropic growth can be uniform across a tissue (Figure 1.3 C), or the level of growth anisotropy can vary across the tissue (Figure 1.3 D). However, anisotropic growth should still be described as a tensor, albeit with different magnitudes in different directions, rather than a vector (which would have a sense, or directional aspect). This is because the growth of cells and tissues is generally not occurring in a certain direction relative to a fixed point. Take a single cell in a tissue, for example: the cell expands in both

directions, rather than in one direction relative to a fixed point. Some cell types, such as pollen tubes, may grow in a more unidirectional manner, but these exceptions are not considered here. Describing growth across a tissue therefore requires a potentially complex set of growth parameters.

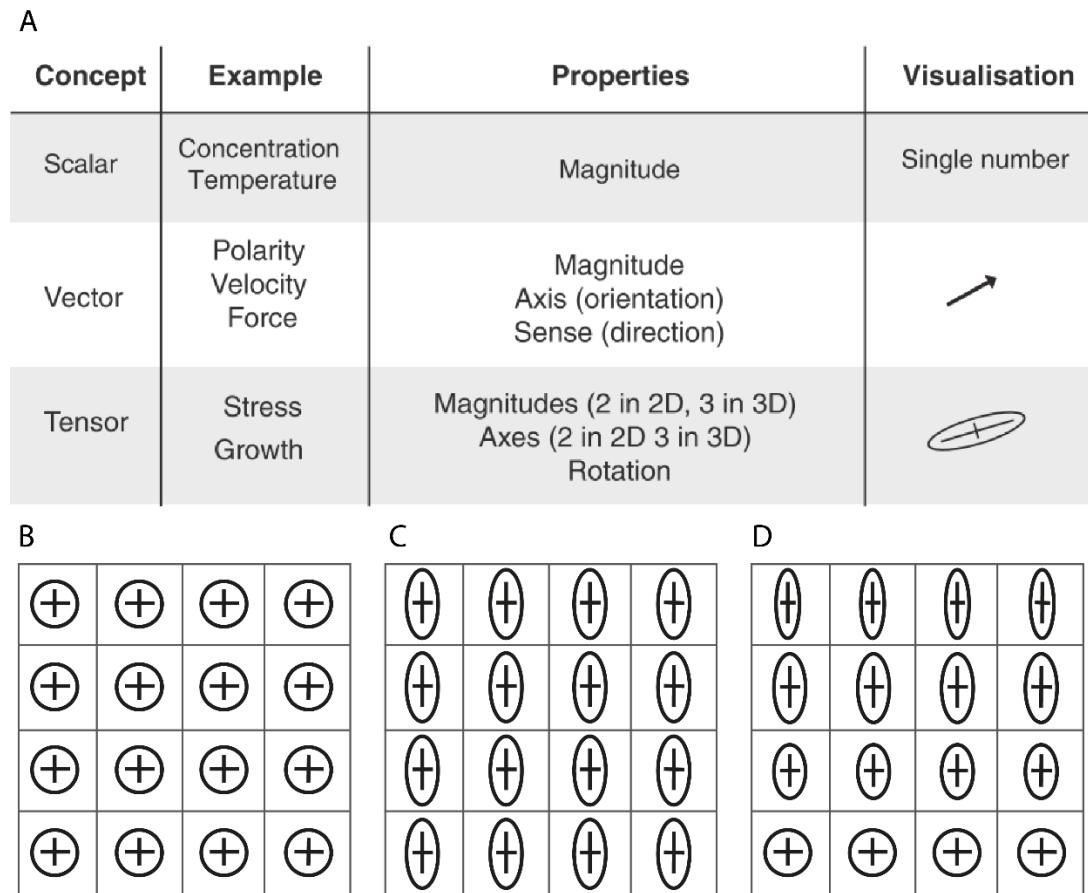


Figure 1.3 Key concepts in describing growth across a tissue.

(A) Summary of concepts key to understanding plant growth, adapted from Whitewoods and Coen (2017). The mathematical concepts of a scalar, vector and tensor can be used to describe different aspects of growth across a tissue. Growth itself is described as a tensor while growth rate is a scalar. (B-D) Growth across a tissue may be described as a field of growth tensors and varies depending on the type of growth. (B) Uniform isotropic growth has tensors with equal magnitudes in all directions. (C) Uniform anisotropic growth has tensors with different magnitudes, but uniform across a tissue. (D) Non-uniform anisotropic growth has tensors which vary in magnitude in multiple orientations across the tissue.

The elements of growth described above can be specified in cells, through the action of genes. However, it is also worth noting that there are properties of growth which are not specified at the cell or tissue level. The rotational element of growth results from the mechanical connectivity of tissue. Hence the specified growth (which would occur if each

part in the tissue could grow without constraints from its surroundings) and the resultant growth (the growth which actually occurs) may differ (Coen and Rebocho, 2016).

Growth at the cellular level equates to cell elongation. Growth rates are dependent on the cell wall extensibility, and cell growth is driven by internal turgor pressure (Lockhart, 1965). The elasticity of the cell wall allows cell expansion in response to turgor pressure, which acts isotropically. If the cell wall properties are uniform, isotropic expansion of the cell can occur. Alternatively, non-uniform cell wall properties allow anisotropic cell expansion. The cell wall properties can be altered by expansins (Cosgrove, 2000; McQueen-Mason and Cosgrove, 1995) and pectin methylesterases (Bosch et al., 2005) which alter cell wall rigidity and hence influence local growth.

Cellulose fibres in the plant cell wall control directional cell reinforcement. The cell wall is more extensible in the direction perpendicular to the deposition of cellulose fibres and can expand along that axis (Williamson, 1990). Cellulose fibres are deposited by cellulose synthase and microtubule alignments provide tracks for this enzyme (Baskin, 2001; Heath, 1974). Microtubule arrays are therefore key to differential cell expansion and may vary on different cell faces allowing potential cell anisotropies (Williamson, 1990). Genes that influence the cell wall properties, microtubule arrays and cellulose deposition can therefore play a role in specifying the growth rates of cells.

At the whole tissue level, growth has been measured using fluorescent ink dots placed on the tissue (Remmler and Rolland-Lagan, 2012), air pore positioning (Solly et al., 2017), ink spots drawn onto the tissue (Das Gupta and Nath, 2015) and marks drawn onto the stem (Bencivenga et al., 2016). In addition, a common method used to measure growth is the analysis of clonal sectors in a tissue. This approach can be used in species with naturally occurring sectors, such as pigment sectors formed by transposon excision in *A. majus* (Green et al., 2010). Clonal sectors can also be induced in transformable species using a Cre-lox recombination system that has been used to induce GFP sectors in plant organs (Gallois et al., 2002). This approach has provided evidence for the anisotropic growth of leaves (Kuchen et al., 2012), petals (Sauret-Güeto et al., 2013) and the meristem (Bencivenga et al., 2016) of *A. thaliana*, as well organs of other species (Bushell, 2016; Eldridge et al., 2016).

For anisotropic growth to be coordinated across a tissue, an axiality system may be required (Coen et al., 2017). A coordinated axiality system can be achieved across a tissue through the coordination of individual cell axialities. A tissue-wide axiality system can then allow growth

directions to be coordinated across a tissue. For example, growth rates can be specified (and modulated by the action of genes) both parallel and perpendicular to the axiality system (Kennaway et al., 2011).

1.2.2.2 *The role of polarity in the growth of plant tissues*

One hypothesis for how the coordinated axial information across a tissue could be established is through a polarity-based axiality system (Kennaway et al., 2011). In a polarity-based axiality system, individual cell polarities can be coordinated across a tissue by a chemical signal. The axiality of a polarity vector can provide the directional aspect of a growth tensor. Growth rates can then be modulated in relation to the axiality system.

Modelling of tissue-level growth using a polarity-based axiality system has been carried out in multiple organs using the software Growing Polarised Tissue Framework (GFtbox, Kennaway et al., 2011). This software relies on the existence of a polarity field across the tissue which can be used to guide growth. 'Organiser' regions, which are hypothesised to be genetically defined, allow the polarity field to be linked to the tissue. Modelling of the *A. majus* flower and petal (Green et al., 2010; Rebocho et al., 2017b) was based on the PIN1 localisation patterns in the petal, as observed by immunolocalisation (Rebocho et al., 2017b). Similarly, in the leaf of barley (*Hordeum vulgare*), SISTER OF PIN1 localisation and reorientation patterns were used to inform modelling of this organ (Richardson et al., 2016). GFtbox modelling of the heart-shaped *Capsella rubella* silicle has also predicted the existence of polarity to guide growth (Eldridge et al., 2016). In *A. thaliana*, both the petal and leaf have been modelled, based on polar PIN1 patterns in these organs (Kuchen et al., 2012; Sauret-Güeto et al., 2013). In all these models, there is a requirement for a tissue-wide polarity field that currently has a limited experimental basis.

Another type of model for the formation of leaf shapes uses information from veins to guide growth of the tissue (Runions et al., 2017). This type of model has a theoretical computational basis with representations of the leaf margin, main veins and the leaf blade (modelled as a triangular mesh and not including individual cells). The patterning of serrations and leaflets at the margin, as well as patterning of the vasculature and the growth of the leaf blade, are then modelled allowing the production of a diverse range of leaf shapes (Runions et al., 2017). However, the biological factors controlling lamina growth in this model are not addressed and the model needs to be tested experimentally. This could be achieved by analysing clonal sectors in parallel with venation patterns in the leaf.

1.2.2.3 Growth without polarity

Stress and growth are both tensors and hence, in principle, mechanical stresses (force per unit area) could be used to directly guide specified growth directions. Growth is not polarised and therefore hypotheses for the control of growth that do not require polarity, particularly given the limited experimental evidence for coordinated polarity in plants, are appealing.

A stress-based axiality system requires a cell to be able to sense stresses and orient its growth accordingly. Microtubules have been shown to reorient around an ablation site in the *A. thaliana* meristem in line with the principle orientation of stresses (Hamant et al., 2008). The meristem is modelled as a pressurised cylinder, under tension due to turgor pressure. This could allow anisotropic cell wall reinforcement, and therefore specify anisotropic growth perpendicular to the principle orientation of stresses. Principle stress orientations could be coordinated across a tissue to allow coordinated anisotropic growth.

A stress-based axiality system has also been used to model growth of the *A. thaliana* sepal (Hervieux et al., 2016). In this work, a global stress field is predicted to arise from differential isotropic growth rates across the sepal. However, in this case, the global stress field needs to be separated from the cells which are modifying their growth in relation to local stresses. The model therefore proposes local and global stress-fields that can be differentially sensed by cells. It is not clear how sensing of stresses, or deciphering local and global stresses, would work at the cell level (Whitewoods and Coen, 2017). Mechanosensitive ion channels have been described in plants (Basu and Haswell, 2017; Haswell et al., 2008) but it is unclear how such channels could measure stresses across a tissue.

In some cases, the growth of planar plant organs has been modelled without the need for an axiality system, as growth has been proposed to be largely isotropic. This was the case in work modelling the thallus of the liverwort *Marchantia polymorpha* (Solly et al., 2017). In this work, a model of the thallus produced using GFTbox (Kennaway et al., 2011) requires a factor, termed APEX, that inhibits growth in the apical region of the thallus. Using only isotropic growth the development of the thallus can be modelled, and recapitulates many of the key processes of thallus development, including bifurcation, branching and expansion (Solly et al., 2017). However, it was found that, in order to extend this model to the thinner thallus of the closely related species *Riccia fluitans*, anisotropic growth may be required (Solly, 2015).

1.2.2.4 *Distinguishing between models*

Distinguishing between stress and polarity-based hypotheses for the control of anisotropic growth is a challenge. One clear difference between models of stress-based axiality and polarity-based axiality is the existence of a polarity field. The existence of a polarity field would not rule out mechanical stresses as playing a role in directing growth orientations. Likewise, experiments showing mechanical stresses may alter growth do not preclude polarity-guided anisotropic growth. However, the lack of evidence for a tissue-wide polarity field would raise a significant issue for a model that relied on polarity to guide anisotropic growth.

Many experiments frequently used to show response to either polarity or mechanical stress may not be straightforward to interpret. For example, stretching and ablation experiments have been shown to alter polarity markers and microtubule alignments (Bringmann and Bergmann, 2017; Heisler et al., 2010; Robinson and Kuhlemeier, 2018). In such experiments it is difficult to negate any wounding response or to measure the stress a tissue is experiencing, but it remains possible that mechanical stresses, or a gradient of mechanical stresses, could alter cell or tissue polarity. Whilst some advances have been made recently in untangling the respective roles of polarity and mechanics in growth, for example in the development of systems controlling and measuring mechanical stresses in tissue (Robinson et al., 2017), it remains a complex topic that is difficult to probe experimentally.

1.3 The leaf as a model for studying polarity

Leaves and roots represent probably the most intensively studied plant organs in terms of development. In leaves, three axes exist: the proximodistal axis from the leaf base to tip, the mediolateral axis from the midvein to the margin, and the adaxial-abaxial axis from the ventral to the dorsal surface of the leaf (Byrne, 2012). Within these three axes, leaves generally exist as flattened tissue and therefore are an appropriate organ for the study of tissue cell polarity. In this work, I focus on leaves for several reasons.

Leaves represent a relatively easily tractable system, amenable to confocal microscopy and live-imaging. The growth dynamics of the *A. thaliana* leaf have been characterised in detail through live-imaging and cell tracking experiments (Kuchen et al., 2012). Such analysis has

allowed detailed modelling of leaf development as a continuous tissue, using biologically extracted parameters for growth rates. Recently, this model has been developed further to include individual cells and cell types (Fox et al., 2018). Both models, generated in GFTbox, require polarity-based axiality to guide growth (Fox et al., 2018; Kuchen et al., 2012). The tissue-wide polarity fields predicted in these models are based on PIN1 polarity patterns in the young primordia (Guenot et al., 2012; Kuchen et al., 2012; Scarpella et al., 2006) and are predicted to be maintained throughout development.

In the model of the leaf by Kuchen et al. (2012), for example, a polarity field is required throughout development. This allows growth to switch to become more perpendicular to this predicted polarity field at later stages. In the model a factor termed 'LATE' is switched on at later stages of development to enhance growth perpendicular to the hypothesised polarity field, and this allows the leaf to form its final shape (Kuchen et al., 2012). However, the polarity patterns in the leaf at later stages of development have so far not been testable experimentally due to a lack of polarity markers at later developmental stages.

In addition to a predicted tissue-wide polarity field for leaf 1 of *A. thaliana*, the leaves of this species also possess serrations. Development of serrations is known to involve PIN1 polarity convergence points (Hay et al., 2006), and this process has also been modelled (Bilsborough et al., 2011; Kuchen, 2011). In serrations, the up-the-gradient model has been combined with observed PIN convergence points and CUP SHAPED COTYLEDON 2 (CUC2) dynamics to form a model for serration development and spacing. This work proposes that CUC2 may be required for cell plasticity, allowing the reorientation of PIN1 to form convergence points along the margin, according to the up-the-gradient model, (Bilsborough et al., 2011). This model has been extended more recently to include gene expression patterns of the AUX/LAX family of auxin importers (Kasprzewska et al., 2015).

The regional polarity of the abaxial-adaxial leaf surfaces has been well studied and is established by the interaction between the dorsal Class III HD-ZIP protein REVOLUTA (REV) (Otsuga et al., 2001) and the ventral protein KANADI1 (KAN1) (Kerstetter et al., 2001). Recent work imaging REV and KAN1 together with PIN1 has shown that PIN1 is expressed in the narrow gap between the dorsal and ventral domains during organ initiation (Caggiano et al., 2017). This work also raises the question of how regional polarity, such as the abaxial-adaxial distinction in a leaf, may interact with and rely on patterns of cellular polarity, such as PIN or other cellular markers, during organ initiation.

Furthermore, *A. thaliana* has multiple mutants with altered leaf shapes that provide a useful resource for understanding elements of leaf growth and polarity. For example, the *kanadi1kanadi2* (*kan1kan2*) double mutant has ectopic outgrowths on its abaxial surface (Eshed et al., 2004) and this system has proved useful in testing models of outgrowth formation involving polarity (Abley et al., 2016). The *kan1kan2* ectopic outgrowths require PIN1 polarity convergence points to form, and expression analysis of PIN1, CUC2, auxin importers and YUCCAs (auxin biosynthetic enzymes) during outgrowth formation has been carried out in this context (Abley, 2014; Abley et al., 2016). This work suggests that the gene expression patterns observed during outgrowth formation in this context are more parsimonious with tandem array models (with the flux and intracellular partitioning) than with convergent alignment models (up-the-gradient) (Abley et al., 2016).

As mentioned previously, the *A. thaliana* epidermis also demonstrates evidence for cell polarity, and some evidence for coordinated tissue polarity, in the stomatal lineage (Bringmann and Bergmann, 2017; Dong et al., 2009; Robinson et al., 2011). There is currently no evidence that polarity in the stomatal lineage is linked to that of PIN proteins, which may indicate that the leaf possesses multiple independent polarity fields.

The detailed understanding of *A. thaliana* leaf growth, a predicted tissue-wide polarity field, multiple contexts where PIN polarity dynamics are involved in outgrowth formation, and the existence of multiple well-characterised polarity fields makes the *A. thaliana* leaf a suitable system in which to study polarity in plant organs.

1.4 Establishment and coordination of polarity in plants

How polarity systems are established in plants is an area of active research, particularly in the case of PIN polarity. PIN proteins transport auxin in a polar manner in plant tissues, and thus auxin has been heavily implicated in the coordination of polarity in plants (Grebe, 2004). Auxin is also known to have a key role in embryogenesis, primordia initiation and shoot architecture, as indicated by a lack of shoot initiation in the *pin1* mutant and in seedlings treated with the NPA (Galweiler et al., 1998; Okada et al., 1991).

1.4.1 Models for polarity establishment and coordination in plants

The observations of PIN protein localisation in different developmental contexts and tissues has given rise to multiple models to account for the polarisation of PINs by auxin. Discussion of the PIN protein family as markers of polarity can be found in section 1.1.3.2.2: the models of how PIN proteins could become polarised and coordinated as part of an axially system are briefly described here and are reviewed in Abley et al., (2016).

In the shoot apical meristem, it has been reported that PIN polarities point towards the site of ectopic auxin application (Bayer et al., 2009); this behaviour has provided the foundation of the up-the-gradient model (Jonsson et al., 2006). In the up-the-gradient model, PIN is polarised towards the neighbouring cell with the highest auxin concentration (Jonsson et al., 2006; Smith et al., 2006). This leads to spontaneous convergence points of PIN with auxin maxima at the centre, and thus parsimoniously illustrates the behaviour of PIN and auxin maxima in the meristem during phyllotaxis (Jonsson et al., 2006; Smith et al., 2006). There are multiple molecular mechanisms that have been proposed to account for the up-the-gradient behaviour, including auxin sensing (Cieslak et al., 2015) and stress-based sensing (Heisler et al., 2010). In the up-the-gradient model, PIN is allocated to the membrane adjacent to the cell wall under the most stress. Auxin is assumed to cause cell wall loosening, which in turn creates a stress difference between the cells, hence the result is PIN orienting towards the cell with the highest auxin concentration (Heisler et al., 2010). However, it remains unclear how cells measure these stress differences (Abley et al., 2016).

An alternative model (with-the-flux model) proposes that PIN proteins localise to membranes with the highest auxin efflux rates (Rolland-Lagan and Prusinkiewicz, 2005). The coordination of PIN polarity across a tissue is therefore a result of auxin flux across the tissue. Flux-based models can account for the patterns of PIN polarity observed during vascular strand formation (Rolland-Lagan and Prusinkiewicz, 2005), and with some added assumptions have also been used to account for phyllotactic patterning (Stoma et al., 2008). How such a flux-sensing mechanism might operate in cells is unclear (Bennett et al., 2014).

A third type of model to account for polarity formation is the intracellular partitioning model proposed by Abley et al., (2013). This model does not focus specifically on the establishment and maintenance of PIN polarity and can account for polarity formation in both plant and animal systems. In this model it is proposed that cells are able to spontaneously polarise, using intracellular partitioning components in the absence of asymmetries in external cues

(such as auxin). Two polarity components exist, each in two forms: A and B are diffusible cytoplasmic forms, and A* and B* are more slowly diffusing membrane bound forms. A* and B* are located at opposite ends of the cell, and through an interaction network (where A* inhibits B*, and B* inhibits A*) can form spontaneous polarisation (Abley et al., 2013). PIN proteins could be recruited by these polarity components. Cell polarisation can then be coordinated by cell-cell coupling, either directly, as in animals, or indirectly as in plants (Abley et al., 2013).

These models accounting for different polarisation behaviours can all explain some aspect of PIN behaviour in developing tissues, but all have biological details or mechanisms which have not been fully supported experimentally. It is also unclear how the same protein may read auxin information in different context-dependent ways, something that may become clearer by studying other systems where these activities are under the control of different PIN1 isoforms (O'Connor et al., 2014). One way to validate and distinguish between models is to test their predictions in different tissue contexts, particularly with respect to gene expression patterns. There are multiple models which now combine the more conceptual model types described above with gene expression patterns, such as in serrations (Bilsborough et al., 2011) and ectopic outgrowths (Abley et al., 2016).

1.4.2 Polarity coordination in the stomatal lineage

In the case of polarised proteins in the stomatal lineage, it is unclear how their polarity is established. Recent work using BRXL2 has implicated mechanical stresses in the coordination of polarity (Bringmann and Bergmann, 2017). This work showed that BRXL2 polarity in the *A. thaliana* cotyledon can respond to mechanical stresses across the tissue when the cotyledon is stretched or cells ablated (Bringmann and Bergmann, 2017). However, given that stress is a tensor and has no direction, it is not mathematically possible for stresses alone to orient polarity (Whitewoods and Coen, 2017).

1.4.3 The need for polarity markers in plants

To further understand how polarity is established and coordinated in plant tissues, and therefore understand mechanisms that might be involved in controlling the growth and development of plant tissues, it is necessary to have suitable markers of polarity. Whilst PIN proteins are well-characterised, their lack of coordinated expression in leaves makes them less useful markers in this organ. In addition, the intrinsic connection between PIN proteins and auxin, which has multiple roles in plant growth and development, complicates their use

as polarity markers. The identification of novel polarity markers in plants, such as the recently identified SOK protein family (Yoshida et al., 2019), may allow testing of models of polarity establishment and coordination, such as the intracellular-partitioning model (Abley et al., 2013), and therefore the testing of hypotheses regarding the control of plant growth and development.

1.5 Aims of this work

This work aims to explore the existence of tissue cell polarity, using the leaf of *A. thaliana* as a model. The work aims to establish whether coordinated tissue-cell polarity exists across the *A. thaliana* leaf throughout development and in cells outside of the stomatal lineage. The existence and characterisation of such a polarity field could provide evidence for the control of anisotropic growth across planar plant organs and could help to elucidate the role of polarity in development. In addition, robust evidence for a polarity field could allow distinction between models of development that currently lack experimental evidence.

In this work, the polarly localised stomatal protein, BASL, is used as a tool to explore the existence of polarity across the leaf. Detailed characterisation of a polarity field across the leaf would allow multiple hypotheses to be tested regarding polarity in plant tissues. Beyond characterisation of any polarity system across the leaf, this project therefore has a number of aims:

- To explore whether tissue cell polarity in leaves exists throughout development.
- To test whether polarity in the leaf is independent of the stomatal lineage.
- To test predictions regarding the role of tissue-wide polarity in the growth and development of leaves and test whether multiple polarity systems exist in leaves.
- To explore the coordination mechanisms underlying tissue cell polarity in leaves.
- To explore the molecular basis for the establishment of polarity using a biochemical approach to search for novel potential factors involved in tissue cell polarity in plant tissues.

2 Evidence for a tissue-wide polarity field in leaves

Introduction

2.1 Polarity in planar plant organs

Several proteins preferentially localised to one end of the cell (i.e. exhibiting cell polarity) have been described in plants. Some of these polarly localised proteins exhibit coordination across planar organs (or regions of organs) in certain contexts, for example PIN proteins in the young primordia (Guenot et al., 2012; Scarpella et al., 2006) and BRXL2 in the stomatal lineage (Bringmann and Bergmann, 2017). Here I focus on the *Arabidopsis thaliana* leaf as a model for studying polarity in plants.

2.1.1 PIN as a marker of polarity

PIN proteins, the family of auxin transporters, are the most well-studied markers of cell polarity and tissue cell polarity in plants. In *A. thaliana*, PIN1 is localised to the distal face of cells in the early leaf primordia, creating a coordinated tissue polarity pattern (Guenot et al., 2012; Scarpella et al., 2006). PIN proteins are also expressed in a polar manner in certain contexts later in development. In serration formation, for example, PIN1 localises to the distal face of cells below the serration tip, and to the proximal or side face of cells in the region above the serration tip, creating PIN1 convergence and divergence points at the serration tip and sinus respectively (Bilsborough et al., 2011; Hay et al., 2006). In the *kanadi1kanadi2* (*kan1kan2*) mutant, PIN1 is expressed during the formation of ectopic *kan1kan2* outgrowths where it forms convergence points (Abley et al., 2016). However, in all of these situations, PIN1 expression is temporally or spatially restricted. In the leaf primordia, polarised PIN1 expression is observed only up to ~150 μm width before disappearing from the epidermis in a non-uniform manner (Figure 2.1 and Abley et al., 2016). In other contexts, such as *kan1kan2* outgrowths and serration formation, PIN1 expression is only observed in a subset of cells in the leaf, usually around the outgrowth (Abley et al., 2016; Bilsborough et al., 2011; Hay et al., 2006). Furthermore, PIN1 expression is not always clearly polarised (Abley et al., 2016).

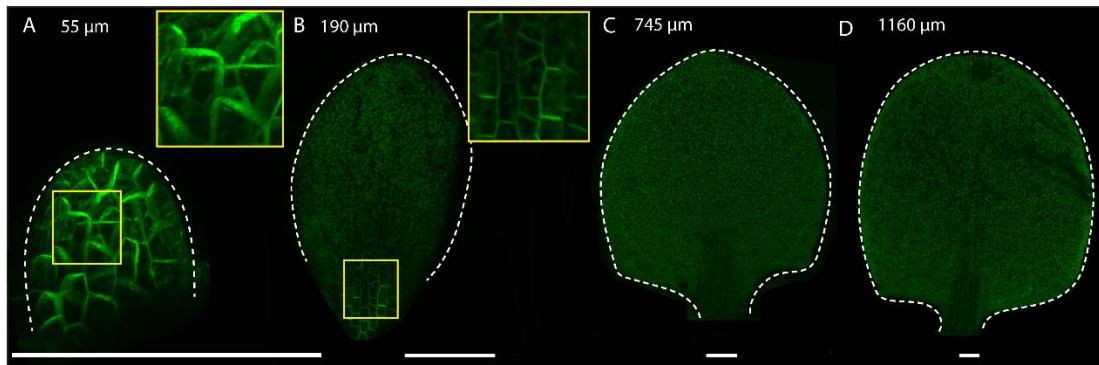


Figure 2.1 *PIN1::PIN1-GFP* expression is visible at early stages of leaf development.

(A) *PIN1::PIN1-GFP* is expressed at very early stages of leaf development, and is polarly localised to the distal end of cells. Polar localisation of PIN1 is shown in inset in yellow box. (B) Expression becomes reduced later in development, disappearing in a non-uniform manner. Here, PIN1 is only visible in the petiole where it appears less polar (inset in yellow box). (C and D) PIN1 expression is not visible in the epidermis of the lamina at later stages. White dotted line shows leaf outline. Leaf widths are shown above each leaf. Scale bars are 100 μm .

At the cellular level, PIN polarity is responsible for the directional transport of auxin (Wisniewska et al., 2006), hence this polarity has major implications for development. Because PIN proteins are part of the mechanism of polar auxin transport, they are therefore potentially connected to any underlying mechanism establishing cell polarity. This raises challenges for using PIN proteins simply as a read-out or marker of polarity, but they do provide some of the only evidence of coordinated polarity in plant tissues.

Computational models, such as those produced using the ‘Growing polarised tissue framework’ (Gftbox) (Kennaway et al., 2011), have highlighted the need for coordinated polarity at the tissue level in the growth of many planar plant organs, particularly in order to orient anisotropic growth (Eldridge et al., 2016; Green et al., 2010; Kuchen et al., 2012; Rebocho et al., 2017b; Richardson et al., 2016). Gftbox has also been used to model liverwort thallus development without a need for polarity (Solly et al., 2017) and other models of plant growth do not invoke tissue cell polarity (Hervieux et al., 2016).

2.1.2 Polarity at later stages of development

In models of *A. thaliana* leaf development produced using Gftbox, coordinated tissue polarity is required in order for the tissue to grow preferentially parallel or perpendicular to a polarity field (Kuchen et al., 2012). The polarity field in this model is supported by observed PIN1 polarity in the primordia (Scarpella et al., 2006). However, the model predicts the existence

of a polarity field throughout development, not just at the primordia stage (Figure 2.2). Indeed, a polarity field throughout development is required in this model to allow growth to switch to become more perpendicular to the predicted polarity field at later stages (in the model, a factor termed 'LATE' enhances perpendicular growth, Kuchen et al., (2012)). Models of other planar organs also require the existence of a polarity field throughout development to allow polarity and growth changes at different developmental stages, for example, in models of the snapdragon flower (Green et al., 2010; Rebocho et al., 2017b). In computer models, it is possible that a polarity field could be established at early developmental stages and attached to the tissue (such as the non-deforming model in Kuchen et al. (2012)). However, it is difficult to see how such a polarity field could remain independent and not deform with the tissue, and how new polarity convergence points, such as those described at serrations and in *kan1kan2* mutants would appear (Abley et al., 2016; Bilsborough et al., 2011). Despite the requirement of some models for a polarity field throughout development, no known polarity marker currently provides experimental evidence for this.

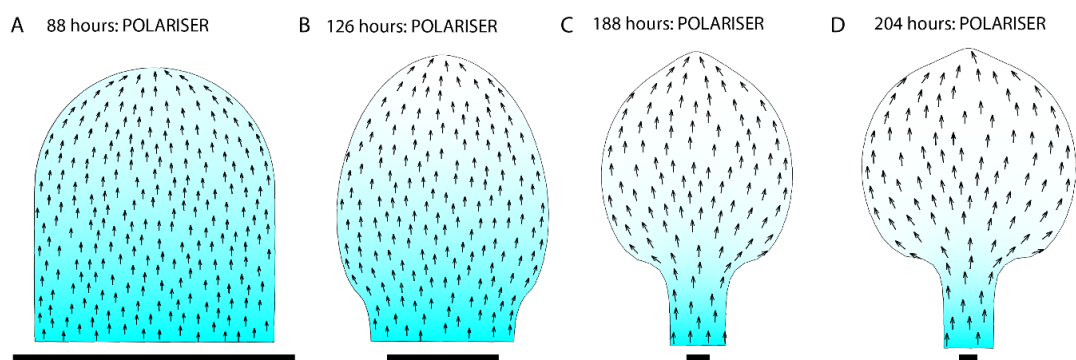


Figure 2.2 Modelling predicts a polarity field throughout *A. thaliana* leaf development. *A. thaliana* leaf model predictions (from model in Kuchen et al. 2012) of polarity field at different stages (progressively later stages A-D), corresponding approximately to the stages of leaf development shown in Figure 2.1. In the model, LATE comes on between stages shown in B and C with the effect of enhancing lateral growth. Blue shows POLARISER gradient. Scale bars 100 μm .

Whilst PIN proteins provide clear evidence for tissue cell polarity in early developmental contexts, their limited expression at later stages of development means this family of proteins cannot provide evidence for tissue cell polarity throughout the development of planar organs. There are, however, other lines of evidence for tissue cell polarity at later stages.

One interesting example is trichomes which, in *A. thaliana*, undergo two successive branching events, the first of which is aligned with the leaf proximodistal axis (Bouyer et al., 2001; Hülskamp et al., 1994). Trichome branching occurs at developmental stages beyond the primordium stage, indicating that cells in later developmental stages may have cell polarity.

Stomata also provide some evidence for cell polarity beyond the primordium stage. Stomata form in an evenly spaced pattern across the leaf epidermis. The cells of the stomatal lineage undergo a spiral pattern of cell divisions, involving the stomatal protein BASL (Robinson et al., 2011). BASL is asymmetrically localised before asymmetric cell division in the stomatal lineage, indicating that these cells have cell polarity. Recent work has indicated that BRXL2, an interactor of BASL, is also asymmetrically localised in the meristemoid mother cells (MMCs) of the stomatal lineage and, in addition, shows proximodistal coordination across the tissue (Bringmann and Bergmann, 2017).

Both trichomes and stomata are features of the leaf epidermis, and thus provide evidence that at least specific cell types in the epidermis may possess polarity throughout development. Recent work in the *A. thaliana* leaf has suggested that growth of the epidermis, perhaps driven by polarity, is the main driving force for overall leaf growth (Fox et al., 2018). This highlights the important role for tissue cell polarity in the epidermis. Root hairs provide further evidence for polarity coordinated across a tissue as they are consistently localised at the rootward end of the root hair cell (Masucci and Schiefelbein, 1994). This is further to the evidence that coordinated cell polarity is important for plant organs at later developmental stages, but roots are not planar organs and will not be considered in detail here.

2.1.3 BASL localisation in stomatal lineage cells

In the stomatal lineage, BASL is asymmetrically localised and plays a role in cell polarity. A polarity switching pattern of cell division in the stomatal lineage has been described and is responsible for the correct spacing of stomata across the leaf (Robinson et al., 2011). BASL localises opposite the site of a new cell wall during asymmetric cell division in meristemoid mother cells (MMCs) (Figure 2.3). *basl* mutants exhibit defects in stomatal patterning, often forming clumped stomata (Dong et al., 2009). The localisation of BASL to a crescent at the cell periphery is critical for its function and preventing peripheral localisation of BASL also leads to *basl* mutant characteristics (Dong et al., 2009). Thus, BASL may represent an

important part of the mechanism of asymmetric cell division in the *A. thaliana* stomatal lineage. Interestingly, whilst BASL appears to be a key player in stomatal lineage patterning in *A. thaliana*, it does not appear to be a protein conserved across the plant kingdom, with only a few known species having strong candidates for BASL homologues (Dominique Bergmann, personal communication). This may indicate a role for other polarity determinants in the stomatal lineage.

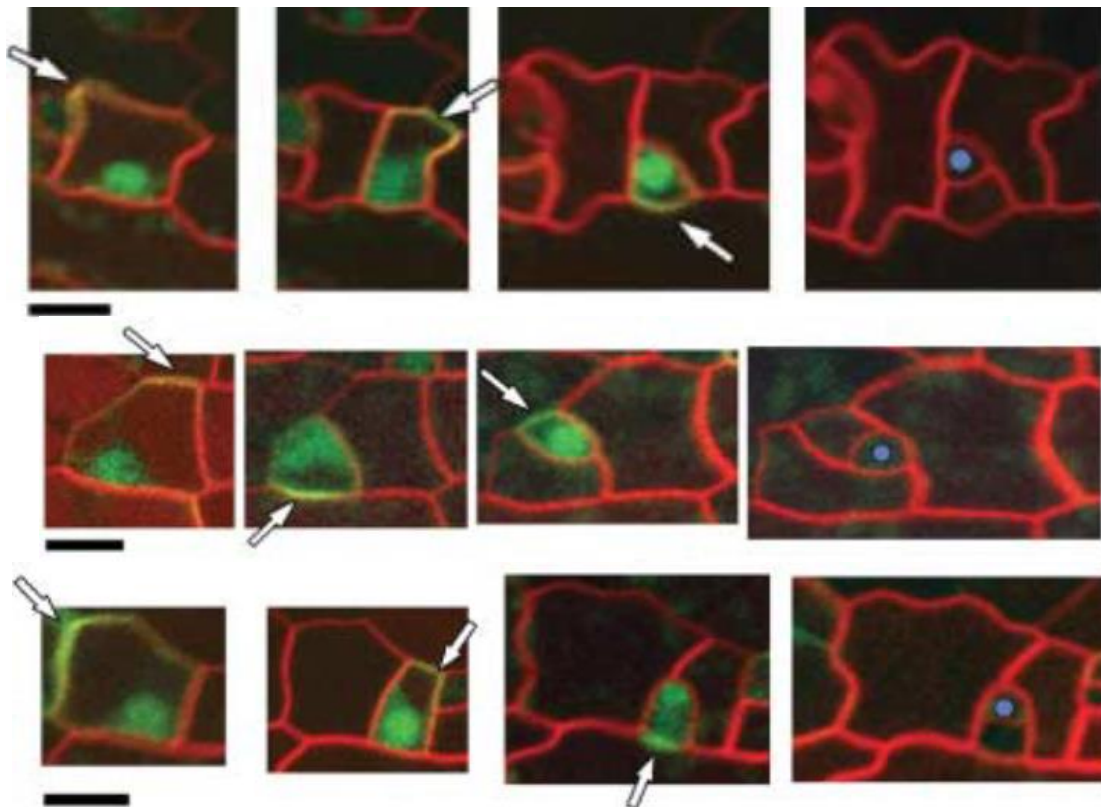


Figure 2.3 *BASL::GFP-BASL* in meristemoid mother cells localises opposite new cell walls. Examples of *BASL::GFP-BASL* showing BASL localised to the cell periphery, opposite the new cell wall and in a spiral pattern. Location of peripheral BASL (arrows) was tracked for three divisions until a GMC (blue) formed. Scale bars are 10 μm . From Robinson et al. (2011). Reprinted with permission from AAAS.

Until recently, it was thought that the polarity of stomatal lineage cells was not coordinated across the tissue. Recent work has shown BRXL2, an interactor of BASL, to be asymmetrically localised within stomatal lineage cells, and, importantly, to exhibit coordination within these cells across the tissue in its native context (Bringmann and Bergmann, 2017). It is unclear whether polarity may also exist outside the stomatal lineage, and at stages where known polarised proteins, such as PIN1, are not expressed.

Modelling work in the *A. thaliana* leaf, and other plant organs, suggests a requirement for coordinated tissue cell polarity across the tissue. For such models to be biologically validated, evidence should be provided for such coordinated polarity. In the case of *Utricularia gibba*, an aquatic carnivorous plant, modelling of the trap shape has predicted a polarity field that has been validated, to some extent, with evidence from the coordinated polarity of quadrifid glands (Bushell, 2016). This example has similarities to the coordination of trichomes on the *A. thaliana* leaf, in that quadrifid glands reveal a coordinated polarity, but that is only visible in a minority of cells across the tissue.

Despite some evidence for physical markers of tissue cell polarity such as trichomes (Bouyer et al., 2001; Hülkamp et al., 1994) and quadrifid glands (Bushell, 2016), and evidence for cell polarity in certain cell types and stages of development, for example with PIN proteins (Bilsborough et al., 2011; Guenot et al., 2012; Scarpella et al., 2006) and with BRXL2 in the stomatal lineage (Bringmann and Bergmann, 2017), the evidence for coordinated tissue cell polarity in plants remains lacking.

One method to explore the existence of polarity across *A. thaliana* leaves is to use known polarity markers and express them in ectopic contexts. This might allow an understanding of how such proteins polarise and become coordinated across a tissue. BASL is a good candidate for overexpressing in leaves, as it is polarised only in the stomatal lineage cells of the leaf where it undergoes a polarity switching mechanism that has been shown to play a role in patterning (Dong et al., 2009; Robinson et al., 2011), but has also been reported to be polarised in ectopic contexts without severe developmental phenotypes (Dong et al., 2009).

2.2 Aims of this work

The aim of this work was to use BASL to explore and characterise tissue cell polarity in *A. thaliana* leaves. This project aims to build on previous work by Jordi Chan who used an inducible system to overexpress BASL in *A. thaliana* leaves. I aim to use BASL as a marker of polarity to characterise tissue cell polarity in *A. thaliana* leaves throughout development, as well as develop tools to quantify polarity. Characterisation of the polarity in the *A. thaliana* leaf could provide insights into how tissue cell polarity may be coordinated and, importantly, may allow the testing of models and hypotheses involving the growth and development of plant planar organs.

The work in this chapter was based on preliminary work by Jordi Chan (John Innes Centre, Norwich), and software was developed in collaboration with Tjelvar Olsson, Matthew Hartley and Jake Newman (John Innes Centre, Norwich).

Results

2.3 Ectopic BASL expression in a wild-type background

To explore how BASL might behave in cells of the *A. thaliana* leaf outside the stomatal lineage, an inducible *35S::GFP-BASL* line was developed using the heat shock system (Figure 2.4) (Gallois et al., 2002) by Jordi Chan, prior to the start of this project. The inducible system allowed BASL expression in cells outside of the stomatal lineage, whilst avoiding any potentially pleiotropic effects of expressing BASL outside of the stomatal lineage (for example cell bulges as has been described previously by Dong et al., (2009)).

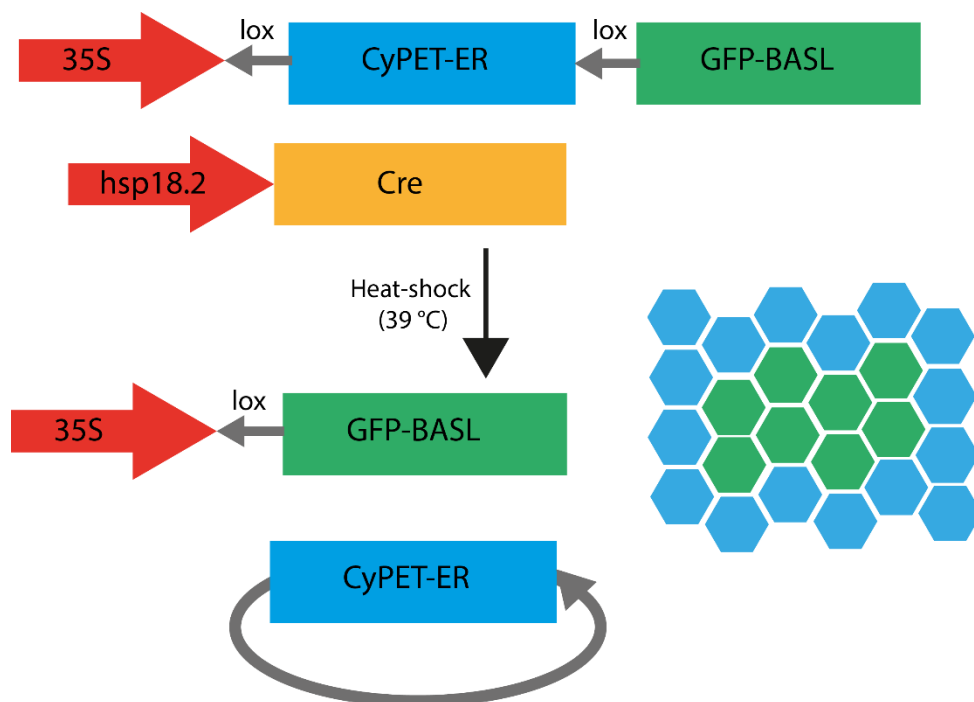


Figure 2.4 A Cre-lox based system was used for inducing BASL expression.

Transgenic plants contain two constructs. One construct has a constitutive promoter (35S, red arrow) driving the expression of a marker gene (CyPET, blue box). The CyPET sequence is flanked by loxP sites and tagged with an ER localisation signal. Downstream of this is a GFP-tagged BASL recombinant sequence (green box). The second construct contains a heat-shock inducible promoter (35S, red arrow) driving the coding sequence of CRE recombinase (yellow box). After CRE expression is induced by heat-shock at 39°C, CRE catalyses recombination at

the lox sites, excising CyPET-ER. This results in GFP-BASL being expressed in random cells under the 35S promoter. The progeny of these cells will also express *35S::GFP-BASL* and go on to form a sector.

2.3.1 Ectopic BASL expression in sectors

To determine where ectopic BASL is localised in individual cells, I induced sectors of *35S::GFP-BASL* using the Cre-lox heat-shock system. I heat-shocked seedlings 4 DAS (days after stratification) for 2-3 minutes at 39°C to induce small sectors of *35S::GFP-BASL*. GFP-BASL expression was imaged typically 48 hours after heat-shock in leaf 1 (Figure 2.5). Sectors with only a few cells expressing BASL were produced. The CRE-lox recombination reaction occurs randomly in cells meaning that, whilst some of the cells BASL was induced in appeared to be non-stomatal lineage cells (for example Figure 2.5 B, C), their lineage could not be fully determined in this experiment.

In sectors composed of two cells, the BASL signal localised in a crescent to the proximal end of both cells (Figure 2.5 B, C). Similarly, in sectors composed of a few cells, BASL was observed as a crescent of signal and was often detected at the proximal end of cells (Figure 2.5 D, E). I refer to this preferential proximal localisation as proximal bias. In these sectors, BASL was often localised to the corners of cells (Figure 2.5 C, E). The localisation of BASL to corners of cells in sectors allowed identification of which cell the BASL signal belonged to, as the BASL crescent tended to span a three-way junction between cells (Figure 2.5 C, E). The proximal bias expression pattern contrasts to endogenous BASL which is transiently expressed in a spiral pattern in the stomatal lineage (Dong et al., 2009). Thus, *35S::GFP-BASL* reveals asymmetric localisation with proximal bias when induced in sectors in young leaves.

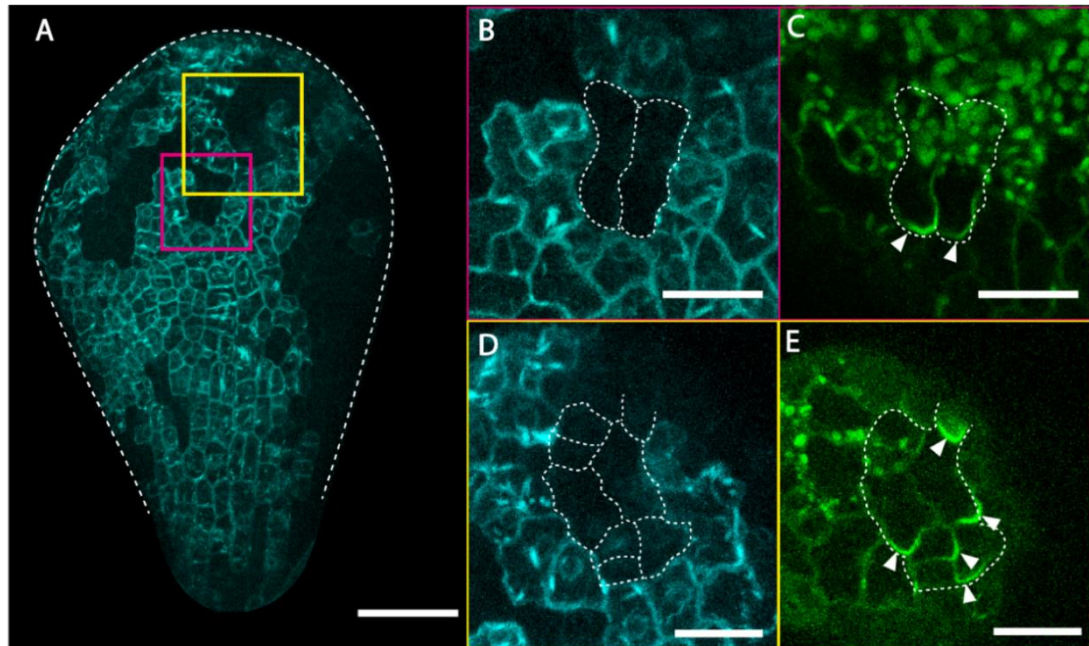


Figure 2.5 *35S::GFP-BASL* localises proximally in sectors in a wild-type background. (A) BASL induced in small sectors across the leaf (magenta and yellow boxes) composed of a few cells. (B and D) Absence of ER-tagged CFP indicates where sectors are induced. (C and E) GFP-BASL signal in the sectors localised to the proximal end of the cells (BASL signal indicated by white arrowhead). White dashed line indicates leaf outline in A, cell outlines in sectors in B and D and sector outlines in C and E. Scale bars are 100 μm in A and 20 μm in B-E.

These results indicate a polarity in cells that might occur in non-stomatal lineage cells, although at this stage of development, it is difficult to be sure whether cells are stomatal lineage cells without other markers to show cell fate. These results indicate not just a cell polarity, but a possible coordinated tissue cell polarity due to the proximal bias observed in ectopic BASL sectors. This raises the question of whether this proximal bias revealed by ectopic BASL could exist across a whole tissue, and whether BASL plays any role in cell polarity and its coordination.

2.3.2 Ectopic BASL expression across the lamina

The proximal bias revealed by induction of *35S::GFP-BASL* in sectors raises the question of how ectopic BASL behaves if induced across the whole leaf lamina, and at different stages of development. To address this question, I heat-shocked seedlings for a longer period of time (typically 20 minutes rather than 2-3) at different developmental stages (heat-shocked between 2 and 7 DAS), to induce *35S::GFP-BASL* expression across the whole leaf tissue. This analysis was carried out on leaf 1, unless otherwise stated.

Evidence for a tissue-wide polarity field in leaves

As observed in sectors, when ectopically expressed across the leaf, BASL signal was observed as a single crescent at the periphery of cells and appeared to show proximal bias across the tissue. This polarly localised and seemingly coordinated pattern of ectopic BASL had previously been observed by Jordi Chan when he developed the heat-shock inducible BASL line. His results showed the interesting patterning and localisation of ectopic BASL, and these preliminary observations became the starting point for my work in analysing, characterising and further exploring the pattern.

In order to assess which cell the BASL signal belonged to, it was important to be able to visualise the cell outlines. I stained leaves with propidium iodide (PI, 2.5 µg/ml) by immersing seedlings in a solution of PI for at least 10 minutes before imaging. This allowed the cell outlines to be visualised and hence enabled allocation of the GFP-BASL signal to specific cells.

I categorised leaves into 4 size classes, based on width (as measured in 2D in Fiji, Schindelin et al., 2012). The size categories (smaller than 200 µm, 200-400 µm, 400-800 µm, and larger than 800 µm) allowed the BASL pattern in leaves of similar sizes to be compared and pooled, and compared to other sizes.

In very young leaves of up to 200 µm in width, asymmetric BASL signal with proximal bias was observed (Figure 2.6 A, D). In some of the smallest leaves imaged, the BASL signal was weak (Figure 2.6 A, D). BASL was often seen across the entire proximal wall of cells in these small leaves, likely due to the small cell sizes (Figure 2.6 D). For leaves of width approximately 200-400 µm, BASL signal also exhibited a proximal bias across the tissue and was often observed in the corners of cells (Figure 2.6 B, E). At these stages, the localisation of ectopic BASL to cell corners results in the signal often spanning a 3-way junction between cells, and hence the signal could be easily assigned to the expressing cell (Figure 2.6 E). Larger leaves of between 400 and 800 µm in width also showed a proximal bias in ectopic BASL localisation (Figure 2.6 C, F). In leaves where pavement cells had clearly formed, the BASL signal was present in a single lobe of the pavement cell (Figure 2.6 F). At all of the stages analysed, BASL signal was not seen in every cell, despite the long heat-shock which should be sufficient to induce *35S::GFP-BASL* expression in all cells. Thus, ectopic BASL exhibits a proximal bias across the lamina at different stages of leaf development.

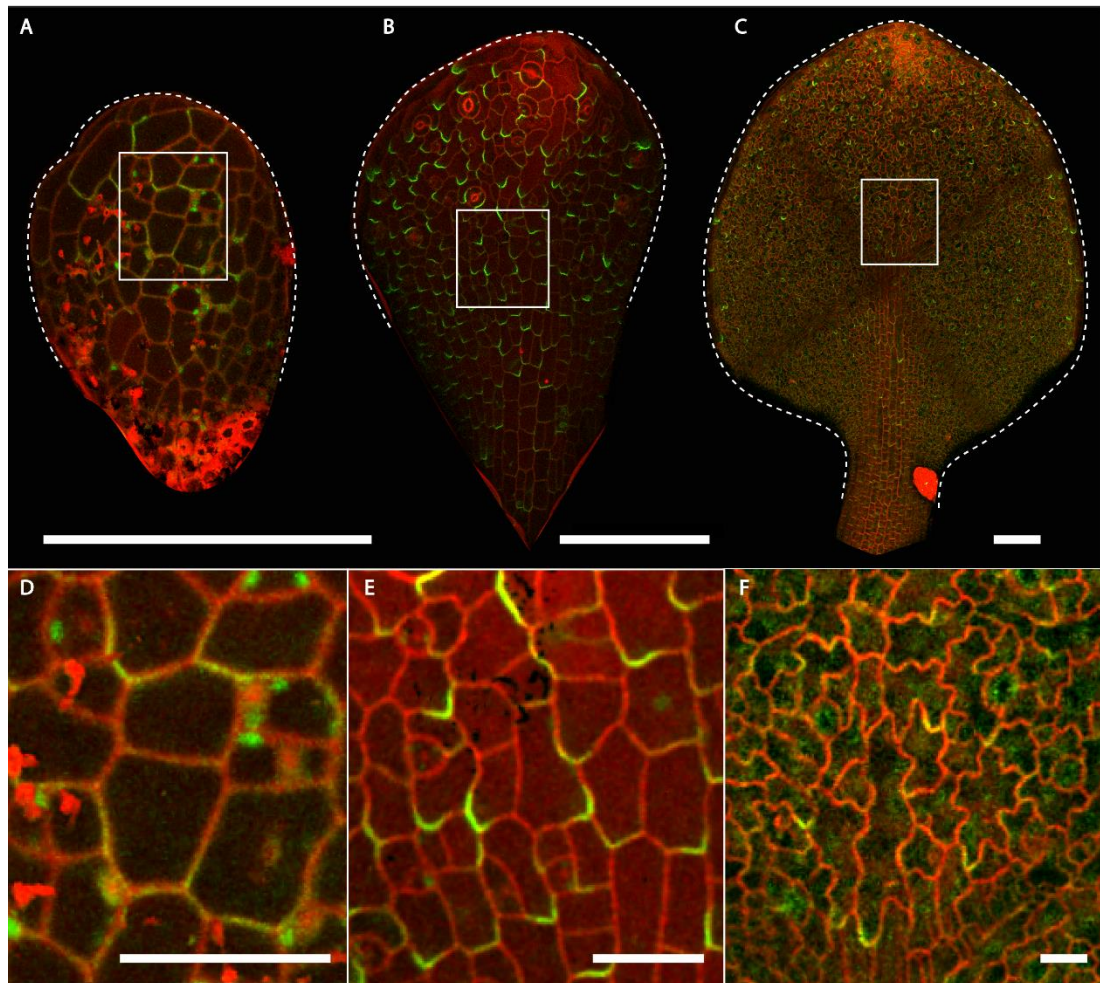


Figure 2.6 *35S::GFP-BASL* exhibits proximal bias across the leaf at different stages of development.

(A-C) Following extended heat-shock, GFP-BASL signal (green) was induced across a whole leaf at different stages of development. Propidium iodide (red) staining allowed visualisation of cell outlines and hence which cell the GFP-BASL signal belonged to. White dashed line indicates leaf outline. (D-F) Close-up regions of A-C (from white boxes). BASL signal was typically observed in a single lobe of pavement cells, at the proximal end of the cell, contributing to a proximal bias across the lamina. Scale bars are 100 μm in A-C and 20 μm in D-F.

2.3.3 Ectopic BASL expression at later stages of development

To better visualise ectopic BASL particularly at later stages, the inducible *35S::GFP-BASL* line was crossed into a plasma-membrane-RFP background (Nelson et al., 2007). This allowed larger leaves with ectopic BASL to be analysed which did not stain as well with propidium iodide. I heat-shocked larger seedlings (typically 7 days after stratification (DAS)) to induce ectopic BASL. In leaves of over 800 μm (up to $\sim 1500 \mu\text{m}$) in width, the ectopic BASL crescent was localised to a proximal lobe of cells, indicating a proximal bias across the leaf (Figure 2.7

A, B), similar to at earlier stages. BASL signal was typically localised to a single lobe of pavement cells, though signal was sometimes localised to the lateral wall of cells, rather than the most proximal lobe of a cell (asterisks in Figure 2.7 B). Thus, ectopic BASL exhibited proximal bias in leaves at later stages of development and localised to the lobe rather than the neck of pavement cells.

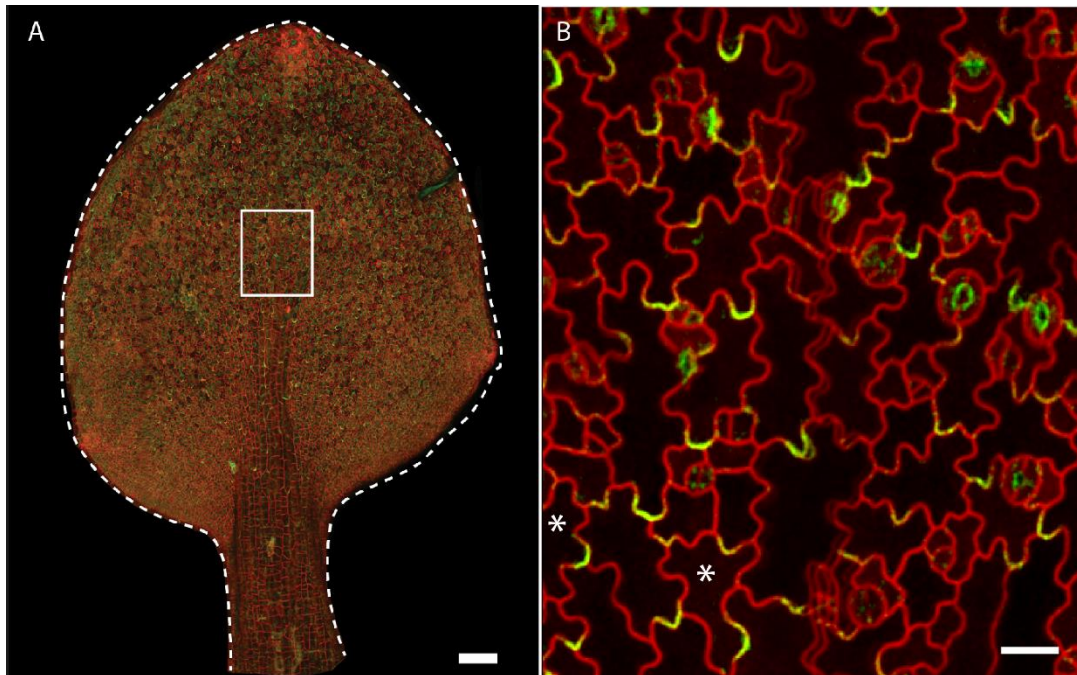


Figure 2.7 *35S::GFP-BASL* localisation is proximal at later stages of development.

Proximal bias is maintained at a later stage of development, using RFP-PM to visualise cell outlines. (A) Following heat-shock, BASL signal can be induced across a whole leaf at later stages of development. RFP-PM allows clear visualisation of which cell the GFP-BASL signal belongs to, and where the signal is localised. White dashed line indicates leaf outline. (B) Region of leaf in A (white box). BASL signal is observed in a single lobe of pavement cells, at the proximal end of the cell. Asterisks indicate cells in which the BASL is not localised to the most proximal lobe of the cell. Scale bar is 100 μm in A and 20 μm in B.

I used multiple criteria to identify which cell the BASL signal belonged to. It was possible to identify the cell to which the BASL signal belonged in cases where BASL overlapped vertices between cells (3-way junctions). In most cases, the BASL crescent did overlap a 3-way junction. In these cases, there was only one possible cell that the BASL crescent could be assigned to (Figure 2.8 A). Analysis of BASL at 3-way junctions confirmed that the BASL signal was seen in the lobe, and not in the necks of pavement cells. A second way I could determine which cell the signal was from was the observation that, in some images, the GFP-BASL signal appeared to bleed slightly into the cytoplasm, again providing clarity regarding which cell to

allocate the signal to (Figure 2.8 B). It is unclear why the signal sometimes appears to bleed into the cytoplasm; this may be due to BASL being saturated at one location, or because part of the top or lower face of the cell has some BASL signal.

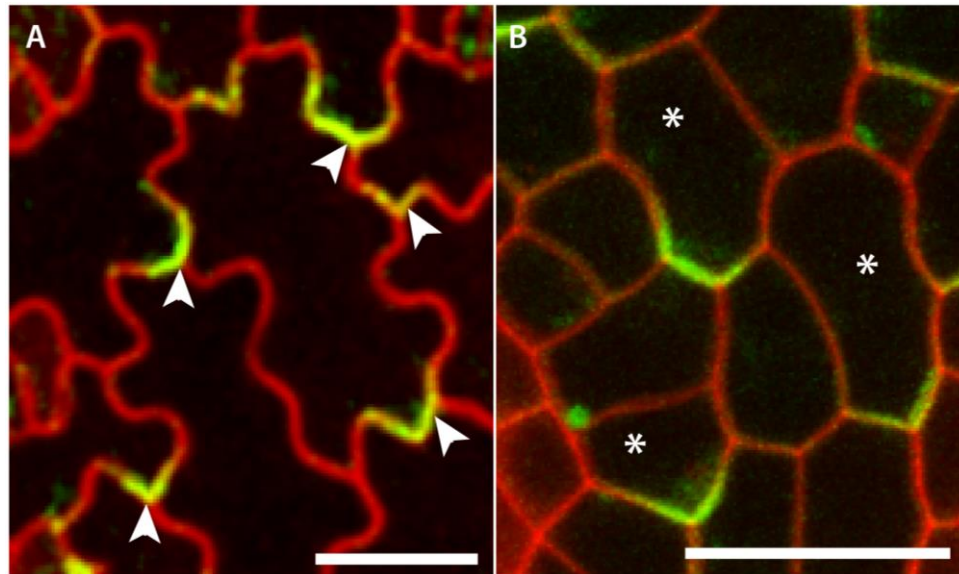


Figure 2.8 Three-way junctions and cytoplasm bleeding allow allocation of BASL signal to a cell.

(A) Three-way junctions between cells makes it clear which cell the GFP-BASL signal belongs to. Cell outlines are visualised with RFP-PM. White arrowheads indicate BASL signal spanning a three-way junction. (B) In some high-resolution images, the GFP-BASL signal appears to bleed into the cytoplasm providing another way to determine which cell the signal belongs to. Cell outlines are visualised with PI staining. White asterisks indicate cells in which the BASL signal appears to bleed into the cytoplasm. Scale bars are 20 μm .

It is worth noting that, at all stages analysed, ectopic BASL signal is not always observable in every cell in the leaf (Figure 2.6 D, E, F and Figure 2.7 B). This observation is despite the long heat-shock the plants received which should induce expression throughout the seedling. It is possible that the heat-shock system does not induce expression equally across the leaf (it was developed to induce sectors across a tissue, (Gallois et al., 2002)). BASL expression is very weak in some cells, and therefore may not be clearly visible when imaging, especially when other cells have much stronger expression. Alternatively, a biological rather than technical reason may account for the lack of BASL in every cell. In the stomatal lineage, BASL expression is dynamic and tightly regulated (Dong et al., 2009; Zhang et al., 2015; Zhang et al., 2016b). It is possible that cells have a mechanism for degrading BASL RNA or protein, in a way comparable to the regulation of BASL in stomatal lineage cells. However, it is unclear

why ectopic BASL would be absent in some cells rather than others. For example, if this was the case, it might be expected that ectopic BASL was not localised in meristemoids, and only in non-stomatal cells. Whilst it is difficult to definitively assign meristemoid identity without genetic markers, BASL can be observed in some presumed meristemoid cells (Figure 2.6 E) and is absent in others that are not obviously in the stomatal lineage (Figure 2.6 E). Thus, ectopic BASL is proximally localised in cells at different developmental stages, but not in every cell and it remains unclear why expression is variable.

2.4 Quantifying the polarity pattern revealed by BASL

2.4.1 BASL vectors indicate cell polarity

The observation that BASL localises to the proximal end of cells outside of the stomatal lineage when ectopically expressed indicates that cells have a proximodistal polarity. By localising to one end of the cell, BASL provides evidence for cell polarity, rather than just cell axiality. An important distinction is that an arrowhead can be assigned to a cell with polarity, but this is not possible in a cell with only axiality (Hejnowicz and Romberger, 1984; Whitewoods and Coen, 2017). In addition, the consistent proximal bias observed when *35S::GFP-BASL* is ectopically expressed suggests that BASL may reveal a coordinated tissue-wide polarity pattern that can be observed throughout development.

As a leaf deforms, a polarity field may deform with it, as has previously been predicted (Kuchen et al., 2012), raising the question of how polarity is oriented at different stages. I needed to be able to quantify the extent of any coordination of BASL polarity. I therefore worked with Tjelvar Olsson and Matthew Hartley (Scientific Computing, John Innes Centre, Norwich) to develop an image analysis pipeline to place vectors on cells using BASL signal, revealing any tissue-level polarity patterns indicated by BASL. Whilst vectors can be assigned by hand, it was important to ensure polarity vectors were assigned without bias. Knowledge of a cell's orientation relative to the leaf could result in a bias with polarity vectors being incorrectly assigned based on expected, rather than observed results.

2.4.2 Automated polarity vectors

One way to avoid subjectivity in assigning vectors to cells is to use automated analysis tools. This has the added benefit of often being less labour intensive and preventing human error

in assigning vectors. An automated analysis tool was developed in collaboration with Tjelvar Olsson. I contributed to ideas and discussion in the development of software, with Tjelvar programming and developing the software using Python.

Initially, we aimed to develop a fully automated tool that could assign BASL vectors without manual input. The automated tool developed by Tjelvar Olsson segmented cells on the leaf using a watershed algorithm. To find the BASL crescent, the point of maximum intensity of the BASL signal was used as one end of the vector. To assign the BASL signal to the correct cell, the assumption that the BASL signal was concave was added (i.e. if an ellipse could be fitted to the signal within a cell). The centre of this ellipse provided the point for the arrowhead of the vector. In some flatter leaves, this software was able to successfully identify BASL signal and assign it to a cell (Figure 2.9 A, B). However, in many other examples, and in the vast proportion of the data collected, there were multiple issues with this approach. In many cases, more than one point of signal in the GFP channel was identified by the software, for example (Figure 2.9, yellow boxes), which could not distinguish between the BASL signal and chloroplast auto-fluorescence in this channel. This was particularly the case if the BASL signal was faint and indistinguishable from background fluorescence. In other cases, the leaves (particularly smaller leaves) were too curved, or the cell outlines too unclear for the fully automated software to successfully segment cells or assign a high proportion of BASL vectors (Figure 2.9 C, D).

Given the issues faced, I decided that the fully automated software may not be suitable for this analysis with the images that I had collected. Further development of this software would require more advanced segmentation tools, and also more criteria or assumptions, (such as a minimum size threshold for the BASL crescent or the allocation of a single BASL vector) in order to be usable with this dataset. I therefore worked with Tjelvar Olsson and Matthew Hartley to explore the possibility of a semi-automated analysis tool with some manual input to correctly identify the BASL signal.

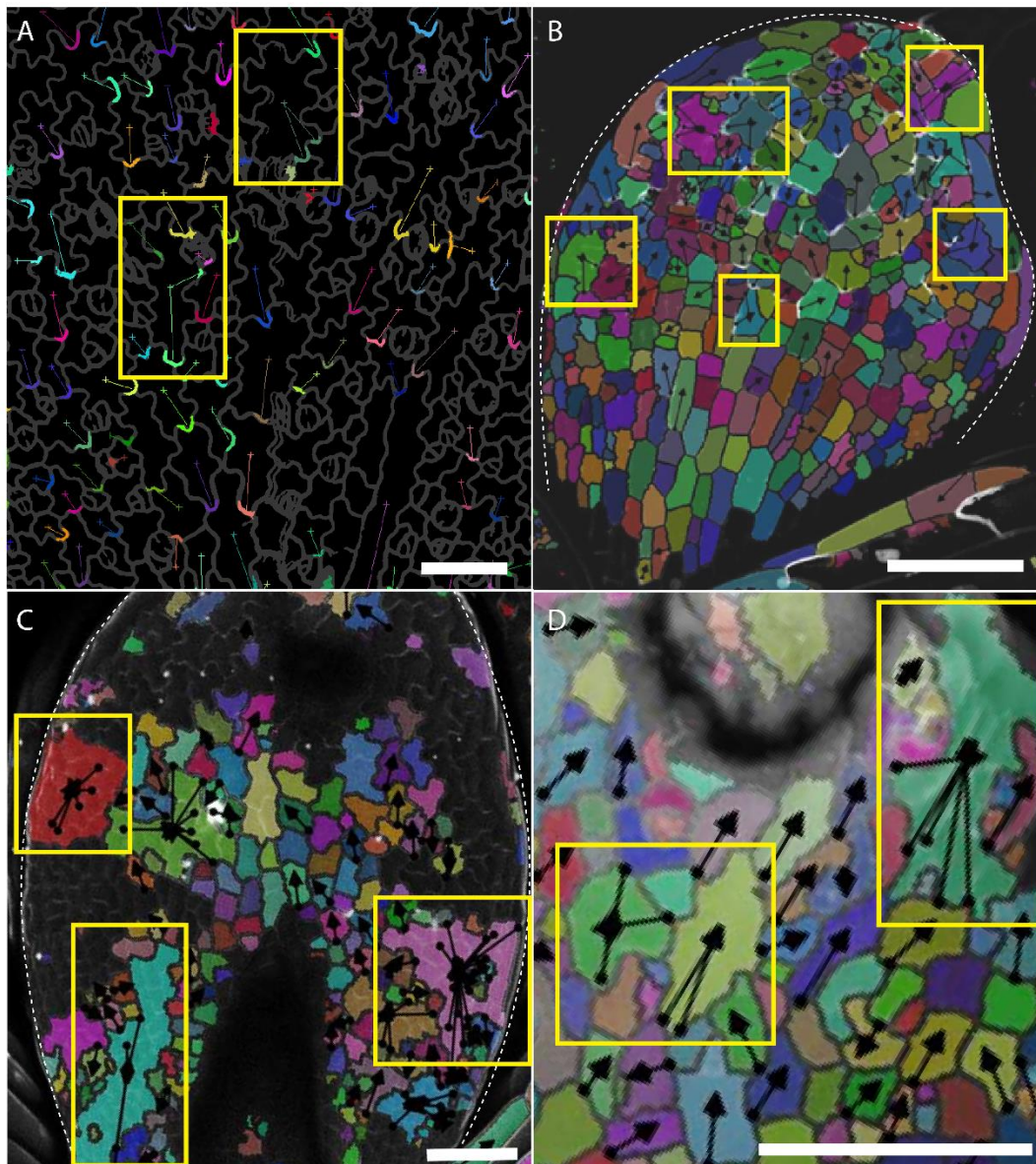


Figure 2.9 Fully automated software could not accurately assign BASL vectors.

(A and B) Leaf examples with successful segmentation, but some incorrectly assigned BASL vectors. In A, the cell outlines are shown in grey and coloured crescents indicate BASL signal that has been identified by the software and used as one end of the BASL vector (also shown in colours). In B, segmented cells are shown in different colours, with BASL vectors shown as black arrows. Yellow boxes indicate examples of cells where multiple BASL vectors have been assigned. (C) Leaf example with poor segmentation and therefore incorrect assignment of BASL vectors. Segmented cells are shown in different colours. Yellow boxes show regions in which multiple vectors have been assigned. In this example, the incorrect segmentation is likely due to poor PI staining and unclear cell outlines across a curved surface. (D) Section of a leaf with poor assignment of BASL vectors due to incorrect segmentation and multiple BASL signals being identified (yellow boxes). Scale bars are 50 μm .

2.4.3 Semi-automated polarity vectors

Following the difficulties of developing fully-automated software within the time and resource constraints, I decided that the priority for any polarity assigning software tool was to be accurate and unbiased, rather than automated and thus a semi-automated software was developed. The software (termed 'Cellsfromleaves' and detailed in section 6.6.1.1) consisted of two parts: (1) fitting the surface and segmenting cells; and (2) random rotation of cells. In addition, a visualisation tool (termed 'Cellsfromleavestagger' and detailed in section 6.6.1.1) was developed to allow BASL signal to be manually identified. The software was developed in collaboration with Tjelvar Olsson and Matthew Hartley (Scientific Computing, John Innes Centre, Norwich). Parts 1 and 2 of the software were coded by Tjelvar Olsson and the visualisation tool was developed by Matthew Hartley.

To overcome the issue of leaf curvature, a pseudo-3D surface was fitted to the leaf using the cell outlines (either RFP-PM or PI stained) (Figure 2.10). This then allowed a more accurate cell segmentation than had been possible using fully automated algorithms. Defining the leaf surface and cell segmentation depended on multiple parameters that could be adjusted on a leaf-specific basis to allow analysis of as many confocal images as possible. For example, wall signal erosion could be added (Figure 2.10 F), small object removal applied (Figure 2.10 D), as well as other standard cell-segmentation processes (Figure 2.10). Projecting cell outlines and BASL signal onto a surface (Figure 2.10 B, K) had the added benefit of removing much of the chloroplast auto-fluorescence signal, also captured within the GFP channel.

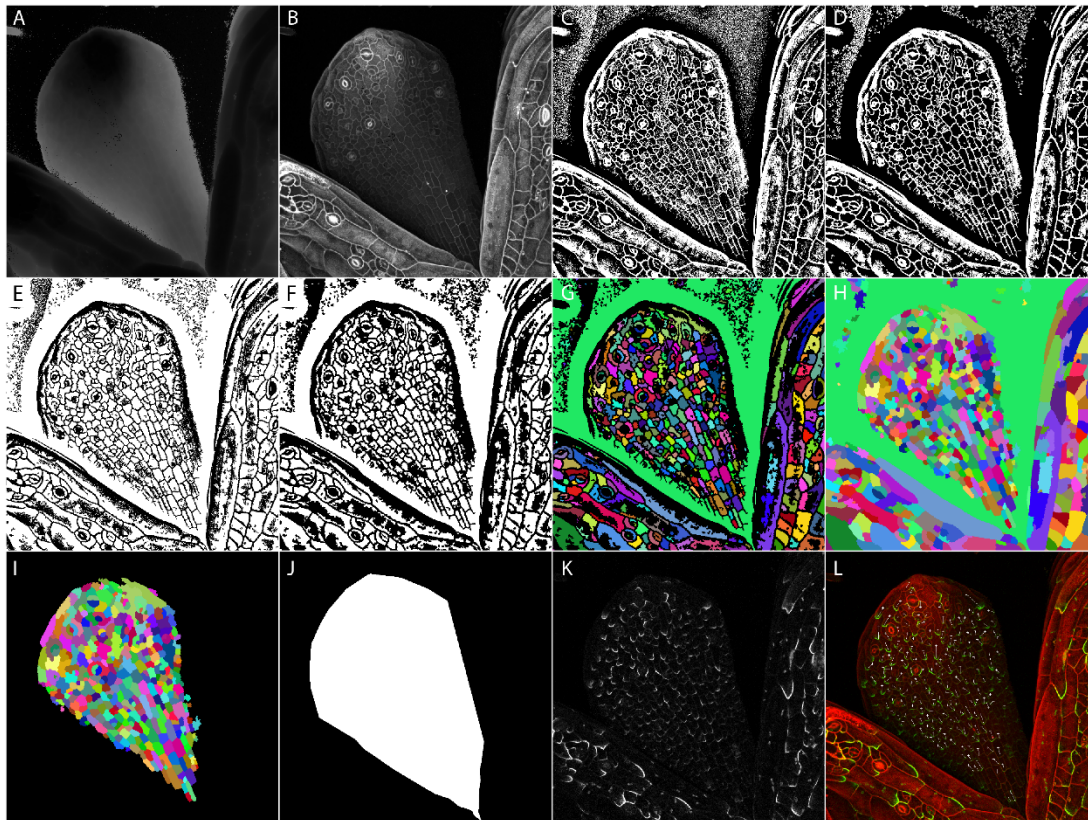


Figure 2.10 Semi-automated image analysis (part 1) creates a surface and segments cells. Example of a leaf in the various stages of semi-automated analysis. (A) A pseudo-3D surface is fitted using the cell outlines. (B) The cell wall signal (either RFP-PM or PI-stain) is projected onto the surface. (C) The signal undergoes thresholding to convert to a binary image. (D) Small objects (of a defined pixel size) are removed to get rid of noise introduced by thresholding. (E) The image is inverted and (F) an optional erode step is used to ensure each cell is enclosed. (G) A connected components algorithm and (H) watershed allow cell segmentation. (I) Cells outside the a given leaf mask (i.e. not within the leaf region) (J) are removed. (K) The BASL signal is projected onto the same leaf surface. (L) Both channels after tensors have been added in part 2 of the software.

To avoid bias in assigning vectors to cells, automatically segmented single cells were randomly rotated in one of four orientations (part 2 of software) (Figure 2.11 B-D). Individual cells were then visualised in the rotated position and the BASL signal (Figure 2.11 E, F) was identified manually by the user (Figure 2.11 G) before the vector information for that cell was re-rotated back to its original orientation (Figure 2.11 H). The centroid of the cell was calculated automatically by fitting an ellipse to a segmented cell. The BASL vector is oriented from the BASL crescent to the cell centroid (Figure 2.11 H and 2.12). I refer to the resulting vector field as the BASL polarity field (Figure 2.11 I). Thus, vectors can be extracted from cells

with BASL signal, using a semi-automated approach, and allowing a BASL polarity field to be visualised across the tissue.

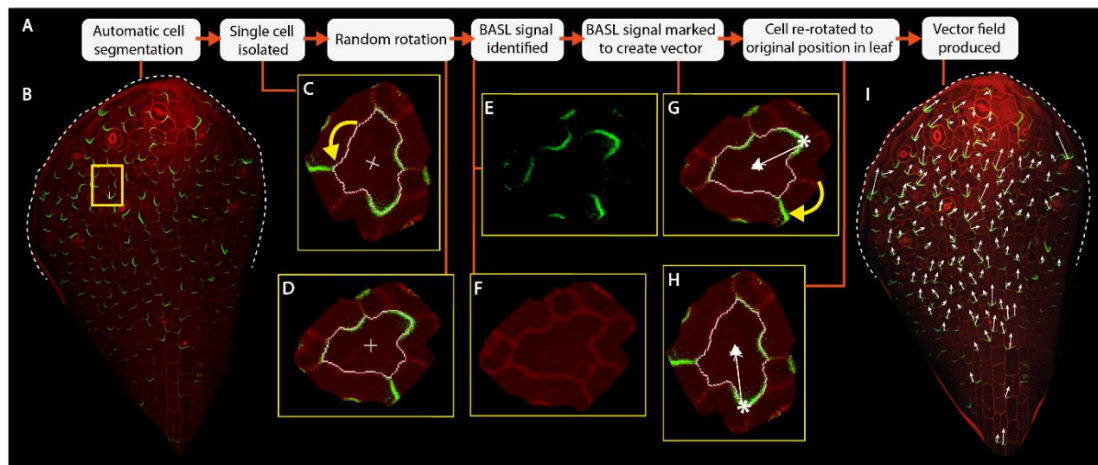


Figure 2.11 Semi-automated image analysis (part 2) rotates cells and allows vectors to be assigned.

(A) Image processing pipeline of 'Cellsfromleaves' software. (B) Raw confocal data is automatically segmented (see Figure 2.10). (C) Individual cells are identified and position of centroid is extracted. (D) Individual cells are randomly rotated in one of 4 orientations. (E and F) BASL signal is identified from merged image of cell and separate colour channels for clearer visualisation (using 'Cellsfromleavestagger' software). (G) BASL signal marked by hand (indicated by asterisk) to create vector, indicated by white arrow. (H) Cell and vector are re-rotated back into original position. (I) Process repeated for every segmented cell to produce a vector field for the leaf. White dashed line in B and I indicates leaf outline.

The resulting vectors describe the BASL polarity for individual cells. The angle of the vector can be calculated in relation to the proximodistal axis of the leaf (black arrow in Figure 2.12). This gives an angle describing the orientation of BASL, where 0° would be BASL in a perfectly proximal position relative to the leaf proximodistal axis (Figure 2.12). Development of this software and image analysis pipeline allowed BASL vectors to be assigned and I could therefore use the resulting vector orientations to further analyse tissue level polarity patterns.

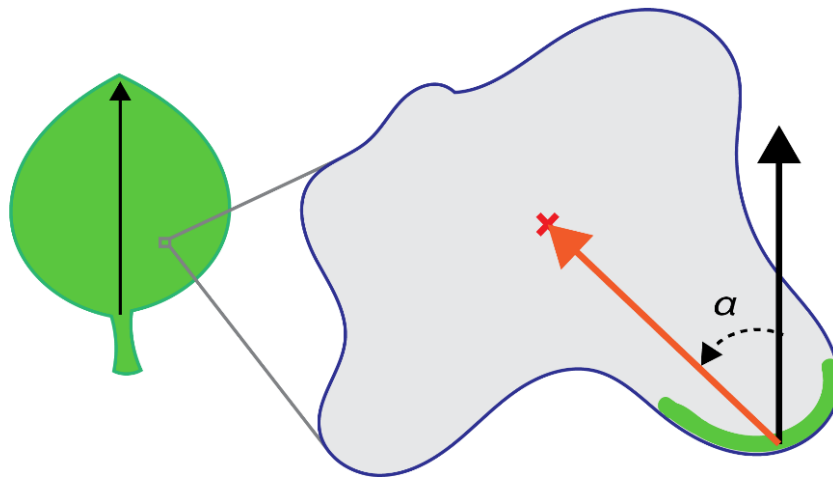


Figure 2.12 BASL vectors are assigned from the BASL crescent to the cell centroid. Vectors were assigned from the centre of the BASL crescent to the computational centroid (red cross) of the cell (orange arrow). This provides the vector angle (α) relative to the proximodistal axis of the leaf (black arrow).

2.4.4 Visualising the BASL vectors

In addition to the software developed for assigning BASL vectors, it was necessary to have a means of visualising the resulting vectors. I collaborated with Jake Newman to develop a program in Matlab (SampleArrows8) to allow the vector output from the previously described software to be visualised. Programming of SampleArrows8 was done by Jake Newman; I contributed ideas and tested the software. The BASL vectors were plotted based on their orientation, according to a colour map (Figure 2.13). This facilitated clear visualisation of patterns and preferential orientations across the leaf (Figure 2.13, A).

2.4.5 Testing the software using randomly generated tensors

In order to test the software and the random rotation method, the software also recorded the vectors before they were re-rotated to their original position. I plotted these non-rotated vectors and this confirmed that the non-rotated vectors were randomly oriented (Figure 2.13 B). When compared to the rotated vectors, the non-rotated distribution did not appear to have any preferential orientation (Figure 2.13, compare A and C with B and D). Thus, the software with random rotation of cells is sufficient to prevent knowledge of a cell's orientation in the leaf and eliminate the subjective bias that could be associated with this.

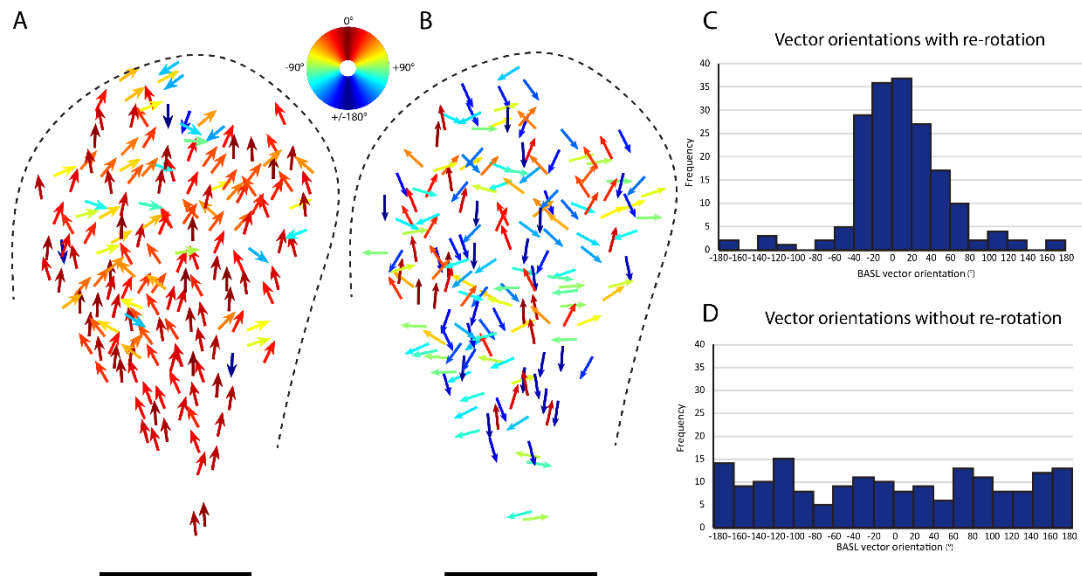


Figure 2.13 Testing re-rotation of semi-automated software.

(A) Example of output from semi-automated software (same leaf as in Figure 2.11) where cells are re-rotated back to their original position. Vectors are coloured based on their orientation, according to the colour map shown, where red represents a proximodistal vector and blue represents a disto-proximal vector. (B) Example of output from semi-automated software (same leaf as in A) where cells are not re-rotated back to their original position resulting in a random distribution of orientations. Vectors are coloured according to the colour map shown. Black dotted lines show leaf outline. Scale bars are 100 μm . (C) Quantification of re-rotated BASL vectors, shown in A, indicating a largely proximodistal distribution. (D) Quantification of BASL vectors not re-rotated, shown in B, indicating a random distribution of vector orientations.

2.5 BASL vectors in wild type

2.5.1 *35S::GFP-BASL* is coordinated across a tissue indicating a polarity pattern

To analyse the pattern revealed across the leaf and quantify any proximal bias, I used confocal images of *35S::GFP-BASL* from leaves heat-shocked at different developmental stages (section 2.3.2 and 2.3.3). Confocal images comprising of GFP-BASL signal and cell outlines (either RFP-PM or PI stained if necessary) were run through the semi-automated software described above (Figure 2.11). The resulting vectors were run through the SampleArrows8 program to plot them according to colour (Figure 2.14 A) and allow visualisation of the vector orientation across the leaves.

Evidence for a tissue-wide polarity field in leaves

For leaves of up to approximately 200 μm in width, the vectors appeared to be largely proximodistal in orientation as shown by predominantly red and orange vectors (Figure 2.14 B). There were a few vectors pointing proximally resulting in a noisy distribution, especially given the relatively low number of vectors on leaves of this size. In leaves of width approximately 200-400 μm , the vectors showed a largely proximodistal orientation (Figure 2.14 C) and seemed to converge slightly towards the leaf tip. In larger leaves of up to 800 μm , the vectors also showed a proximal bias across the tissue, again with some noise (Figure 2.14 D). In leaves of over 800 μm in width, the proximal bias was also visible. At these later stages, the vectors in the lower half of the lamina appeared to diverge from a proximodistal orientation and point diagonally, as shown by yellow and green vectors, indicating a splaying out polarity pattern (Figure 2.14 E). It was important to analyse multiple leaves in order to ensure all regions of the leaf were sampled and in order to provide enough vectors to have statistical power. I therefore carried out the analysis described above on multiple leaves of varying sizes (Figure 2.15).

I plotted the vector orientations as histograms using data pooled from at least four leaves of similar sizes to quantify the polarity pattern across the leaf. Using multiple leaves, I was able to quantify and assign at least 800 BASL vectors in each size category. The histograms of BASL orientation at each leaf size indicate a proximodistal polarity pattern, with a peak at 0° degrees representing proximodistal BASL vectors (Figure 2.14 F-I). Notably, whilst it is possible to mathematically pool the vector orientations from leaves in each size category, creating a visual representation of the averaged vectors is conceptually and computationally more challenging as an average leaf shape would need to be generated, averaging vectors in their associated positions. In this work, I therefore used multiple leaf examples where possible and was able to pool the vector orientations for statistical purposes, but additional work would need to be carried out in order to generate an average leaf image combining raw data from multiple leaves.

Across all leaves analysed (pooled from all leaf sizes), the proportion of BASL vectors outside the range -80° to 80° was 14%, compared to 45% that would be expected for randomly distributed angles. Thus, ectopic BASL reveals a coordinated proximodistal polarity pattern across the leaf lamina at different stages of development.

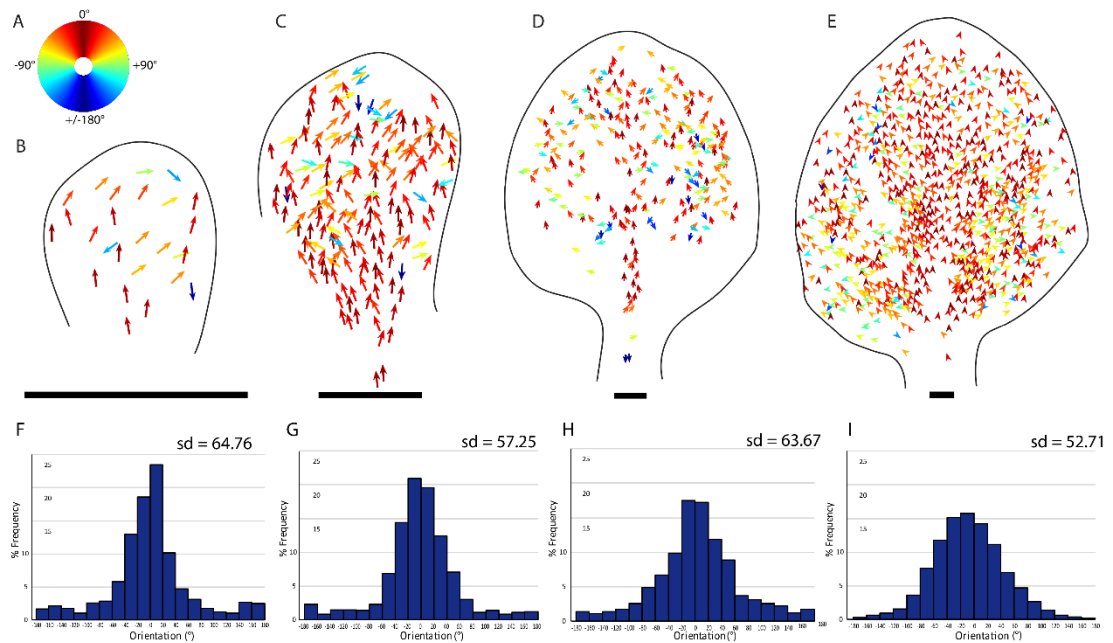


Figure 2.14 Analysis of the vector field shows a coordinated pattern across the leaf at different stages.

(A) Colour wheel used to plot orientation of vectors. (B-E) BASL vectors from individual cells coloured according to colour wheel indicating ectopic BASL orientation in single representative leaves of different sizes: (B) up to 200 μm , (C) 200-400 μm , (D) 400-800 μm , (E) > 800 μm width respectively. Additional examples are shown in Figure 2.15. Black outlines indicate leaf outline. Scale bars are 100 μm . (F-I) Histograms showing frequency of ectopic BASL vector orientation, pooled from multiple individual leaves. (F) up to 200 μm width ($n=1042$ cells from 15 leaves), (G) 200-400 μm width ($n=1464$ cells from 9 leaves), (H) 400-800 μm width ($n=890$ cells from 4 leaves) and (I) > 800 μm width ($n=3642$ cells from 4 leaves). 0° degrees represents proximodistal vector. Standard deviation for each histogram shown.

The leaves varied in how much of the leaf lamina contained vectors, but all showed a proximodistal pattern. In some cases, leaves were not well segmented, often due to poor PI-staining. This was particularly the case in the proximal lateral lamina. If cell segmentation was completely incorrect, or BASL location was ambiguous, polarity was not assigned to the cell. This could also result in a lack of vectors in some regions of the leaf. In addition, as mentioned previously, not all cells had an observable BASL crescent. Despite poor segmentation in some leaves, overall, the ectopic BASL pattern was largely proximodistal at all developmental stages analysed (Figure 2.15). Furthermore, at all stages, the BASL vectors appeared to be most coordinated in a proximodistal manner in the midvein region of the leaf (Figure 2.15).

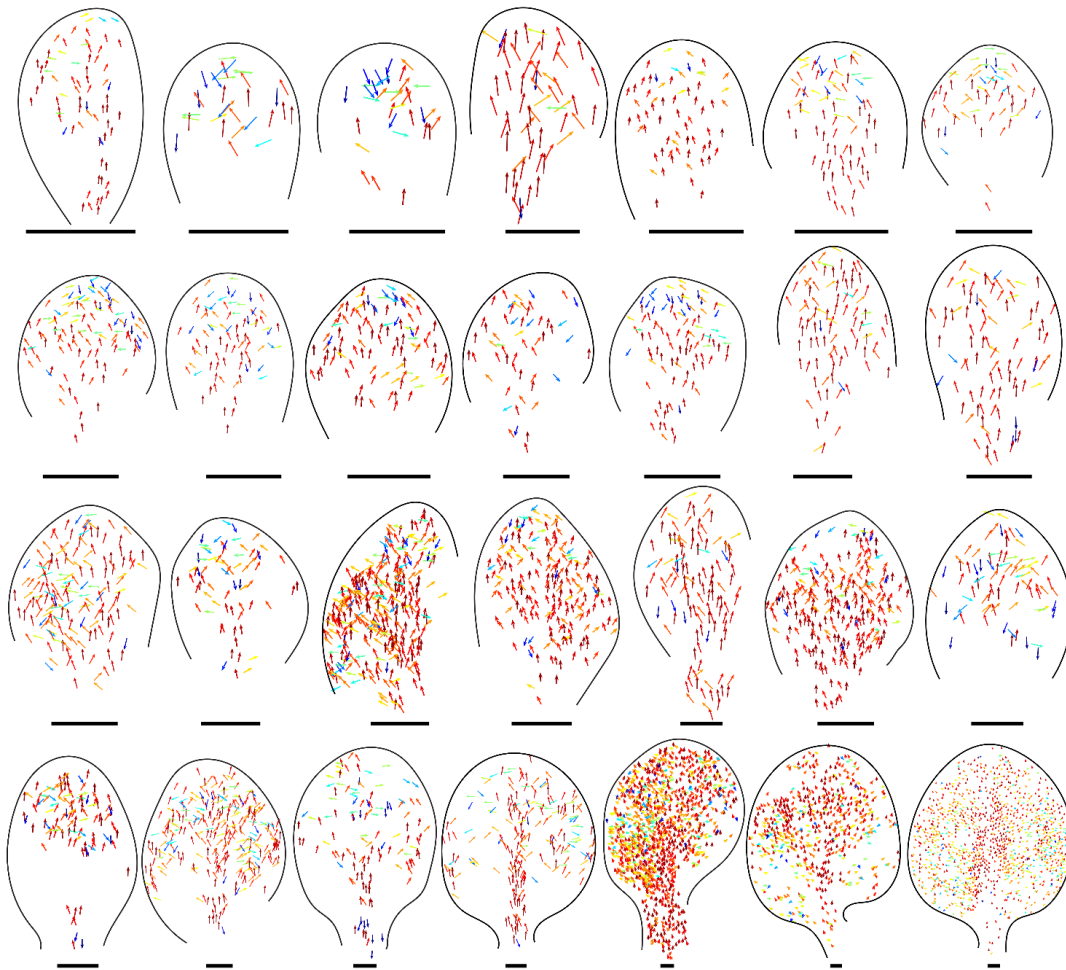


Figure 2.15 Additional wild-type leaves with *35::GFP-BASL* vectors confirm a proximo-distal polarity field.

Ectopic GFP-BASL vectors analysed in additional wild-type leaves using semi-automated software, showing a proximo-distal pattern at all stages analysed. Vector orientation coloured according to colour map in Figure 2.14 A. Leaves ordered from smallest to largest width. Black lines show leaf outlines. Scale bars 100 μ m.

2.5.2 Down-sampling allows tissue-level patterns to be visualised

In leaves with many thousands of cells it can be difficult to visualise tissue-level patterns such as the splaying out of the polarity field. To analyse the splaying out of the polarity field, I needed to be able to average the vectors. The SampleArrows8 program was developed to allow the vectors on large leaves well-populated with vectors to be down-sampled. This was achieved using a grid across the leaf to define evenly spaced points, and then averaging the vector orientations within a certain radius (grid cell) from those points (Figure 2.16 A). It was important to choose an appropriate grid cell size in order to have a sufficient number of data points for averaging, but not so large that grid cells overlapped and data points were used

more than once (Figure 2.16 B). Due to the use of circles for grid cells (which is computationally most straightforward), there were some 'gaps' between grid cells. Vectors in these gaps were not used in down-sampling. The down-sampled vectors were then coloured according to their orientation to reveal tissue-wide patterns (Figure 2.16 C).

Down-sampling the BASL vectors for leaves of over 800 μm revealed a divergent pattern across the leaf lamina. Vectors in the midvein appeared highly coordinated in a proximodistal orientation while those in the lamina diverged away from the midvein (Figure 2.16 B, C). Thus, at later stages of leaf development the polarity field revealed by BASL is divergent, rather than proximodistal parallel to the midvein.

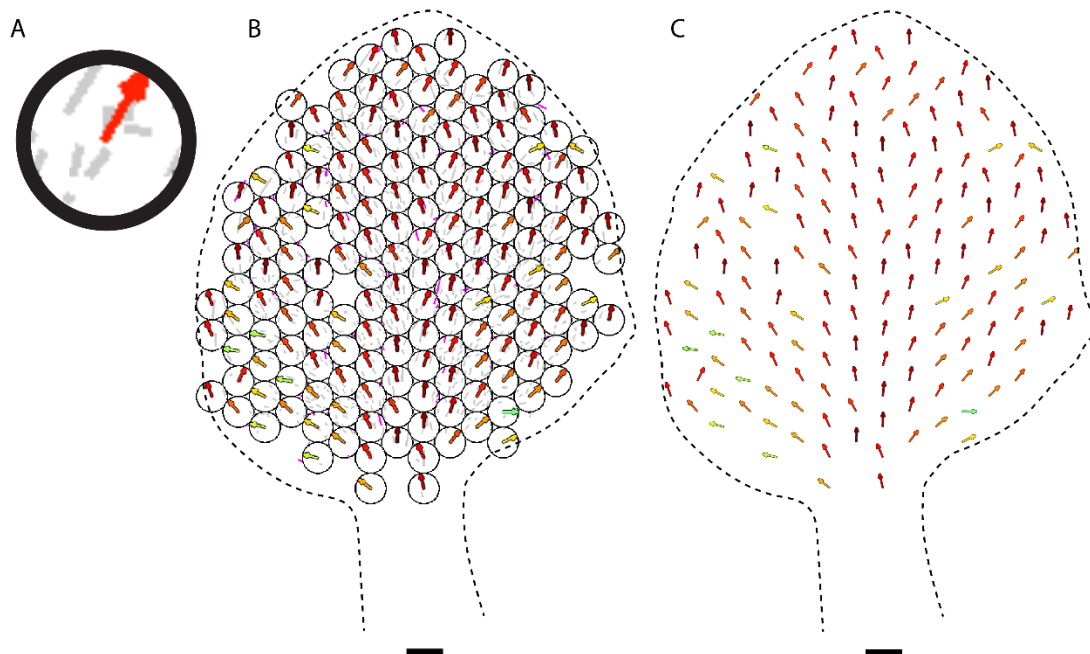


Figure 2.16 Down-sampling allows tissue-wide patterns to be visualised.

(A) Example of circular grid cell used for down-sampling. Grey lines show raw data, red arrow shows average vector for this grid cell. (B) Representative leaf of $> 800 \mu\text{m}$ width (same example as in 2.14 E) showing grid circles used for down-sampling. Average vectors for each grid circle shown (coloured arrows), and BASL vectors plotted according to colour map in 2.14 A). (C) Down-sampled output of leaf shown in B showing divergent polarity field. Dotted black lines show leaf outline. Scale bars are $100 \mu\text{m}$.

2.5.3 Higher-order leaves suggest a divergence of BASL vectors towards serrations

The proximodistal polarity field revealed by ectopic BASL throughout development shows that such a polarity field exists during the stages of leaf 1 development that have been previously modelled. To test whether this polarity field is maintained in stages beyond those analysed so far, I induced ectopic BASL in older seedlings and analysed the BASL polarity. I heat shocked seedlings ~24 DAS and analysed the pattern of ectopic BASL. In leaf 7, at approximately 3500 μm in width, a proximodistal BASL polarity field was observed when the leaf was analysed using the previously described software (Figure 2.17 A). This pattern was confirmed by down-sampling the BASL pattern revealing a strongly proximodistally coordinated pattern in the midvein region (Figure 2.17 B, D).

Leaves formed later in development also develop multiple clear serrations, unlike leaf 1, which forms one small pair of serrations (Biot et al., 2016). I noticed that in the proximal region of the leaf lamina, the polarity pattern diverged, similar to leaf 1 (compare Figure 2.17 B with Figure 2.16 C). In the lateral lamina, many cells indicated a divergent polarity which appeared to approximately coincide with the positioning of the serration, illustrated by yellow and green vectors in this region (Figure 2.17 C). However, many of the cells in this region, particularly margin cells, did not have clear enough BASL, or good enough segmentation to assign BASL polarity to. In addition, some cells in this region showed a polarity that appeared to remain more proximodistal, hence additional leaves of this size and stage need to be analysed to further explore this observation. However, this could indicate that the divergent polarity pattern observed in the lamina of leaf 1 could perhaps be accounted for by the lateral expansion of the lamina and the development of serrations. In addition, the analysis of BASL in higher order leaves indicates that the polarity field is maintained to more mature stages of development.

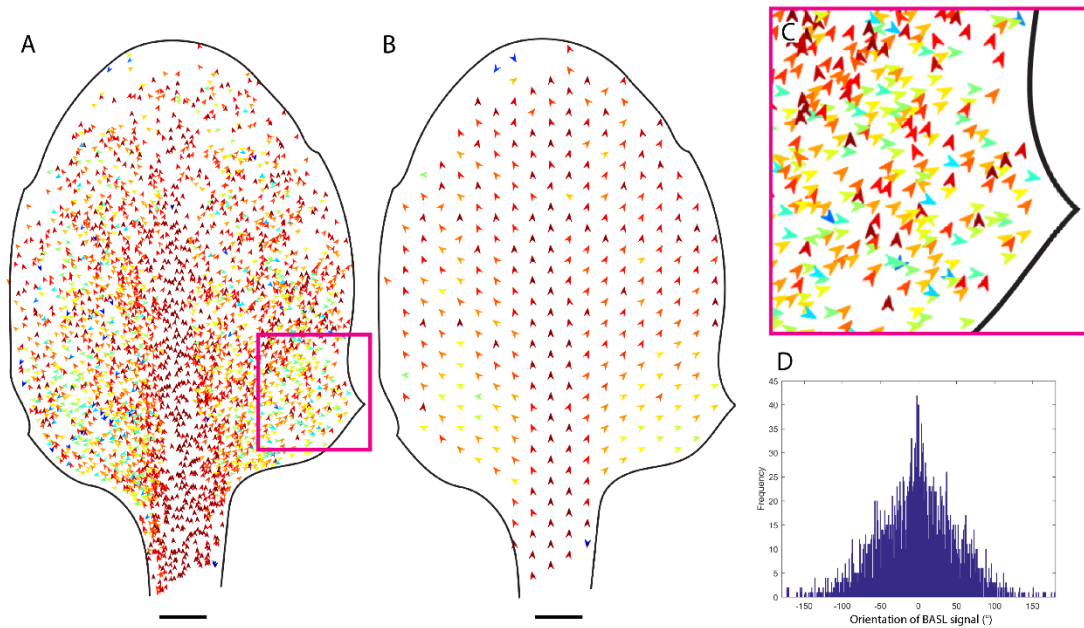


Figure 2.17 Larger, higher order leaves show a proximodistal polarity field and divergence towards serrations.

(A) Ectopic BASL vectors in leaf 7, plotted according to the colour map shown in Figure 2.14 A. Predominantly red and orange vectors are seen, with more yellow and green vectors in the lower lamina. (B) Leaf 7 ectopic BASL vectors down-sampled showing a divergent proximodistal polarity field (same leaf as in A). Black outlines show leaf outline. Scale bars are 500 μm . (C) Close up region shown in magenta (from A) showing the predominance of divergent yellow and green vectors around the serration. (D) Histogram showing quantification of vectors shown in A. Note this figure contains data from a single leaf and additional leaves of this size and stage need to be analysed.

2.6 Size of BASL crescent

BASL is not normally expressed outside stomatal lineage cells, thus suggesting that the observed ectopic BASL expression reveals a polarity field that does not itself depend on BASL function. Moreover, *basl* mutants do not exhibit a clear tissue-level polarity phenotype outside the stomatal lineage cells (Dong et al., 2009). Ectopic BASL might therefore bind to interacting partners, for example proteins or lipid domains, that are located proximally in each cell. I refer to these hypothetical interacting partners as providing a proximal molecular address. This proximal address may exist in epidermal cells regardless of developmental stage, accounting for why induction of ectopic BASL reveals a proximodistal polarity field throughout development. The localisation of BASL to cell corners, or to a single lobe of pavement cells may reflect a single address located at the proximal extrema of the cell (i.e. lobes and corners).

Evidence for a tissue-wide polarity field in leaves

The proximal address may be held autonomously at a fixed length or increase in length as the cell grows. To distinguish these possibilities, I measured the length of the ectopic BASL domain at different developmental stages in a wild-type background. Domain length varied from $\sim 5\mu\text{m}$ to $\sim 45\mu\text{m}$ and, on average, the BASL domain length increased approximately threefold for a tenfold increase in cell perimeter (Figure 2.18 A). Interestingly, this increase in size was at a rate lower than the rate of increase in cell perimeter, so that it became a smaller proportion of the cell perimeter (from $\sim 30\%$ to $\sim 5\%$ as cell perimeter increased tenfold) (Figure 2.18 B). This finding suggests that the proximal address does not have a fixed size limit but may be restricted through interactions with other factors in the cell.

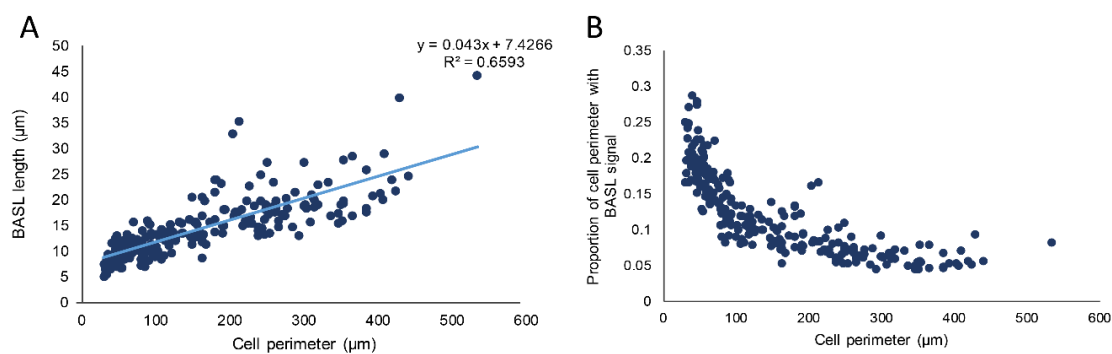


Figure 2.18 BASL crescent increases in size but does not maintain a constant proportion of the cell perimeter.

(A) Length of BASL crescent plotted against cell perimeter for leaves of various sizes. (B) BASL crescent plotted as a proportion of cell perimeter showing proportion decreases as cell perimeter increases.

2.7 BASL crescent appears as a distinct domain after heat-shock

There are multiple ways in which BASL might become localised to a crescent at the proximal end of a cell. One hypothesis is that BASL may appear in a diffuse pattern after heat-shock and then coalesce on its proximal location. This would indicate that perhaps BASL interacting with another protein or complex was responsible for creating this proximal address. Alternatively, BASL may become localised to its proximal location straight away which might suggest that the proximal address was already positioned and recruited BASL as it was expressed.

To understand the potential nature of the molecular address that BASL may interact with and distinguish between these hypotheses, I imaged BASL appearing after heat-shock. Seedlings were heat-shocked as normal and placed in an imaging chamber (Chan et al., 2007). Previous experiments had shown that proteins induced using the Cre-lox heat-shock system tended to appear by 24 hours after heat-shock (Samantha Fox, personal communication). Leaves were imaged every hour for 24 hours, or until BASL signal appeared. Time-lapse imaging leaves after heat-shock induction showed that rather than coalescing, ectopic BASL appeared in the proximal location from approximately 12 hours after heat-shock induction and gradually intensified (Figure 2.19). This supports the hypothesis that ectopic BASL does not itself induce cell polarity but marks a pre-existing polarity.

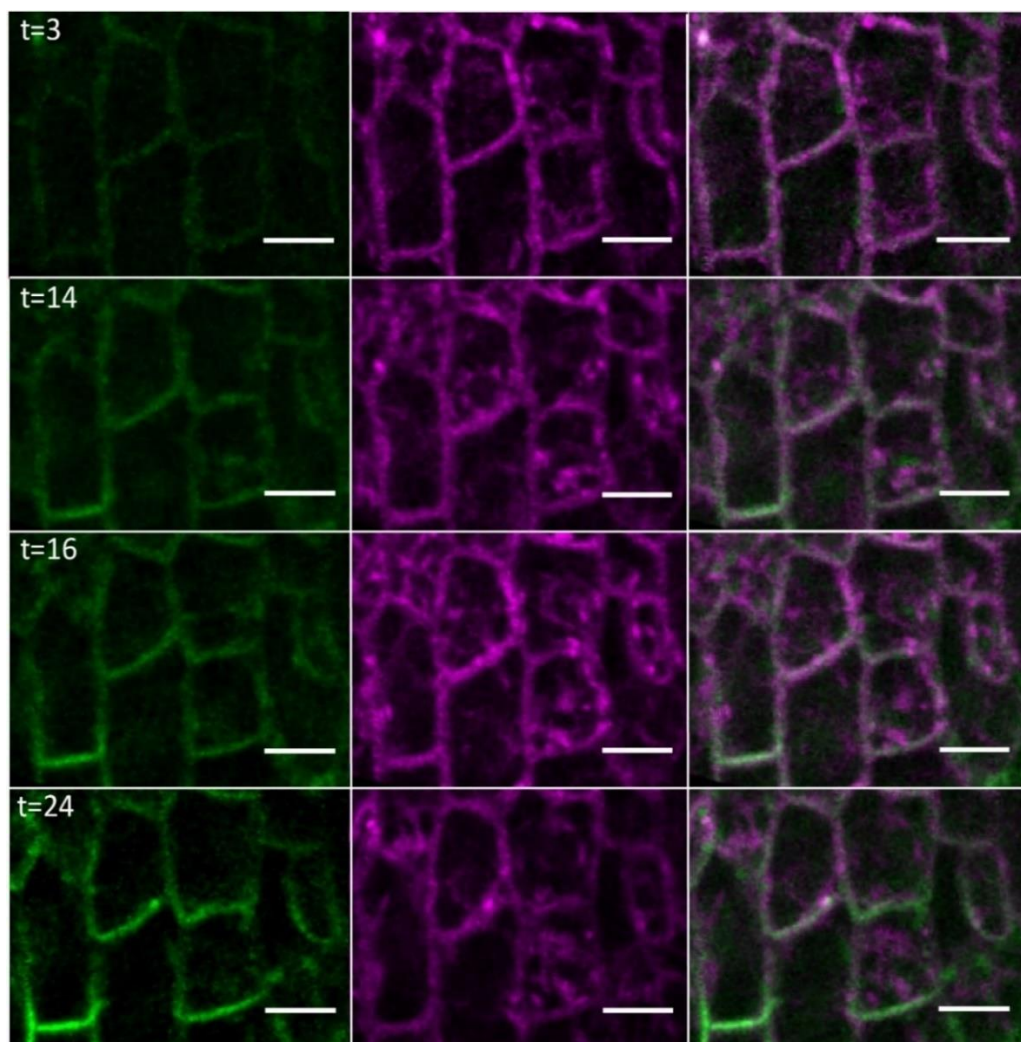


Figure 2.19 Time lapse imaging after *35S::GFP-BASL* induction shows gradual increase in signal intensity.

(A) *35S::GFP-BASL* induction in a wild type background at 3 (A), 14 (B), 16 (C), and 24 (D) hours after heat-shock. At 3 hours, no GFP-BASL signal is seen, comparable to uninduced leaves. Left hand panels show GFP-BASL expression appearing at the proximal end of cells with increasing intensity. Middle panels show ER-localised CyPET inside the lox sites,

coloured magenta for clear visualisation. Right hand panels show combined GFP-BASL and ER-CyPET channels. Scale bars are 10 μm . Images are maximum projections of multiple z-slices to accommodate movement of the leaf during imaging.

2.8 Ectopic BASL polarity is more coordinated in the midvein, and less coordinated at the tip

Whilst the overall polarity pattern is proximodistal, BASL does not localise proximally in every cell (as seen in Figure 2.14 B-E). In addition, some regions of the leaf display a divergent BASL polarity pattern (Figure 2.14 E). The variation observed in the orientations of BASL polarity can therefore be described in terms of local variation and global variation. Global variation may include the splaying out pattern across the lamina and the observation that the polarity pattern is not proximodistal across the whole leaf. The local variation includes the observation that polarity is more highly coordinated in the midvein compared to other regions, as well as the noisiness of the pattern. It is useful to distinguish between these types of polarity variation as there may be distinct reasons underlying the variable coordination locally and globally.

2.8.1 Local variation in BASL polarity differs across the lamina

One way of exploring the coordination in the variation of the vectors is to analyse the coordination in the grid cells (similar to downsampling), as each grid cell will have a local variance (Figure 2.20 C). This was done using the SampleArrows8 software which uses circular variance to allow variance calculations for vectors (Berens, 2009). Circular variance is indicative of the spread of vectors but, unlike linear variance, is bounded in the interval [0, 1]. The circular variance will be 0 or close to 0 if all vector orientations point in the same direction (Figure 2.20 Ci), and 1 if they are spread out evenly around a circle (i.e. randomly distributed, Figure 2.20 Cii) (Berens, 2009). Thus, circular variance is a measure of the local heterogeneity of the polarity vectors. I used SampleArrows8 to calculate the circular variance for samples in a given grid cell. The downsampled vector of each grid cell was coloured according to its variance (using the colour scheme in Figure 2.20 D) and plotted at its relative position on the leaf. Circular variance was only assigned if there were at least three vectors in a grid cell. This allows regions of the leaf that are more or less coordinated to be highlighted.

At the later stages of development that were imaged, the polarity of the midvein appeared to be highly coordinated (Figure 2.20 A, B, white arrows). The lamina also showed fairly high local coordination (lower circular variance) despite the divergent vector field indicating that this divergence is a feature of the polarity pattern rather than local noise. Grid cells in the lamina at the distal end of the leaf showed slightly less local coordination (Figure 2.20 A, B). The local variance of each grid cell was plotted on a histogram indicating that the circular variance of most grid cells was below 0.3 (Figure 2.20 D). Thus, there is high local coordination of the BASL polarity pattern with some regions of the leaf showing higher local coordination than others.

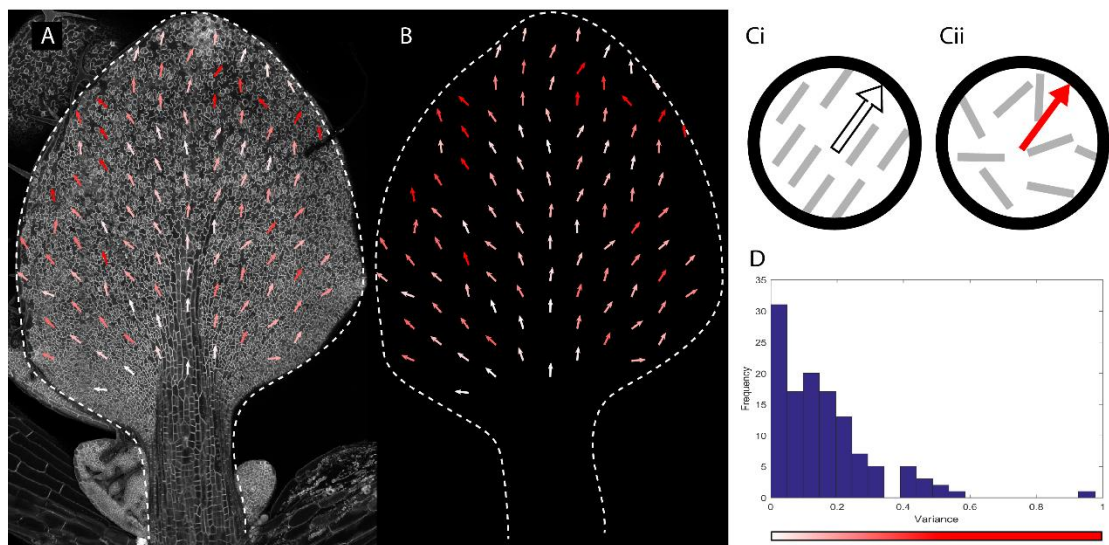


Figure 2.20 Ectopic BASL vectors are locally coordinated, particularly in the midvein region. (A) Leaf showing local variation in ectopic BASL polarity using circular variance. Lowest variance is observed in the midvein, with higher towards the tip. Down-sampled arrows shown with variance coloured according to scale in E. (B) Leaf (in A) without background image for clearer visualisation of variance colour. Leaf outline shown in white dotted line. (C) Schematics showing how circular variance is calculated. For each grid cell, polarity vectors (grey) are down-sampled (as in Figure 2.16) and coloured according to the variance within the grid cell. (Ci) If vectors in a grid cell are all aligned with no variation, the circular variance is 0 and the average vector (arrow) is coloured white. (Cii) If vectors in a grid cell are randomly aligned, the circular variance is 1 and the average vector (arrow) is coloured red. (D) Quantification of circular variance for each grid cell for the leaf in A. Most of the grid cells have highly coordinated ectopic BASL polarity (circular variance <0.3).

2.8.2 Local variation in BASL vector could be due to stomatal lineage cells

Whilst the ectopic BASL polarity is highly coordinated in some regions (Figure 2.20 A), there are some BASL vectors that do not show a proximodistal direction (Figure 2.14 E). Some of the local variation in the BASL polarity field seen across the tissue could be due to BASL orientations in cells of the stomatal lineage where endogenous BASL is known to switch polarity (Robinson et al., 2011). I imaged regions of the leaf over the course of four days and observed the patterns of ectopic BASL expression in presumed stomatal lineage cells (based on shape, size and division patterns in the absence of markers) (Figure 2.21). Where BASL expression was observed in the stomatal lineage, it appeared to follow the expected endogenous pattern of BASL, localising to the wall furthest away from a new cell wall following division (Figure 2.21). This is distinct from the expression pattern observed when BASL is overexpressed in pavement cells, becoming polarised to the proximal end of the cell, and therefore could suggest a possible reason for some of the local variation observed in leaves.

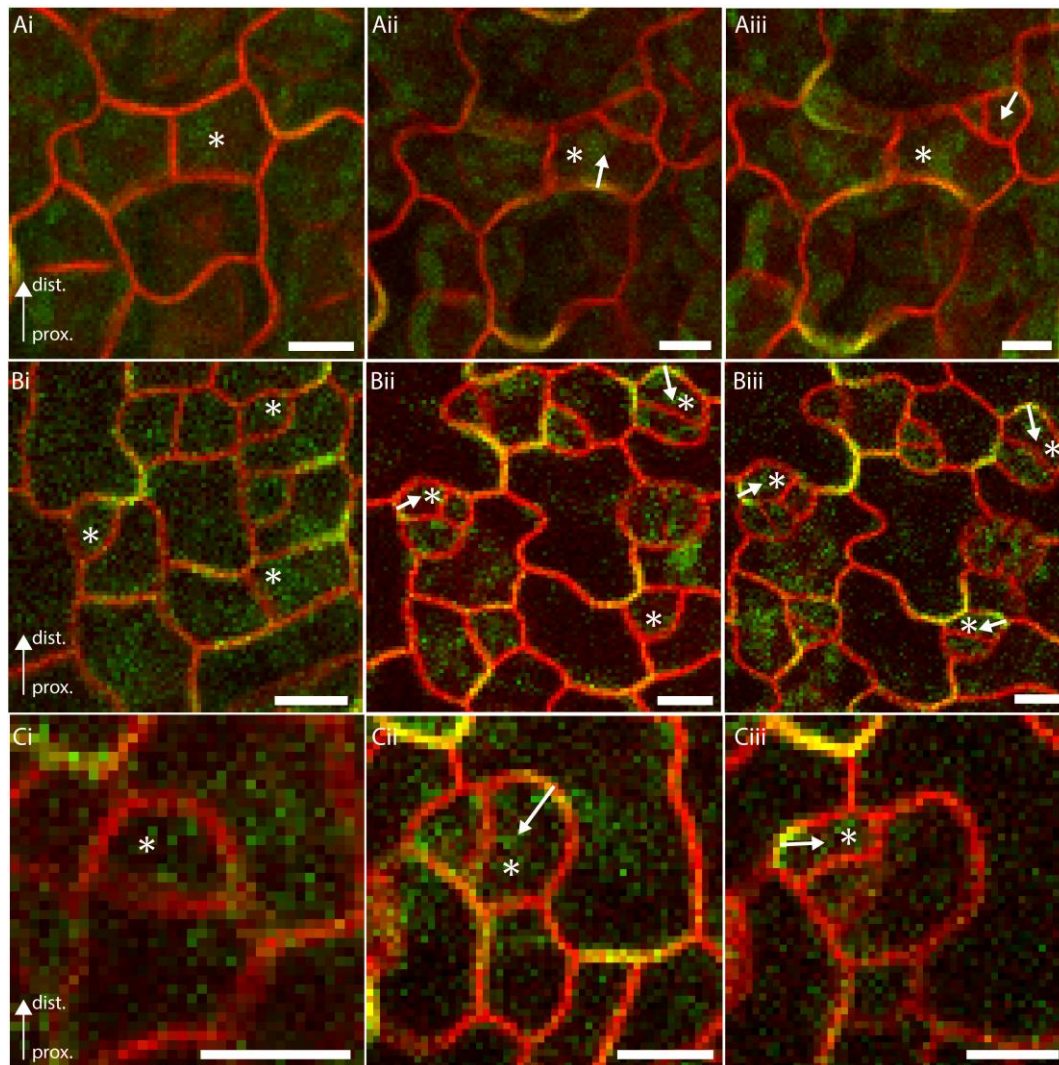


Figure 2.21 *35S::GFP-BASL* in meristemoids shows a spiral polarity pattern.

Three examples of induced *35S::GFP-BASL* in meristemoids, from a leaf imaged over four days. Panels i and ii are ~48 hours apart, panels ii and iii are ~24 hours apart. Cell outlines visualised using RFP-PM. White asterisks indicate meristemoids undergoing stomatal divisions. *35S::GFP-BASL* tends to localise opposite the new cell wall (white arrow). Proximodistal axis indicated. Scale bars are 10 μm .

Furthermore, I noticed that many cells assumed to be in the stomatal lineage did not exhibit clear BASL signal. BASL is known to be transient in stomatal lineage cells, and it therefore seems likely that BASL is under tight regulation in these cells which could, for example, involve degradation mechanisms. One hypothesis, therefore, is that ectopic BASL is often degraded in stomatal lineage cells, and hence often not visible.

To further explore whether cells of the stomatal lineage may contribute to the local variation observed in the ectopic BASL polarity pattern in leaves, I examined the localisation of BASL around stomatal cells. In most cases, the BASL did not appear to be disrupted by the stomata

and was localised to a proximal lobe of cells. However, in multiple instances, BASL signal in cells adjacent to stomata appeared to be localised to the wall closest to the stomata (Figure 2.22). In some cases, this localisation still marked the proximal end of cells (Figure 2.22 B), while in others, this resulted in BASL marking the distal end of the cell (Figure 2.22 A). In some cells, the BASL signal appeared to be possibly disrupted by stomatal lineage cells, localising to the wall adjacent to the meristemoid and not a lobe of the cell (Figure 2.22 C). Thus, it appears that cells of the stomatal lineage can disrupt the proximal localisation of BASL in some instances and contribute to the local variation in BASL polarity pattern observed in leaves.

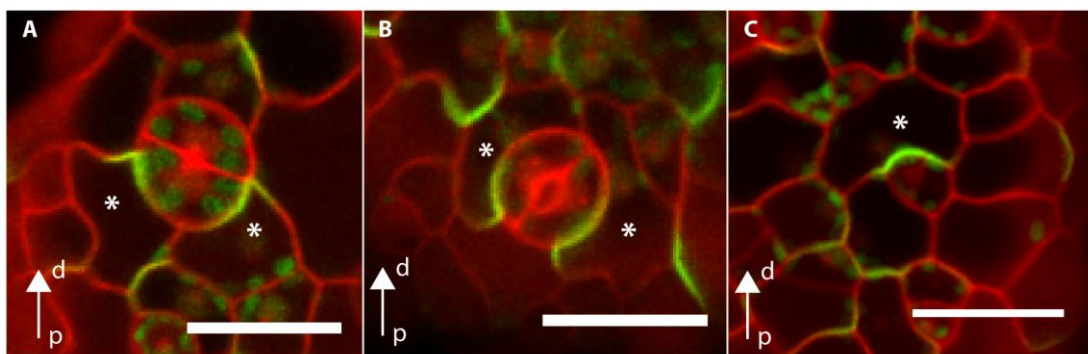


Figure 2.22 Proximodistal patterning of ectopic BASL may be disrupted by stomata. Examples where *35S::GFP-BASL* signal in cells adjacent to stomata (A, B), or stomatal lineage cells (C) appears to be disrupted by stomata. Cells with potentially disrupted BASL vectors are indicated (white asterisks). Cell outlines visualised using PI. Proximodistal axis is indicated. Scale bars are 20 μm .

2.9 Ectopic BASL reveals a polarity field independent of stomatal lineages

Wild-type leaves are composed of a number of cell types: stomatal lineage cells, and non-stomatal lineage cells, including pavement cells and trichomes. Pavement cells can be formed from cells that do not enter the stomatal lineage, and also from stomatal lineage ground cells (SLGCs) (Lau and Bergmann, 2012). SLGCs can differentiate into pavement cells, or they can adopt meristemoid mother cell fate and undergo asymmetric spacing divisions to create new meristemoids positioned away from the existing stomatal lineage cells, thus providing a spacing mechanism for stomatal patterning in *A. thaliana* (Lau and Bergmann, 2012).

The results described above using ectopic BASL indicate that a tissue-wide polarity field can indeed be extended to the non-stomatal cells of the leaf. This raises two important questions. Firstly, whether the tissue-wide ectopic BASL pattern is dependent on or connected to the stomatal lineage, and whether such a pattern could be observed independently of the stomatal lineage. Secondly, whether stomatal patterning could be adding complexity to a proximodistal polarity revealed by BASL (such as through the non-proximal localisation of BASL within the meristemoids (Figure 2.21) and in the cells surrounding the stomata (Figure 2.22)). It is possible that there might be two polarity fields interacting (or not) in the stomatal lineage. In order to explore these questions, I exploited the *speechless* (*spch*) mutant which does not make stomata.

I crossed the heat-shock inducible *35S::GFP-BASL* line into the *speechless* background which does not make stomata or meristemoids (MacAlister et al., 2007). As in wild-type leaves, I typically imaged GFP-BASL expression 48 hours after heat-shock and used propidium iodide to stain the leaves and allow visualisation of the cell outlines. When induced in *speechless* leaves of varying sizes (up to 200 μm , 200-400 μm and 400-800 μm in width), BASL localised to a crescent at the proximal end of cells (Figure 2.23), similar to that observed in wild-type background leaves. As in wild-type background leaves, in leaves where lobed pavement cells had formed, ectopic BASL localised proximally in a single lobe (Figure 2.23 B). Thus, the coordinated polarity field revealed by ectopic BASL in leaves at different stages of leaf development is independent of the stomatal lineage.

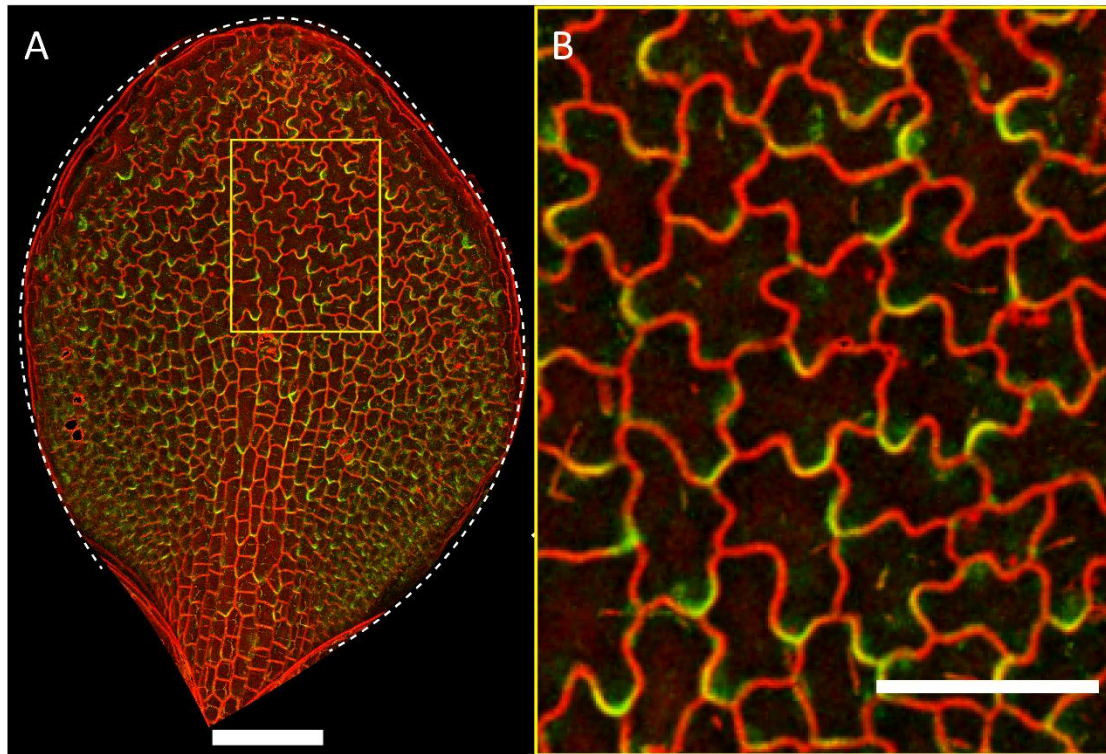


Figure 2.23 Inducible 35S::GFP-BASL in *speechless* leaves localises proximally. (A) *speechless* leaf with induced 35S::GFP-BASL and (B) enlarged section of leaf (yellow box) showing localisation of 35S::GFP-BASL (green). Propidium iodide (PI) staining shows cell outlines (red). Scale bar 100 μ m in A and 50 μ m in B.

To quantify the extent of proximal bias in *spch*, I imaged multiple leaves and processed them using the custom-developed software described previously (Figure 2.11) to assign unit vectors to cells expressing ectopic BASL (Figure 2.24 and Figure 2.25). At all developmental stages analysed (50 - 800 μ m leaf width), BASL vectors were largely proximodistally oriented in *spch*, as indicated by predominance of red and orange vectors (Figure 2.24 B-D). Some vectors deviated from this proximodistal pattern, though very few vectors pointed proximally (blue vectors in Figure 2.24 B-D and Figure 2.25). *speechless* leaves of over 800 μ m in width were not imaged due to slower growth in this mutant compared to wild-type (Fox et al., 2018). As in wild-type leaves, the proximodistal coordination appeared to be strongest in the midvein region (Figure 2.24 C, D).

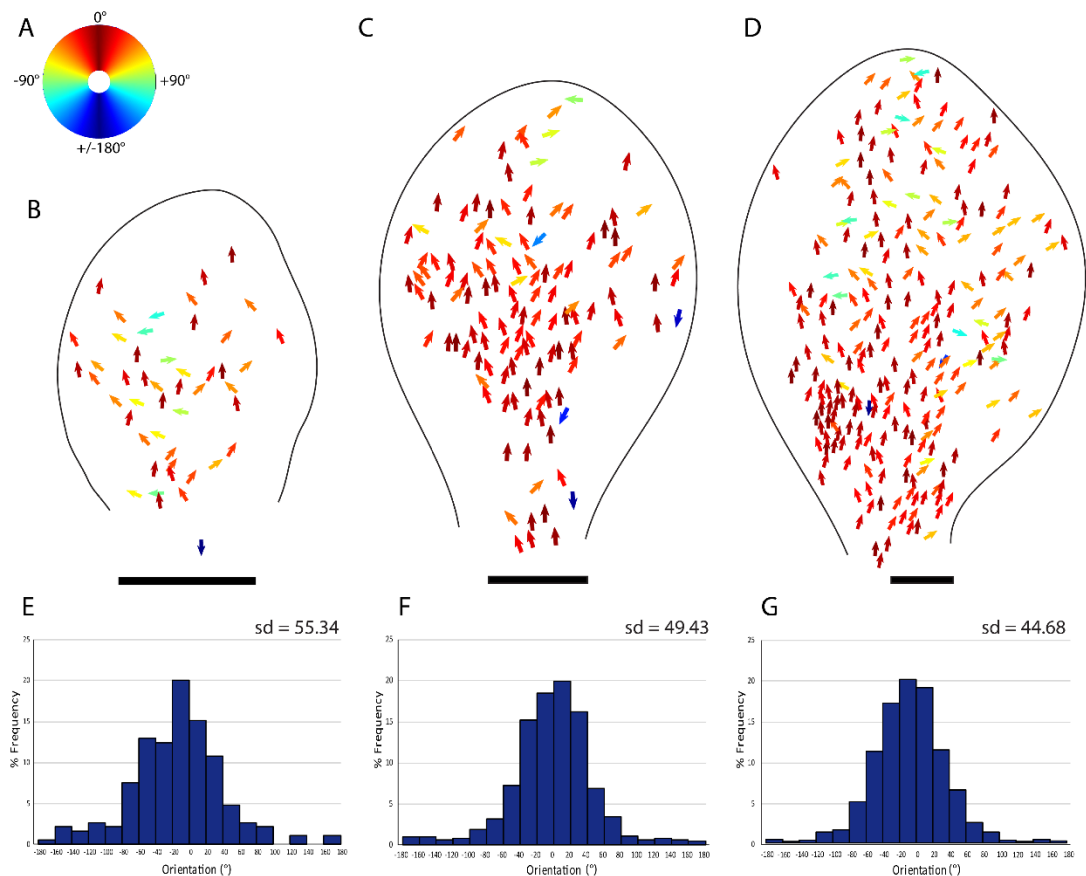


Figure 2.24 Analysis of the ectopic BASL vector field in *speechless* shows a coordinated pattern across the leaf at different stages.

(A) Colour wheel used to plot orientation of vectors. (B-D) BASL vectors from individual cells of *speechless* leaves, coloured according to colour wheel indicating ectopic BASL orientation in representative leaves of different sizes: (B) up to 200 μm , (C) 200-400 μm and (D) 400-800 μm width respectively. Additional examples are shown in Figure 2.23. Black outlines indicate leaf outline. Scale bars are 100 μm . (E-G) Histograms showing frequency of ectopic BASL vector orientation in *speechless*, pooled from multiple individual leaves. (E) up to 200 μm width ($n=185$ cells from 4 leaves), (F) 200-400 μm width ($n=1199$ cells from 12 leaves) and (G) 400-800 μm width ($n=2063$ cells from 9 leaves). 0° degrees represents proximodistal vector. Standard deviation for each histogram shown.

BASL vector orientations from multiple *spch* leaves were pooled according to leaf size and plotted in histograms (Figure 2.24 E-G). For all leaf sizes analysed, the histograms peak at 0°, similar to in a wild-type background, indicating that the majority of BASL vectors were in the same direction as the midline vector. I conducted a chi-squared test on the proportion of vectors outside the range -80° to 80° for comparable leaf sizes. This showed that proportion of vectors outside the range -80° to 80° was significantly higher for wild type (14%) than for *spch* (<10%) (Chi-squared, $p < 10^{-5}$) (Table 2.1). Thus, the ectopic BASL polarity field in a *spch* background is more coordinated than ectopic BASL polarity in a wild-type context.

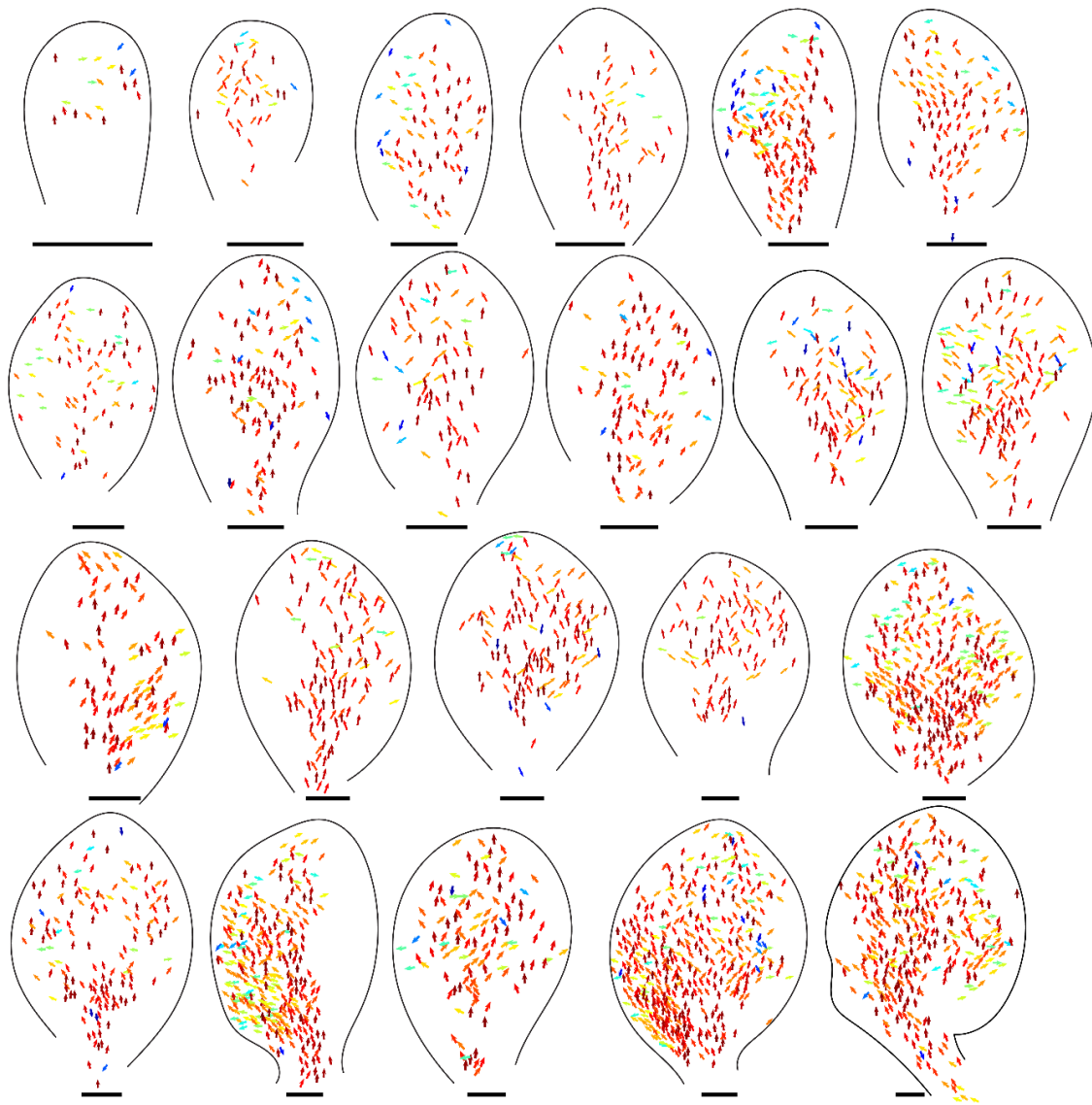


Figure 2.25 Additional *speechless* leaves with *35::GFP-BASL* vectors confirm a proximo-distal polarity field.

Ectopic GFP-BASL vectors analysed in additional *speechless* leaves using semi-automated software, showing a proximo-distal pattern at all stages analysed. Vector orientation coloured according to colour map in Figure 2.24 A. Leaves ordered from smallest to largest width. Black lines show leaf outlines. Scale bars 100 μm .

2.10 Endogenous BASL

The observation that ectopic BASL in a wild-type leaf is significantly less coordinated than in *spch* may be accounted for by more variable BASL polarity orientation in the stomatal lineage cells. This is also suggested by the observation of disrupted proximal localisation of BASL in some meristemoids (Figure 2.21). Moreover, Bringmann and Bergmann (2017) show BRXL2

polarity vector orientation within stomatal lineage cells to be $\sim 65\%$ within the -80° to $+80^\circ$ range. This indicates that polarity in the stomatal lineage may be less coordinated than that in non-stomatal lineage cells, as shown here by ectopic BASL in *spch* which is $\sim 90\%$ within the -80° to $+80^\circ$ range.

To test whether BASL is polarised in a coordinated manner within the stomatal lineage and may be contributing to the variation observed in wild-type leaves, I imaged leaves with *BASL::GFP-BASL*, and analysed them using the software pipeline described previously. *BASL::GFP-BASL* was asymmetrically localised within individual cells as well as being expressed in the nucleus (Figure 2.26), as previously described (Dong et al., 2009; Robinson et al., 2011). Although not obvious from inspection of a single leaf (Figure 2.26 A, B), when multiple leaves are pooled, proximodistal coordination was observed for *BASL::GFP-BASL* vectors (61% within the range -80° to 80° , Figure 2.27) similar to the level of coordination reported for BRXL2 (Bringmann and Bergmann, 2017). Thus, BASL is coordinated in its native context in the stomatal lineage.

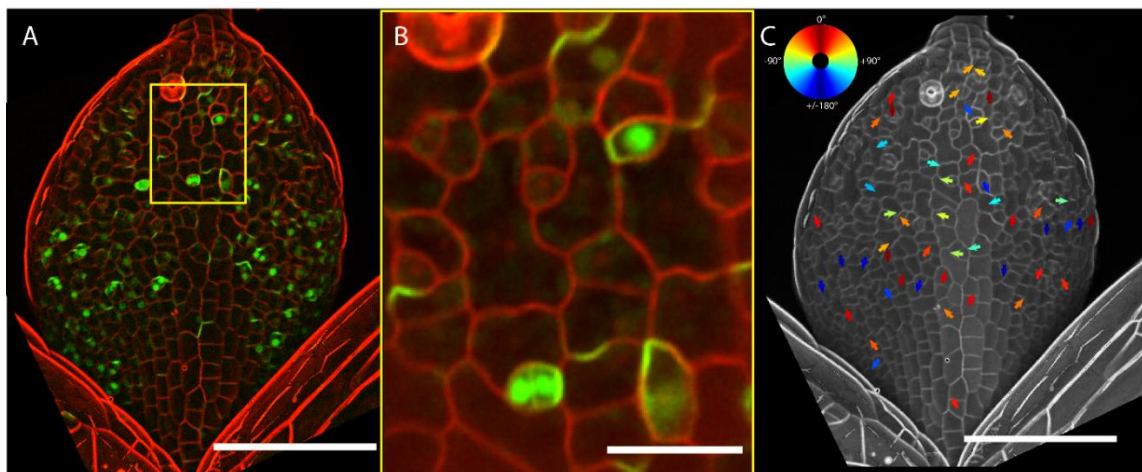


Figure 2.26 *BASL::GFP-BASL* reveals proximodistal coordination in the stomatal lineage. (A) Example leaf showing *BASL::GFP-BASL* expression (from 50–200 μm width range). Yellow box shows area in B. Scale bar 100 μm . (B) Close up region of leaf in A showing *BASL::GFP-BASL* expression is seen only in stomatal lineage cells and is asymmetrically localised, as well as having nuclear localisation. PI staining shows cell outlines. Scale bar 20 μm . (C) BASL vectors from leaf in A shown, coloured according to colour wheel (shown) indicating orientation. Scale bar 100 μm .

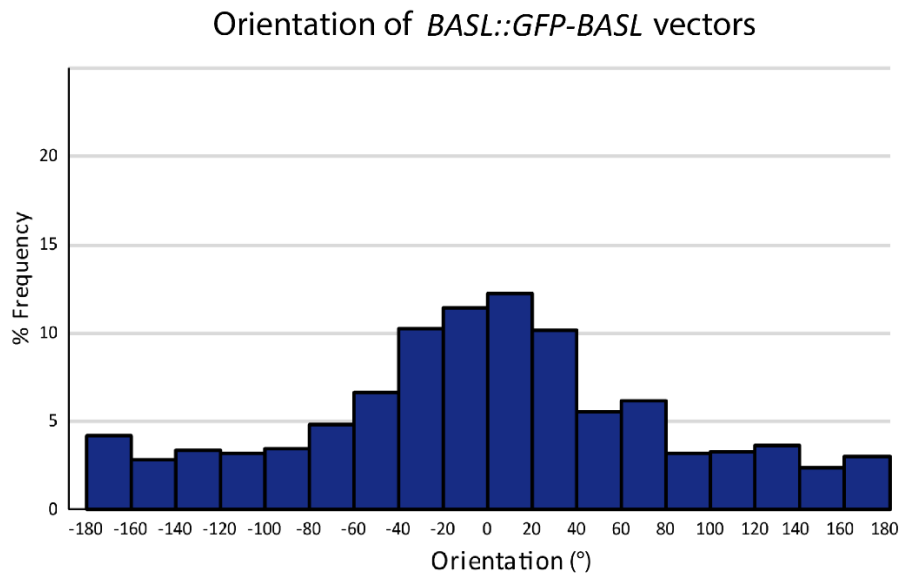


Figure 2.27 Quantification of *BASL::GFP-BASL* vectors indicates coordination.

Histogram showing frequency of *BASL::GFP-BASL* vector orientation, pooled from multiple leaves from 50-800 μm width range, showing coordination of BASL polarity (n=1319 cells from 21 leaves, $\sigma=82.3$).

Endogenous BASL polarity (*BASL::GFP-BASL*) was significantly less coordinated than for ectopic BASL in *spch* (67% compared to 91% within the range -80° to 80° , $p < 10^{-5}$, Table 2.1, Figure 2.28). Coordination of ectopic BASL polarity in a wild-type background showed an intermediate distribution (85% within the range -80° to 80°) (Figure 2.28), and was significantly more coordinated than *BASL::GFP-BASL* ($p < 10^{-5}$, Table 2.1), suggesting that it reflects a mixture of two patterns: a strongly coordinated proximodistal pattern in non-stomatal lineage cells and a weaker coordinated pattern in stomatal lineage cells.

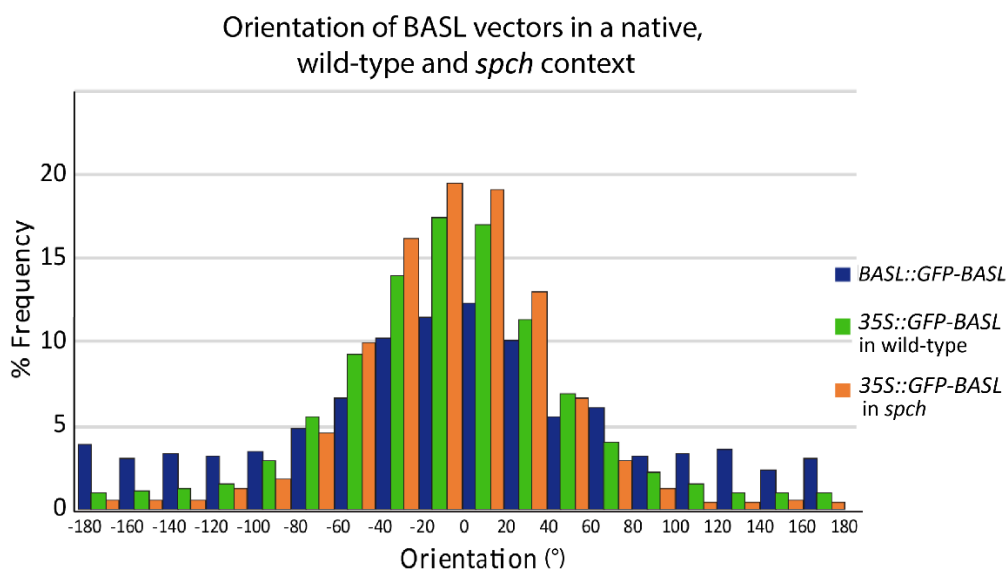


Figure 2.28 *35S::GFP-BASL* in a wild-type background shows intermediate coordination between *spch* and native BASL.

Quantification of BASL vectors in *BASL::GFP-BASL* (blue), *35S::GFP-BASL* in a wild-type background (green) and *35S::GFP-BASL* in a *spch* background (orange) showing relative levels of polarity coordination. Ectopic BASL polarity in *spch* is the most coordinated, ectopic BASL in wild-type has intermediate coordination, and *BASL::GFP-BASL* is the least coordinated. Each genotype pooled from at least 20 leaves from 50-800 μm . $p < 10^{-5}$ for each pairwise chi-squared comparison between genotypes (Table 2.1).

Table 2.1 Two-way chi-squared tests for comparing BASL vector orientation across genotypes.

Chi-squared tests comparing BASL vector orientation across genotypes, based on number of vectors within the range -80° to $+80^\circ$ compared to outside this range. Note that as the distributions were not normal I used a non-parametric test.

Genotype comparison	n = BASL vectors	n = leaf number	Chi-squared (df=1)	P value
<i>35S::GFP-BASL</i> WT vs <i>35S::GFP-BASL</i> in <i>spch</i>	<i>35S::GFP-BASL</i> in WT = 7038 <i>35S::GFP-BASL</i> in <i>spch</i> = 3447	<i>35S::GFP-BASL</i> in WT = 33 <i>35S::GFP-BASL</i> in <i>spch</i> = 26	85	$p < 10^{-5}$
<i>35S::GFP-BASL</i> in WT vs <i>BASL::GFP-BASL</i>	<i>35S::GFP-BASL</i> in WT = 7038 <i>BASL::GFP-BASL</i> = 1319	<i>35S::GFP-BASL</i> in WT = 33 <i>BASL::GFP-BASL</i> = 22	260	$p < 10^{-5}$
<i>35S::GFP-BASL</i> in <i>spch</i> vs <i>BASL::GFP-BASL</i>	<i>35S::GFP-BASL</i> in <i>spch</i> = 3447 <i>BASL::GFP-BASL</i> = 1319	<i>35S::GFP-BASL</i> in <i>spch</i> = 26 <i>BASL::GFP-BASL</i> = 22	456	$p < 10^{-5}$

Two hypotheses could account for the weaker polarity coordination in the stomatal lineage. One is that the proximal address becomes reoriented in stomatal lineage cells, and ectopic BASL follows this pattern. Alternatively, stomatal lineage cells contain two addresses (i.e.

two regions with BASL-interacting factors): a proximal address and an address specific to stomatal lineage cells, which could be competing for BASL localisation. The proximodistal polarity observed in endogenous BASL may be an indication of the two polarity fields interacting and the stomatal spiral pattern being deflected by the non-stomatal proximodistal polarity. Furthermore, competing molecular addresses would account for why BASL is sometimes proximal in meristemoid cells and sometimes localised in a spiral pattern more consistent with its native expression pattern (Figure 2.21) (Robinson et al., 2011). The ectopic BASL polarity field shown here in a wild-type and *spch* is independent of the stomatal lineage and therefore may have a different signal or address localising BASL in cells outside of the stomatal lineage. It is possible that there may be an underlying proximodistal polarity field, such as that revealed here by ectopic BASL, that the stomatal lineage could alter or co-opt for patterning the stomatal lineage.

2.11 Discussion

2.11.1 Characterising the ectopic BASL polarity pattern

2.11.1.1 *Ectopic BASL reveals a coordinated polarity field throughout development*

I have explored the existence of a leaf-wide polarity field using ectopic expression of BASL. Initial work indicating coordination of the polarity pattern was done by Jordi Chan prior to the start of this project. I have used an inducible *35S::GFP-BASL* line to analyse ectopic BASL in sectors, showing that BASL localises proximally even in sectors composed of only a couple of cells. I have shown that ectopic BASL localises in a polar manner in epidermal cells, including non-stomatal cells and that the BASL crescent tends to localise to corners, or a single proximal lobe of pavement cells. By heat-shocking seedlings of different stages I have also shown, using quantitative analysis, that ectopic BASL reveals a coordinated polarity field in leaf one throughout early development (from primordium to over 1000 μm in width). The polarity field revealed by ectopic BASL in leaves may represent an underlying coordinated polarity field, though the origin of this coordinated field remains unknown.

The ectopic BASL polarity field shown here is not observable in every cell of the leaf. This could be simply due to very low and unobservable expression levels in some cells, or a lack of uniformity in the expression of BASL using the heat-shock system (although seedlings were

heat-shocked for long enough that every cell should be expressing *35S::GFP-BASL*). An alternative explanation for the lack of BASL expression in every cell is that BASL may be inherited through cell division, and that it only appears after a delay in recently divided cells. This could be tested by live-imaging of BASL through multiple cell divisions. Despite this, the polarity field described here is observable in a much higher proportion of epidermal cells than just the stomatal lineage (Bringmann and Bergmann, 2017), or trichome cells (Bouyer et al., 2001; Hülskamp et al., 1994) where polarity was previously described.

The BASL polarity field can also be revealed in larger, higher-order leaves where the pattern also splays out in the lower lamina. In this case, splaying out may be due to growth perpendicular to the proximodistal axis or, alternatively, could be a result of BASL polarity being deflected by serrations which are more prominent in higher-order leaves. The large higher-order leaves imaged here were not of high enough image quality to analyse BASL polarity in detail around serrations, but this would be an informative context in which to analyse ectopic BASL polarity in relation to a specific growth pattern. Furthermore, analysis of BASL around serrations could provide an understanding of the relationship between BASL and PIN1 polarity as PIN1 polarity is known to show polarity reversal forming convergence and divergence points around serrations (Bilsborough et al., 2011; Hay et al., 2006). The relationship between BASL and PIN1 polarity is explored in Chapter 3.

I have shown that the ectopic BASL polarity field splays out in a divergent pattern in later stages of development and in higher-order leaves. The divergence of the polarity field at later stages may arise as a result of the lamina growing more in the mediolateral direction while the petiole remains narrow, as previously modelled by Kuchen et al. (2012). In such models, a fixed polarity field becomes curved and deformed with the tissue. Alternatively, the divergence could occur due to propagation of a signal in a divergent pattern across the lamina. Due to the mechanical connectivity of the tissue, and the unknown origin of the polarity field described here, these hypotheses remain indistinguishable.

The BASL polarity field described here is markedly different to polarity fields previously described in plants for a number of reasons. Firstly, the polarity field can be revealed at all stages of leaf development, unlike, for example, PIN polarity which occurs transiently in specific developmental contexts (Bilsborough et al., 2011; Guenot et al., 2012; Scarpella et al., 2006). Furthermore, BASL typically localises to a single lobe of pavement cells, unlike Rho of plant (ROPs) which localise to multiple lobes of pavement cells (Fu et al., 2002) and are often linked to polarity formation in pavement cells (Yang, 2008). Previous work has

suggested a possible link between BASL polarity and the ROP pathway (Dong et al., 2009). In the hypocotyl cells of *rop2* mutants, BASL-mediated cell outgrowths (which are reported with non-inducible ectopic BASL) appear to be abrogated, consistent with BASL acting upstream or independent of the ROPs (Dong et al., 2009). The possible connection between BASL and the ROP pathway cannot account for the localisation to a single lobe, rather than multiple lobes as is the case with ROPs (Fu et al., 2002). It would be interesting to explore this further, perhaps by ectopically expressing BASL in mutants of the ROP pathway. This might also provide further insight into the localisation of BASL in lobe-less cells, which are a common phenotype of *rop* mutants (Fu et al., 2002).

2.11.1.2 The ectopic BASL polarity pattern is independent of the stomatal lineage

By overexpressing BASL in the *speechless* mutant, I found that the ectopic BASL polarity field is independent of the stomatal lineage. This contrasts with the polarity field described by Bringmann and Bergmann (2017) which is only observed in stomatal lineage cells and thus is the first example of a coordinated tissue-wide polarity field, throughout leaf development, that is independent of the stomatal lineage. The degree of coordination observed for ectopic BASL in both a wild-type and *spch* background is higher than that previously described in the stomatal lineage for *BRXL2::BRXL2-GFP* in a wild-type background, in which only ~65% of vectors are within the -80° to 80° range (Bringmann and Bergmann, 2017) and therefore have a proximodistal orientation. It would be informative in the future to analyse ectopic BASL polarity in larger *spch* leaves ($>800 \mu\text{m}$) to allow comparison of the polarity divergence at this stage compared to wild-type.

The increased coordination of *35S::GFP-BASL* in a *spch* background suggests that the stomatal lineage contributes to the variation in BASL localisation in a wild-type context. This is consistent with the results described in this chapter where ectopic BASL localisation appears to be disrupted by stomata (Figure 2.22), and meristemoids (Figure 2.21). Meristemoids and stomata are known to grow more quickly than surrounding cells (Andriankaja et al., 2012). The disruption caused by the stomata could therefore be a result of mechanical disruption, which would be consistent with the observation that BRXL2 localisation can be altered by mechanical stresses (Bringmann and Bergmann, 2017). Alternatively, this deflection from a proximal position may be due to ligand signalling from the stomatal lineage cells. EPIDERMAL PATTERNING FACTOR 1 (EPF1), for example, is active in determined stomatal lineage cells and has been reported to influence BASL orientation in neighbouring MMCs (Bringmann and Bergmann, 2017; Dong et al., 2009; Hara et al., 2007).

In this chapter I have also shown that, similar to BRXL2 (Bringmann and Bergmann, 2017), BASL is coordinated in the stomatal lineage, albeit to a much lesser extent than when ectopically expressed. The spiral polarity switching pattern of BASL in the stomatal lineage has been described previously (Robinson et al., 2011), though overall tissue-level coordination has not been previously reported for BASL (unlike for the BASL-interactor BRXL2 (Bringmann and Bergmann, 2017)). I hypothesise that the polarity switching of BASL in the stomatal lineage may be responsible for the lower levels of polarity coordination observed in the stomatal lineage. Although polarity is critical for stomatal spacing in *A. thaliana* (Dong et al., 2009; Robinson et al., 2011), it is unclear why proximodistal coordination within the stomatal lineage would be functionally important.

One hypothesis that could account for the observation of an endogenous BASL pattern in the stomatal lineage cells, even when BASL is overexpressed, is that there are competing proximal addresses in stomatal lineage cells. Stomatal lineage cells could contain a proximal address (remaining at the proximal end of cells), and a stomatal address which could localise opposite the new cell wall. In non-stomatal cells, the proximal address appears to dominate, while in stomatal cells, there may be more correspondence to the stomatal address, perhaps in a cell-type dependent manner.

2.11.2 Development of software to quantify the polarity field

Through analysing the ectopic BASL polarity field qualitatively, it became clear that quantitative analysis was necessary to allow comparison of the polarity field between genotypes and in a non-biased manner. I worked with computer scientists to decide on the key priorities for development of a polarity quantification tool. After trialling a fully-automated tool, we decided that a semi-automated tool that segmented cells and randomly rotated them before manual identification of BASL signal was more useful. This software, developed by Tjelvar Olsson and Matthew Hartley, with later Matlab code for visualisation by Jake Newman, was more useful in this context as it allowed me to analyse much more of the confocal data. The random rotation element of the software was crucial in preventing bias when assigning BASL vectors, and hence providing confidence in the output.

The software at present requires specific requirements in terms of input images (2-channel z-stack .tif images) and requires in depth understanding of the adjustable parameters in order to achieve a well-segmented output. The tool could be developed further in order to make it more widely usable, for example, by creating a more user-friendly interface for

parameter searching, or to integrate it into existing software used by the developmental biology community (e.g. MorphoGraphX, Barbier de Reuille et al., 2015). In addition, for some high-resolution images, it may be possible to develop fully automated polarity quantification.

These tools may be the first to allow a non-biased approach to assigning polarity. Previously, polarity has been assigned to cells by hand (Abley et al., 2016; Bringmann and Bergmann, 2017). While software such as Fiji (Schindelin et al., 2012) can be used to randomise images for analysis, this is the first case in which random rotation of cells has been used to remove bias when assigning polarity. The importance of correctly and objectively assigning polarity is particularly clear where polarised proteins may be less clearly linked to a specific cell than BASL, such as is often the case with PIN polarity (Abley et al., 2016; Bilsborough et al., 2011; Sauret-Güeto et al., 2013).

2.11.3 Concluding remarks and future work

This work aimed to characterise the polarity field revealed by ectopic expression of BASL in the *A. thaliana* leaf. The polarity described provides evidence for the existence of tissue-wide polarity across the *A. thaliana* leaf, at different developmental stages, as has previously been predicted (Abley et al., 2013; Kuchen et al., 2012).

The existence of such a polarity field supports models requiring polarity fields (Kuchen et al., 2012). Currently, the polarity field has been described and characterised in detail, but links need to be made to any potential role it may have in growth and development. This could be done using growth analysis, for example tracking, as well as analysis of the polarity field in different developmental contexts, such as serration development or *kanadi1kanadi2* mutants. The latter experiments would also allow testing of the relationship between BASL polarity and PIN polarity and are explored in the next chapter.

One key line of exploration will be to analyse ectopic BASL polarity in relation to PIN polarity and determine if these polarity fields are linked, or independent. It is possible that PIN and BASL polarity systems are linked, and are both able to respond to elements of a more fundamental polarity system, for example, to different elements of a molecular address or intracellular partitioning mechanism (Abley et al., 2013). In addition, it will be useful to explore potential mechanisms for coordinating the ectopic BASL polarity field. If found to be linked to PIN polarity, this could be done using auxin treatments or auxin transport inhibitors.

Importantly, the mechanism underlying the establishment and coordination of the ectopic BASL polarity field remains unknown. Exploring the potential mechanisms underlying its coordination could provide insight into the fundamental mechanisms of polarity in plants. This could be achieved using biochemical approaches to identify novel interactors of ectopic BASL which could suggest potential candidates for the molecular address I hypothesised: this is addressed in Chapter 4. Alternatively, it may be useful to explore potentially likely candidates that have a link with BASL, such as the ROP family, which has been shown to possibly play a role in the same pathway (Dong et al., 2009), and is hypothesised to have a similar role in plant polarity to that of homologous Cdc42 proteins in animals (Goldstein and Macara, 2007; Menke and Scheres, 2009; Suzuki et al., 2002).

Overall, this project has shown the existence of a tissue-wide polarity field throughout *A. thaliana* leaf development that is independent of the stomatal lineage. This supports some models of growth that require a polarity field and, excitingly, could suggest the existence of fundamental polarity factors and determinants in plants. This system can be used to further study the role of polarity and patterning in *A. thaliana* leaf development, as well as the patterns and mechanisms of tissue cell polarity more broadly in the plant kingdom.

3 Testing predictions of a tissue-wide polarity field

Introduction

3.1 The role of a tissue polarity field

The tissue-wide polarity field revealed in *A. thaliana* leaves using BASL, and described in the previous chapter, represents the first time a tissue polarity field, that had previously been predicted (Coen and Rebocho, 2016; Kennaway et al., 2011; Kuchen et al., 2012) has been described in plant planar organs throughout development in multiple cell types. In this chapter, I will explore some of the predictions and questions raised by the existence of a tissue cell polarity field in plants.

Evidence for a coordinated tissue-wide polarity field through development has been described previously in animal systems, such as the milkweed bug *Oncopeltus* (Lawrence, 1966) and *Drosophila*. In *Drosophila*, the existence of a tissue cell polarity field that has an important role in development has been well documented and shown to be essential for the correct anatomy and function of many tissues and organs (Goodrich and Strutt, 2011; Thomas and Strutt, 2012).

3.1.1 Polarity at the tissue level

Coordinated tissue-wide polarity fields have been hypothesised to play a role in the development of plant planar organs (Eldridge et al., 2016; Green et al., 2010; Kuchen et al., 2012; Rebocho et al., 2017b; Richardson et al., 2016). Specifically, at the tissue level, polarity has been proposed to be one mechanism for orienting anisotropic growth (Coen et al., 2017; Whitewoods and Coen, 2017). Growth can then be oriented parallel or perpendicular to the polarity field allowing the formation of simple and complex organ shapes through the action of genes and regulatory factors. Growth orientations and polarity have previously been correlated (Bringmann and Bergmann, 2017; Kuchen et al., 2012) but forming causative links between polarity and growth would ideally require experiments modulating either polarity or growth which remains technically challenging, not least because the mechanisms underlying both are not fully understood.

Testing predictions of a tissue-wide polarity field

An alternative hypothesised mechanism for the coordination of anisotropic growth is mechanical stresses (Hamant et al., 2008; Hervieux et al., 2016). This hypothesis suggests that growth can be specified in relation to the principle orientation of stresses across a cell or tissue.

Whilst it is difficult to see how mechanical stresses, which do not have a directional aspect (no arrowhead), could establish polarity (which does have an arrowhead), it remains possible that a gradient of stresses could create directionality to establish polarity. In addition, mechanical stresses could modulate an existing polarity field. This has been reported for BRXL2 which has been shown to be responsive to mechanical stress by stretching a cotyledon and laser ablation (Bringmann and Bergmann, 2017). A stress gradient or axial information from mechanical stresses could be combined with other tissue-organising mechanisms, such as polarity organisers.

3.1.2 Polarity at the cell level

At the cell level, polarity may also play a role in the coordination of anisotropic growth. Cellular growth can be isotropic or anisotropic and is controlled by turgor pressure and cell wall extensibility (Cosgrove, 2016). Turgor pressure provides an isotropic pressure for growth, while cell wall extensibility can be anisotropic due to the non-uniform cellulose reinforcement of the wall (Cosgrove, 2005). A polarity system could provide the directional information needed for non-uniform cell wall reinforcement and it would be interesting to investigate links between the tissue-cell polarity field revealed by BASL, and the cytoskeleton.

Pavement cells are often considered to be multi-polar and polarity in these cells has been linked to the ROP signalling pathway and the formation of lobes (Yang, 2008). ROPs indicate the multi-polar nature of pavement cells, shown by the localisation of ROP2 to the lobes of pavement cells (Fu et al., 2002; Fu et al., 2005). This is markedly different to the described ectopic BASL polarity field and exploring the relationship between BASL and ROPs further may provide insights into how and why ectopic BASL localises to a single lobe of pavement cells.

3.1.3 Continuous versus discrete polarity

When modelled across a tissue, for example using GFtBox (Kennaway et al., 2011) polarity is considered and defined as a mathematical vector where every point in space has an

associated vector. In this type of modelling, the tissue is considered as a continuous sheet, without cells allowing polarity to be modelled as a continuum. In a biological tissue, this mathematical definition of polarity is confounded by the existence of cells. This means that, instead of each point in space having an associated vector, each cell can have a vector. However, because cells are discrete rather than continuous entities, this means that cell polarity has to be assigned relative to another point, such as the cell centroid or leaf axis. In different situations, it can be helpful to consider a tissue as a continuous canvas, or a collection of cells, but the associated mathematical differences raise issues that will be explored in this chapter.

3.2 Ectopic BASL polarity in relation to PIN polarity

PIN proteins represent the best studied polarity markers in plants and much work has been conducted regarding the polarisation mechanisms of PINs (Boutté et al., 2005; Křeček et al., 2009; Tanaka et al., 2013; Wisniewska et al., 2006). The polarity field revealed by ectopic BASL resembles that for PIN1 localisation at early stages of leaf development with some notable differences. Firstly, whereas ectopic BASL localises proximally, PIN1 in epidermal cells localises distally (Guenot et al., 2012; Scarpella et al., 2006). Secondly, the ectopic BASL polarity field described in this work is tissue-wide and can be induced at all stages of leaf development. This contrasts with PIN1 polarity which is only visible in the very early stages of leaf development (Guenot et al., 2012; Scarpella et al., 2006) and in specific developmental situations where new outgrowths form, such as during serration formation (Bilsborough et al., 2011; Hay et al., 2006).

It is possible that the ectopic BASL polarity field described in the previous chapter is connected to PIN polarity, either directly or indirectly. For example, PIN proteins could be involved in establishing polarity in the primordia, with a system (which BASL reveals) maintaining polarity throughout development. Auxin sources and sinks are able to modulate PIN polarity and coordination (Abley et al., 2016; Cieslak et al., 2015; Rolland-Lagan and Prusinkiewicz, 2005) and could hypothetically also be a coordination mechanism for BASL polarity. Alternatively, PIN and ectopic BASL polarity could be independent.

3.2.1 Testing of a polarity field in developmental contexts

The existence of a polarity field across the leaf throughout development does not necessarily indicate a role for polarity in the development of planar plant organs. However, experiments elucidating the relationship between PIN polarity and ectopic BASL polarity could indicate a role for this polarity field in the formation of plant organs.

3.3 Mechanisms underlying the establishment and maintenance of polarity

A key question following the discovery of a tissue-wide polarity field, maintained through development, is how such a polarity field is generated. This can be broken down into understanding how polarity is established initially, and how it is coordinated and, unlike PIN1 polarity, maintained throughout development (Abley et al., 2016).

3.3.1 Establishment of polarity

One plausible mechanism for the initial establishment of tissue cell polarity is intracellular partitioning, as suggested by Abley et al., (2013). This model requires two polarity components (A and B), which are diffusible and cytoplasmic, and their respective membrane bound, slowly-diffusing forms (A* and B*). A* and B* are localised to opposite ends of the cell and, through local feedback and inhibition, and small random fluctuations, are able to spontaneously polarise in cells. Polarised cells can then become coordinated by direct or indirect cell-cell coupling mechanisms (Abley et al., 2013). It is possible that the polarity mechanisms controlling localisation of ectopic BASL to the proximal end of cells is part of an intracellular partitioning cell-cell coupling mechanism. Whilst the molecular components of the intracellular partitioning mechanism have not been verified, PIN1 remains a plausible candidate for establishing cell polarity (although notably the auto-inhibitory behaviour required for intracellular partitioning has not been shown). Analysis of BASL localisation compared to PIN1 could aid understanding of the possible molecular components of an intracellular partitioning model.

3.3.2 Maintenance and coordination of polarity

Auxin has been suggested as part of the mechanism for polarity coordination in a cell-cell coupling model (Abley et al., 2013) and is known to play a key role in the development of plant organs. Inhibition of polar auxin transport, such as using *N*-1-naphthylphthalamic acid (NPA), could indicate whether polar auxin transport is required for the coordination of ectopic BASL.

Another possible system involved in the coordination of polarity across plant tissue is plasmodesmata. Plasmodesmata allow the passage of small molecules and signals between cells and thus represent a plausible mechanism for the coordination of signals involved in the maintenance of polarity across a tissue. These regulated channels between cells are known to be involved in transport, defence and development (Cheval and Faulkner, 2018; Lucas and Jung-Youn, 2004; Yadav et al., 2014). Whilst many mechanistic aspects of plasmodesmata function, particularly in a developmental context, remain unknown, research is increasingly highlighting the fine-tuned and dynamic regulation of these channels (Cheval and Faulkner, 2018; Cui and Lee, 2016; Tilsner et al., 2016).

3.4 Aims of this work

The work in this chapter aims to test some key predictions associated with the existence of a coordinated tissue-wide polarity field. I address the differences in understanding polarity as a continuous or discrete system through analysis of ectopic BASL polarity in contexts where cell shape is altered. This allows separation of polarity and cell shape which may be closely correlated in most anisotropic cells. I will also use BY-2 cells to test the role of the tissue in cell polarity and the coordination of polarity by expressing ectopic BASL in BY-2 cells.

In addition, I test the relationship between the ectopic BASL polarity field described and PIN1 polarity. I analyse situations in which PIN1 and BASL are both expressed such as primordia, and also situations where PIN1 polarity reversals are seen, such as serrations (Bilsborough et al., 2011; Hay et al., 2006) and ectopic outgrowths (Abley et al., 2016) which can shed light on the role of BASL in a developmental context.

Finally, I aim to explore possible mechanisms involved in coordinating and establishing the ectopic BASL polarity field. I test known coordination mechanisms, for example polar auxin

transport and plasmodesmata, and systems known to be involved in polarity, for example microtubules and mechanical stresses. Whilst the discovery of a highly coordinated polarity field, described in Chapter 2, is interesting, it raises many important questions, and would have significant relevance if it were shown to have a physiological or developmental role, or to interact with known polarity systems.

Results

3.5 Polarity and cell shape

The ectopic BASL polarity field described in the previous chapter shows striking similarities with the polarity field previously proposed to account for orientations of growth in the leaf of *A. thaliana* (Figure 3.1, A compared to B) (Kuchen et al., 2012). The observed polarity field diverges at later stages, and hence appears to be more similar to a deforming model of the leaf, where the polarity field diverges as the tissue grows, as a result of the tissue connectivity (Figure 3.1 B), compared to a non-deforming model where the polarity field remains fixed proximodistally and does not diverge at later stages (Figure 3.1 C).

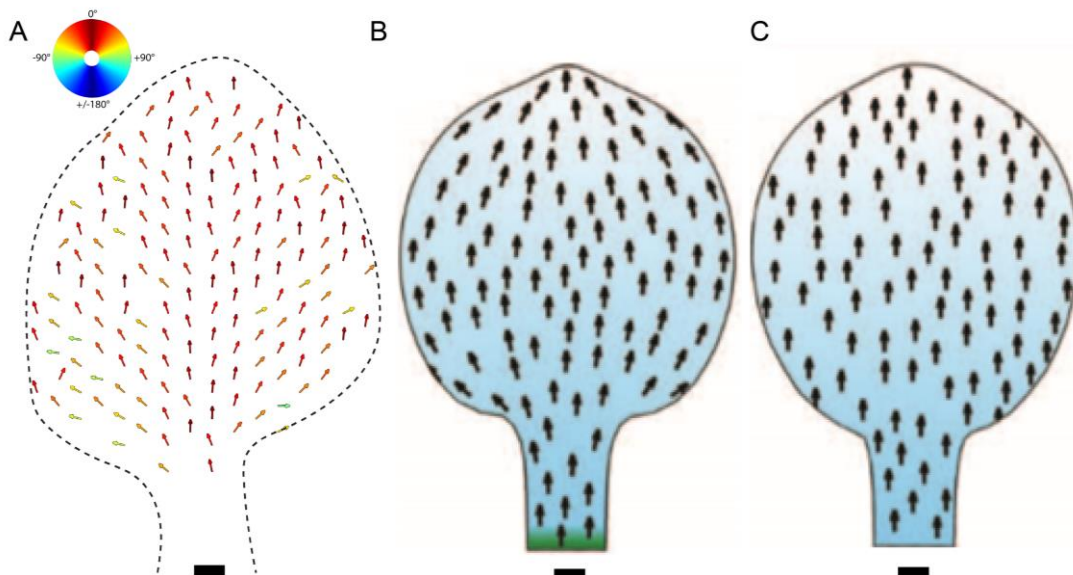


Figure 3.1 The downsampled ectopic BASL polarity pattern resembles the predicted polarity of the deforming organiser-based model from Kuchen et al. (2012).

(A) Downsampled ectopic BASL pattern in a wild-type leaf of width over 800 μm with vectors plotted according to colour map shown (see also Figure 2.16 C). (B) Deforming organiser-

based model of the leaf and (C) Non-deforming organiser-based model of the leaf from Kuchen et al. (2012). Leaf of approximately a similar stage to that shown in A. Black arrows indicate the predicted polarity field, cyan indicates the gradient of POLARISER in the model. Scale bars are 100 μm . B and C adapted from Kuchen et al. (2012). Reprinted with permission from AAAS.

3.5.1 Artefact of cell anisotropy and polarity

However, as highlighted in section 3.1.3, this similarity between the predicted polarity of computational models and biological data is not straightforward. This is because differences between the continuous mathematical polarity in the model and the discrete cell-based biological data. The way polarity is assigned in relation to another point confounds the interpretation of the polarity pattern. Here I use the cell centroid in assigning polarity to cells, as is the case in other published studies (Bringmann and Bergmann, 2017). This leads to the cell shape having a confounding effect on polarity.

For example, suppose BASL is proximal in a circular cell (Figure 3.2 Ai). If that cell becomes elongated diagonally, either through growth or diagonal division, polarity will also become diagonal due to polarity vectors being assigned to the cell centroid (Figure 3.2 Aii). This deviation from proximal occurs even though there has been no change in the positioning of the BASL signal. This anisotropic cell (Figure 3.2 Aii) would then appear to have the same polarity vector as a cell in which the polarity was initially divergent or not proximal (Figure 3.2 Bi, Bii). The confounding effect of cell shape therefore makes it very difficult to distinguish between a polarity field that is parallel to the midline but appears divergent due to cell shape anisotropy (Figure 3.2 Aii), and one that diverges across the tissue, irrespective of cell shape (Figure 3.2 B). In models where polarity fields have been predicated using GFtBox (Kennaway et al., 2011; Kuchen et al., 2012), the lack of cells means that there is no confounding effect of cell shape.

Testing predictions of a tissue-wide polarity field

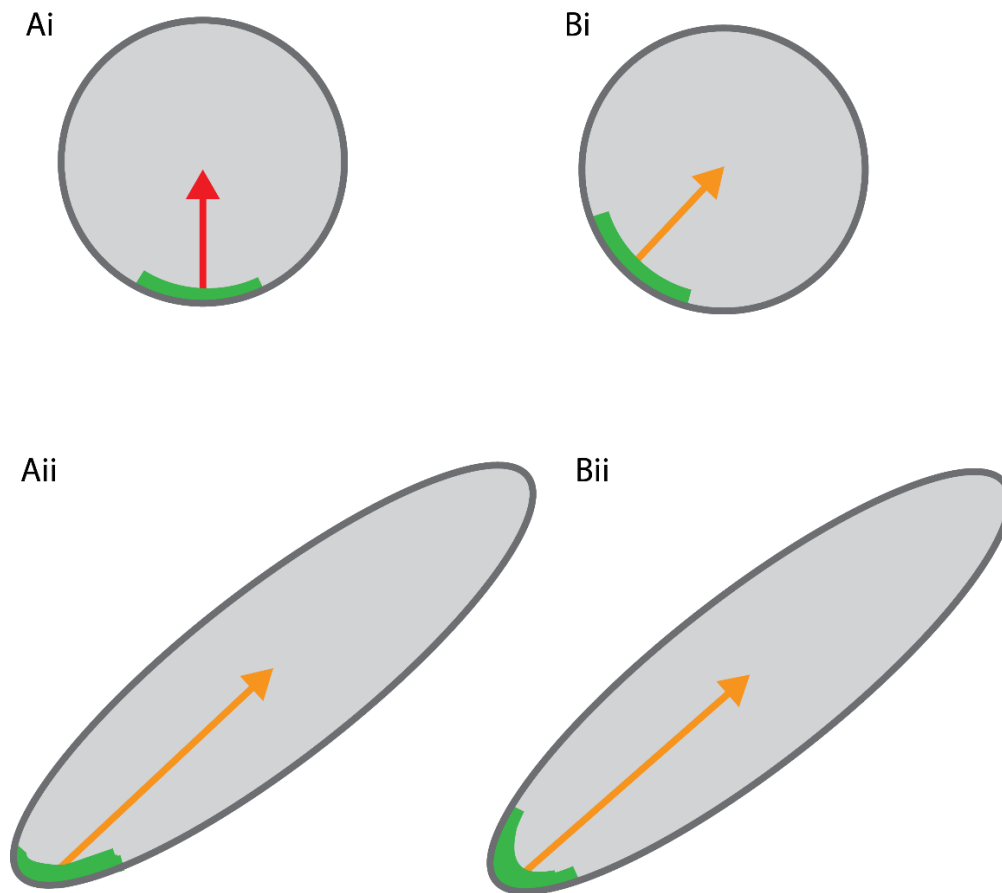


Figure 3.2 Polarity and long axis information is correlated in anisotropic cells.

(Ai) Schematic of an isotropic cell with BASL localised to the proximal end and (Aii) schematic of an anisotropic cell where the BASL localised at the proximal end has become deflected due to deformation of the cell shape (through growth or division). (Bi) Schematic of an isotropic cell with BASL localised to one side and (Bii) schematic of an anisotropic cell where the BASL localised at one side has become deflected due to deformation of the cell shape (through growth or division).

Importantly, this may also be relevant to published work where polarity is often assigned in relation to the cell centroid (Bringmann and Bergmann, 2017). While any observed correlations between growth or cell shape and polarity may be a result of polarity guiding growth, the alternative scenario that growth or cell shape influence polarity cannot be ruled out. Indeed, it is difficult to see how a polarity could be assigned to anisotropic cells in a way that does not correlate with the cell long axis.

3.5.2 Ectopic BASL polarity is correlated with cell shape anisotropy

To determine if the BASL polarity field observed is correlated with cell shape and whether it could therefore be a result of cell shape anisotropy, I first needed to be able to extract and

quantify cell shape information from leaf images. I collaborated with Jake Newman to develop the 'CellLongAxisCorr7' script in Matlab (referred to as CellLongAxis script) which allowed the long axis of each segmented cell to be calculated and multiple angles quantified. The CellLongAxis script was programmed by Jake Newman, Jake and I tested and further developed the software together, and I used the script for analysis.

When applied to leaf images, this script allowed cell long axes to be assigned to cells (by fitting an ellipse to each segmented cell) and coloured according to the same colour map as used previously (Figure 3.3 A). Notably, the colour map is only half that of Figure 3.1 as the information being visualised here has axiality and not polarity, and hence an arrowhead cannot be assigned. I plotted the orientations of the cell long axis for cells in numerous leaves and this confirmed that cell long axes tended to be oriented in line with the leaf midvein axis (Figure 3.3 B). Similar proximodistal axiality for cells in the *A. thaliana* leaf have previously been shown (Fox et al., 2018; Kuchen et al., 2012).

Visualising the overall pattern of cell long axes across a whole lamina with hundreds, or even thousands of cells is not easy. I therefore used the SampleArrows script (developed by Jake Newman and described in Chapter 2 and Materials and methods) to down-sample the cell long axis information across the leaf. This was achieved in a similar way to down-sampling of the BASL vectors (see Chapter 2) using a grid. However, whilst vectors can be averaged by adding them, mathematically, this is not possible for tensors. Instead, down-sampling of the cell long axis orientations was achieved by gathering cell orientations within a certain radius, normalising and superimposing them onto the same axis, and then performing principle component analysis (PCA) on the resulting cloud of points.

Down-sampling of the cell long axis orientations confirmed that, on average, cells were preferentially elongated in a divergent proximodistal (axial) pattern across the leaf lamina. Cell long axis orientations in the midvein region were highly coordinated in line with the midvein axis, while those in the proximal lamina had a more divergent angle away from the midvein (Figure 3.3 C).

Testing predictions of a tissue-wide polarity field

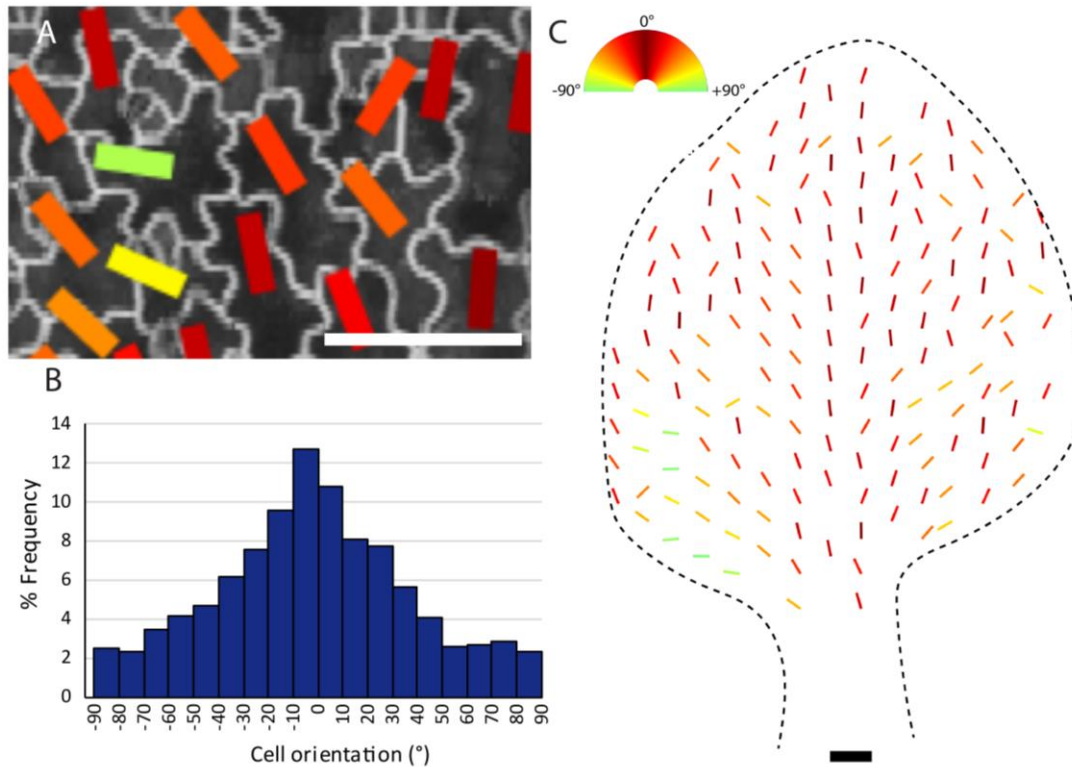


Figure 3.3 Cell long axes across the leaf are similar to proximodistal polarity orientations. (A) Close-up of cell orientations, plotted for cells that BASL vectors can also be assigned to, according to colour map in C. Scale bar 20 μm . (B) Histogram of orientation of cell long axis relative to leaf midvein vector (see Figure 3.3) for leaf of width 800 $\mu\text{m}+$ (shown in C). (C) Cell long axis data for leaf of width 800 $\mu\text{m}+$ (same leaf as in Figure 3.1 A), down-sampled and plotted according to colour map shown, showing splaying out of cell orientations across proximal lamina (yellow and green lines). Note, due to elongation axis being tensors and not vectors, only half of the full colour map is used. Dotted line shows leaf outline. Scale bar 100 μm .

The pattern of cell orientations strongly resembles the down-sampled ectopic BASL orientations for the same leaf (compare Figure 3.3 C with 3.1 A). This suggests the BASL vector orientations may be correlated with the cell long axis orientations. The CellLongAxis script was used to calculate and output a number of angles, such as the angle between the assigned ectopic BASL vector and the cell long axis orientation for each cell (Figure 3.4).

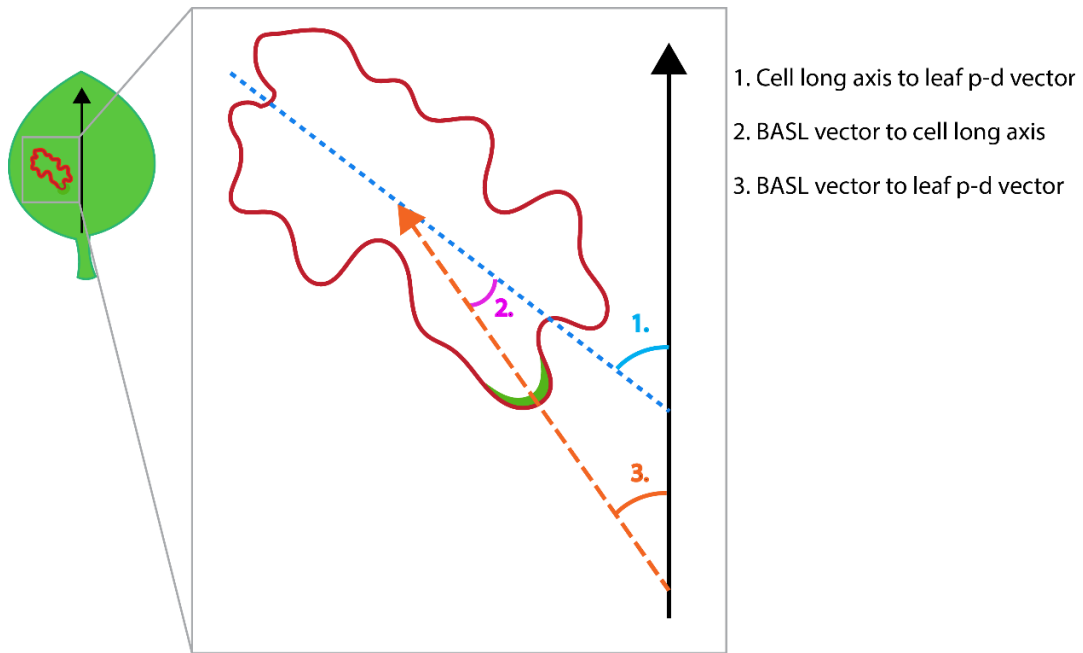


Figure 3.4 Angles between the cell long axis and BASL vector can be calculated.

Schematic shows the three measurable angles involving the cell long axis and ectopic BASL vector for a pavement cell. (1) The angle between the cell long axis (blue dotted line) and leaf proximodistal (p-d) vector (black arrow). (2) The angle between the BASL vector (orange dashed line, see Figure 2.12 for how this is calculated) and the cell long axis. (3) The angle between the BASL vector (orange dashed line) and the leaf proximodistal vector (black arrow).

I used the CellLongAxis script to calculate the angle between the ectopic BASL vectors and the orientation of the cell long axis (Figure 3.4). If the ectopic BASL vector and the cell long axis orientation were perfectly aligned, this angle would be zero. Plotting this angle for multiple leaves confirmed that there was a strong correlation between the BASL vector and the orientation of the cell long axis (Figure 3.5).

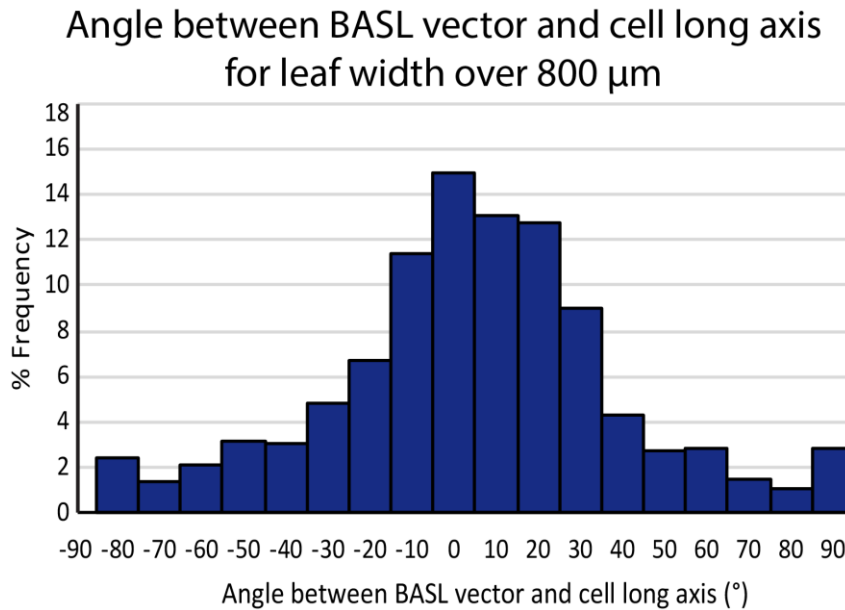


Figure 3.5 The ectopic BASL vectors correlate with the cell long axis.

Histogram showing frequencies of angle between BASL vector and cell long axis (for leaf of width over 800 μm shown in Figure 3.1 A), indicating correlation between BASL vector and cell long axis orientation. See Figure 3.4 for how this angle is calculated.

Multiple hypotheses could account for the correlation between the divergent pattern of ectopic BASL axiality and the cell long axis, though the causative nature of this correlation is unclear. One possibility is that the divergent pattern of ectopic BASL vector orientations could be a consequence of the mechanical connectivity of the tissue which could alter or distort the polarity field as the tissue grows (Coen et al., 2017; Kuchen et al., 2012) (Figure 3.6). However, cell shape anisotropy (itself a result of growth) may also influence polarity because of the way polarity is assigned to cells (Figure 3.2 and Figure 3.6). Alternatively, polarity could provide orientation information to influence or guide growth or cell shape anisotropy (Figure 3.6) (Coen et al., 2017; Whitewoods and Coen, 2017).

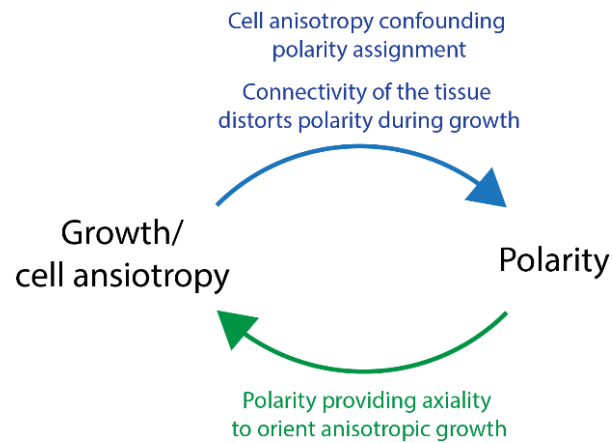


Figure 3.6 A two-way relationship exists between polarity and growth/cell anisotropy.

Diagram shows possible interconnected relationship between polarity and growth or cell shape. Polarity may provide axial information to orient anisotropic growth (green arrow and text). Growth may influence polarity through connectivity of the tissue distorting a polarity field. Cell anisotropy may influence the measure of polarity due to how polarity is assigned to anisotropic cells (blue arrow and text).

3.5.3 Isotropic cells allow uncoupling of cell shape and polarity

One way to separate the effect of cell shape from polarity assigning is to analyse isotropic cells. In isotropic cells, the cell anisotropy cannot influence the polarity vector allowing a clearer distinction between a proximal polarity signal (Figure 3.2 Ai) and a diagonal or divergent signal (Figure 3.2 Bi). To explore the potentially confounding effect of cell shape on assigning polarity, I analysed BASL vectors in a subset of cells from the wild-type background which had a nearly isotropic shape.

3.5.3.1 Cell eccentricity can be used as a proxy for cell shape anisotropy

The CellLongAxis script allowed determination of a cell's eccentricity (ratio of the distance between the foci of the ellipse fitted to a cell and its major axis length), which was used as a mathematical proxy for anisotropy (Gomez et al., 2016; Rangamani et al., 2013). Eccentricity is a measure of circularity: shapes with an eccentricity of 0 would be a perfect circle, through to an eccentricity of 1 which would be a line (Figure 3.7). Quantifying the properties of complex shapes, such as pavement cells, is challenging (Carter et al., 2017; Zhang et al., 2011). Recent work has developed Fourier Analysis to allow quantification of such shapes (Sánchez-Corrales et al., 2018) but this is mathematically and computationally complex hence the simpler measure of eccentricity was used here.

Testing predictions of a tissue-wide polarity field

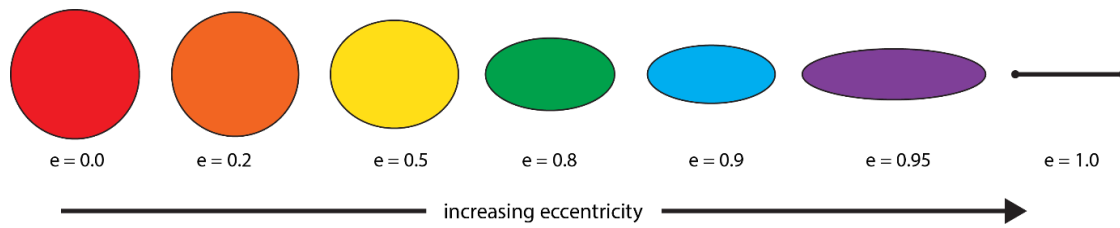


Figure 3.7 Eccentricity can be used as a measure of cell shape.

Illustration of the eccentricity of different ellipses, from 0 (a perfect circle), to 1 (a straight line). Eccentricity is a mathematical measure of the round-ness of an ellipse and is used here as a proxy for cell anisotropy. Eccentricity is the ratio of the distance between the foci of the ellipse fitted to a cell and its major axis length.

In order to get a number of cells that could be classed as isotropic, or near isotropic, an eccentricity of 0.6 and below was used as the threshold for isotropy. This provided a number of cells on leaves over 800 μm in width that would be assigned near isotropic and visually appeared fairly isotropic (Figure 3.8).

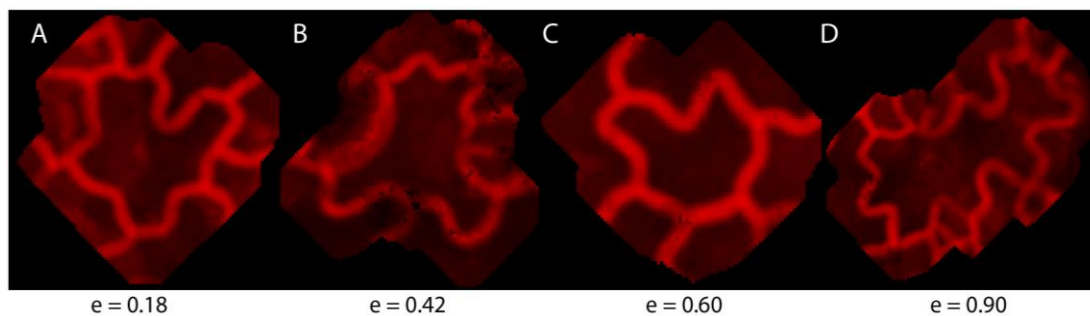


Figure 3.8 Cells with eccentricity of below 0.6 were considered near isotropic.

Examples of cells with their eccentricities, calculated computationally using the CellLongAxis script. Cells with an eccentricity of less than 0.6 (A-C) were considered near isotropic, while cells with an eccentricity higher than 0.6 were considered anisotropic (D).

3.5.3.2 BASL in isotropic cells shows a divergent pattern

I analysed the near-isotropic cells (with an eccentricity of less than 0.6) in leaves over 800 μm in width in a wild-type background that had been assigned ectopic BASL vectors. Plotting the cell long axis orientations for near isotropic cells indicated that there was no preferential orientation (Figure 3.9). This confirmed that the cells selected were sufficiently isotropic; if anisotropic cells had been selected, the histogram would show a peak at 0 degrees, similar to Figure 3.3 B.

Cell long axis orientation for near isotropic cells

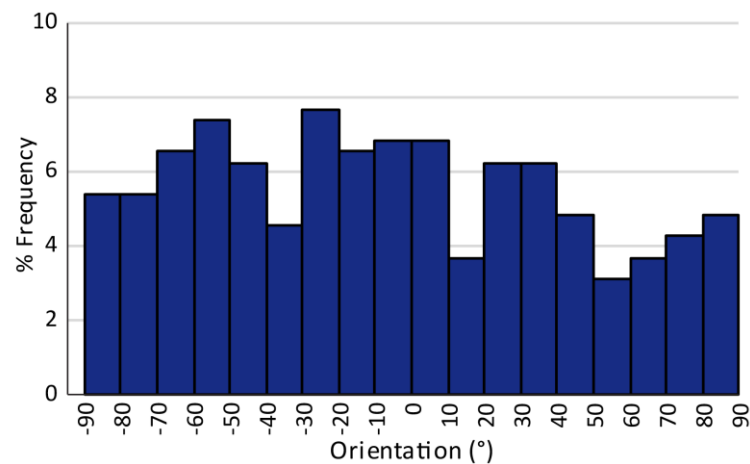


Figure 3.9 Near-isotropic cells show no predominant orientation of cell long axis. Histogram showing cell long axis orientation relative to the midline vector for near isotropic cells (total from 4 leaves greater than 800 μm in width), showing that this subset of cells has no preferential long axis orientation.

In this subset of near isotropic cells, the ectopic BASL vectors showed a preferential proximodistal orientation, including the splayed-out pattern in the proximal region of the lamina, indicated by predominately red and orange vectors (Figure 3.10). This pattern was observed across four leaves of width over 800 μm (Figure 3.10) and appeared similar to if a subset of cells was taken from the BASL vectors in wild type.

Testing predictions of a tissue-wide polarity field

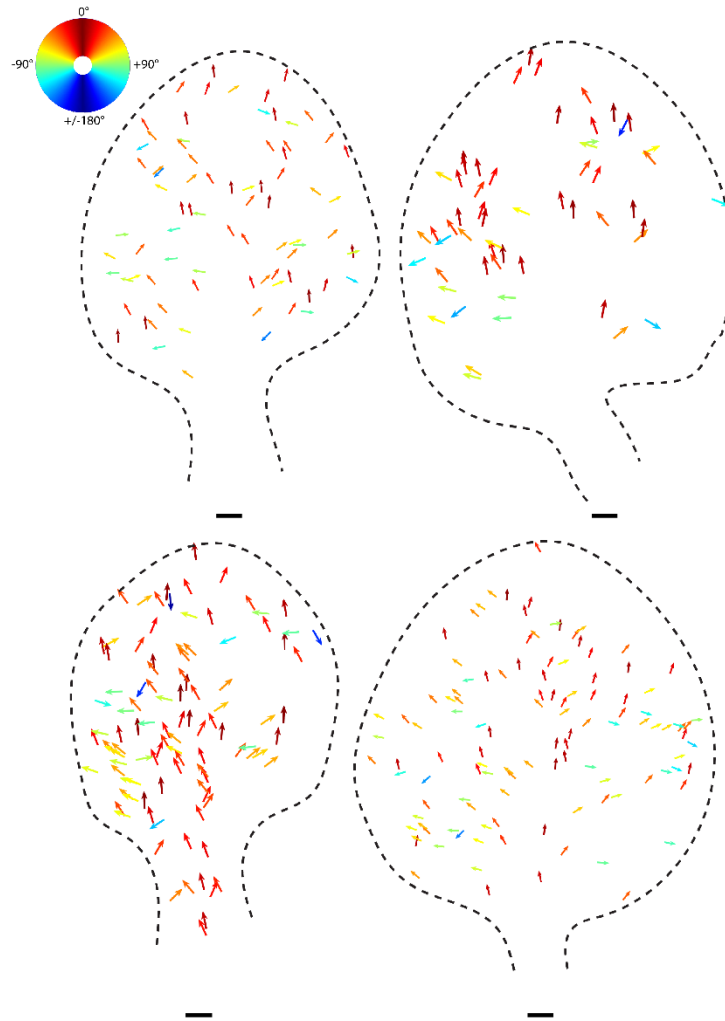


Figure 3.10 Ectopic BASL vectors in near-isotropic cells of large leaves were predominantly proximal-distal.

Ectopic BASL vectors in near-isotropic cells of four leaves, all greater than 800 μm in width. BASL vectors were plotted according to the colour map shown. Black dotted line indicates leaf outline. Scale bars are 100 μm .

Furthermore, the histogram of ectopic BASL vector orientations in near-isotropic cells closely resembled that for all cells across the leaf (Figure 3.11 compared to Figure 2.14 I). This confirmed that the ectopic BASL localised proximally and the polarity field in this small subset of cells reflected that described across the whole leaf.

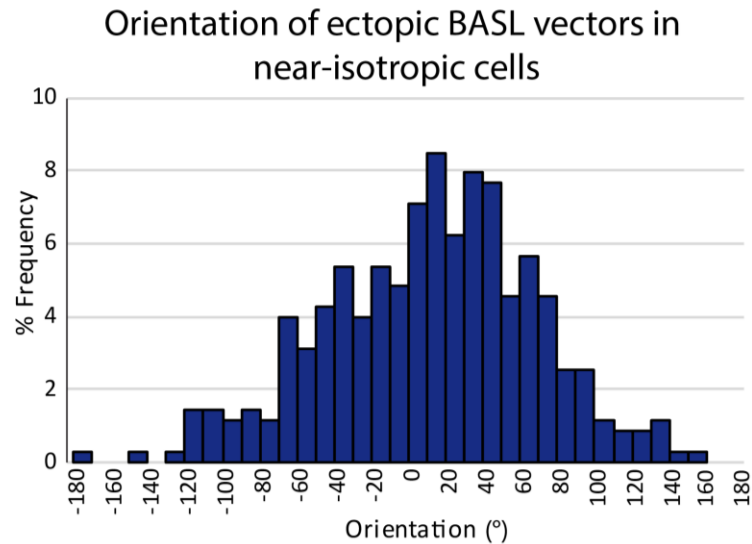


Figure 3.11 Quantification of ectopic BASL vectors in near isotropic cells showed preferential proximodistal orientation.

Ectopic BASL vector orientations for near-isotropic cells relative to leaf midvein, data pooled from 4 leaves with widths over 800 μm .

To more clearly visualise the pattern of BASL vectors in isotropic cells across the leaf, I subdivided multiple large leaves of over 800 μm into nine regions, based approximately on the midvein region and dividing the lamina horizontally into thirds. I measured the assigned ectopic BASL orientations from isotropic cells in each region using Fiji (Schindelin et al., 2012). I then averaged the BASL vector orientations in each of the nine sections to give an average vector for each region of the leaf, independent of cell shape anisotropy (Figure 3.12, Table 3.1). This showed that, in near isotropic cells of the four large leaves analysed, the ectopic BASL vectors were divergent across the lower lamina and proximodistal in the midvein region. Thus, the observed divergent proximodistal polarity field is not dependent on cell shape anisotropy.

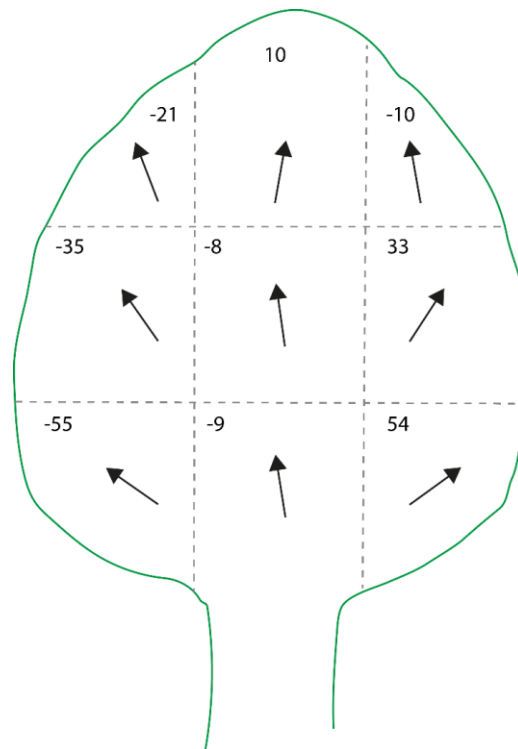


Figure 3.12 Average BASL vector angles from isotropic cells in subdivided regions show a divergent proximodistal pattern.

Schematic of large leaf illustrating the average BASL vector orientation in each section of a subdivided leaf from four leaves over 800 μm width. Average vectors are shown by black arrows in each section, average angle of BASL vector is shown in each section. Sections marked approximately by grey dotted line, approximate average leaf outline shown in green. Corresponds to data from individual leaves shown in Table 3.1.

Table 3.1 Average vectors from isotropic cells in regions of additional subdivided leaves.

The first row of data shows average vectors for regions of leaf shown in top left panel of Figure 3.10, the bottom 3 rows show average vectors for leaves in 3 additional leaves (shown in Figure 3.10), all over 800 μm in width.

Top left	Top middle	Top right	Mid left	Mid middle	Mid right	Bottom left	Bottom middle	Bottom right
-41.1	38.9	-19.3	-24.1	4.5	35.3	-40.5	-28.0	42.8
-45.3	8.4	19.6	-57.4	-3.5	64.3	-60.4	-4.2	66.6
3.7	11.6	-15.9	-28.0	-20.6	7.2	-36.6	-15.5	19.6
-1.1	3.5	-26.6	-29.3	-13.2	25.0	-83.0	10.5	86.9

These results indicate that ectopic BASL polarity shows a divergent pattern at later stages of leaf development that is not simply a consequence of the way polarity is assigned in relation to the cell centroid. The divergent polarity pattern described for leaves at later stages of development may be a consequence of the mechanical connectivity of the growing tissue (blue arrow and text Figure 3.6); indeed, the splaying out at later stages rather than early stages would suggest this. In addition, the possibility remains that polarity guides growth (green arrow and text Figure 3.6). Live-tracking data may allow any causative link to be made more conclusively, however, a correlation between BASL polarity and growth would likely still be observed because growth is largely anisotropic across the leaf (Kuchen et al., 2012) and the issue of assigning polarity in anisotropic cells would arise (Figure 3.2). It is therefore challenging to explore the relationship between polarity (as measured in relation to the cell centroid) and growth without confounding effects of cell shape.

3.6 Uncoupling polarity and cell long axis orientation

3.6.1 Cells not in line with proximodistal axis also allow separation of cell shape and polarity

Given that most pavement cells in the *A. thaliana* epidermis are approximately aligned with the proximodistal axis of the leaf, as shown in Figure 3.3, it is challenging to uncouple cell shape from polarity. It is possible that the localisation of BASL to the proximal end of cells is due to preferential localisation to the long axis of a cell. Notably, this hypothesis would require BASL localisation to also respond to additional signals allowing consistent localisation to the proximal rather than distal end of the cell long axis.

To test whether BASL localised preferentially to one end of the cell long axis, I used the CellLongAxis software to select the subset of cells in the leaf epidermis in which the long axis was more than 50 degrees from the proximodistal midline vector and were also anisotropic (eccentricity of more than 0.6). The CellLongAxis software indicated the BASL polarity axis (Figure 3.13, green line), the cell long axis (Figure 3.13, blue line), and also the axis through the most proximal point in the cell (Figure 3.13, red line). The most proximal point was determined mathematically using the lowest y-coordinate of the cell: it was helpful in order to assign BASL localisation in relation to the cells, but it is not clear how a cell could determine the mathematical extrema and therefore this is not a biologically relevant measure. Cells

Testing predictions of a tissue-wide polarity field

could be assigned to one of five categories depending on the BASL localisation: BASL localisation to one end of the cell long axis (Figure 3.13 A), localisation to the most proximal point (lowest y-coordinate) of the cell (Figure 3.13, B), localisation that did not align with the mathematical proximal point of the cell but a neighbouring proximal lobe (Figure 3.13 C), cells where the most proximal point and long axis were too close to distinguish between (Figure 3.13 D), and cells in which the BASL vector is not clearly localised to the one end of the long axis or a most proximal lobe (Figure 3.13 E).

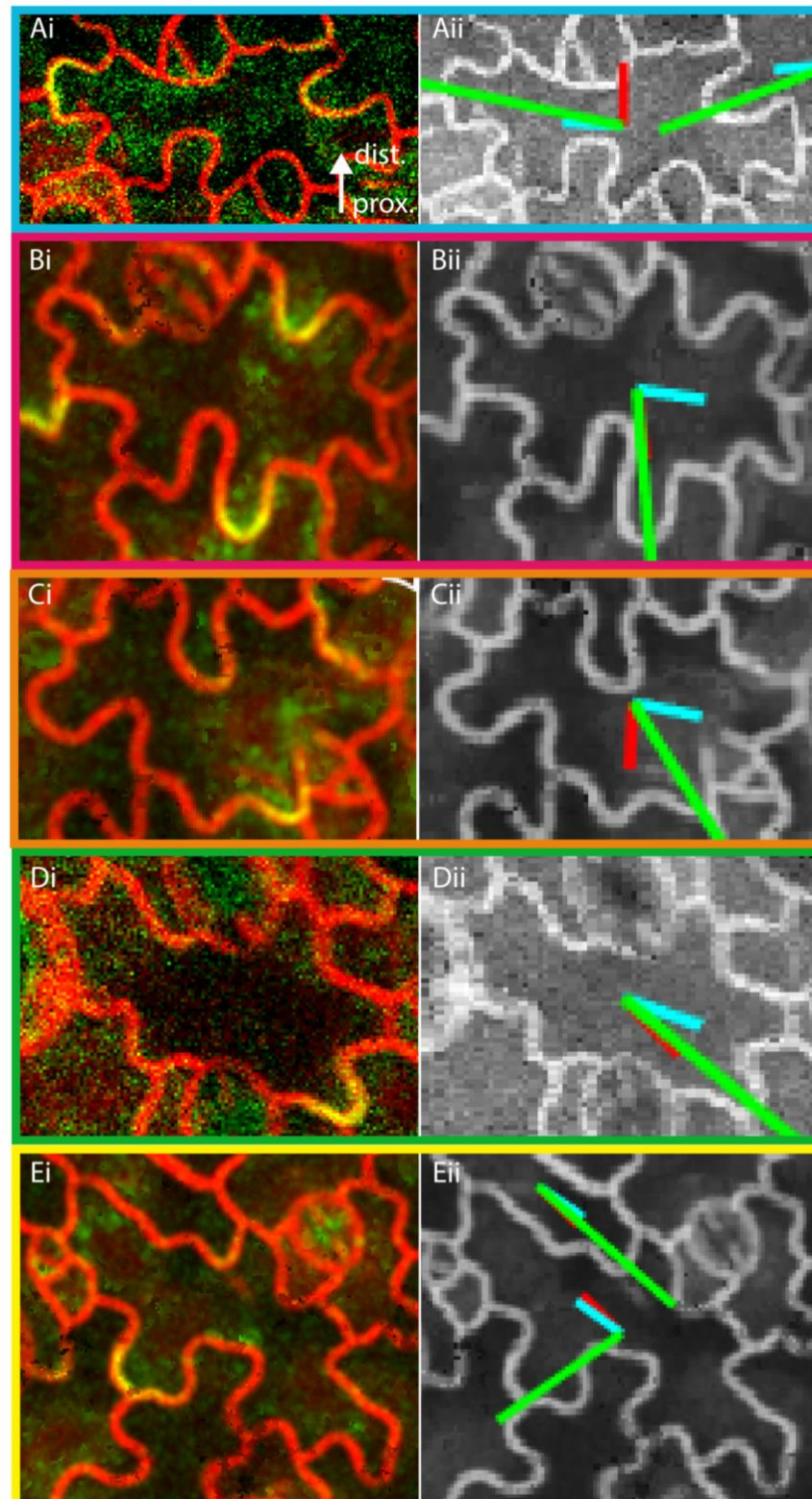


Figure 3.13 BASL localisation in anisotropic cells oriented more than 50° from the leaf proximodistal axis was variable.

Examples of ectopic BASL localisation in anisotropic cells (eccentricity >0.6) in which the long axis was more than 50° from the leaf proximodistal axis. Left hand panels show BASL localisation, right hand panel shows output of CellLongAxis software that indicates the axis of the BASL vector (green), cell long axis (blue) and axis through most proximal point (lowest y-coordinate) of the cell (red) for each corresponding cell (axes from surrounding cells also

Testing predictions of a tissue-wide polarity field

visible in Aii and Eii). Cells could be assigned to one of 5 categories: (A) BASL localisation to one end of the cell long axis; (B) localisation to the most proximal point of the cell; (C) localisation that did not align with the mathematical proximal point of the cell but a neighbouring proximal lobe; (D) cells where the most proximal point and long axis were too close to distinguish between and (E) cells in which BASL did not clearly localise to one end of the long axis or a most proximal lobe. Coloured boxes show relation to sectors of pie chart in Figure 3.14. Examples in A and D are from one leaf, B, C and E are from another leaf. Leaf proximodistal axis is shown in A and applies to all cells.

I carried out visual analysis and categorisation of 165 cells from two leaves that had numerous anisotropic cells not in line with the leaf proximodistal axis (Figure 3.14). Across these two leaves, only ~18% of cells had BASL localised to near one end of the cell long axis suggesting that BASL is not marking the long axis of cells. In ~25% of cells, the long axis and most proximal point of the cell couldn't be distinguished while in over 50% of cells analysed ectopic BASL localised to the most proximal point of the cell, or a proximal lobe (Figure 3.14). This data indicated that there was no overall consistent localisation of BASL in relation to the cell long axis and that there was more of a tendency to mark a proximal lobe of cells. In wild-type leaves where cells tend to align with the leaf proximodistal axis, this qualitative analysis is not conclusive, but provides preliminary evidence that BASL tends to localise proximally rather than to one end of the cell long axis.

Breakdown of ectopic BASL localisation in cells where the long axis is mediolateral

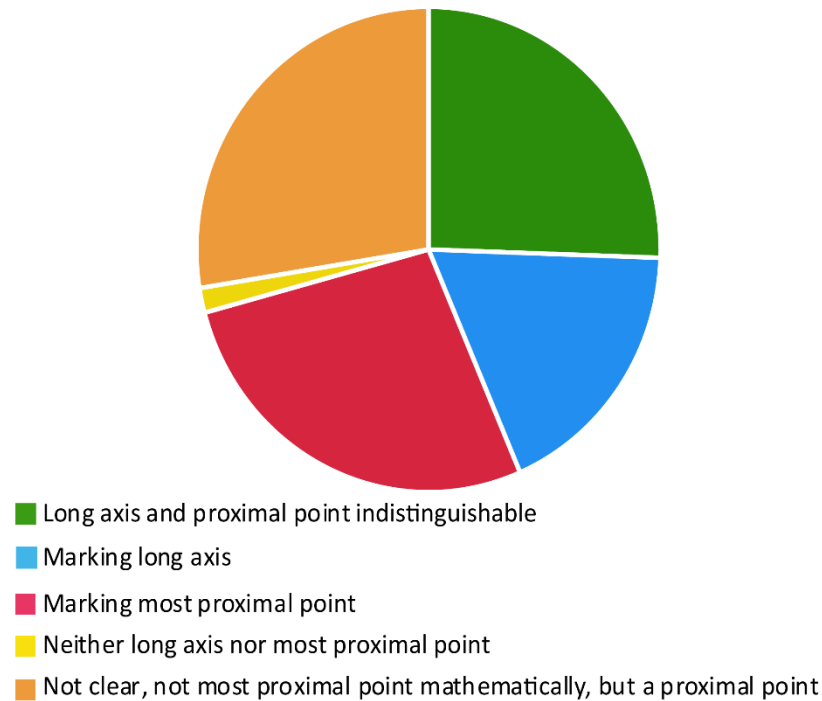


Figure 3.14 Ectopic BASL localises to a proximal lobe in more than 50% of anisotropic cells aligned approximately with the mediolateral axis in a wild-type leaf.

Pie-chart shows proportion of cells in a wild-type leaf with BASL localising to each of the five categories described (long axis and proximal point indistinguishable (green), BASL marking one end of the long axis (blue), BASL marking the most proximal point (i.e. lowest y-coordinate, red), BASL localising to neither long axis nor most proximal point (yellow) and BASL not clearly marking the cell long axis but localising to a proximal lobe of the cell (orange). Section colours correspond to coloured boxes in examples in Figure 3.13. 165 cells from 2 leaves of width >800 μm were analysed.

3.6.2 *gap1gap2* mutant allows uncoupling of polarity and cell geometry

As described above, in a wild-type leaf, the long axis of most cells is approximately aligned with the leaf proximodistal axis (Figure 3.3). Cells in which the long axis is not aligned with the proximodistal axis allow uncoupling of cell polarity and cell shape, but in a wild-type leaf, these are relatively rare and analysis of BASL localisation in this subset of cells was variable (Figure 3.13 and 3.14).

Previous work had observed that the epidermal cells of the Rho GTPase activating proteins double mutant (RhoGAP, (Stöckle et al., 2016), here referred to as *gap1gap2*) appear to have a high proportion of cells in which the cell long axis is not aligned with the proximodistal axis

(Jordi Chan, personal communication). The *gap1gap2* double mutant is therefore a useful tool in exploring how BASL polarity localises independent of cell axis orientation. I crossed the *gap1gap2* double mutant to the inducible *35S::GFP-BASL* line to test if anisotropic cells whose long axes are aligned perpendicular to the midvein localise BASL to their long-axis, or to the proximal end (Figure 3.15).

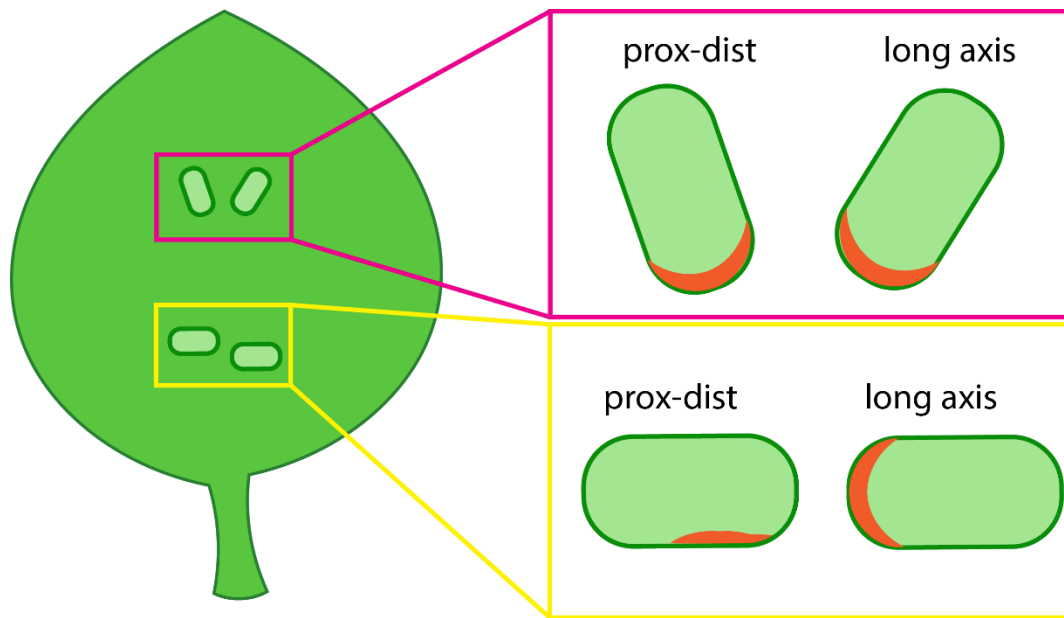


Figure 3.15 Cells in *gap1gap2* in which the long axis is not aligned with the proximodistal axis of the leaf allow uncoupling of polarity and cell orientation.

Cells in a *gap1gap2* mutant appear to be often not aligned with the leaf proximodistal axis, allowing separation of proximodistal polarity and cell long axis orientation. Cells in the magenta box indicate wild-type orientations; they tend to be aligned parallel to the leaf midline and a marker (orange) of the proximodistal axis is indistinguishable from a cell long axis marker (although this could be proximal or distal). The yellow box indicates cells not aligned with the leaf proximodistal axis (more common in the *gap1gap2* mutant). In such cells, a proximodistal signal would localise to the bottom of the cell, while a long axis marker would localise to an end (or both ends).

I also crossed the *gap1gap2* double mutant with the inducible BASL line that also had an RFP-plasma membrane line to allow visualisation of the cell outlines. This confirmed the observation that the cell long axes in *gap1gap2* cotyledons were often perpendicular to the proximodistal axis (Figure 3.16). I used the cotyledons for analysis with BASL as they appeared to have more cells in which the cell long axis was perpendicular to the proximodistal axis. The unusual cell orientations observed in this mutant are likely to be a

result of faulty division planes, which have previously been described in the root (Stöckle et al., 2016).

Another interesting feature of the *gap1gap2* mutant is that the pavement cells are lobeless (Figure 3.16). This simplified the analysis of polarity in this mutant as the pavement cells could contribute to making the polarity pattern more complex. This also allowed the cell long axis to be visualised more easily. The lack of lobed pavement cells is likely due to the interference with the ROP pathway, known to be involved in the formation of pavement cell lobes (Fu et al., 2005), although this feature of the mutant has not been described as previous work was conducted largely in roots (Stöckle et al., 2016).

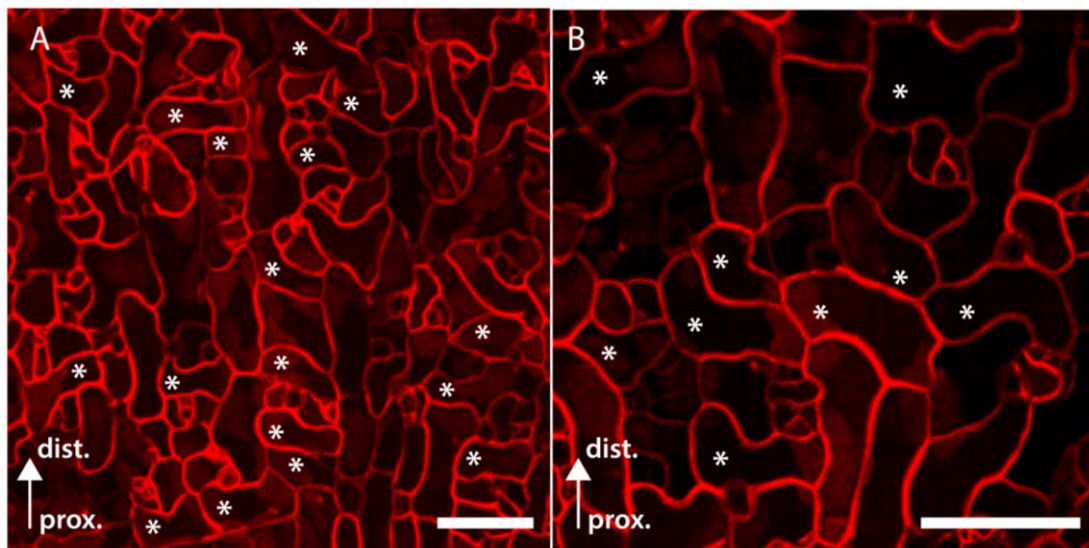


Figure 3.16 *gap1gap2* mutant has multiple cells in which the long axis is not proximodistally aligned.

(A, B) Two representative examples of lobeless pavement cells in the *gap1gap2* double mutant. RFP-PM allow visualisation of cell outlines. Images are from two different cotyledons. Cells with a long axis approximately perpendicular to the proximodistal axis (shown) are marked with a white asterisk. Scale bars are 100 μm .

Despite the unusual shape of the cells in this mutant, and altered cell divisions, the leaves and cotyledons maintain a relatively wild-type shape (Figure 3.17). One noticeable difference is that the cotyledons of the *gap1gap2* mutant tend to be elongated compared to the wild-type (Figure 3.17). This may be due to the altered division patterns, although it has not been characterised previously.

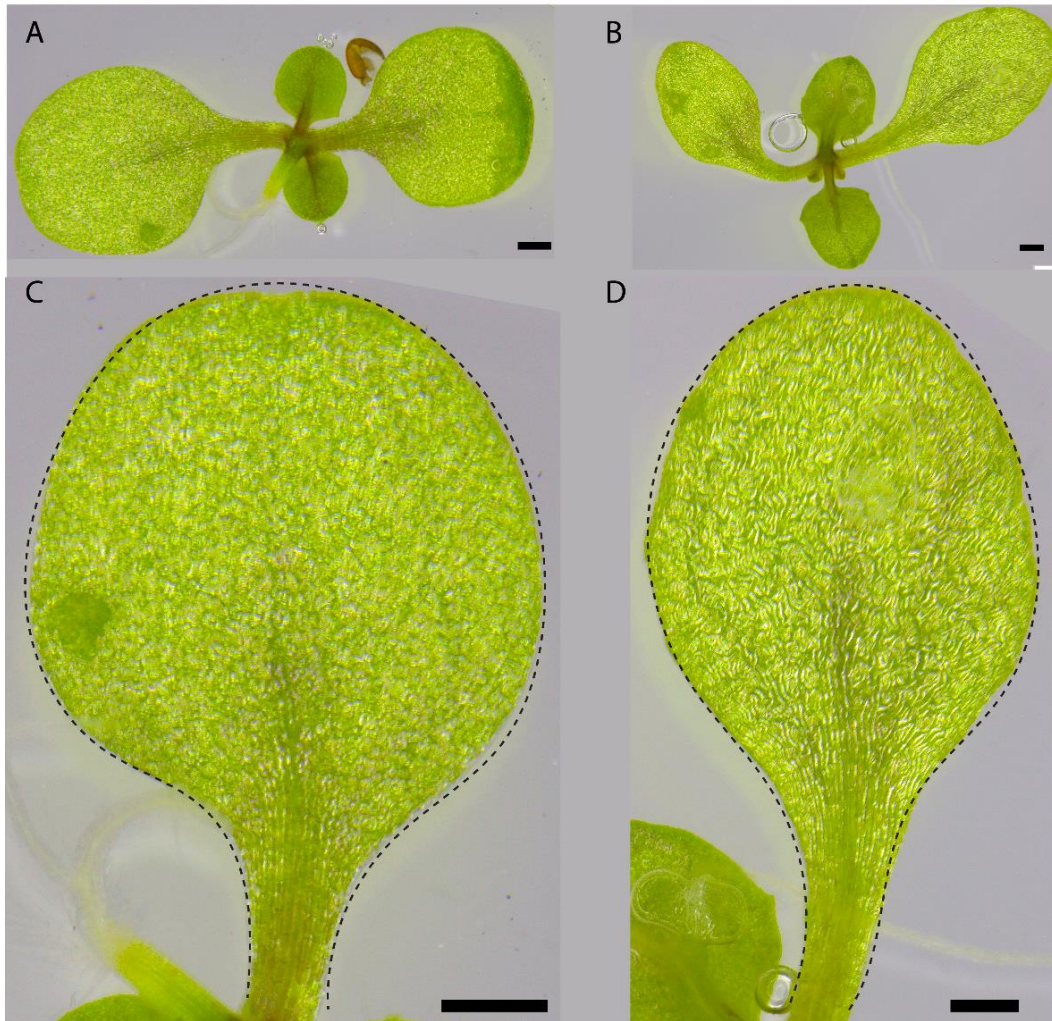


Figure 3.17 *gap1gap2* cotyledons have an elongated cotyledon shape compared to wild type.

(A) Wild-type seedling (Col-0) and (B) *gap1gap2* seedling 6DAS, grown on plates. (C) Close-up region of A showing rounded cotyledon in wild-type. (D) Close-up region of B showing elongated cotyledon in *gap1gap2*. Black dotted lines show cotyledon outline. Scale bars are 500 μm .

I heat-shocked *gap1gap2* seedlings carrying *35S::GFP-BASL* for 20 minutes 4 or 5 DAS to induce BASL expression across the leaf and cotyledon. In the cotyledon, a number of cells could be found that had a long axis aligned perpendicular to the proximodistal axis (outlined in magenta in Figure 3.18). In these cells, BASL tended to localise to the proximal end of the cell, which was generally along the long wall of the cell (Figure 3.18 B, C). The BASL signal was not always observed in the centre of the cell, sometimes towards one end of the other, but was typically not observed marking either end of the long-axis of perpendicular cells. In cells that did align the with proximodistal axis, BASL tended to localise proximally (Figure 3.18 B and C), as in wild-type.

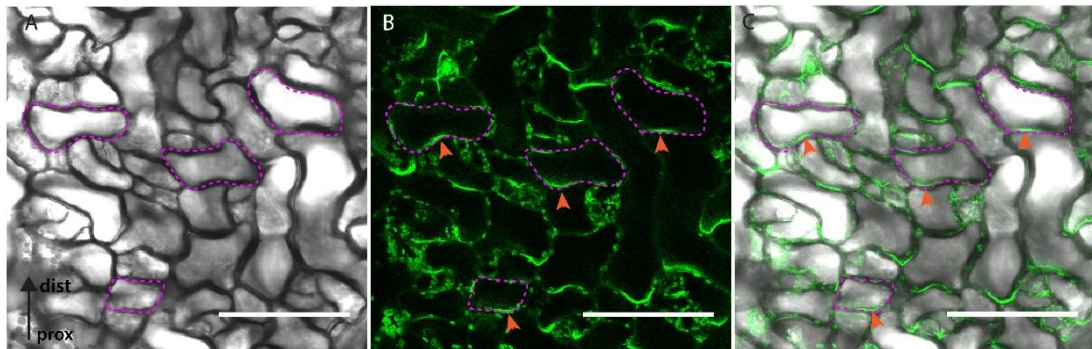


Figure 3.18 *35S::GFP-BASL* in a *gap1gap2* cotyledon is typically proximally localised. *35S::GFP-BASL* induced in a *gap1gap2* cotyledon, showing the cell outlines (Bright-field, A), GFP-BASL signal (B), and combined cell outlines and BASL signal (C). Four cells in which the long axis is approximately perpendicular to the proximodistal axis are highlighted with magenta dotted line. BASL signal in these cells is proximally localised, indicated with orange arrowheads (B and C). Proximodistal axis is shown in A. Scale bars are 100 μm .

To visualise the cell outlines more clearly in the *gap1gap2* mutant, I induced BASL in *gap1gap2* seedlings and stained with PI. As before, 5-day old seedlings were heat-shocked for 20 minutes and stained with PI before imaging. This allowed a clearer visualisation of the cell outlines in the cotyledon and confirmed that the BASL signal tended to localise to the proximal end of cells in which the long axis was perpendicular to the proximodistal axis (Figure 3.19). The BASL signal was sometimes observed in the centre of a cell wall (example in Figure 3.19 A), and sometimes localised to one end of the long edge of the cell (example in Figure 3.19 B). This confirms that ectopic BASL tends to mark the proximal end of cells, rather than either end of the long axis of cells (yellow box in Figure 3.15).

The absence of lobes in the *gap1gap2* mutant also indicates that ectopic BASL localises proximally independent of lobes. The PHGAP proteins (absent in this mutant) are part of the ROP pathway (Stöckle et al., 2016) that has previously been linked to cell polarity, albeit multi-polar cells, rather than a single polarity (Yang, 2008). The ability of BASL to polarly localise in the absence of this functional pathway suggests that ectopic BASL polarity is at least partly independent of this signalling pathway. However, previous work has suggested a potential involvement of BASL acting upstream of the ROP pathway, given that BASL-mediated cell outgrowths are abrogated in *rop2* mutant hypocotyls (Dong et al., 2009). Quantification of ectopic BASL localisation in the *gap1gap2* mutant is required in order to

further understand the role of BASL in marking the proximal end of cells, and any potential role in cell growth.

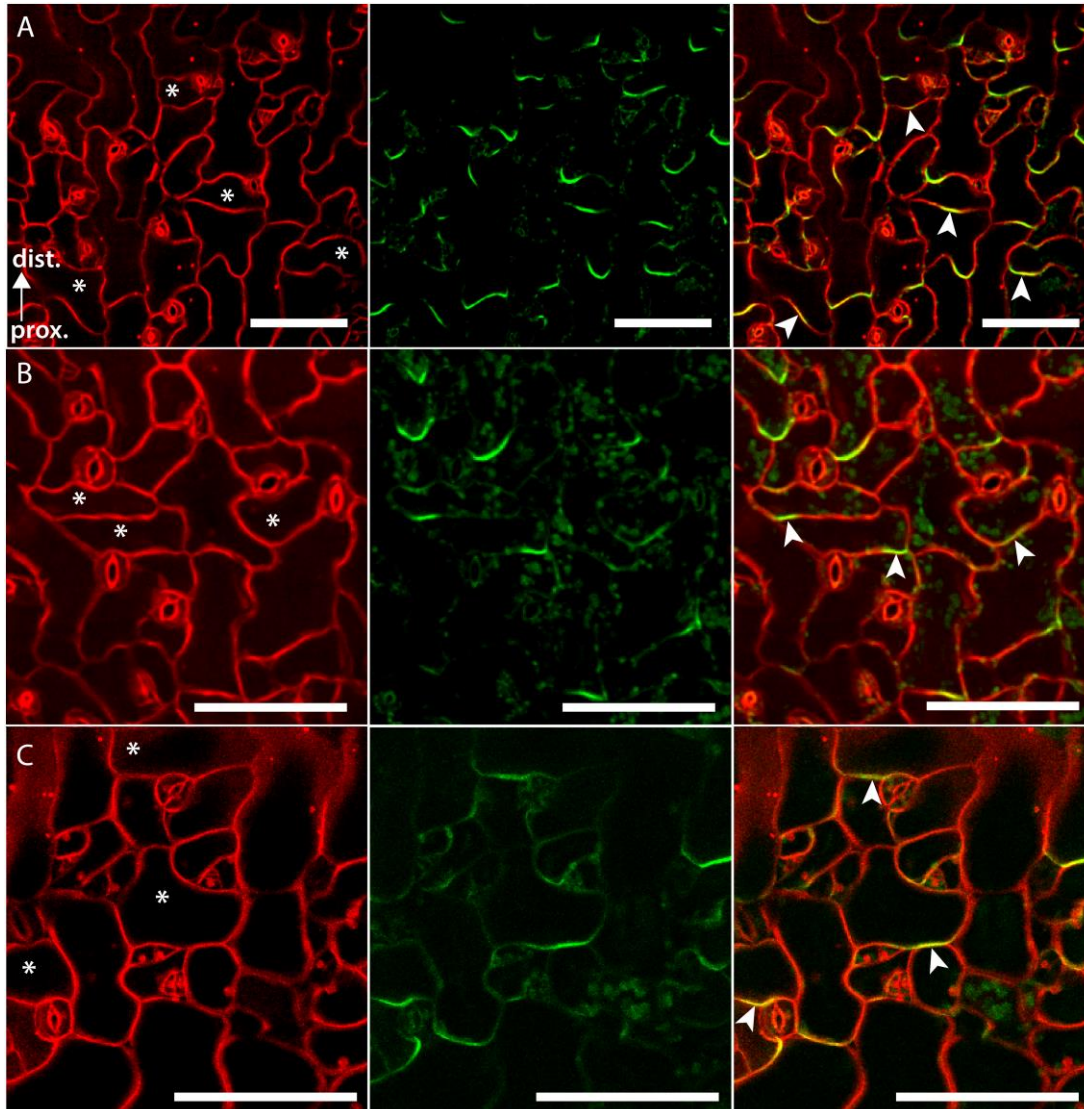


Figure 3.19 *35S::GFP-BASL* in *gap1gap2* cotyledons, stained with PI.

Examples of *35S::GFP-BASL* induced in a *gap1gap2* cotyledon (A, B, C each show a separate cotyledon). Left hand panels show cell outlines with PI staining, cells with long axes approximately perpendicular to the proximodistal axis are indicated with an asterisk. Middle panel shows *35S::GFP-BASL* signal. Right hand panel shows combined cell outlines and *35S::GFP-BASL* signal. GFP-BASL signal in the cells indicated in left hand panel is highlighted by a white arrowhead. Uppermost two cells with asterisks in A show examples where BASL localises to the centre of the cell wall. Leftmost two cells with asterisks in B show examples where BASL is localised to the end of the cell. Proximodistal axis (same for all three examples) is shown in A. Scale bars are 100 μm .

3.7 Relationship to PIN polarity

One key question that arises from the ectopic BASL polarity field described in this work is whether this polarity field is connected to PIN polarity, either directly or indirectly, or whether the two are independent. It is possible that both polarity markers are part of a common system, with PIN involved in early establishment of polarity and ectopic BASL revealing a polarity that is maintained through to later stages. Equally, BASL could be an independent polarity system with different underlying polarisation mechanisms.

To test the relationship between the ectopic BASL polarity and PIN1 polarity, I developed a line with inducible *35S::mCherry-BASL*, in a *PIN1::PIN1-GFP* background with the aim of analysing the localisations of ectopic BASL and PIN1 in different contexts. Other PIN family members have different localisations and polarities that may also be worth exploring: I used PIN1 here as it has a well-characterised polar distribution in young primordia and serrations (Bilsborough et al., 2011; Guenot et al., 2012; Hay et al., 2006; Scarpella et al., 2006).

Whilst PIN proteins are polarly localised, their polarity orientation in relation to a single cell can be difficult to assign; in some cases only PIN axiality can be inferred (Abley et al., 2016). When PIN polarity can be assigned, the vectors are usually oriented pointing towards the PIN signal (Abley et al., 2016; Hay et al., 2006; Sauret-Güeto et al., 2013). This contrasts to the vectors that I assign for BASL polarity from signal to centroid (red arrow, Figure 3.20 A). By assigning BASL vectors this way, the tissue-wide polarity patterns can be compared to those predicted by modelling of the leaf (Kuchen et al., 2012). In addition, although PIN1 and BASL localise at the opposite ends of the cell, the cell can be considered to have a single intrinsic polarity, marked by two different proteins (Figure 3.20). This could be due to multiple different molecular addresses responding to an underlying polarity system. If PIN1 and BASL colocalised at one end of a cell (Figure 3.20 B), the vectors would appear to point in different directions, and would indicate a cell with unusual PIN or BASL localisations (Figure 3.20 B).

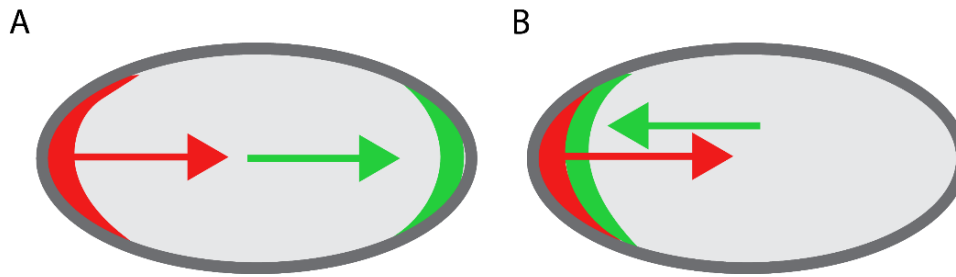


Figure 3.20 PIN and BASL vectors are assigned differently.

Schematic showing how PIN and BASL vectors may be assigned in cells expressing both polarity markers. I assign BASL vectors from the signal to the cell centroid (red). PIN vectors are usually assigned pointing towards the signal (rather than away from it as in BASL) (green). (A) In cells where PIN and BASL are localised at opposite ends of the cell, the vectors would therefore be pointing in the same direction indicating an overall cell polarity. (B) In cells where PIN and BASL localise together, the vectors would be pointing in opposite directions.

3.7.1 BASL and PIN in early leaf

PIN1 is reported to be polarised in primordia, before expression disappears from the epidermis in a non-uniform manner when the leaf is approximately 100 μm in width (Abley et al., 2016; Guenot et al., 2012). I previously confirmed these approximate stages of PIN1 dynamics by imaging the *PIN1::PIN1-GFP* reporter in early leaves (Figure 2.1). Ectopic BASL expression could be induced and observed in very young leaves, from approximately 50 μm in width, indicating that ectopic BASL and PIN1 expression could overlap temporally.

To determine the relationship between PIN1 and BASL localisation in primordia, I used the line with inducible *35S::mCherry-BASL* and *PIN1::PIN1-GFP*, allowing both polarity markers to be visualised in the same cells. In order to visualise ectopic BASL at very early stages of development, seedlings were heat-shocked when they had just emerged from the seed coat (2 DAS).

Induction of ectopic BASL in young leaf primordia showed that it localised to the proximal end of cells at a time when PIN1 was polarly localised to the distal end of cells (Figure 3.21), indicating that these two polarity markers could be co-expressed. As described previously, the ectopic BASL localised to a distinct crescent in cells and was not visible in every cell of the leaf. By contrast, PIN1 had a broader distribution, localising across the whole wall of a cell, making its polarity harder to assign to individual cells (Figure 3.21 B, C). This difference in localisation domains of BASL and PIN has also been described previously where PIN1 and *35S::GFP-BASL* distributions have been compared in the root (Dong et al., 2009).

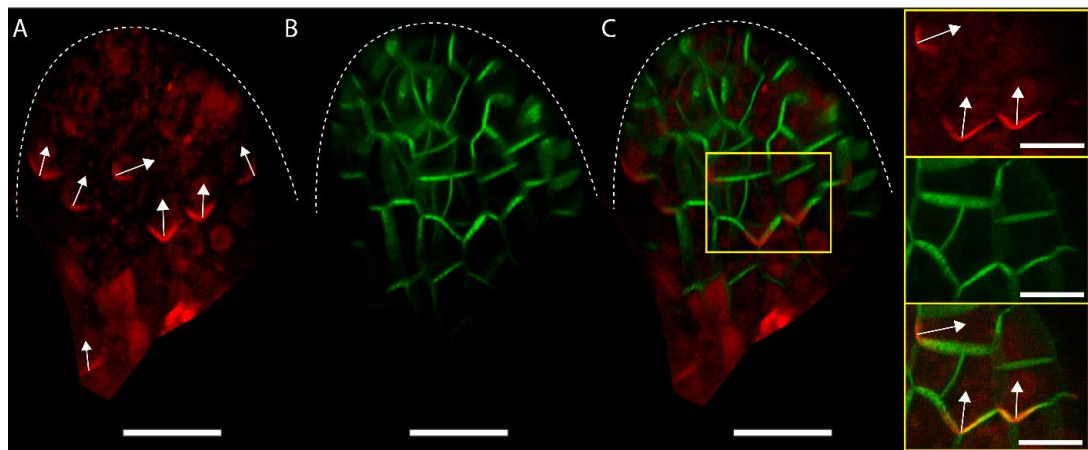


Figure 3.21 *35S::GFP-BASL* localised at the opposite end of cells to PIN1 in primordia.

(A) Young leaf showing inducible *35S::mCherry-BASL* localised to the proximal end of cells and to cell corners. White arrows indicate manually assigned BASL polarity based on the curvature of the BASL crescent. (B) *PIN1::PIN1-GFP* expression for leaf in A shows PIN1 localised to the distal face of cells. (C) *35S::mCherry-BASL* and *PIN1::PIN1-GFP* channels combined. Yellow box indicates close up section. White dotted lines indicate leaf outline. Scale bars 20 μm in A-C and 10 μm in close up regions of C.

I found the inducible *35S::mCherry-BASL* line appeared to be more variable than the inducible *35S::GFP-BASL* line. BASL signal was frequently observed in the nucleus as well as in a crescent at the cortex. Whilst this was also sometimes the case with the inducible *35S::GFP-BASL* line, it was more obvious in the mCherry line, possibly due to differences in the fluorophore and/or insertion site. The BASL signal was sometimes also more patchy in the mCherry line than in the inducible *35S::GFP-BASL* line, again, possibly due to differences in insertion sites, and the multiple generations the *35S::GFP-BASL* line had been taken through. In the *35S::mCherry-BASL* line, the proximal localisation of BASL remained the same in multiple independent lines indicating that, while expression levels may be variable, this feature of ectopic BASL remains constant. Furthermore, the mCherry fluorophore used when I made this line was difficult to image in very young primordia due to autofluorescence. This may have been worsened by the seedlings being stressed by a heat-shock treatment. As a result, images of whole primordia with PIN1 and clear *35S::mCherry-BASL* were difficult to obtain.

I imaged other young primordia or regions of primordia with *35S::mCherry-BASL* and *PIN1::PIN1-GFP* and confirmed that BASL and PIN1 tended to localise opposite each other in young leaves, even when tissue-level patterns were obscured (Figure 3.22). In individual cells with both BASL and PIN expression, BASL tended to localise proximally, opposite to the distal

PIN1 localisation (Figure 3.22). This situation resembled the hypothesis shown in Figure 3.20

A.

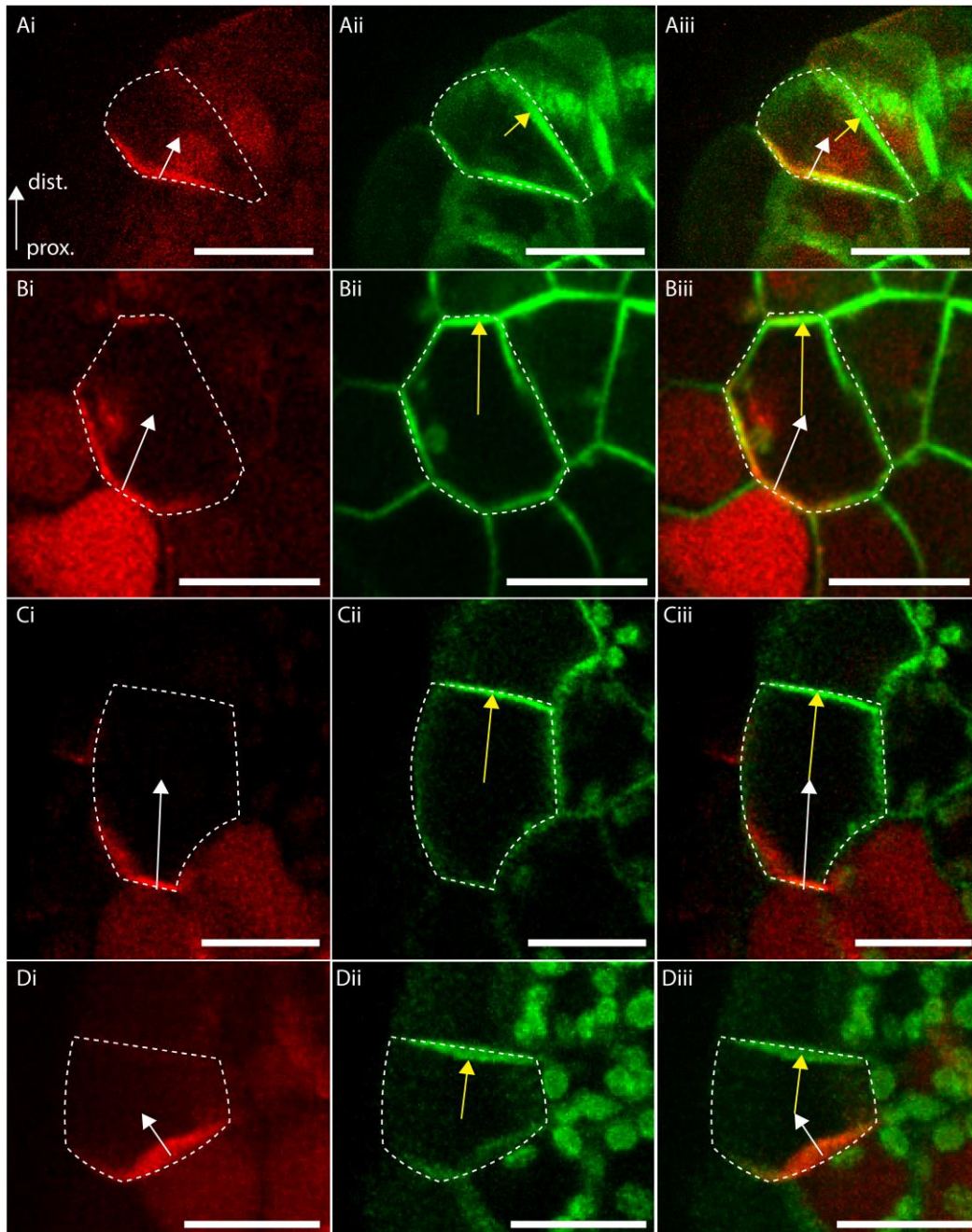


Figure 3.22 Ectopic BASL and PIN1 localised to the opposite ends of individual cells.

Examples of *PIN1::PIN1-GFP* and induced *35S::mCherry-BASL* in young leaves, heat-shocked 3DAS and imaged 2 days later (A and B) or 3 days later (C and D). Cells are oriented according to the leaf proximodistal axis in all cases (shown in A). Left hand panel shows ectopic *35S::mCherry-BASL* with white arrows manually assigned according to Figure 3.20 from BASL signal to the centroid. Middle panel shows *PIN1::PIN1-GFP* expression in the same cell with yellow arrows showing orientation of PIN1, according to Figure 3.20, from the centroid to the PIN signal. Note polarity of PIN1 is difficult to assign. Right panel shows combined channels with white arrows (BASL) and yellow arrows (PIN). White dotted outlines show cell outline. Scale bars are 10 μm .

3.7.2 BASL in serrations

The localisation of ectopic BASL to the proximal end of the cell in young primordia where PIN1 is polarised distally, and the maintenance of this proximal localisation throughout development may suggest that BASL is a proximal marker in all situations. This would contrast to PIN1 polarity which is known to be involved in, and necessary for, outgrowth and organ formation (Abley et al., 2016; Hay et al., 2006). To further test the role of the polarity field revealed by ectopic BASL, it would be interesting to alter the polarity field. However, this is technically difficult, particularly when the origins and mechanisms underlying the BASL polarity field are unknown. One way to explore polarity reversals or disruptions and to further test the relationship with PIN is to analyse situations in which PIN1 polarity is known to change.

One such situation where PIN1 is reported to show reversals is in developing serrations where PIN1 at the margin is distally localised below a serration outgrowth, and proximally localised above the serrations outgrowth (Bilsborough et al., 2011; Hay et al., 2006). This pattern is repeated along the margin as multiple serrations develop resulting in the formation of PIN1 convergence points at the serration tip, and divergence points at the sinus of the serration (Bilsborough et al., 2011).

There are therefore two possibilities for how BASL polarity would behave around a serration outgrowth (Figure 3.23). Either, BASL may remain proximally localised, even in the cells at the top of the sinus where PIN is reversed. In this case, BASL and PIN would likely be seen at the same end of cells in this region of the serrations (Figure 3.23 A). This might suggest that PIN and BASL are distinct and that the polarity field revealed by ectopic BASL does not play a role in the formation of outgrowths. Alternatively, it is possible that ectopic BASL will reorient in a similar way to PIN1. In this case, BASL may be localised to the proximal end of cells below the serration, and in the distal end of cells above the serration outgrowth, forming convergence and divergence points like that reported for PIN1 (Bilsborough et al., 2011; Hay et al., 2006). In this case, I would expect to observe PIN1 and BASL at opposite ends of the cells in all regions of the developing serration (Figure 3.23 B).

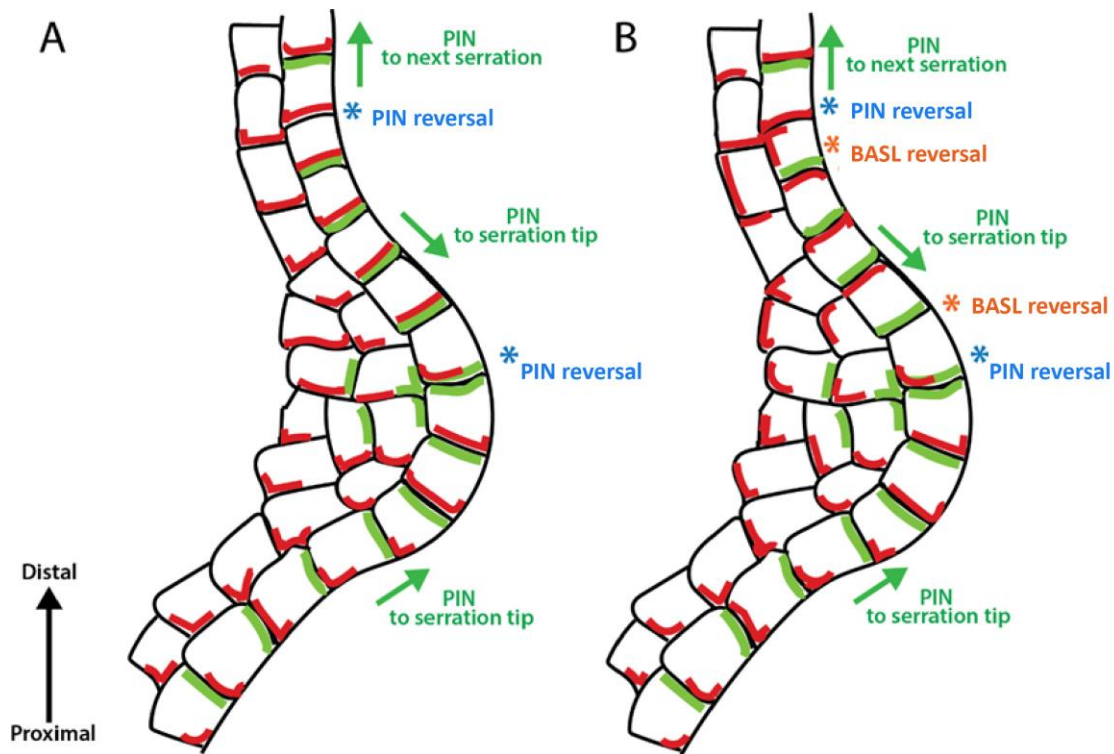


Figure 3.23 Two hypotheses illustrate possible BASL behaviour at serrations.

Schematic of two hypotheses for how BASL will behave at serrations in relation to previously reported PIN1 expression. In both cases, PIN1 (green) localises to the distal end of cells below the serration outgrowth, and at the proximal end of cells above the outgrowth forming a PIN convergence point at the serration tip, and a divergence point at the sinus (blue asterisks). In (A), BASL (red) localises at the proximal end of all cells and is therefore localised to the same end of the cell as PIN1 in cells above the serration outgrowth. In (B), BASL (red) localises to the proximal end of cells, apart from those above the serration outgrowth where PIN1 reorients. In these cells, BASL localises to the distal end of cells and is therefore always localised opposite PIN1, mirroring the convergence and divergence points (orange asterisks).

I heat-shocked seedlings for 20 minutes at later stages of development (~8 DAS) to induce *35S::GFP-BASL* expression in later leaves as leaf 1 does not develop clear serrations (Biot et al., 2016). I imaged PIN1 and BASL in later leaves, for example leaf 5 (Figure 3.24), where more pronounced serrations form (Biot et al., 2016).

Induction of ectopic BASL at later stages showed that co-expression with epidermal PIN1 expression was only observed in developing serrations (Figure 3.24 A-C). Below the developing serration tip, ectopic BASL was proximally localised (Figure 3.24 A, C, D). Above the serration sinus, ectopic BASL was also proximal (Figure 3.24 F). In the distal region of the serration outgrowth, a region of reversed ectopic BASL polarity was observed where BASL localised to the side or distal wall of cells (yellow arrows, Figure 3.24 E). This resulted in the

formation of ectopic BASL convergence and divergence points (Figure 3.24 A), mirroring the polarity pattern of PIN1 previously described (Bilsborough et al., 2011; Hay et al., 2006), with BASL localising to the opposite end of the cell compared to that reported for PIN1.

Imaging of BASL and PIN1 at serrations was complicated by the 3D curvature at serrations which made it difficult to image the epidermis and marginal cells and to see all the relevant cells in one plane. To overcome this issue, the panels in Figure 3.24, particularly D-F are projections of a few z-slices from the relevant area in order to allow clear visualisation of the cells in each region. I also imaged multiple different serrations, on higher order leaves (typically leaf 4 or 5) and confirmed that there was consistently a group of cells at the distal end of the serration in which BASL polarity was altered (Figure 3.25).

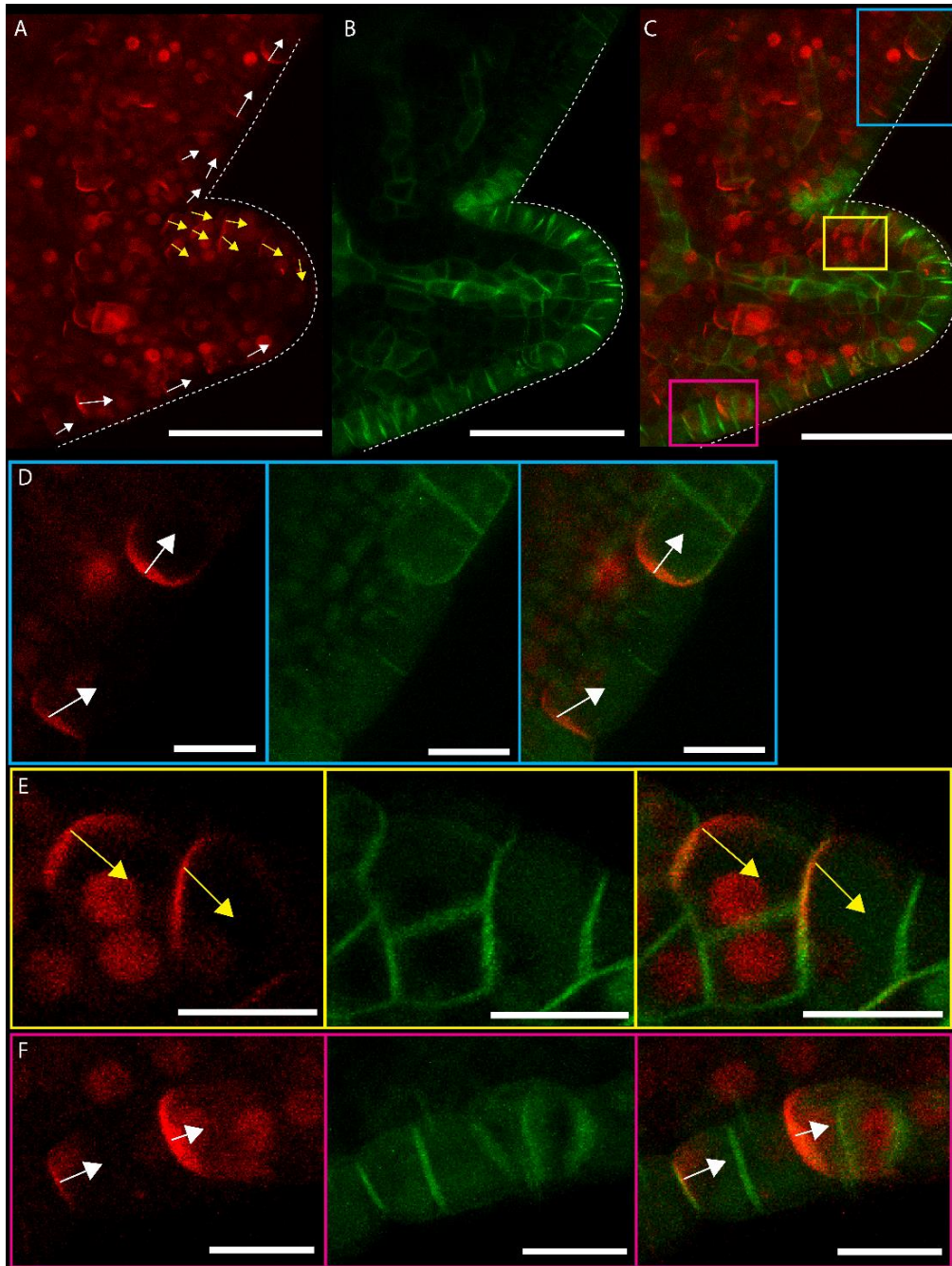


Figure 3.24 Ectopic *35S::mCherry-BASL* mirrors *PIN1* convergence and divergence points at serrations.

(A) Serration of leaf 5 showing *35S::mCherry-BASL* expression (projection). Arrows indicate manually assigned BASL polarity based on the curvature of the BASL crescent, yellow arrows highlight cells in which BASL is not proximally localised and contributes to convergence and divergence points. (B) *PIN1::PIN1-GFP* expression at serration shown in D (projection allowing visualisation of margin cells). (C) *35S::mCherry-BASL* and *PIN1::PIN1-GFP* channels combined. White dotted lines indicate serration outline. Scale bars 50 μm in A-C. (D-F) Regions of serration shown in A-C in blue, yellow and magenta boxes respectively. Z-slices selected to allow visualisation of particular cells due to 3D curvature of serrations. Left panel shows *35S::mCherry-BASL*, middle shows *PIN1::PIN1-GFP*, right shows combined channels. Arrows indicate manually assigned BASL polarity based on the curvature of the BASL crescent. Scale bars are 10 μm .

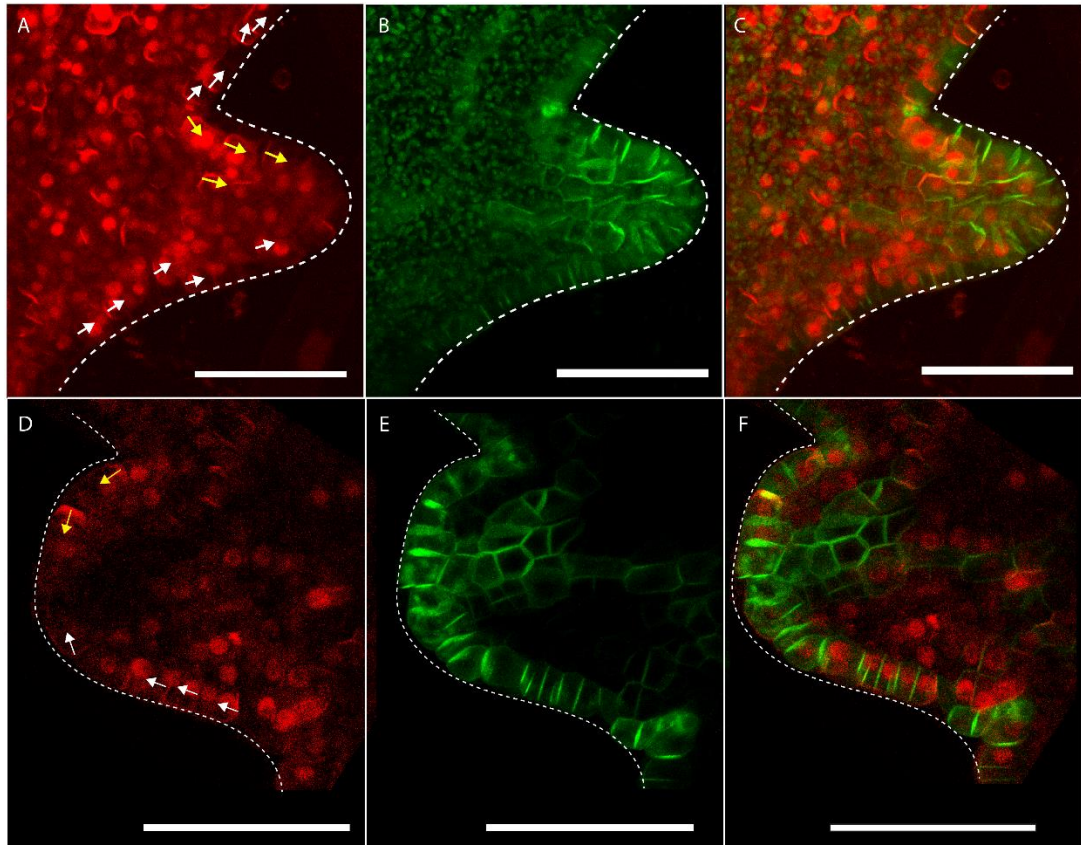


Figure 3.25 Regions of reversed BASL polarity can be seen in the distal region of serrations. Two examples of induced *35S::GFP-BASL* and *PIN1::PIN-GFP* polarity at serrations of leaf 4 (A-C) and leaf 5 (D-F). (A and D) *35S::mCherry-BASL* expression at serration shows BASL convergence points (projections). Arrows indicate manually assigned BASL polarity based on the curvature of the BASL crescent; yellow arrows highlight cells in which BASL is not proximally localised and contributes to convergence and divergence points. (B and E) *PIN1::PIN1-GFP* expression at serration shown in A and D respectively. (C and F) *35S::mCherry-BASL* and *PIN1::PIN1-GFP* channels combined for serration shown in A and D respectively. Z-slices selected to allow visualisation of particular cells due to 3D curvature of serrations. White dotted lines indicate serration outline. Scale bars are 50 μm .

In some serrations, the PIN1 expression was clear and polarised (Figure 3.25 E), whilst in others it was less clear. By contrast, the localisation of BASL to cell corners made it relatively easy to tell which cell expression was related to, compared to PIN1 expression which does not have a preference for corners (e.g. polarity in Figure 3.25 A and D compared to B and E). This makes ectopic BASL a useful marker of polarity in situations where PIN polarity may be difficult to assign and where the direction of polarity, rather than the axial information, is important, for example when comparing and testing models of polarity and growth (Abley, 2014; Abley et al., 2016).

Testing predictions of a tissue-wide polarity field

The observation that BASL polarity forms convergence points at the serration suggests that the underlying polarity system that ectopic BASL reveals has a role in outgrowth formation. However, it is unclear whether this is an active role in which this polarity reversal leads to outgrowth formation, or whether this reversal forms as a consequence of outgrowth formation.

I was able to image PIN1 and ectopic BASL in serrations at earlier stages of development (heat-shocked ~6 DAS). In these leaves, as with primordia, imaging the *35S::mCherry-BASL* was difficult due to auto-fluorescence. In the few examples I was able to image, I observed multiple cells towards the distal region of the serration in which BASL was distally localised. However, this work needs to be repeated to conclusively decipher the timings and consistency of BASL reorientation at early stages of serration development. In the future, it would be informative to time-lapse image serration formation using this line or take carefully staged snapshot images of serration development to establish the timing of BASL reorientation in relation to outgrowth formation.

3.7.3 Ectopic BASL in *kanadi1kanadi2* outgrowths

Another context where PIN polarity reversals are reported is in the ectopic 3D outgrowths of the *kanadi1kanadi2* double mutant (referred to as *kan1kan2*) (Abley et al., 2016). These outgrowths form on the abaxial side of leaves of the *kan1kan2* mutant (Eshed et al., 2004) and may be considered intermediates between serrations and leaf primordia, having aspects in common with both. *kan1kan2* outgrowths have elevated auxin at their tips, dependent on patterns of auxin biosynthetic enzyme expression (Wang et al., 2011). The formation of these outgrowths is preceded by *PIN1::PIN1-GFP* convergence points that form within the proximodistal pattern of PIN1 in the epidermis (Figure 3.26, Abley et al., 2016).

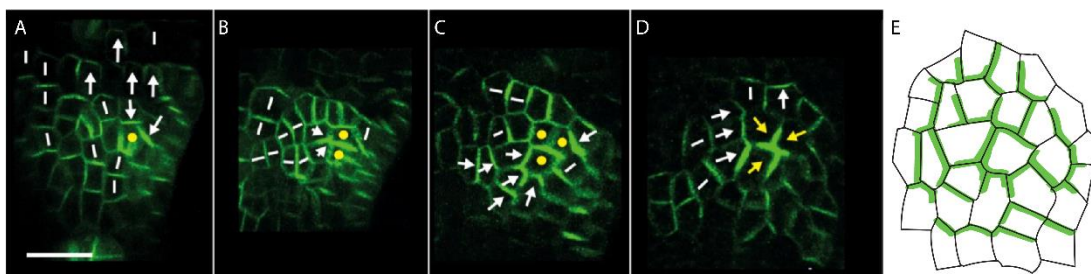


Figure 3.26 PIN1 forms ectopic convergence points at the tip of *kanadi1 kanadi2* outgrowths, preceding outgrowth formation.

(A-D) Adapted from Abley et al., (2016). *PIN1::PIN1-GFP* convergence points at the tip of an emerging *kan1kan2* outgrowth, prior to the emergence of an ectopic outgrowth. Images are (A) 58 hours, (B) 46 hours and (C) 24 hours before (D) outgrowth formation. Yellow dots,

arrows and lines indicate the cells that form the centre of convergence in (D). Arrows indicate inferred PIN1 polarities and lines indicate inferred axes of PIN1 distributions. Scale bars are 20 μm . The scale bar in A applies to all panels in A-E. (E) Schematic illustrating the convergence of PIN1 (green) in cells, preceding the *kan1kan2* outgrowth.

The *kan1kan2* outgrowths therefore represent another developmental situation in which the relationship between PIN1 and ectopic BASL polarity can be tested. As with serrations, there are two hypotheses for the behaviour of ectopic BASL at *kan1kan2* outgrowths (Figure 3.27). One hypothesis is that BASL may remain proximally localised around a *kan1kan2* outgrowth, even where PIN1 reorients. This would result in cells towards the distal region of the outgrowth with PIN1 and ectopic BASL localised to the same end of cells (Figure 3.27 A). Alternatively, ectopic BASL may reorient mirroring PIN1 reorientation. BASL would therefore localise opposite PIN1 and localise to the distal end of cells above the outgrowth (Figure 3.27 B).

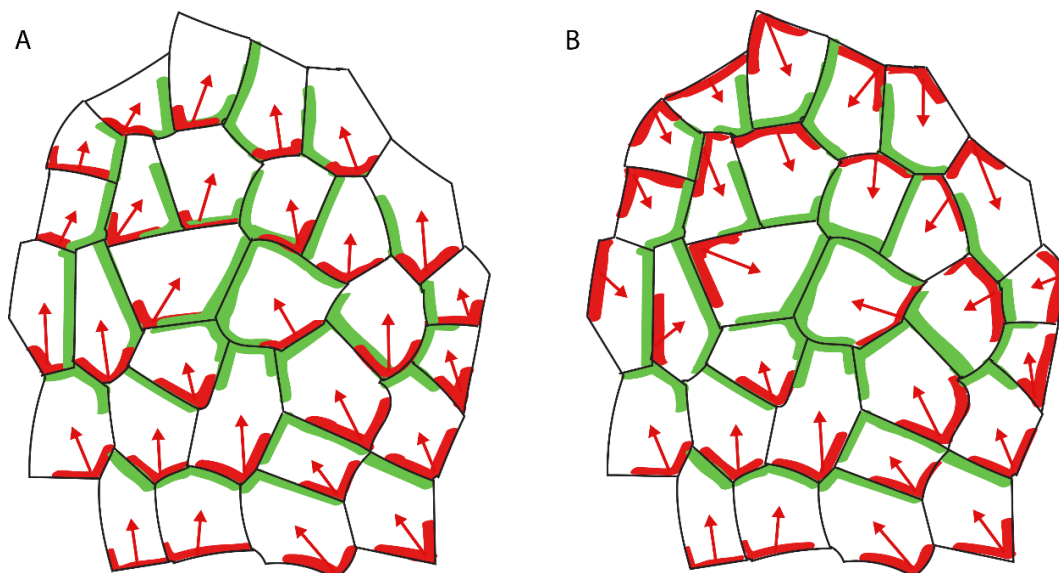


Figure 3.27 Two hypotheses could account for ectopic BASL behaviour at *kan1kan2* outgrowths.

Schematic of two hypotheses for how ectopic BASL will localise at *kan1kan2* outgrowths in relation to previously reported PIN1 expression. In both cases, PIN1 (green) forms a convergence point, localising to the distal end of cells below the outgrowth, and at the proximal end of cells above the outgrowth. In (A), BASL (red) localises at the proximal end of all cells and is therefore localised to the same end of the cell as PIN1 in cells in the distal region of the *kan1kan2* outgrowth. In (B), BASL (red) mirrors PIN1 polarity and forms a convergence point, localising to the proximal end of cells below the outgrowth, and the distal end of cells above the outgrowth. Red arrows indicate hypothesised ectopic BASL polarity, black lines indicate cell outlines.

Testing predictions of a tissue-wide polarity field

To test the behaviour of ectopic BASL around *kan1kan2* outgrowths, I initially used the inducible *35S::GFP-BASL* line to time lapse image GFP-BASL at developing outgrowths. I heat-shocked seedlings 3 DAS and imaged them over consecutive days. Before an outgrowth was visible on the abaxial surface of the leaf, ectopic BASL appeared to be proximally localised in cells where expression could be seen (Figure 3.28 A), though expression was not visible in all cells of the epidermis. I used PI staining to visualise the cell outlines and transferred the plants back to plates in between imaging each day. Over the following 2 days, an ectopic outgrowth formed (Figure 3.28 Biii, Ciii) but no reorientation of BASL was seen (Figure 3.28 Bii, Cii). However, the region of most importance when imaging the outgrowths was the axil of the outgrowth (closest to the leaf) and this was often obscured and difficult to image so whilst these results did not show BASL reorientation, this may be a result of the imaging techniques used. I also noticed that there was often very little, or no, BASL expression in cells of the outgrowth itself. The reasons for this are unknown but could be due to low or non-uniform expression of the 35S promoter in young tissue and this may also interfere with the observation of any BASL reorientation.

I also tried transferring the heat-shocked seedlings to a tracking chamber for time lapse imaging, similar to the method used by Abley et al., (2016) (data not shown). This was challenging due to not knowing which regions of the leaf to image, a lack of plasma membrane marker, and was confounded by the fact that *kan1kan2* outgrowths form less frequently on leaves grown in the imaging chamber (Abley et al., 2016). The preliminary experiments with this line revealed a need for imaging earlier in development before the outgrowth was obscured for imaging and a need for a PIN1 marker so that imaging could be focused on the area where an outgrowth would form.

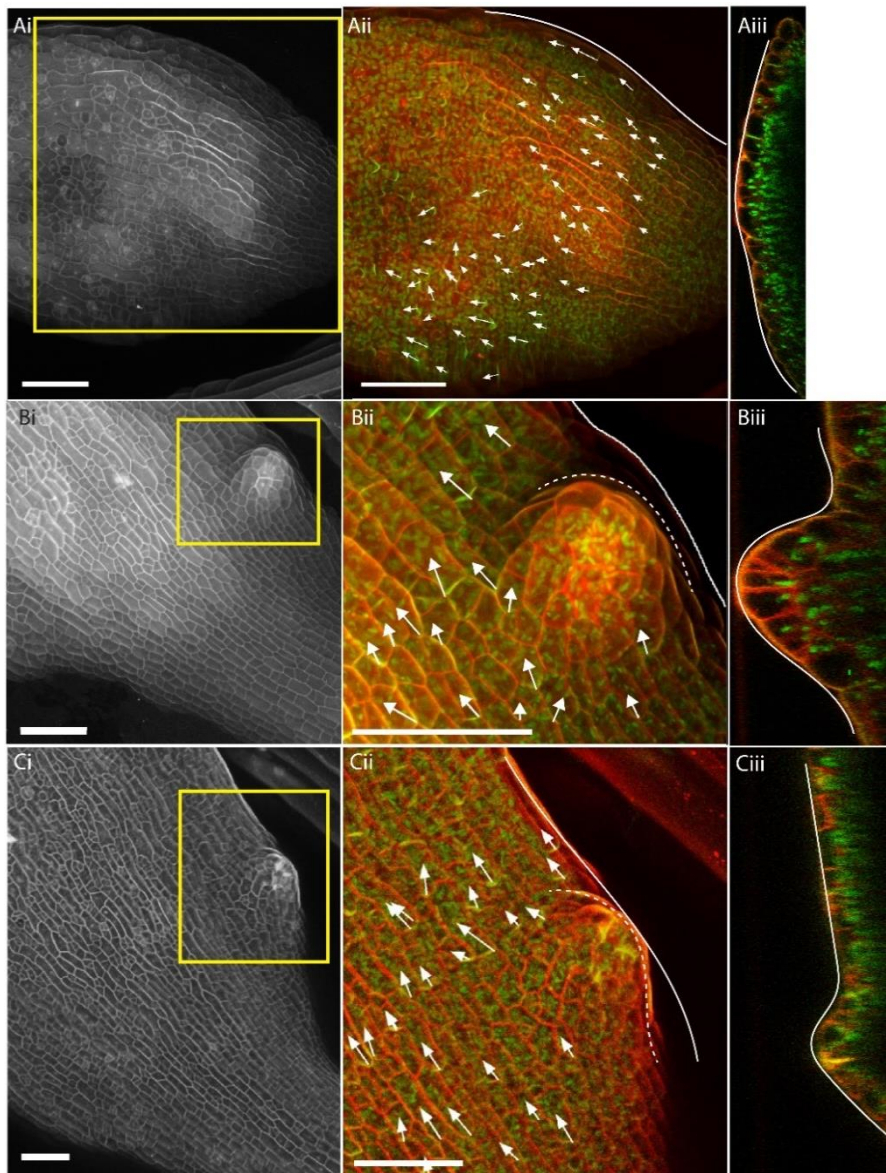


Figure 3.28 No reorientation of ectopic BASL was seen during time-lapse imaging of *kan1kan2* outgrowths.

Abaxial surface of a *kan1kan2* leaf heat-shocked 3 DAS to induce ectopic BASL expression and imaged (A) 3 days later, (B) 4 days later and (C) 5 days later. Left panels show leaf surface and cell outlines. Yellow box shows close-up region in (ii). Middle panels shows *35S::GFP-BASL* expression and cell outlines (PI stained). White arrows show manually assigned BASL vectors where expression could be seen. White dotted line shows outgrowth which is visible in Bii and Cii. Right panels show orthogonal views of the respective stages, cut through at 40 degrees rotation compared to (ii) so panels are proximodistally orientated. White lines in (ii) and (iii) indicate leaf outline. Scale bars 50 μ m.

I heat-shocked seedlings containing *PIN1::PIN1-GFP* and inducible *35S::mCherry-BASL* at 4 DAS and imaged them 3 days later. The PIN1 marker provided an indication of whereabouts the outgrowth would form, and therefore where to look for BASL reorientation. In some

leaves, I did not observe a clear BASL reorientation (Figure 3.29). BASL was not observable in every cell, but in some cells in the distal region of the outgrowth where PIN1 and BASL could both be seen, BASL appeared to be proximally localised, with a few examples of BASL localised to a side wall (Figure 3.29). In the example shown in Figure 3.29, an upregulation of PIN1 is seen, but the orthogonal cross-section of the leaf does not indicate that any outgrowth has formed yet (Figure 3.29 D).

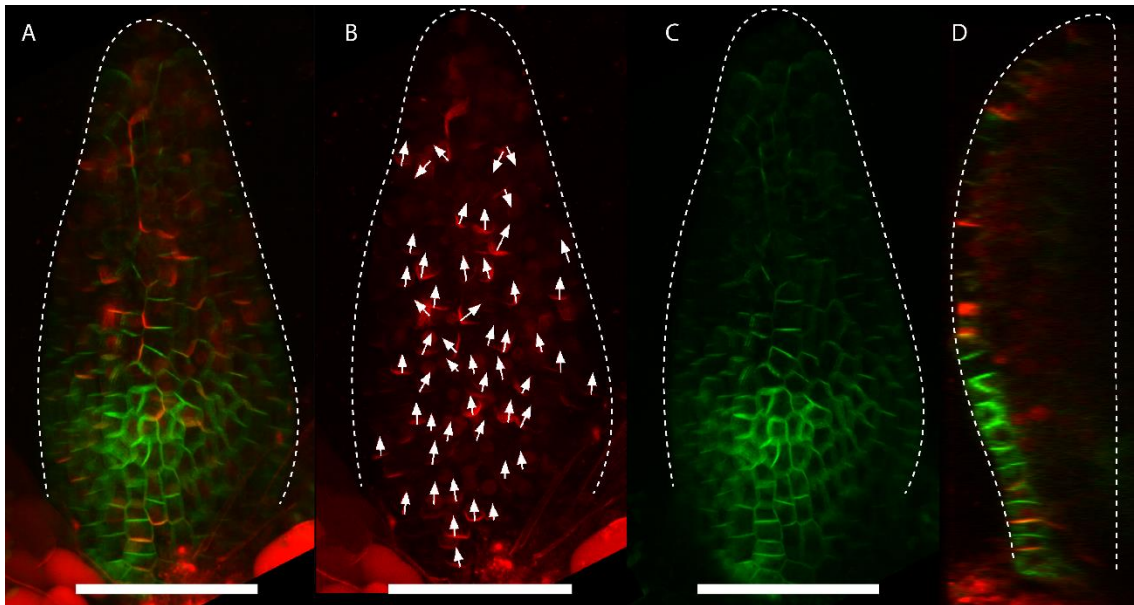


Figure 3.29 Ectopic BASL remains proximal in cells in some *kan1kan2* leaves. (A) Abaxial surface of *kan1kan2* leaf (7 DAS) with *PIN1::PIN1-GFP* and induced *35S::mCherry-BASL*. (B) Induced *35S::mCherry-BASL* in *kan1kan2* leaf (same as in A) with manually assigned arrows indicated BASL polarity. White arrows indicate cells in which BASL is proximally localised, or cells not in the lower half of the lamina where outgrowth formation occurs. (C) *PIN1::PIN1-GFP* expression in *kan1kan2* leaf (shown in A and B). Increased expression in the lower third of the leaf suggests ectopic outgrowth formation. (D) Orthogonal view of leaf in A-C but no outgrowth is visible at this stage. Dotted white lines show leaf outline. Scale bars 50 μm .

In other cases, BASL did appear to be localised to the distal end of some cells around the outgrowth (Figure 3.30). The example in Figure 3.30 shows multiple cells where BASL localises to the distal or side wall (Figure 3.30 B). PIN1 polarity was difficult to assign and therefore it was hard to be sure if PIN1 and BASL were at opposite ends of the cell (Figure 3.30 C). In this case, the orthogonal section of the leaf indicated a subtle change in shape suggestive of early outgrowth formation (Figure 3.30 D). These preliminary results suggest that BASL may reorient in the cells around *kan1kan2* ectopic outgrowths, possibly once outgrowths have formed, (i.e. after reorientation of PIN1).

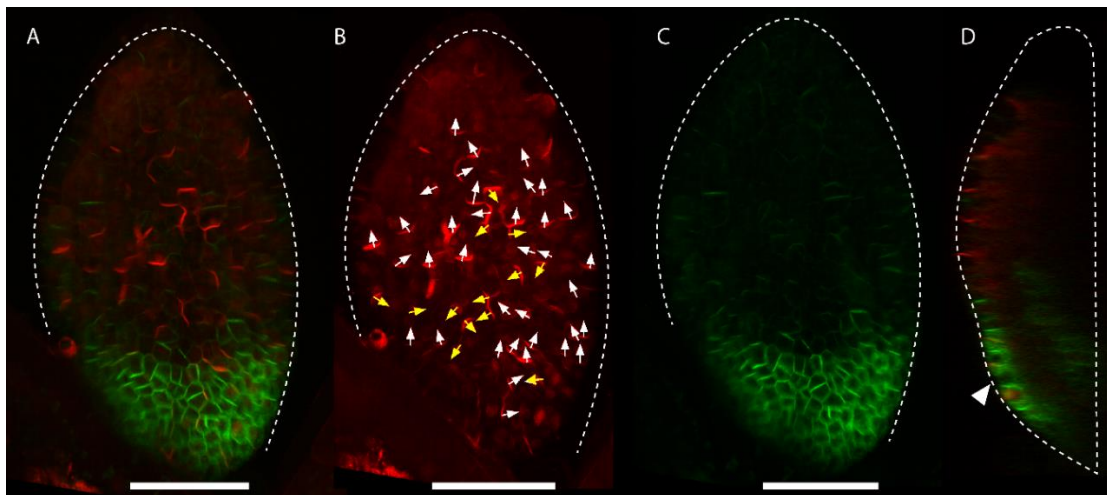


Figure 3.30 Ectopic BASL reorients in some cells around some *kan1kan2* outgrowths. (A) Abaxial surface of *kan1kan2* leaf (7 DAS) with *PIN1::PIN1-GFP* and induced *35S::mCherry-BASL*. (B) Induced *35S::mCherry-BASL* in *kan1kan2* leaf (same as in A) with manually assigned arrows indicated BASL polarity. White arrows indicate cells in which BASL is proximally localised, yellow arrows indicate cells in which BASL is distally or side-wall localised. (C) *PIN1::PIN1-GFP* expression in *kan1kan2* leaf (shown in A and B). Increased expression in the lower third of the leaf suggests ectopic outgrowth formation. (D) Orthogonal view of leaf in A-C showing outgrowth formation (white arrowhead). Dotted white lines show leaf outline. Scale bars 50 μm .

My observations in this mutant indicate that the stage of outgrowth formation may be crucial to observe BASL polarity reorientations, and that this may occur only in a small number of cells. It is challenging to decipher whether BASL localisation to the side or distal wall represents developmentally relevant behaviour, or is associated with the variation known to exist in ectopic BASL polarity (Chapter 2, Figure 2.20). In future experiments, it will be necessary to time lapse image multiple individual *kan1kan2* leaves at higher resolution in order to provide more conclusive analysis of ectopic BASL behaviour in this context.

3.7.4 BASL and PIN in roots

Another interesting context in which to analyse the relationship between BASL, PIN1 and other PINs in the root. In the root, members of the PIN family localise to different faces of cells in different regions of the root (Feraru and Friml, 2008). In the central stele region, PIN1 localises polarly to the basal end of the cell (rootward end) (Křeček et al., 2009; Omelyanchuk et al., 2016; Steinmann et al., 1999). PIN2 localises to the basal side of cortical cells and at the apical side of the root epidermal cells (Abas et al., 2006; Feraru and Friml, 2008; Müller et al., 1998), whilst PIN3 is apolar in roots (Feraru and Friml, 2008). This illustrates the ability

Testing predictions of a tissue-wide polarity field

of PIN proteins to localise to different cell faces in a tissue-specific manner as PIN1 is at the distal or shootward end of cells in the young leaf (Guenot et al., 2012; Scarpella et al., 2006). This raises the question of whether PIN1 and BASL localise at opposite ends in the root, as they do in primordia (Figure 3.21 and Figure 3.22) and serrations (Figure 3.24 and 3.25), or whether roots represent a situation where PIN1 and BASL colocalise (Figure 3.20 B).

In order to image PIN and BASL in the root, I heat-shocked seedlings 4 DAS and imaged both markers in the root tip. Ectopic BASL was localised to the rootward end of cells (Figure 3.31 A). The proximal localisation of BASL was clearest in the epidermis but was apparent throughout the root. PIN1 was localised primarily in the stele, as previously reported, and was localised at the rootward end of cells (though signal was sometimes not clear enough to assign clear polarity to, Figure 3.31 B) (Křeček et al., 2009; Omelyanchuk et al., 2016; Steinmann et al., 1999). The key region to analyse BASL localisation in was therefore the stele, where expression would overlap with PIN1. I found BASL expression was difficult to see in this region in many cells (Figure 3.31 A and C). In cells where BASL expression was observable, it was localised to the proximal or rootward end of cells, as in the rest of the root (Figure 3.31 D, top panel). PIN1 expression was not very clear in these cells (Figure 3.31 D, middle panel), but appeared to be localised at the bottom of cells, as previously described, possibly sharing localisation domains with BASL in these cells (although this is difficult to confirm in these images, Figure 3.31 D, bottom panel).

Further imaging of both polarity markers in the stele is required in order to confirm the localisation of PIN1 and ectopic BASL to the same end of cells. However, this preliminary result suggests that the relationship between PIN1, auxin and ectopic BASL localisation may be tissue-context dependent. This result also confirms that of Dong et al., (2009), where *35S::GFP-BASL* was reported to localise to the lower end of cells in different regions of the root (Dong et al., 2009).

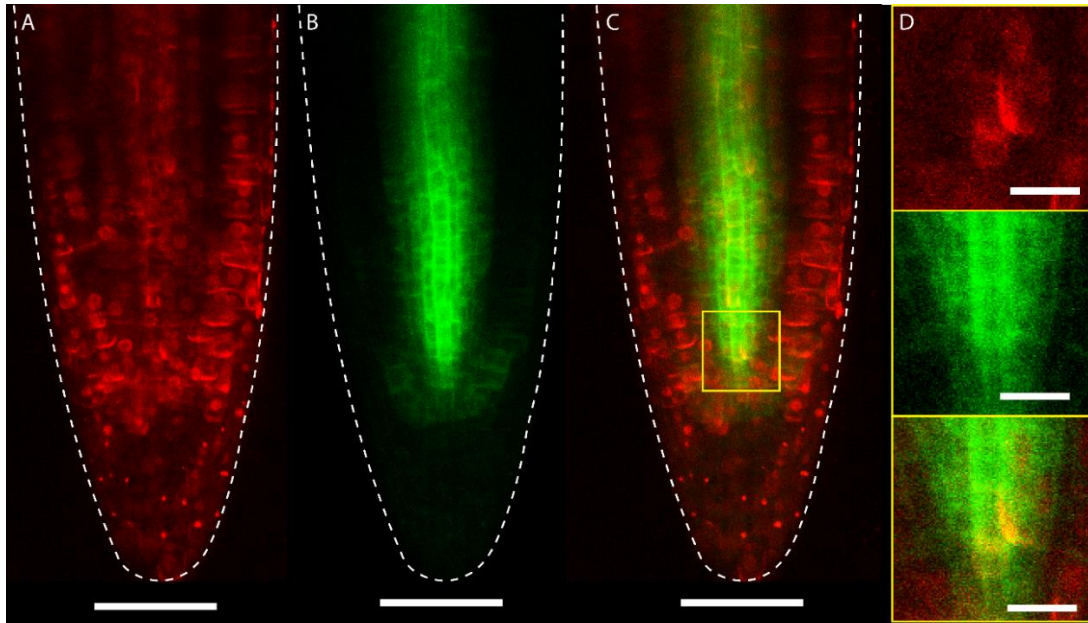


Figure 3.31 *PIN1::PIN1-GFP* and *35S::mCherry-BASL* may both localise proximally in root cells.

Root with (A) ectopic *35S::mCherry-BASL*, (B) *PIN1::PIN1-GFP* and (C) channels combined. (D) Close-up of region shown in yellow box in C. Top panel is *35S::mCherry-BASL*, middle is *PIN1::PIN1-GFP* and bottom is combined channels. White dotted line indicates root outline. Scale bars 50 μm in A-C and 10 μm in D.

3.8 Coordinating polarity across a tissue

The mechanisms that position ectopic BASL at the proximal end of cells remains unknown. Given that BASL here is overexpressed under the 35S promoter, it is likely that the polarity field revealed is not itself dependent on BASL function. Instead, I hypothesise, that BASL interacts with other factors that are localised to the proximal end of cells forming a proximal address. The identity of this proximal address and the mechanisms associated with positioning the proximal address remain unknown. In order to explore the possible mechanisms by which BASL is polarly localised, I tested how factors that have previously been associated with the formation of cell polarity and the coordination of signals across a tissue affect BASL polarity. These factors include polar auxin transport, microtubules and plasmodesmata.

3.8.1 Ectopic BASL and inhibiting auxin transport with NPA

It has been proposed that polar auxin transport is required for the polar localisation of PIN proteins, though there are multiple hypotheses for the mechanism by which this occurs

Testing predictions of a tissue-wide polarity field

(Abley et al., 2013; Bilsborough et al., 2011; Cieslak et al., 2015; Jonsson et al., 2006; Mitchison, 1980; Rolland-Lagan and Prusinkiewicz, 2005; Smith et al., 2006). At serrations, polar auxin transport involving a feedback loop is thought to orient PIN1 towards the serration tip (Bilsborough et al., 2011). Polar auxin transport would be one possible coordination mechanism that could allow BASL coordination across the tissue, particularly given the relationship with PIN1 at serrations.

To test the role of polar auxin transport in BASL localisation, I grew seedlings containing inducible *35S::GFP-BASL* and transferred them to liquid media containing the auxin transport inhibitor N-1-naphthylphthalamic acid (NPA) (either 10 μ M or 100 μ M), before heat-shocking them for 20 minutes to induce BASL. I then imaged the leaves of these seedlings and found BASL was still able to localise to the proximal end of cells in these leaves, at both concentrations (Figure 3.32), similar to the DMSO control (data not shown). This suggests that blocking polar auxin transport is not sufficient to prevent BASL polarisation and coordination. However, it is possible that polar auxin transport is required for the establishment of ectopic BASL polarity, but not the maintenance of it.

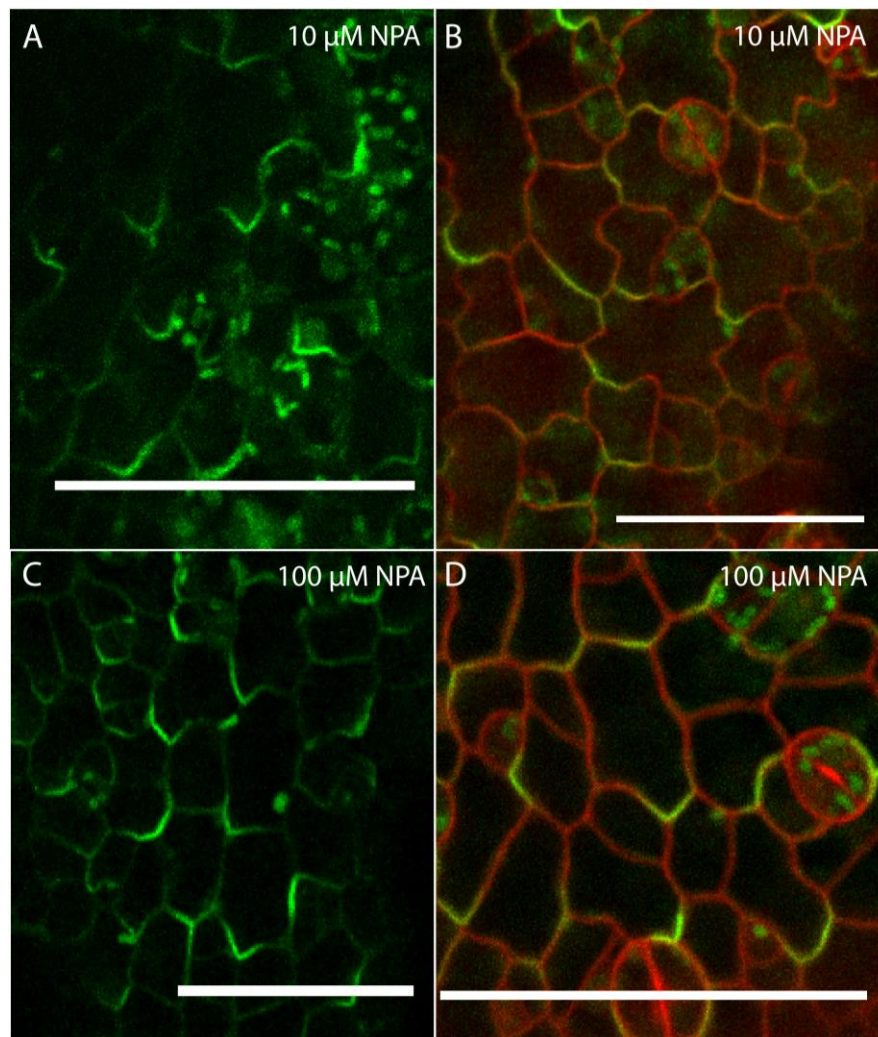


Figure 3.32 Ectopic BASL remains polarised in leaves following treatment with NPA.

(A, B) Ectopic *35S::GFP-BASL* remains polarised to the proximal ends of cells in leaves treated with 10 μM NPA. The leaf in B was also treated with PI to allow visualisation of cells outlines. (C, D) Ectopic *35S::GFP-BASL* remains polarised to the proximal ends of cells in leaves treated with 100 μM NPA. The leaf in D was also treated with PI to allow visualisation of cells outlines. Scale bars are 50 μm .

I therefore grew seedlings on 100 μM NPA from germination before inducing ectopic BASL 2 DAS. In NPA treated seedlings, which exhibited root and leaf shape phenotypes (Figure 3.33 A-D, Casimiro et al., 2001; Hay et al., 2006), ectopic BASL was still proximally localised (Figure 3.33 E), as in the DMSO control (Figure 3.33 F). This indicates that BASL can still polarise and be coordinated across the tissue in the absence of polar auxin transport, when inhibited using NPA.

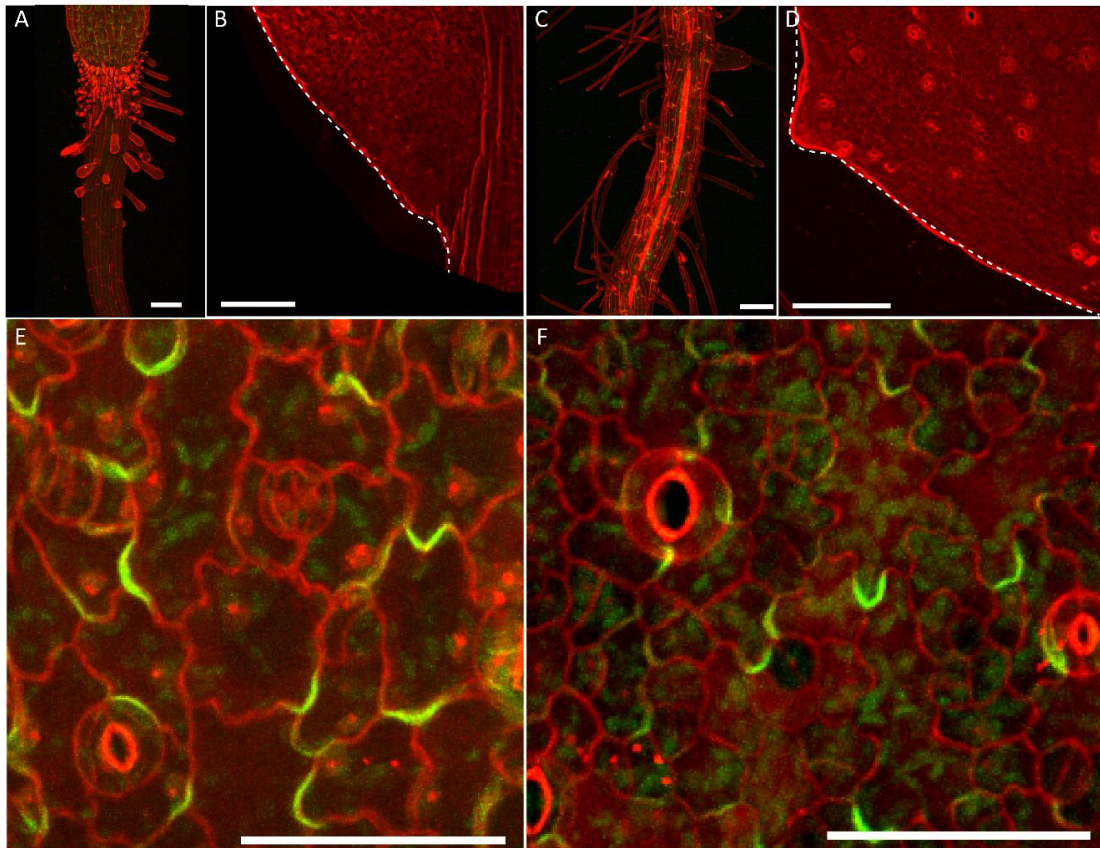


Figure 3.33 Ectopic BASL is able to localise polarly in leaves germinated on NPA.

(A) Root of NPA (100 μ M) treated seedlings did not produce lateral roots or fully developed root hairs. (B) Leaf outline of NPA (100 μ M) treated seedlings did not produce a wild-type serration. (C) Root and (D) leaf outline of DMSO treated seedlings showing lateral roots and root hairs, and serration respectively. Dotted white line indicates leaf outline. Scale bars 100 μ m in A-D. (E) *35S::GFP-BASL* induced in leaves grown on 100 μ M NPA remained proximal. (F) *35S::GFP-BASL* induced in leaves grown on DMSO control. PI staining shows outlines. Scale bars in E-F are 50 μ m.

3.8.2 Ectopic BASL and microtubules

The cytoskeleton has often been linked to the coordination of cellular growth (Bichet et al., 2001; Hamant et al., 2008; Hervieux et al., 2016; Hervieux et al., 2017; Uyttewaal et al., 2012), and has previously been associated with formation of cell polarity (Asnacios and Hamant, 2012; Heisler et al., 2010). Bringmann and Bergmann (2017), reported a role for the microtubule severing protein KATANIN in the coordination of BRXL2 polarity across the leaf; in the *katanin* mutant BRXL2 was able to polarise, but the coordination across the tissue was lost.

It is therefore possible that microtubules, or other components of the cytoskeleton, are involved in the positioning of ectopic BASL. Microtubules could be involved in positioning of the proximal address or in the interaction between ectopic BASL and the proximal address. Using drugs is a common way to probe the impact of the cytoskeleton in various cellular processes (Bringmann and Bergmann, 2017; Fu et al., 2005; Geldner et al., 2001; Hamant et al., 2008).

To test if microtubules are required for positioning ectopic BASL, I destabilised microtubules with 20 μ M oryzalin, before heat-shocking seedlings to induce BASL. I wanted to test whether microtubules were required for the establishment of the ectopic BASL polarity field, rather than the maintenance of BASL's proximal localisation. I imaged *35S::TUA6-GFP* seedlings (Ueda et al., 1999) after 4 hours of 20 μ M oryzalin treatment and confirmed that microtubules were no longer intact (Figure 3.34 A), compared to the DMSO control (Figure 3.34 B). The *35S::TUA6-GFP* and inducible *35S::GFP-BASL* seedlings were then heat-shocked for 20 minutes and kept in oryzalin-containing media for 2 days. 2-days after heat-shock, *35S::TUA6-GFP* seedlings were imaged again confirming that the microtubules were still depolymerised (Figure 3.34 C, D). In the oryzalin treated *35S::GFP-BASL* plants, BASL remained polarised and localised to the proximal end of cells (Figure 3.34 E, F), as in the DMSO control (Figure 3.34 G). The lack of lobes on the pavement cells in oryzalin-treated seedlings compared to the control (compare Figure 3.34 E to Figure 3.34 G) also confirmed that the treatment had depolymerised microtubules, as they are required for pavement cell lobing (Ambrose and Wasteneys, 2008; Ambrose et al., 2007; Fu et al., 2005). I also stained seedlings with PI to visualise the cell outlines (Figure 3.34 F). These findings suggest that microtubules are not required for the polarisation of ectopic BASL.

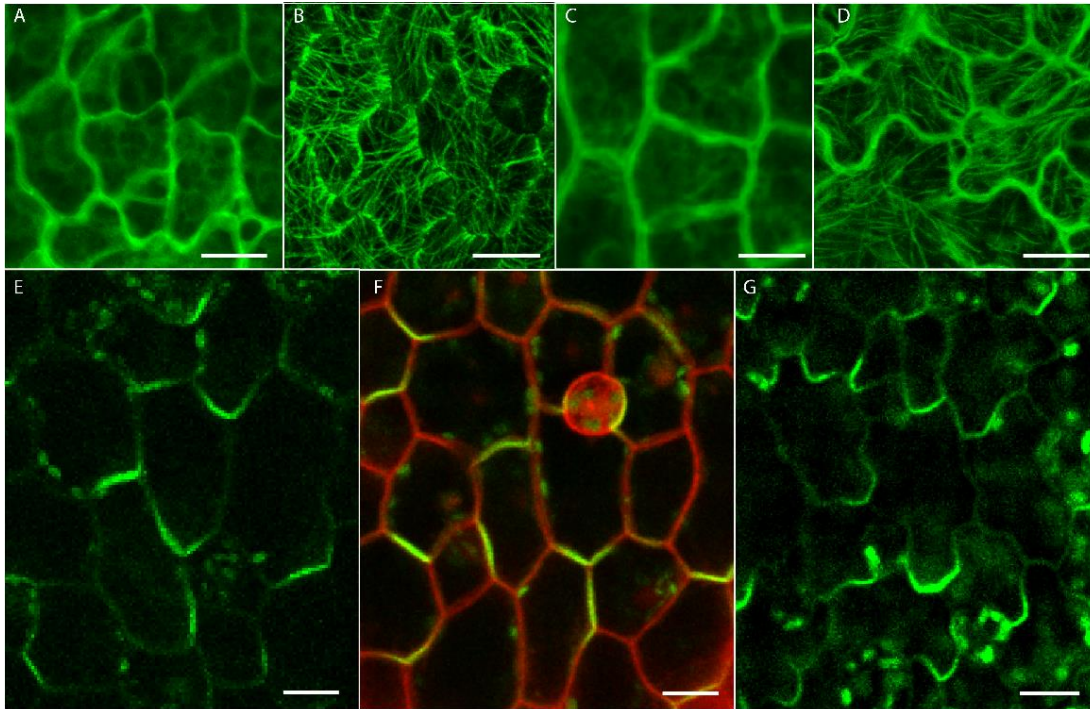


Figure 3.34 *35S::GFP-BASL* localisation remains proximal in cells treated with oryzalin. (A) *35S::TUA6-GFP* after treatment with 20 μ M oryzalin for 4 hours showing microtubules depolymerised. (B) *35S::TUA6-GFP* after treatment with DMSO equivalent to 20 μ M oryzalin for 4 hours showing microtubules intact. (C) *35S::TUA6-GFP* after treatment with 20 μ M oryzalin for 2 days showing microtubules still depolymerised. (D) *35S::TUA6-GFP* after treatment with DMSO equivalent to 20 μ M oryzalin for 2 days showing microtubules remain intact. (E) *35S::GFP-BASL* remains proximally localised after treatment with 20 μ M oryzalin for 2 days. (F) *35S::GFP-BASL* remains proximally localised (cell wall stained with PI (red)) after treatment with 20 μ M oryzalin for 2 days. (G) *35S::GFP-BASL* proximally localised after treatment with DMSO equivalent to 20 μ M oryzalin for 2 days.

3.8.3 Coordination of ectopic BASL in leaves with closed plasmodesmata

To test the impact of closing plasmodesmata on the coordination of ectopic BASL polarity, I crossed the inducible *35S::GFP-BASL* line into a line carrying *35S::mCherry-TMCT* which is reported to have reduced intercellular flux through plasmodesmata, as shown by flux assays and an increase in callose deposition (Caillaud et al., 2014). These plants are often stunted as a result of constitutively closed plasmodesmata, although the phenotypes appear to be variable and somewhat environmentally sensitive. I heat-shocked seedlings 7 DAS and imaged them 2 days later. I found that ectopic *35S::GFP-BASL* remained proximally localised in a coordinated manner in the leaves of this line (Figure 3.35 A).

In some seedlings, and particularly in cotyledons, I also observed unusual pavement cell shapes (Figure 3.35 B). The lobes of the pavement cells were often spiky, rather than rounded as is normally the case. In this line, this phenomenon seemed to be patchy, not occurring consistently across all leaves and cotyledons, or all regions of these organs. Unusual pavement cell shapes in this line and other lines with disrupted plasmodesmata has been reported previously (Christine Faulkner, personal communication), although it is not known why this occurs. In regions of the cotyledon where cells appeared spiky, BASL was typically localised to the proximal end of the cell (Figure 3.35 C). Interestingly, BASL was sometimes seen in two proximal lobes of the cell, rather than the usual single lobe (Figure 3.35 C, cells with asterisks), though this was not seen in all cases and would require further investigation in order to be robust. I had previously observed this on rare occasions in particularly large cells of the leaf (data not shown), but the occurrence of double-labelled cells appeared more frequent in section of the cotyledons with closed plasmodesmata. This observation should be analysed quantitatively with adequate controls, such as analysis of BASL patterning in a wild-type cotyledon, in order to allow conclusions to be drawn.

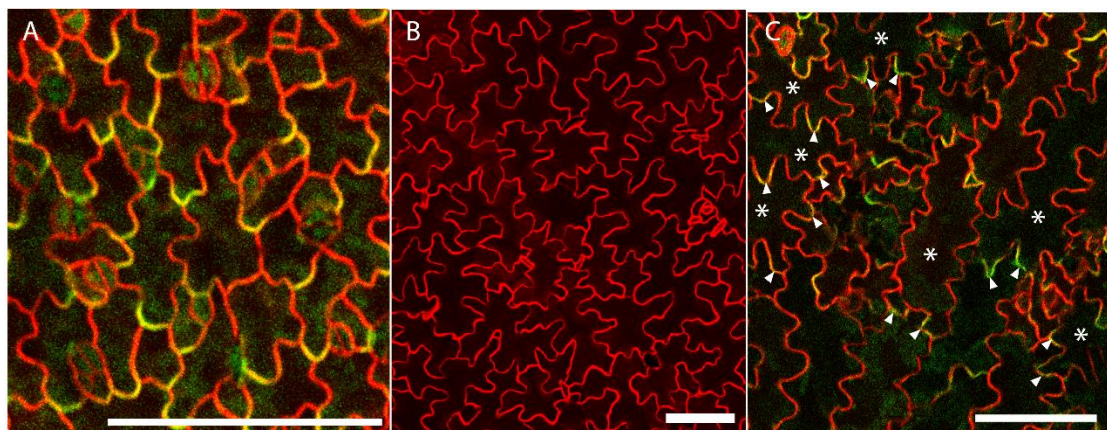


Figure 3.35 Ectopic BASL localises to the proximal end of cells when induced in leaves and cotyledons with constitutively closed plasmodesmata.

(A) *35S::GFP-BASL* induced in *35S::mCherry-TMCT* line with constitutively closed plasmodesmata. BASL localised to the proximal end of cells. (B) *35S::mCherry-TMCT* cotyledons showing spiky lobes in pavement cells. (C) *35S::GFP-BASL* induced in cotyledons with constitutively closed plasmodesmata showing spiky cells. BASL localised to the proximal end of cells and to two lobes in some cases (cells with asterisks). Scale bars are 100 μm .

3.9 BASL and response to mechanical stress

A key consideration in the establishment of polarity is the role of mechanical stresses. The ability of mechanical stresses to reorient or be involved in the establishment and coordination of cell polarity in plants is something that has been hypothesised (Asnacios and Hamant, 2012; Bhatia et al., 2016; Bringmann and Bergmann, 2017). However, experiments untangling the role of mechanical stresses in polarity can be very difficult to interpret for a number of reasons: mechanical cues and polarity are likely both involved in the growth of tissues and cells, mechanical stresses in a tissue remain very difficult to accurately measure, and, until now, polarity markers distinct from PINs have not been well characterised.

Recent work by Bringmann and Bergmann (2017) illustrated that the localisation of BRXL2, an interactor of BASL, can be altered by mechanical forces. This work quantified BRXL2 polarity across the leaf and cotyledon and reported a statistically significant difference in BRXL2 polarity in cotyledons that had been mechanically stretched compared to those that had not (Bringmann and Bergmann, 2017). Such a result has significant implications in the understanding of tissue cell polarity. However, these results are difficult to interpret conclusively and are complicated primarily by two factors. Firstly, it is necessary in such experiments that a leaf or cotyledon is experiencing the expected mechanical stress, but this cannot be easily measured or tested. Whilst some new techniques are being developed for measuring stresses (Robinson et al., 2017), this was not used in the work of Bringmann and Bergmann (2017). Secondly, in this work, a statistical approach was used to compare stretched cotyledons with un-stretched cotyledons. Any differences observed could therefore be due to other factors, such as analysing different regions of the cotyledon. It would be useful to be able to conduct a similar experiment imaging leaves or cotyledons while they were still being stretched, and also comparing the localisation of a polarity marker before and after stretching in the same tissue.

In order to test the effect of mechanical stress on BASL polarisation, I worked with an undergraduate student (Jamie Spooner) who developed a device to image cotyledons whilst under tension. The work outlined below was largely conducted by Jamie, with supervision from myself, and is included here as preliminary data relevant to understanding the ectopic BASL polarity field.

In order to image the same leaf, before, during and after stretching, a device needed to be developed that could stretch leaves, such as the prototype device used in Bringmann and

Bergmann (2017) and could also fit under a confocal microscope. A device was built, similar to that used in Bringmann and Bergmann (2017) (following discussions with members of the workshops team at the John Innes Centre) but using a vice mechanism rather than simply stretching by hand. During his undergraduate project, Jamie Spooner redesigned this device and used the same basic idea to build a stretching device that would allow stretching and imaging at the same time (Figure 3.36 A).

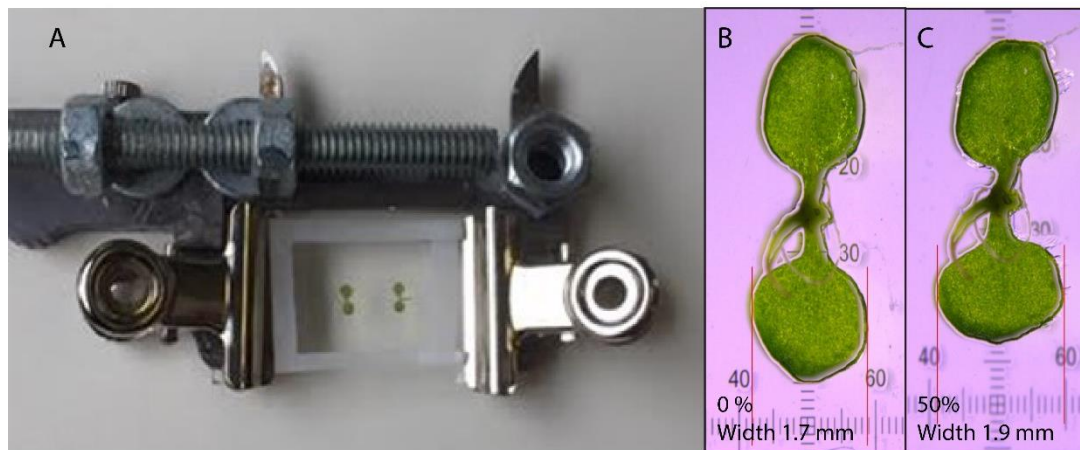


Figure 3.36 A small stretching device allowed seedlings to be imaged whilst being stretched.

(A) The stretching device (built by Jamie Spooner) uses a vice mechanism glued onto 2 bulldog clips so that, when the screw is turned, the bulldog clips move apart. Silicone-based membrane is attached between the clips and seedlings stuck onto the membrane. Membrane and adhesive are the same as used in Bringmann and Bergmann (2017). (B and C) An *A. thaliana* seedling attached to the membrane and imaged (B) before stretching and (C) whilst being stretched. The percentage in B and C shows the amount the membrane has stretched. Leaf width in B and C is shown. Images in B and C are taken by Jamie Spooner.

Using this device, it was possible to stretch the membrane by 50% and observe a change in cotyledon shape, becoming wider in the direction of stretch (Figure 3.36 B and C). Jamie was then able to induce ectopic BASL expression by heat-shock, attach seedlings to a membrane and stretch them; imaging before stretching (Figure 3.37 A, left panel), straight after stretching the membrane (Figure 3.37 A, middle panel), and after seven hours (Figure 3.37 A, right panel). Imaging BASL in cotyledons before and after stretching (after 7 hours) did not reveal any change in the relative BASL localisation in individual cells (Figure 3.37 B and C), although the positioning relative to the leaf may have varied as a result of rotation and growth of the tissue (Figure 3.37).

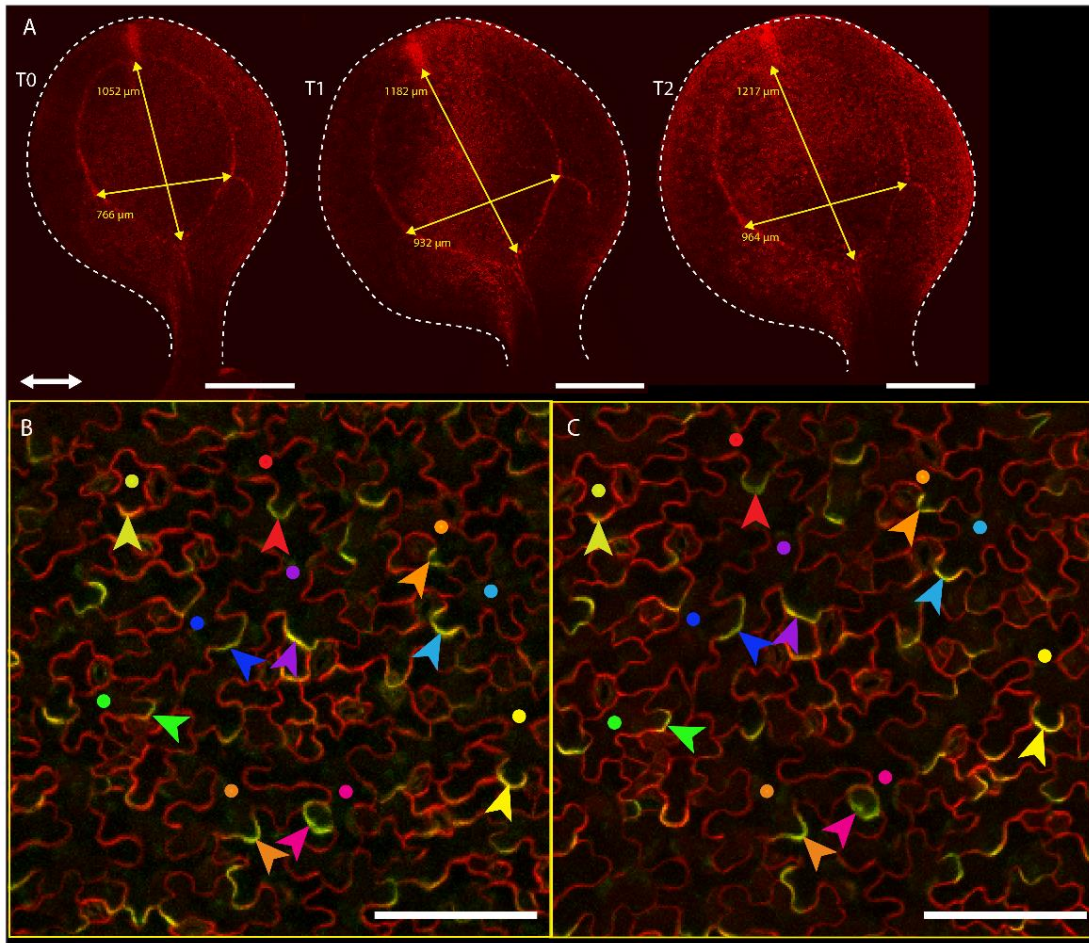


Figure 3.37 Mechanical stretching of a cotyledon showed no ectopic BASL reorientation. (A) Cotyledons expressing inducible *35S::GFP-BASL* and RFP-PM were imaged whilst stuck to the stretching device at various stages. T0 (left panel) shows the cotyledon before the membrane is stretched, T1 (middle panel) is whilst the membrane is being stretched by 50% (imaged just after stretching) and T2 (right panel) is the same cotyledon after being stretched for 7 hours. Scale bar in A is 500 μm. (B) Cotyledon shown in A at T0 (before stretch) and (C) at T2 (50% stretch for 7 hours). BASL signal is marked by coloured arrowheads, corresponding to the cell with the same coloured dot. Colours are maintained between B and C and show BASL localisation to the same lobes at both time points. Sale bars in B and C are 100 μm. Images taken by Jamie Spooner.

These results may indicate that mechanical stresses do not alter BASL polarity, which contrasts to the result shown by Bringmann and Bergmann (2017) with BRXL2. However, a number of reasons may account for these differences including the difficulties in ensuring the cotyledon remained adhered to the membrane, and the use of BASL in an ectopic context, compared to BRXL2 in a native context.

3.10 Testing polarity outside of a tissue context using BY-2 cells

The work of the previous chapter illustrates that BASL reveals a polarity field that is independent of the stomatal lineage. Work by Abley et al., (2013) hypothesises that polarity is a fundamental property of individual cells and predicts that cells can polarise in the absence of external cues in a non-tissue context. Within a tissue, it is not easy to remove external cues. To test ideas associated with polarity outside of a tissue context, I used BY-2 cells, a tobacco cell line commonly used in cell biology work (Nagata et al., 1992). These chains of cells represent a potentially informative situation in which to test not only the existence of polarity outside the usual plant tissue context (although notably, these cells still have neighbours), but also to probe possible polarity coordination mechanisms. I transformed BY-2 cells with *35S::GFP-BASL*. Transformation of the cell lines with the inducible *35S::GFP-BASL* line would require multiple transformations with different constructs and therefore, for simplicity, I used the non-inducible *35S::GFP-BASL* line. However, analysis using the inducible line in the future may be informative.

I found that BASL localised to one end of cells within the chain of BY-2 cells in varying patterns. In some cells chains, the BASL signal appears to be partially coordinated, often localising to the same end of a number of sequential cells, and sometimes then switching to the opposite end mid-way through a chain of cells (Figure 3.38 A). The ends of a chain of cells usually had BASL signal associated with them (Figure 3.38 A-D). In some cases, BASL appeared to be localised to a region where there was also a protrusion or outgrowth in the cell or was associated with a potentially unusual division plane (Figure 3.38 B). As observed in cells in the leaf, BASL often localised to the corners of BY-2 cells (Figure 3.38 A, B). Generally, each cell had one BASL domain but, in some cells, multiple domains were observed (Figure 3.38 C, D). Where this was observed, the domains were usually, but not always, localised at the opposite short ends of the cells (Figure 3.38 C, D). The observation of multiple BASL domains was often in larger cells (Figure 3.38 C), but not always (Figure 3.38 D) and may suggest that this phenomenon is linked with cell size or age.

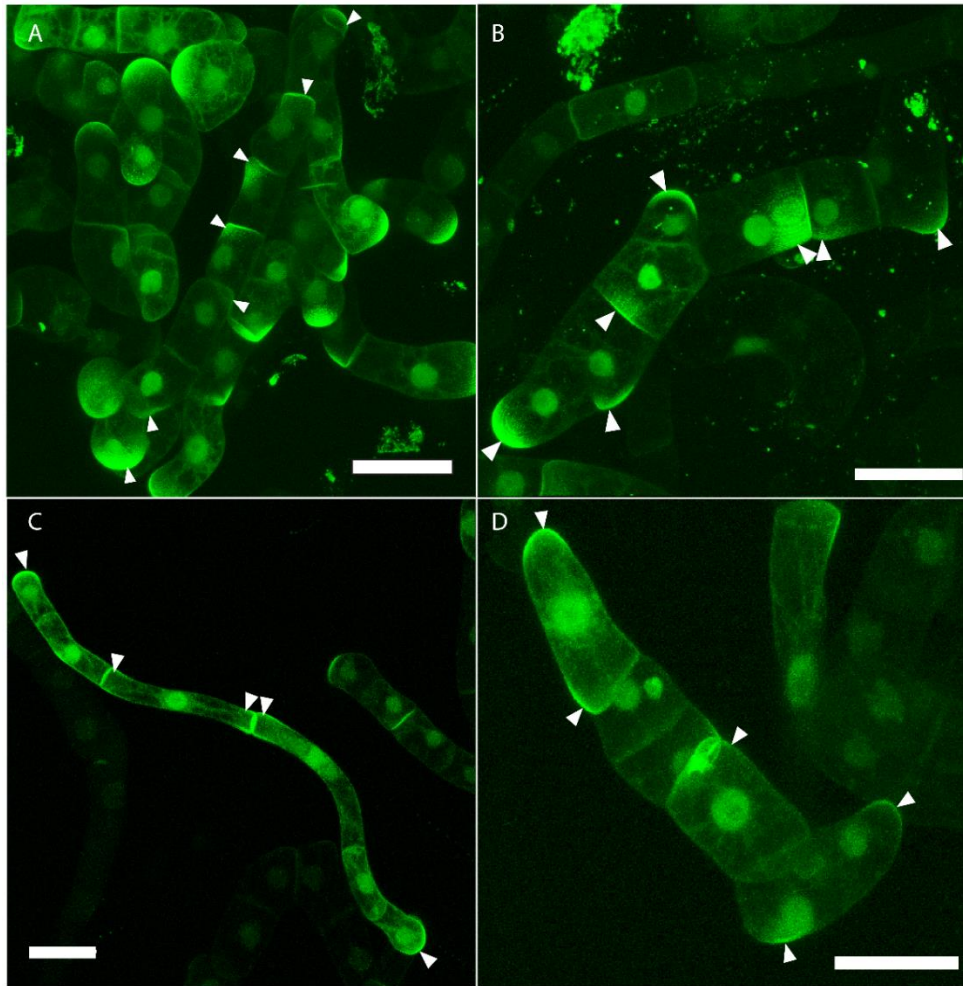


Figure 3.38 *35S::GFP-BASL* in BY-2 cells is polarly localised.

Examples of *35S::GFP-BASL* expressed in BY-2 cells. White arrowheads indicate BASL signal. (A) BASL signal localised to one end of the upper five cells, and the lower end of the lower two cells. (B) BASL signal localised to one end of each cell. In the third cell from the left, the signal is not localised to the corner and the fourth cell has an unusual division branching from another cell. (C) Example of a chain of cells where BASL localised to both short ends of some cells. (D) Example of a chain in which the end cells have 2 BASL domains. Scale bars are 50 μm .

The polarisation of BASL to ends and corners of BY-2 cells is intriguing and differs from the reported axial localisation of PIN1 in BY-2 cells (Boutté et al., 2005). However, these cells are linked to one another and therefore cannot provide a context in which to test the spontaneous polarisation of a single cell, as predicted by modelling (Abley et al., 2013). In order to test whether BASL can remain polarised in a single cell context, I digested the cell wall of BY-2 cells using cellulase and pectolyase to form protoplasts.

I imaged the protoplasts after 4-6 hours of digestion and found that, in some protoplasts, BASL was still able to polarise to one side (Figure 3.39). BASL signal was not observed in all protoplasts (Figure 3.39 B, C), and in some cases the protoplast had very bright GFP signal that did not appear polarised (Figure 3.39 A). Cases where polarised BASL signal was observed indicate that BASL polarisation does not require a cell wall. To further confirm this, staining of the cell wall, for example with calcofluor, could be conducted to verify that the cell wall was completely removed. In addition, numbers of protoplasts with polarised BASL should be quantified.

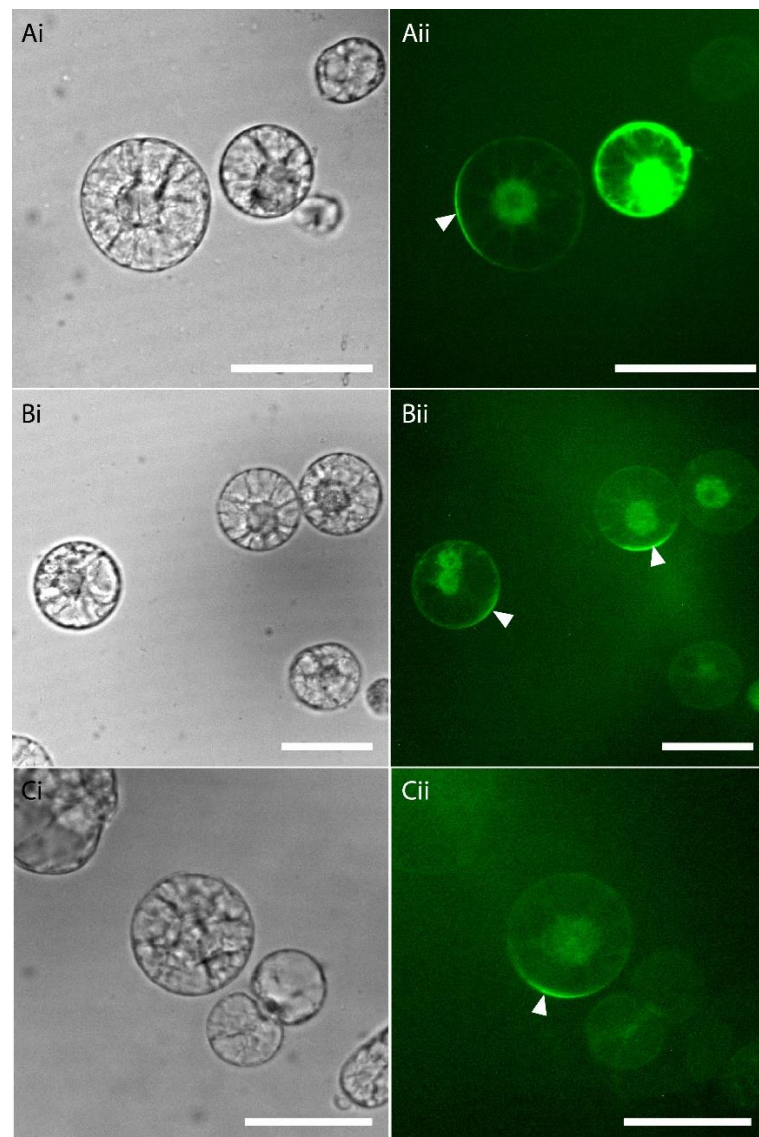


Figure 3.39 Ectopic BASL can be polarised in individual BY-2 protoplasts.

Example of BY-2 protoplasts (formed from BY-2 cells expressing *35S::GFP-BASL*) imaged after 4-6 hours of cell wall digestion. Left hand panel shows bright field image, right hand panel shows GFP channel. (A) Some protoplasts had very bright apolar GFP signal. (B, C) Some protoplasts did not express BASL. In other protoplasts, BASL is polarised (white arrow). Scale bars are 50 μm .

Testing predictions of a tissue-wide polarity field

These results provide evidence that polarity can exist in a single plant cell, as suggested by Abley et al., (2013) and that the cell wall is not required, although it remains possible that the cell wall plays a role in the coordination of polarity.

Protoplasts can be regenerated into cell chains (Hasezawa and Syono, 1983) in a process controlled by the cytoskeleton (Zaban et al., 2013). It would be interesting to test whether BASL is able to remain polarised in regenerated protoplasts and whether the polarity revealed by BASL could play a role in the anisotropic elongation, growth and division of regenerating protoplasts. To test whether BASL remains polarised in a stable manner in protoplasts and whether this might provide insights into the control of cell growth, I transferred protoplasts (digested for 5 hours in enzyme solution) into FMS (Fukuda, Murashige and Skoog) media overnight for regeneration (Hasezawa and Syono, 1983; Zaban et al., 2013). I imaged the protoplasts the next day and was still able to observe polarised BASL in some protoplasts (Figure 3.40). This indicates that the polarity of BASL may be stable in protoplasts, although going forward it will be important to use cell wall staining to ensure that all cells are protoplasts before transferring to regeneration media. I observed some cells with polarised BASL and with an unusual shape (Figure 3.40 C) which could indicate regeneration but, after only a few hours, it is more likely that these cells had not fully lost their cell wall.

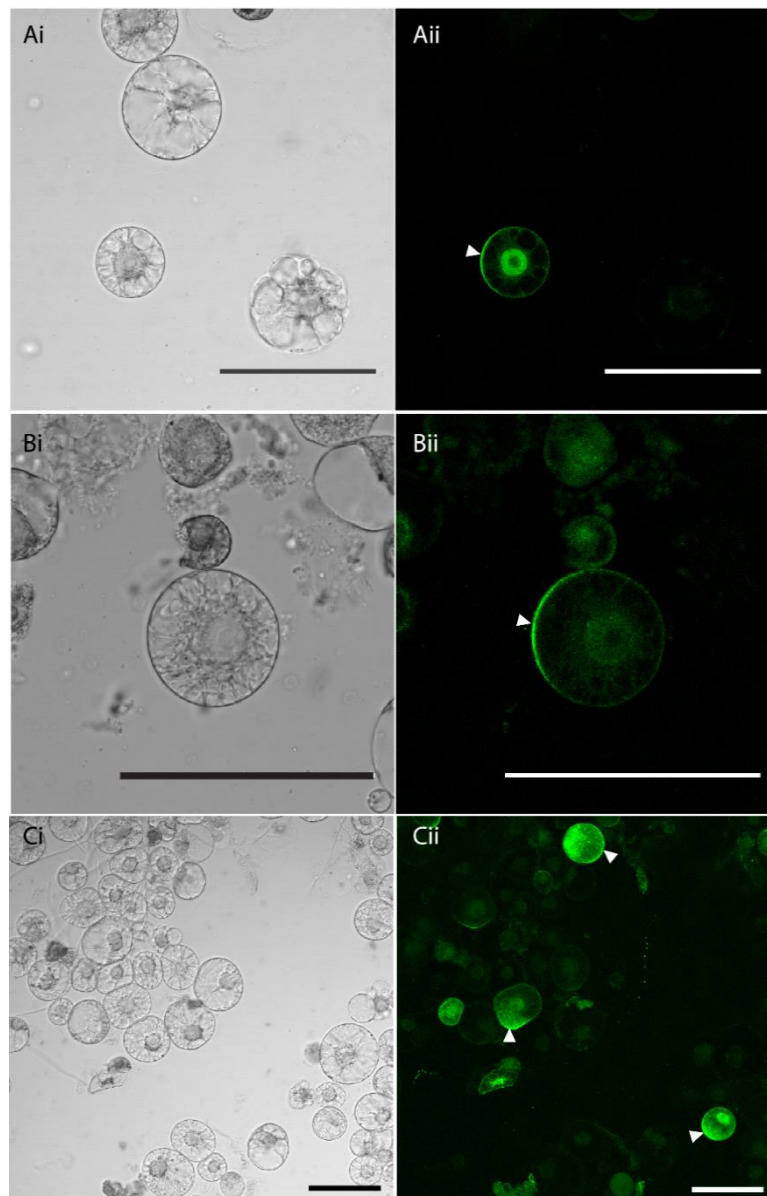


Figure 3.40 BASL remains polarised in protoplasts resuspended in regeneration media overnight.

Examples of protoplasts expressing *35S::GFP-BASL* that were transferred to regeneration media (FMS media) after 5 hours of cell wall digestion. Protoplasts were imaged after being in FMS media overnight. Left hand panel shows bright field image, right hand panel shows GFP channel. White arrowheads indicate where BASL is polarised in a protoplast. Scale bars are 100 μm .

I also used the protocol in Zaban et al., (2013) to attempt to regenerate protoplasts over three days. I incubated protoplasts in FMS media in the dark in sealed petri dishes for three days before imaging. I could not confirm that all cell wall had been removed prior to this and hence this experiment should be repeated, ensuring this is the case using cell wall staining. The protoplasts were alive after three days and some showed polarly localised BASL (though

many did not). The protoplasts had not all kept their spherical shape and were often bulbous and unusual shapes (Figure 3.41). In these cells, BASL was often localised to the end of outgrowths (Figure 3.41) and, in some cases, there appeared to be multiple BASL domains (Figure 3.41 A and C). In addition, I observed cells with two nuclei possibly indicating a failure in cytokinesis (Figure 3.41 A), although notably I also occasionally observed this in non-regenerated protoplasts (Figure 3.39 B).

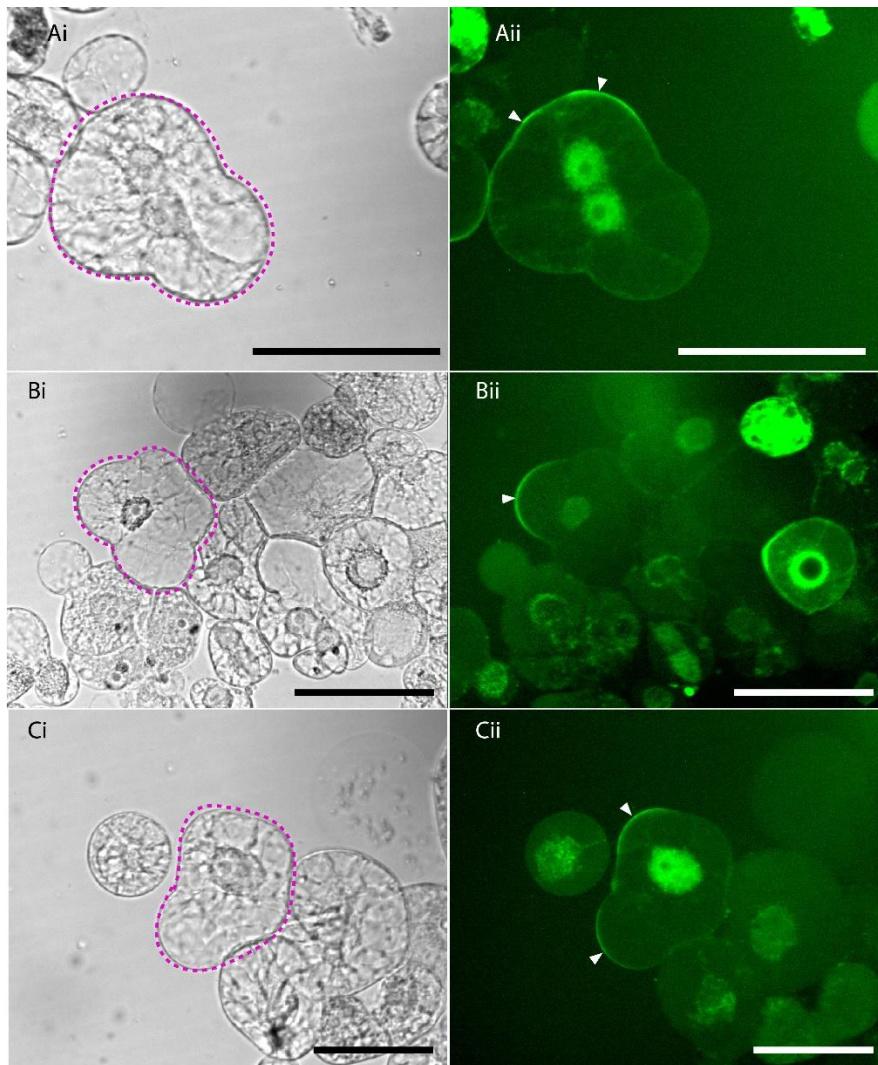


Figure 3.41 BASL localises to the end of outgrowths in regenerating protoplasts. Examples of regenerating protoplasts with BASL. Cells were often unusual shapes and not all cells had BASL signal. When observed asymmetrically, BASL was often localised to the tips of cell bumps and was sometimes observed in multiple domains (A and C). Left hand panel shows bright field image, right hand panel shows GFP channel. Magenta outline shows individual cells with unusual shapes. White arrowheads indicate where BASL is polarised in a protoplast. Scale bars are 50 μm .

These preliminary results are difficult to interpret conclusively as cells were not confirmed to have lost their cell wall before protoplast regeneration and results of BASL localisation in protoplasts and regenerating protoplasts were variable. The regeneration of protoplasts with polarised BASL could indicate that polarity has a role in outgrowth formation. Primarily, these results highlight a need for more detailed studies using BASL in protoplasts.

3.11 Discussion

3.11.1 Relationship between cell anisotropy, cell orientation and polarity

For a tissue-wide polarity field, as described in Chapter 2, to have a significant developmental or physiological relevance, it needs to be analysed in relation to the growth of cells or tissues. Whilst previous studies have shown that cell polarity, or predicted polarity, may be correlated with growth directions (Bringmann and Bergmann, 2017; Kuchen et al., 2012), here I have highlighted the issues associated with making links between polarity and growth or cell anisotropy in anisotropic cells. I show that, indeed, BASL polarity and cell shape are correlated and I have also analysed ectopic BASL polarity in near-isotropic cells. This showed that the ectopic BASL polarity field diverges at later stages of development independent of cell anisotropy and this divergent polarity pattern is not simply a consequence of the way polarity is assigned to the centroid of anisotropic cells.

The issue of assigning cell polarity arises because of the differences between a continuous mathematical polarity field, often used in computational modelling, in which every point has a vector, and a discrete polarity field that can exist in a biological tissue with cells. This distinction between these types of polarity field should be made clear, particularly if modelling work using a continuous polarity field also contains discrete cells, such as in Fox et al., (2018).

There is a two-way relationship between polarity and growth, as indicated in Figure 3.6 and thus it remains difficult to draw conclusions about causality in the relationship between polarity and growth. Growth may alter polarity due to mechanical connectivity of the tissue, as shown in the deforming organiser-based model in Kuchen et al. (2012) and polarity could

plausibly provide directional information to guide growth, as has been previously predicted (Coen et al., 2017; Kennaway et al., 2011; Kuchen et al., 2012).

In addition, cell divisions further complicate the relationship between growth and cell polarity. Future work could involve live-tracking of ectopic BASL dynamics, particularly in regions of the leaf with more isotropic cells and where the confounding effect of cell shape is therefore reduced. Crossing the ectopic BASL line into different shaped leaves, such as *as1* which has rounded leaves (Byrne et al., 2000; Ori et al., 2000) or *angustifolia* which has long narrow leaves (Kim et al., 2002; Tsuge et al., 1996) could also prove useful, for example, through live-tracking and comparison of growth directions and polarity patterns to wild-type.

I have shown that, in addition to cell shape having a confounding effect on cell polarity, cell long axis orientation also adds complexity to understanding properties of the polarity field. I show that, in a wild-type leaf, the majority of cells approximately align with the proximodistal axis of the leaf. To uncouple the relationship between cell polarity and cell long axis orientation, I analysed ectopic BASL localisation in cells in which the long axis was approximately mediolaterally aligned in both wild-type leaves and the *gap1gap2* cotyledon and show that BASL tended to localise to the proximal long wall of the cell. This analysis, both in wild-type and *gap1gap2*, suggests that the proximal address with which BASL interacts does not localise to one, or both ends of the cell long axis. Whilst the mechanisms involved in positioning the proximal address remain unknown, it could indicate that the proximal address is responsive to a proximally or distally emanating signal, for example, as suggested in a cell-cell coupling model of polarity establishment (Abley et al., 2013) and in models of *A. thaliana* leaf development (Kuchen et al., 2012).

3.11.2 BASL in relation to the ROP pathway and the cytoskeleton

Discussion of pavement cell polarity, involving the ROP pathway, usually refers to pavement cells being multi-polar. The preference of BASL to localise to a lobe, rather than a neck of pavement cells, partly resembles the localisation of ROP2 to lobes (Fu et al., 2002; Fu et al., 2005), and might suggest a link between the ROP pathway and the polarity system underlying BASL localisation. However, it is difficult to see how a BASL could interact with the ROP pathway and remain localised to a single lobe. Pavement cell polarity has also been linked to auxin signalling and the cytoskeleton (Chen et al., 2015; Xu et al., 2010) providing a possible link between the polarity of a single cell (involving the cytoskeleton and ROP pathway), and plausible mechanisms for tissue-wide coordination (involving auxin).

It would be interesting to test the localisation of inducible BASL in *rop* mutant lines, such as *rop2*. In this work, I used *gap1gap2* to analyse the role of BASL in cells that do not align with the leaf midvein axis. The PHGAP proteins (absent in this mutant) are known to interact with multiple ROPs and show comparable localisation patterns (Stöckle et al., 2016). Pavement cells in the *gap1gap2* mutant lack lobes but BASL remains proximally localised in a distinct domain. This shows that BASL localisation is not dependent on lobes and may be independent from the ROP pathway. Dong et al., (2009) suggest that BASL may act upstream or independently of ROPs due to the lack of BASL-induced cell outgrowths in a *rop2* mutant. It would be interesting to quantify this further and perhaps model growth and division in the *gap1gap2* mutant background. The cell orientation pattern is somewhat confounded by the stomatal divisions. Crossing *gap1gap2* to *speechless* and inducing ectopic BASL in a *gap1gap2spch* background would be useful to remove the spiral stomatal divisions which complicate the analysis of polarity in the double mutant.

I show that ectopic BASL is able to polarise in a coordinated manner in leaves treated with oryzalin. This suggests that microtubules are not directly involved in the establishment of the polarity. However, microtubules and the cytoskeleton represent an important plausible mechanism linking polarity with cell outgrowths and hence further work, for example, perturbing other parts of the cytoskeleton with drugs, or analysing inducible BASL in mutants with compromised cytoskeletons will be crucial to understanding the link between cell polarity and cell growth or development.

3.11.3 Relationship of ectopic BASL polarity field and PIN

I have shown that BASL and PIN1 localise to the opposite sides of cells in the *A. thaliana* leaf primordia. Ectopic BASL tends to localise to cell corners in a distinct crescent whilst PIN1 tends to localise across the whole face of the cell. This difference in domains and localisation patterns might suggest that BASL does not simply localise antagonistically to PIN1 and that there may be different mechanisms underlying how the two proteins localise at the membrane.

I have also analysed ectopic BASL and PIN1 expression at serrations and *kan1kan2* outgrowths where PIN1 is known to undergo polarity reorientations and form convergence points (Abley et al., 2016; Bilsborough et al., 2011; Hay et al., 2006). At serrations, I found that ectopic BASL reorients to localise at the distal of side wall of cells, thus mirroring the convergence points of PIN1. It would be interesting to further analyse the dynamics of BASL

Testing predictions of a tissue-wide polarity field

localisation during serration development. This might allow more detailed understanding of the timing of outgrowth formation relative to polarity reversal. If, for example, polarity reoriented before outgrowth formation occurred, this could provide evidence for polarity directing growth. In the absence of such experiments, these observations show a relationship between PIN1 and BASL polarity, but do not currently allow further understanding of the link between polarity and growth. In my imaging of *kan1kan2* outgrowth formation, I observed some cells where ectopic BASL appeared to reorient where outgrowth formation was likely to occur. However, there were other instances where reorientation was not seen and therefore further work is required to draw conclusions about BASL polarity in this context. I often could not observe BASL signal in the young *kan1kan2* outgrowth, perhaps due to using the 35S promoter.

The observed changes in ectopic BASL polarity at serrations and possible changes around *kan1kan2* outgrowths may suggest interaction between tissue cell polarity, marked by BASL, and regional polarity factors, such as KANADI and possibly CUC proteins. In future, ectopic BASL polarity could also be studied in relation to CUC2 expression, for example, by inducing CUC2 sectors and observing BASL dynamics. Similarly, ectopic BASL may provide a tool for understanding how individual cell polarities respond to regional polarity factors during leaf organogenesis. Experiments using ectopic KANADI and HD-ZIP expression, such as those carried out by Caggiano et al., 2017, may elucidate any role of cell polarity in leaf and outgrowth formation.

The observation that ectopic BASL mirrors PIN1 polarity at serrations suggests the two polarity systems are linked. A feedback loop involving auxin transport and epidermal PIN1 expression has been shown to be necessary for serration formation: serrations cannot form in a *pin1* mutant, but epidermal PIN1 expression is sufficient to restore serrations (Bilsborough et al., 2011). PIN1 at serrations is therefore not simply a polarity marker, but part of the feedback process needed for outgrowth formation (Bilsborough et al., 2011). The mirrored behaviour of PIN1 and ectopic BASL at serrations suggests that the polarity revealed by ectopic BASL is coupled to the same polarity-coordinating mechanism as for PIN1. Whether this is a direct relationship between ectopic BASL and PIN polarity or whether both polarity markers somehow interact with or respond to a common underlying polarity system is not clear. The hypothesised molecular address to which ectopic BASL is directed may be

linked to auxin transport, or another common underlying polarity system to which PIN can also respond.

I show that growing plants on NPA, or transferring them to NPA after inducing BASL, does not prevent coordinated ectopic BASL polarisation. This indicates that polar auxin transport may not be the mechanism positioning BASL to the proximal end of cells, but further mechanistic work is required, such as testing BASL in *pin* mutants and biochemical analysis, to understand the factors and mechanisms responsible for BASL polarisation. It is also worth noting that NPA does not necessarily inhibit all polar auxin transport in tissues and that, if some auxin transport occurs, its role in polarity coordination cannot be ruled out. PIN does not fully disappear from the membrane when treated with NPA. Some reports suggest that PIN becomes apolar following NPA treatment (Hay et al., 2006) while other studies are less clear (Heisler et al., 2005; Scarpella et al., 2006); these differences may partly arise due to the difficulty in assigning PIN polarity.

Whilst the work here focusses on leaves, the root represents a further context in which to analyse the relationship between PIN and BASL. My preliminary imaging suggests that BASL, like PIN1 in the vasculature, localises to the rootward end of root cells. This would represent an unusual context in which PIN1 and BASL colocalise, although further imaging is needed to confirm this, and it needs to be confirmed that PIN1 and BASL are both proximal in the same cell type or same cell. It was previously shown that, in the vasculature of equivalently staged roots (notably not in the same roots), both PIN1 and BASL localise to the rootward end of cells (Dong et al., 2009). Different members of the PIN family localise differently in a cell type dependent manner in roots (Křeček et al., 2009), for example, PIN2 localises at the apical end of cells in the root epidermal cells but is basal in cortical cells (Feraru and Friml, 2008; Müller et al., 1998). The relationship between PIN and BASL may therefore be cell-type dependent and further investigations, for example, in *pin* mutants and during root hair development, may provide useful contexts in which to further understand PIN and BASL polarity. In addition, the results described here raise the question of how ectopic BASL polarity is established with respect to the meristems of the plant, both the shoot apical meristem and the root meristem.

3.11.4 Role of plasmodesmata in polarity coordination

I tested the role of plasmodesmata as a potential mechanism involved in the coordination of polarity across a tissue. I used a line with constitutively closed plasmodesmata (previously

Testing predictions of a tissue-wide polarity field

shown by reduced flux and increased callose deposition, Caillaud et al., 2014) and induced BASL in this context. I found ectopic BASL could still be polarised in these leaves and also observed spiky cells in this line where BASL was sometimes localised to two proximal lobes. It would be interesting to explore this further in the future, quantifying this phenomenon.

These results show that BASL can be coordinated across a tissue even in leaves with reduced intercellular flux due to increased callose deposition at plasmodesmata, although notably, it is challenging, or perhaps impossible, to completely close plasmodesmata throughout development due to their essential role. It might be possible to close plasmodesmata more using inducible constructs. I would have anticipated any effects of plasmodesmatal closure to affect cell-cell coordination, which does not appear to be the case. It is therefore possible that signals involved in coordinating polarity are still able to move through the plasmodesmata. It is interesting that plasmodesmata closure can also lead to cell shape phenotypes and, whilst the reason for this remains unknown, plasmodesmata could play an indirect role in polarity coordination, for example via auxin transport, and thus may warrant further investigation in the future.

3.11.5 Mechanics and polarity

I started to develop tools to test the role of mechanical stresses in the coordination of tissue cell polarity and then worked with and supervised an undergraduate project student, Jamie Spooner, who carried out this preliminary work. He developed a tool, based on that used in Bringmann and Bergmann (2017), that also allowed leaves or cotyledons to be imaged on a confocal microscope whilst being stretched. This is an advance on the statistical methods used previously (Bringmann and Bergmann, 2017) but is relatively simple and easy to make, unlike some more sophisticated tools recently developed (Robinson et al., 2017).

The initial experiments indicated that mechanical stresses do not alter BASL polarity, which contrasts to the result shown by Bringmann and Bergmann (2017) with BRXL2. A number of reasons may account for these differences. It was difficult to ensure the cotyledon remained flat and stuck to the membrane for the period of stretching. This is important in order to ensure that the cotyledon was experiencing tension throughout the experiment and is likely a difficulty found by Bringmann and Bergmann (2017). Without being able to measure the stress being experienced by the tissue, using more advanced methods such as Robinson et al., (2017), it is possible that slippage of the leaf on the membrane occurred. Furthermore, over the period of a few hours, the leaf or cotyledon would have grown which may also serve

to reduce the tension experienced by the tissue. The direct comparison between stretched and unstretched leaves made in this work on a small section of tissue using ectopic BASL is not directly comparable to the statistical approach using native BRXL2 line used in Bringmann and Bergmann (2017). Whilst these differences may not account for the different results obtained, it is necessary to repeat these experiments, ideally using the method allowing imaging whilst stretching rather than a statistical approach, in order to verify any conclusions.

3.11.6 BASL in BY-2 cells

I conducted preliminary work using *35S::GFP-BASL* in BY-2 cells to explore polarity outside of a tissue context and in protoplasts. I showed that BASL tends to localise to the ends of BY-2 cells, sometimes both ends, and has a preference for cell corners, much like in leaves. In some cell chains, BASL localisation seemed coordinated across multiple cells, but this observation requires quantification to be conclusive. This localisation pattern of BASL is markedly different to the axial localisation of PIN1 in BY-2 cells (Boutté et al., 2005).

BY-2 cells also offer a context in which to study polarity inheritance at cell division. In the stomatal lineage, endogenous BASL localises opposite the new cell wall, creating a spiral pattern of polarity, as described by Robinson et al., (2011) and shown in Chapter 2 of this work. It is possible that ectopic BASL also follows this pattern of inheritance. If we take a single cell with proximally localised ectopic BASL and follow this pattern of inheritance in a single file of cells, the polarity would become disrupted with some proximodistal polarity vectors, and some disto-proximal polarity vectors (Figure 3.42 A, Bi, Ci). This division rule alone would not account for the consistent proximal localisation of BASL in cells. Alternatively, BASL could be localised proximally in daughter cells following divisions through an unknown mechanism. In this case, if we start with a cell with proximally localised BASL, the proximodistal polarity would be amplified through rounds of division (Figure 3.42 A, Bii, Ciii). A combination of polarity inheritance rules at cell division is also possible, for example, dependent on cell type and this could lead to a largely proximodistal polarity in cell files, with polarity vectors that deviate from proximodistal in some cells (Figure 3.42 Cii). Whilst the rules governing polarity inheritance at cell division remain unknown, the work in Chapter 2 suggests that BASL localisation opposite the new cell wall is not sufficient to generate the patterns of ectopic BASL seen here. There may be additional rules for polarity inheritance in non-stomatal cells. BY-2 cells showed coordinated BASL in some cell files and not in others and therefore could indicate a role for multiple polarity inheritance rules. BY-2 cells

expressing ectopic BASL represent a useful tool to further understand polarity inheritance at cell divisions due to their characteristic growth and division in cell files, and their amenability to live-imaging. In addition, it would be interesting to generate BY-2 or suspension cell lines that lacked SPCH (and therefore lacked any stomatal fate) and compare the inheritance of polarity in these cells.

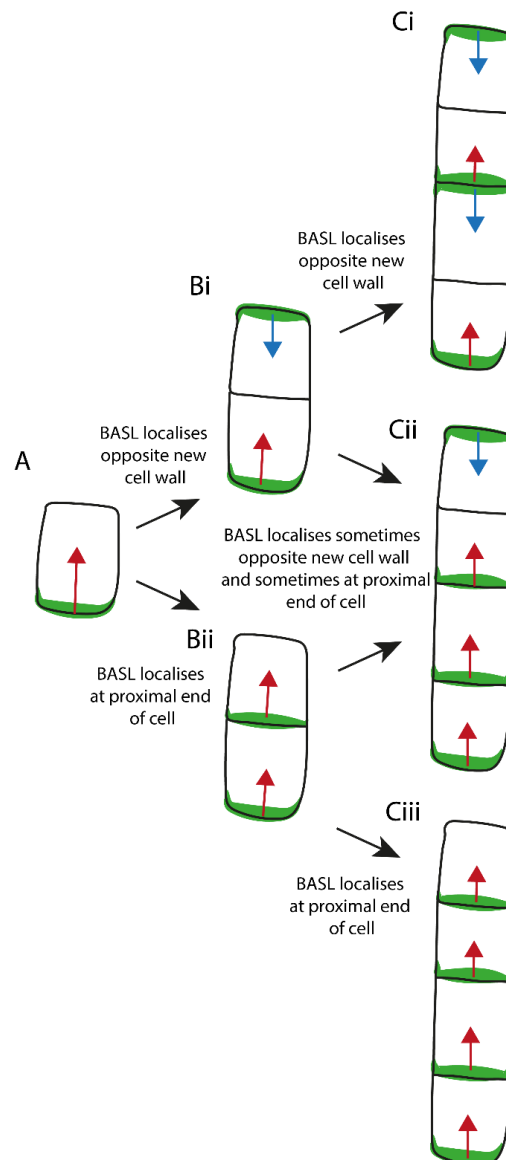


Figure 3.42 Possible hypotheses for BASL polarity being inherited at cell division.

(A) Ectopic BASL (green crescent) localised at the proximal end of a cell could be inherited in different ways at cell division. (Bi) Ectopic BASL could remain proximal in daughter cells following division, or (Bii) ectopic BASL could localise opposite the new cell wall following division. (Ci-iii) After multiple divisions, proximodistal may have been (Ciii) amplified or (Ci) disrupted, depending on how BASL polarity is inherited. (Cii) A combination of polarity inheritance rules at cell division is also possible and would lead to different pattern of polarity. Red and blue arrows indicate polarity orientation, based on the colour scheme used in Chapter 2.

I also showed that BASL can be polarly localised in protoplasts and that this localisation is not lost within minutes (as is reported to be the case with PIN1 in protoplasts when cell-cell contact is lost, Boutté et al., 2005). This provides preliminary evidence for the existence of polarity systems in plant cells in a non-tissue context and may therefore support a model of polarity establishment involving intracellular partitioning (Abley et al., 2013), though the molecular components of such a system remain unknown. I show some evidence for the polar localisation of BASL in regenerating protoplasts which, to some extent, may correspond to the cell outgrowths observed with *35S::GFP-BASL* in roots (Dong et al., 2009). The anisotropic elongation of BY-2 protoplasts in response to geometric cues has been shown to be dependent on auxin (Zaban et al., 2015). It would be informative to conduct similar experiments exploring the role of auxin in BY-2 cells using BASL as a polarity marker. My results thus far are inconclusive but highlight a need for multiple avenues of future work. Through developing this BY-2 line, I have provided tools that might be able to address the role of the cytoskeleton and cell division in cell polarity, the relationship between polarity and growth, and perhaps the molecular and biochemical mechanisms underlying polarity establishment and maintenance.

3.11.7 Concluding remarks and future work

This work aimed to test hypotheses and address questions that arise following the characterisation of a tissue-wide polarity field. In particular, I focussed on the uncoupling of cell shape and cell orientation from polarity, the relationship between ectopic BASL polarity and PIN1 polarity, and tested the role of plausible polarity coordination methods. I used mutants to test the role of BASL in different contexts, as well as analysing ectopic BASL in different developmental contexts including serrations. I also tested possible systems involved in polarity establishment and coordination through perturbing the cytoskeleton and plasmodesmata, and stretching cotyledons. The results from these experiments highlight a need for further investigation. For example, further controls and experiments are required to understand why these results with BASL and mechanical stress differ from those of Bringmann and Bergmann (2017).

This work has shown that PIN1 polarity and BASL polarity are linked, through the analysis of both polarity markers at serrations. This would suggest that PIN and BASL polarity are also linked in other situations. The analysis undertaken in this project focuses on epidermal BASL in the leaves. The vasculature and roots represent two contexts in which PIN polarity is

Testing predictions of a tissue-wide polarity field

markedly different to that in the leaf epidermis. Further imaging, including more time lapse imaging (as in Abley et al. (2016)) and imaging different plant organs with both BASL and PIN may provide further insights regarding the relationship between these markers of polarity and polarity fields. In addition, other mutants, such as *pin* mutants, *rop* mutants, and those with different leaf shapes, combined with live tracking, may allow further insights into the role of BASL polarity in relation to known polarity systems and allow the role of polarity in growth to be better understood.

Auxin is considered a likely polarity coordination mechanism and the link between BASL and PIN polarity indicates that there are indeed shared features between BASL and PIN polarity. Future work investigating the role of auxin in the establishment and maintenance of BASL polarity will be informative. It remains possible that the polarity system underlying the ectopic BASL polarity field is linked to auxin directly, but it may also be the case that auxin is responsive to other unknown systems underlying polarity. BY-2 cells may represent a useful way to probe the fundamentals of the underlying polarity system through drug applications and biochemical approaches.

Whilst I have described the ectopic BASL polarity field and tested its role in different contexts, a key question remains of what BASL interacts with to reveal this polarity field. I hypothesise that there is a molecular address in cells which is composed of unknown molecular components. Discovery of these components will be key to uncovering the mechanisms involved in the establishment of tissue cell polarity in plant planar organs. To carry out such investigations, as biochemical approach, such as co-immunoprecipitation, is required to identify interactors of BASL and potential novel polarity candidates.

4 Exploring mechanisms of polarity coordination

Introduction

4.1 Interactors of BASL

The work in the previous chapters focuses largely on the heat-shock inducible system to overexpress *35S::GFP-BASL* across the tissue. Given that BASL is not endogenously expressed in most cells of the leaf but localises to a specific small domain when overexpressed, it seems likely that BASL is binding to or interacting with molecular components at the proximal end of cells. In previous chapters, I termed this the 'proximal address'. This address is most likely composed of a protein, or scaffold of proteins, with which BASL interacts, but it could also include other molecular components, such as lipid components, or a combination of these factors.

Given that the localisation pattern of ectopic BASL in the leaf appears to be quite different from any known polarity markers, such as PINs or native stomatal polarity factors such as BRXL2, it is possible that the identification of the proximal address could reveal novel plant polarity components. Identification of the underlying factors involved could aid the understanding of how polarity is established and maintained in plant cells and would allow testing of models of polarity. For example, it is possible that the components of the proximal address could be part of the intracellular partitioning model of polarity (Abley et al., 2013), such as components A/A* and B/B* which remain unknown.

To explore and identify potential interactors of BASL, I used two approaches. Firstly, I made use of a previous screen that used the Split-ubiquitin system to identify putative interactors of membrane proteins (Jones et al., 2014). Although it lacks membrane binding domains, BASL was used as a bait protein in this study allowing me to probe this database for potential BASL interactors. Secondly, I used a biochemical approach to try and extract BASL and any interacting protein partners.

4.1.1 Using the Membrane-linked Interactome Database

A recent high-throughput study used a mating-based Split-ubiquitin system (mb-SUS) to identify putative interactions of membrane and signalling proteins (Jones et al., 2014). The mbSUS assay allows the identification of cytosolic and membrane bound interactions and

uses the ubiquitin-degradation pathway as a sensor for protein-protein interactions. The work by Jones et al., (2014) tested 6.4×10^6 pairs of proteins and identified ~12000 interactions, confirming a small proportion of these in planta. One of the proteins used as bait in this work was BASL and this database therefore could provide potential BASL interactors that warrant further investigation as candidates involved in the molecular address.

4.1.2 Using a biochemical approach to identify BASL interactors

Like yeast-2-hybrid approaches, co-immunoprecipitation (co-IP) is frequently used as a method to confirm interactions between proteins. Co-IP has the advantage of being able to examine protein-protein interactions in cells and native tissues. It can also be coupled to mass-spectrometry (mass-spec) analysis and, due to advances in mass-spec and peptide and protein databases, can also be used to identify novel interacting components of proteins of interest. This approach has been used to identify novel protein interactions in many areas (Avila et al., 2015) including flowering time regulation (Qüesta et al., 2016), development (Fàbregas et al., 2013) and plant immunity (Kadota et al., 2014; Weis et al., 2013).

Recent work has identified the SOK family of proteins which are polarly localised in *A. thaliana* and contain a well-conserved N-terminal DIX domain (Yoshida et al., 2019). This domain is a protein-protein interaction identified in Dishevelled polarity regulation in animals (Schwarz-Romond et al., 2007) and this domain allows SOK proteins to interact and potentially form a polar protein scaffold. Using a co-IP with mass spectrometry approach, common and distinct interactors of SOK proteins have been identified (Dolf Weijers, Maritza van Dop, personal communication).

4.2 Aims of this work

The aim of this work was to explore potential interactors of BASL in its ectopic context in order to elucidate molecular components of the proximal address. This work makes use of an existing database of potential protein interactions as well as using a biochemical approach to try and identify novel BASL interactors. Identification of novel BASL interactors, identified from the ectopic BASL polarity patterning, could allow further understanding of the mechanisms underpinning the establishment of tissue cell polarity in plants. This in turn may

reveal insights into the role of polarity in development and allow the testing of computational models.

Results

4.3 Membrane-linked Interactome Database candidates

The recent high-throughput screen for membrane and signalling protein interactions by Jones et al. (2014) used a mating-based Split-ubiquitin system (mb-SUS) to test interactions between $\sim 6.4 \times 10^6$ protein pairs. This work identified ~ 12000 potential protein interactions in *A. thaliana* and confirmed a small proportion of these in planta (Jones et al., 2014). A positive result in the mb-SUS screen occurs if an interaction between two proteins, fused to the N- and C- terminal parts of ubiquitin (Nub and Cub), brings these regions in proximity which reconstitutes a ubiquitin protein. This is then recognised by a ubiquitin specific protease which cleaves the Cub fusion protein to release a transcription factor (TF). The TF can then activate marker genes by entering the nucleus and this is detected by growth on selective media (Figure 4.1). Jones et al. (2014) tested interactions in two primary assays and then tested positive interactions in two secondary assays at different stringencies and reported interactions that tested positive in all four assays as MIND1 (Membrane-linked Interactome Database version 1). Protein interactions that also tested positive, but not in all four assays were also included in an online database.

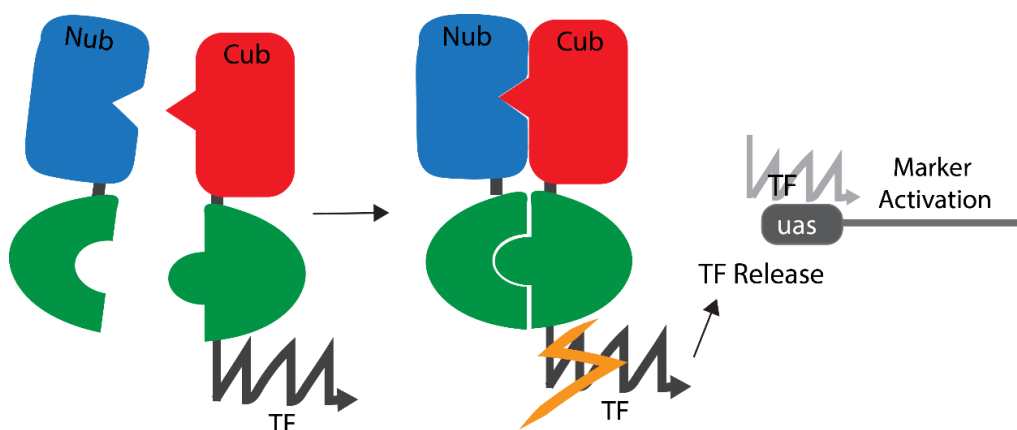


Figure 4.1 The mb-SUS screen was used to identify interactions with membrane proteins. Bait proteins are fused to N- and C- terminal domains of ubiquitin (Nub and Cub). If the proteins interact, the Nub and Cub moieties are brought into contact and reconstitute a

ubiquitin protein (green). This can then be recognised by an endogenous ubiquitin specific protease that cleaves the Cub fusion protein to release a transcription factor (TF). The TF is then free to enter the nucleus and activate marker genes whose expression indicates physical interaction between the proteins of interest. Based on Jones et al. (2014).

BASL was one of the proteins used as bait in this assay, though was predicted to localise to the nucleus by SUBAcon (a consensus algorithm for unifying the subcellular localization data of the Arabidopsis proteome) which was the protein localisation software used here (Hooper et al., 2014). The study undertaken by Jones et al. (2014) identified 32 potential interactors of BASL (listed in Appendix B, section 7.2). The study found no BASL-interactors that were positive for both assays in the primary Split-ubiquitin screen and both of the assays in the secondary screen. However, as noted in the study, this does not preclude that they are biologically important interactions and they were therefore included in the open-access online database. This work reported six candidates that were positive for both assays in the primary screen, and for one out of two assays in the secondary screen (Table 4.1) and I focussed on these candidates to test their localisation in planta. These six candidates were a receptor-like kinase (RLK, AT4G20790), a Cornichon-family protein (AT3G12180), VPS60.1 SNF7-family protein (AT3G10640), wall-associated kinase 3 (WAK3, AT1G21240), IQ-domain 6 protein (IQD6, AT2G26180) and purple acid phosphatase 3 (PAP3, AT1G14700) (Table 4.1 and see also Table 7.1).

Table 4.1 Six candidates from Jones et al. (2014) were the best putative BASL interactors. The six candidates that were positive BASL interactors in both of the Split-ubiquitin assays of the primary screen, and one out of two assay in the secondary screen are listed, with their GO Biological process or molecular function (from TAIR).

Candidate	Gene ID	SUBAcon localisation	GO Biological Process/molecular function
RLK	AT4G20790	Plasma membrane	Protein autophosphorylation
Cornichon	AT3G12180	Plasma membrane	Vesicle-mediated transport
VPS60.1	AT3G10640	Nucleus	Protein, vacuolar and vesicle-mediated transport
WAK3	AT1G21240	Plasma membrane	Cell surface receptor signalling pathway, protein phosphorylation
IQD6	AT2G26180	Nucleus	Calmodulin binding/microtubules
PAP3	AT1G14700	Extracellular	Dephosphorylation

4.3.1 Testing putative BASL interactors in *N. benthamiana*

Before testing the localisation of the putative interactors, I first transiently expressed *35S::GFP-BASL* in *N. benthamiana* to test how ectopic BASL would localise in this system. I generated the *35S::GFP-BASL* construct (71253) which contained the same GFP-BASL module as the heat-shock inducible BASL line. (In this chapter, I refer to this GFP variant as GFP-1). I imaged leaves 2 days after infiltration and found that, as in *A. thaliana*, ectopic BASL localised to a distinct domain in the pavement cells of *N. benthamiana* (Figure 4.2 A). Unlike in *A. thaliana* however, the BASL signal was typically observed in multiple lobes of pavement cells, though was not present in all lobes. In addition, the signal was not necessarily restricted to proximal lobes. BASL signal was also frequently observed in the nucleus (Figure 4.2 A). Whilst there are key differences between the localisation of ectopic BASL in *N. benthamiana* and *A. thaliana* which may be worth exploring in detail and quantifying in the future, the localisation of BASL to restricted domains in lobes of pavement cells remains similar in both contexts.

I cloned the six most promising candidates from the online interactome database of Jones et al., (2014) using Golden Gate cloning and tagged them with mCherry. I used mCherry so that the candidates could be co-expressed with *35S::GFP-BASL* and mCherry would also allow FRET-FLIM experiments to be conducted with these constructs in the future. I aimed to image the constructs in *N. benthamiana* following transient expression to test their localisations and, if potentially interesting, they could be stably transformed into *A. thaliana*. I chose to use the 35S promoter to express the genes and ensure they were expressed in the leaf and also to provide similar levels of expression to ectopic BASL. It is, however, possible that, as with BASL, the localisation of proteins can vary depending on the promoter, hence it could be useful in future to also test the localisation of these candidates using their native promoters.

Despite multiple attempts, I was not able to clone the L1 containing the WAK3 gene. The coding sequence of this gene underwent recombination when in *E. coli*, even when using cells to lower recombination. I therefore decided not to continue with WAK3 due to the difficulties expressing it in *E. coli*. WAK3 does, however, represent a potentially interesting interactor: it might be possible in the future to use different cloning strategies, or to use *wak3* mutants to explore this as a potential BASL interactor.

The remaining five genes were tagged at the N or C terminal end, depending on similar studies in the literature, and transiently co-expressed with *35S::GFP-BASL* in *N. benthamiana*.

Exploring mechanisms of polarity coordination

The RLK and VPS60 protein were tagged with mCherry at the C-terminus, as with previously tagged proteins in these families (Li et al., 2002; Nickerson et al., 2010), and the cornichon, IQD6 and PAP3 proteins were tagged at the C-terminal end (Bürstenbinder et al., 2017; Wudick et al., 2018; Zamani et al., 2014). I imaged *N. benthamiana* leaves with 35S::GFP-BASL and mCherry-tagged putative interactors 2 days after infiltration.

The RLK showed a clear plasma-membrane localised signal (Figure 4.2 B), similar to the localisation of many other RLKs (Greeff et al., 2012; Osakabe et al., 2013; Shiu and Bleeker, 2001). Co-expressed ectopic BASL remained localised to distinct domains in the lobes of pavement cells. Whilst the localisation of this gene does not show the same localisation pattern as ectopic BASL, it is not possible to rule out interactions without further analysis: it is possible that the two proteins could be interacting where BASL is localised. Both 35S::mCherry-Cornichon (AT3G12180, construct 71334) and 35S::mCherry-IQD6 (AT2G26180, construct 71337) were observed in punctate spots, usually near the edge of the cell (Figure 4.2 C and E respectively). IQD6 has previously been reported to localise to nuclear bodies (Bürstenbinder et al., 2017). These localisations were quite unclear but did not appear to co-localise with BASL. The lack of localisation to any distinct organelle might suggest that both constructs were being mis-targeted. It might be possible to tag the genes in different positions to obtain more convincing localisation patterns for these two putative interactors. Alternatively, it is possible that they are not expressed in pavement cells or leaves and hence do not show a clear localisation pattern when overexpressed in this context. When 35S::VPS60.1-mCherry (AT3G10640, construct 71335) was expressed in *N. benthamiana*, it appeared to localise possibly to the cytoplasm (Figure 4.2 D). Transvacuolar strands were visible and there was also some possible localisation to the endoplasmic reticulum and nuclear envelope (Figure 4.2 D). This agrees with previous reports of VPS60.1 localising to the cytoplasm and endosomes (Nickerson et al., 2010). 35S::PAP3-mCherry (AT1G14700, construct 71338) signal was observed very faintly at the plasma membrane, though the signal appeared a little 'fuzzy' (Figure 4.2 F).

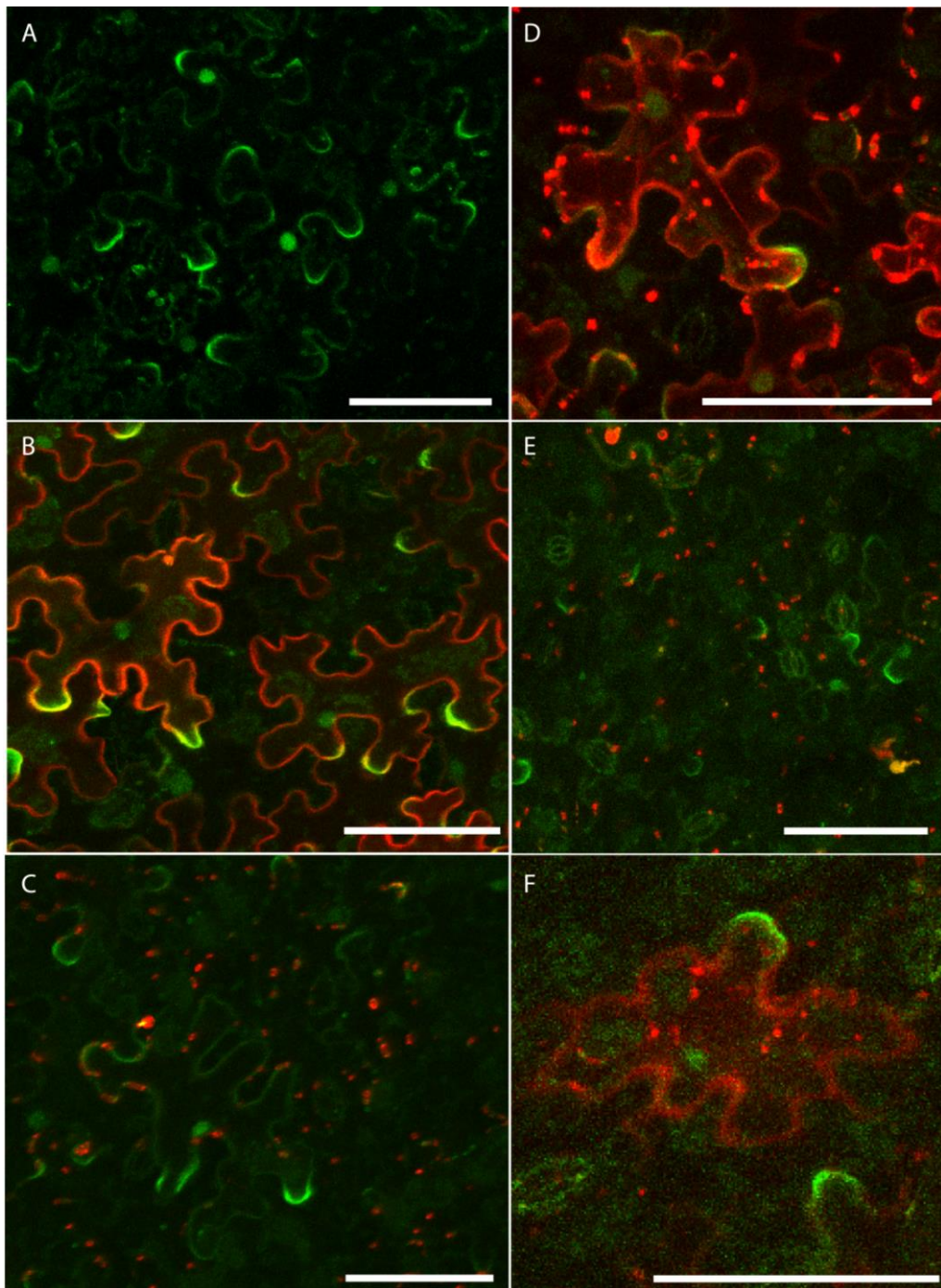


Figure 4.2 Putative BASL interactors showed differing subcellular localisations in *N. benthamiana*.

(A) *35S::GFP-BASL* in *N. benthamiana*. Ectopic BASL signal is also shown in each subsequent panel due to co-expression with the putative interactors. (B) *35S::RLK-mCherry* (AT4G20790, construct 71332) localises to the plasma membrane. (C) *35S::mCherry-Cornichon* (AT3G12180, construct 71334) localises in punctate distinct spots, usually near the edge of the cell. (D) *35S::VPS60.1-mCherry* (AT3G10640, construct 71335) localises possibly to the cytoplasm. Transvacuolar strands are visible, and possibly also the endoplasmic reticulum and nuclear envelope. (E) *35S::mCherry-IQD6* (AT2G26180, construct 71337) localises possibly in vesicles. (F) *35S::PAP3-mCherry* (AT1G14700, construct 71338) localises possibly

to the plasma membrane, though faintly. All leaves were imaged 2 days after infiltration. Scale bars are 100 μm .

Out of the five candidates tested transiently in *N. benthamiana*, none of them showed a localisation pattern resembling that of BASL. It might be expected that any interactors of BASL should localise to, or close to, the membrane, given that this is where ectopic BASL localises. Two of the candidates, *35S::mCherry-Cornichon* (AT3G12180, construct 71334, Figure 4.2 C) and *35S::mCherry-IQD6* (AT2G26180, construct 71337, Figure 4.2 E) did not localise to the membrane. This may be due to mis-expression, or because these proteins are not membrane-targeted. The rice cornichon-family protein OsCNIH1 is localised to the endoplasmic reticulum (Rosas-Santiago et al., 2015) when tagged at the C-terminal end, whilst cornichon-family proteins in *A. thaliana* localised to endo-membranes, punctate structures that colocalise with endoplasmic reticulum markers, and the plasma membrane in some instances when N-terminal tagged (Wudick et al., 2018). This may indicate that the localisation of this protein should be tested with both N- and C-terminal tags. The localisation pattern I observed for PAP3 may agree with previous reports of members of this gene family localising between the plasma membrane and cell wall (Zamani et al., 2014). Given that the RLK, VPS60.1 and PAP3 (construct 71332, 71335 and 71338 respectively) all showed possible plasma-membrane or cytosolic localisations. I therefore decided to create stable transformation lines in *A. thaliana* with these three constructs to analyse their expression further in the system I had previously characterised BASL expression in.

4.3.2 Testing putative BASL interactors in *A. thaliana*

To test the localisation of the candidates in *A. thaliana* that appeared membrane bound, I stably transformed *A. thaliana* with the constructs 71332 (*35S::RLK-mCherry*), 71335 (*35S::VPS60.1-mCherry*) and 71338 (*35S::PAP3-mCherry*). I imaged various parts of the stably transformed plants, including the true leaf, cotyledon and root or hypocotyl, to characterise the localisation of these genes when overexpressed.

The RLK (construct 71332) localised to the plasma membrane in the leaf, cotyledon and very faintly in some cells of the root (Figure 4.3 A-C). In the root, the signal was weaker and less clear, and there was also some signal possibly in the nucleus (Figure 4.3 C). This localisation confirmed the plasma membrane localisation observed in *N. benthamiana* (Figure 4.2 B) and agrees with the membrane localisation of other RLKs (Greeff et al., 2012). However, in this context, it does not indicate any obvious polar localisation. *35S::VPS60.1-mCherry* (construct

71335) also showed a clear plasma membrane localisation in leaves (Figure 4.3 D). In the cotyledon, a very faint plasma membrane localisation was observed, with much stronger expression in the stomata and meristemoid cell (Figure 4.3 E). This localisation was intriguing and could indicate a role in the stomatal lineage that may warrant further investigation. Signal was also weak in the root and may localise to the plasma membrane and nucleus or endoplasmic reticulum (Figure 4.3 F) which is similar to the localisation observed for this construct in *N. benthamiana*. The PAP3 protein (construct 71338) appeared to localise to the plasma membrane in the leaf, cotyledon and hypocotyl (Figure 4.3 G-I), but in a rather unusual non-uniform manner. This localisation could indicate localisation to the region in between the plasma membrane and cell wall, as was previously reported for AtPAP9 (Zamani et al., 2014).

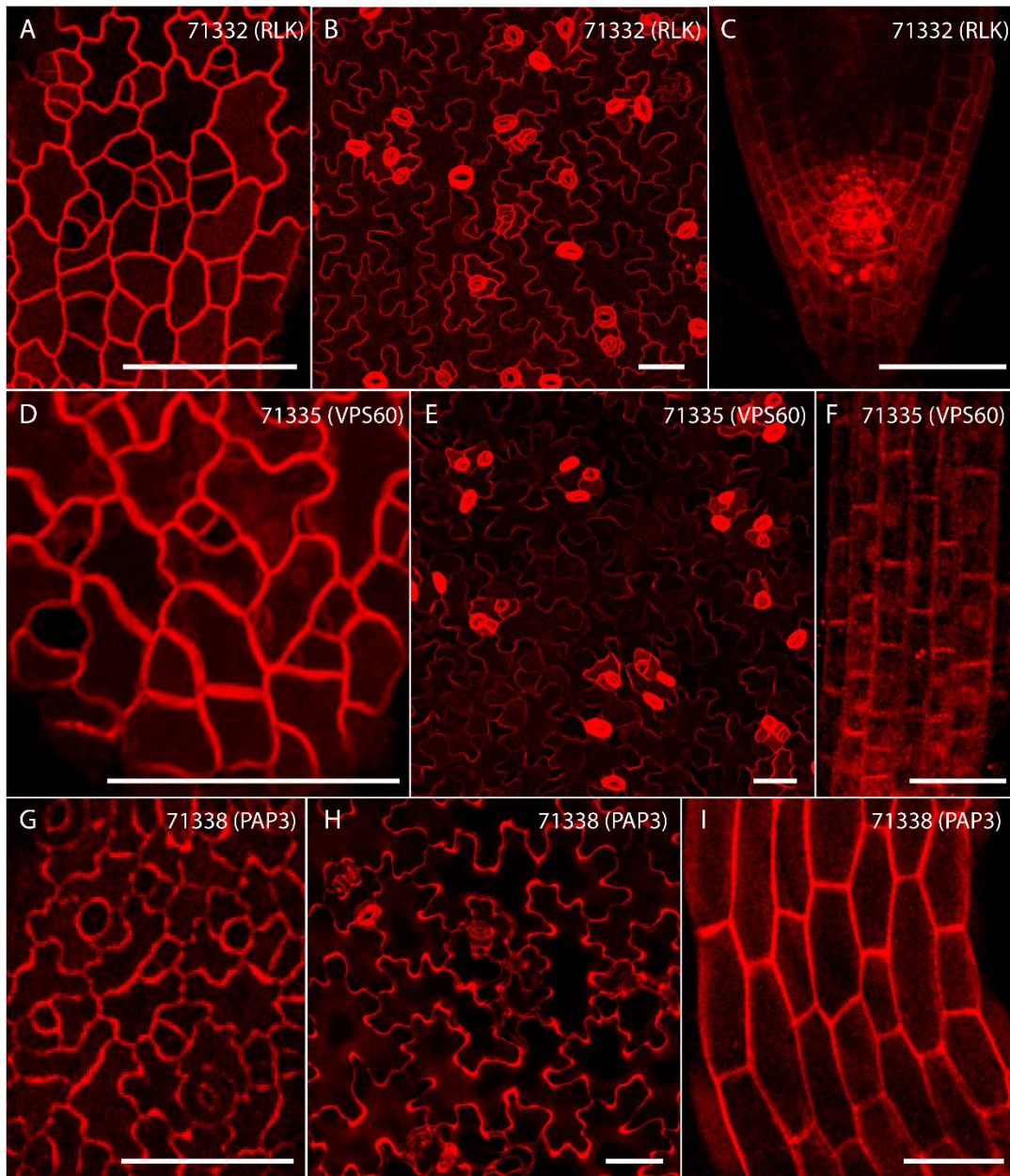


Figure 4.3 Multiple putative BASL interactors were plasma membrane localised in *A. thaliana*.

Three putative BASL interactor candidates from transient expression in *N. benthamiana* were stably transformed into *A. thaliana* under the 35S promoter and tagged with mCherry. Regions of the plant were imaged 7 DAS. (A-C) 35S::RLK-mCherry (71332) expression in (A) the leaf, (B) cotyledon and (C) root. All images are from the same insertion line carrying 2 copies (iDNA genetics). (D-F) 35S::VPS60.1-mCherry (71335) expression in (D) the leaf, (E) cotyledon and (F) root. Images are from three different insertion lines, carrying 3, 1 and 11 copies (in D, E and F respectively, iDNA genetics). (G-I) 35S::PAP3-mCherry (71338) expression in (G) the leaf, (H) cotyledon and (I) hypocotyl. All images are from the same insertion line carrying 2 copies (iDNA genetics). Scale bars are 50 μ m.

The localisation of these three gene products under the 35S promoter in *A. thaliana* did not provide any clear indication of polar localisation. The proteins were all reported to interact with BASL interactions in the Split-ubiquitin assay previously described by Jones et al. (2014), but it is possible they do not interact in planta. Alternatively, the proteins may interact with BASL, but not localise to the proximal end of the cell, as BASL does, when overexpressed. Further analysis with these candidates, and those that I found to be misexpressed in *N. benthamiana*, would be required to understand and clarify any interaction with BASL.

4.4 Protein extraction looking for BASL interactors

To try and identify novel interactors of BASL, I used a biochemical approach. This involved initially trying to extract BASL from leaf tissue of both *A. thaliana* and *N. benthamiana* before carrying out co-immunoprecipitation to pull down potential binding partners that could be identified using mass-spectrometry and might play a role in conferring polarity. The methods used in the following biochemistry work are detailed in the Materials and methods, Section 6.9 and thus are only briefly outlined here, noting any specific differences or adaptations in each iteration of experiments. In this chapter, I distinguish between variants of GFP in different constructs: the GFP variant used in the inducible BASL line (used in Chapter 2 and 3), and some constructs in this chapter, is referred to as GFP-1, and a second variant used in this chapter (eGFP) is referred to as GFP-2 for clarity.

4.4.1 Total protein extraction in *A. thaliana*

I initially carried out total protein extractions to try to extract BASL from the tissue. I first carried out total protein extraction in *A. thaliana* expressing heat-shock induced 35S::GFP-BASL (GFP-1 as used in Chapter 2 and 3) using non-heat shocked plants as a negative control (i.e. plants carried the same construct, but were not expressing BASL). I heat-shocked seedlings for 20 minutes 7 DAS and confirmed expression by confocal microscopy (data not shown) before collecting ~1.5 g of leaf material four days after heat-shock. The total protein extraction was carried out using a basic extraction buffer (see extraction buffer 1, section 6.9.3.1). After centrifugation, I retained the supernatant fraction and the pellet to test if BASL remained in the pellet fraction. I boiled the samples in 2 x SDS-page buffer for 15 minutes to denature proteins. I then ran the supernatant and pellet fractions for the two samples on a 10% SDS-page gel (Figure 4.4 A) and carried out a western blot (Figure 4.4 B, see section 6.9.7

and 6.9.8 for details). In the non-heat shocked supernatant sample, and to a lesser degree in the pellet fraction, I observed a band of approximately 30 kDa on the western blot (Figure 4.4 B, lanes 1 and 3). This band was likely CyPET as antibodies are generally unable to distinguish GFP and CFP variants, and the non-heat shocked plants were expressing ER-targeted CyPET. I did not observe any signal in the heat-shocked samples, indicating that BASL had not been extracted or was too low in concentration to detect (Figure 4.4 B, lanes 2 and 4).

I repeated this approach using the same extraction method (extraction buffer 1), but including a *35S::TUA6-GFP* control sample as a positive control. Notably, the GFP variant in the inducible *35S::GFP-BASL* line (GFP-1) was not the same as that in the tubulin line, which raises limitations of using this line as a control, but a control line with the GFP-1 was not available in *A. thaliana*. For this western blot, I used a more sensitive ECL exposing kit (SuperSignal™ West Femto Maximum Sensitivity Substrate) than in the previous attempt in case GFP-BASL was present at a concentration too low to detect. As before, I observed a band of approximately 30 kDa in the non-heat shocked sample (Figure 4.4 C, lane 1). This band appeared stronger on this blot, probably as a result of the more sensitive exposure. There was a weaker band of the same molecular weight (~30 kDa) in the heat-shocked sample (Figure 4.4 C, lane 2). This band is at the correct position for GFP or CyPET meaning it is either GFP that has been cleaved from BASL during the extraction, or it is CyPET protein from before heat-shocking that has not been degraded. GFP-BASL would be 56 kDa and therefore does not correspond to the observed band. I observed a band at approximately 80 kDa in the *35S::TUA6-GFP* sample which represents the appropriate molecular weight Tubulin-GFP (Figure 4.4 C, lane 3).

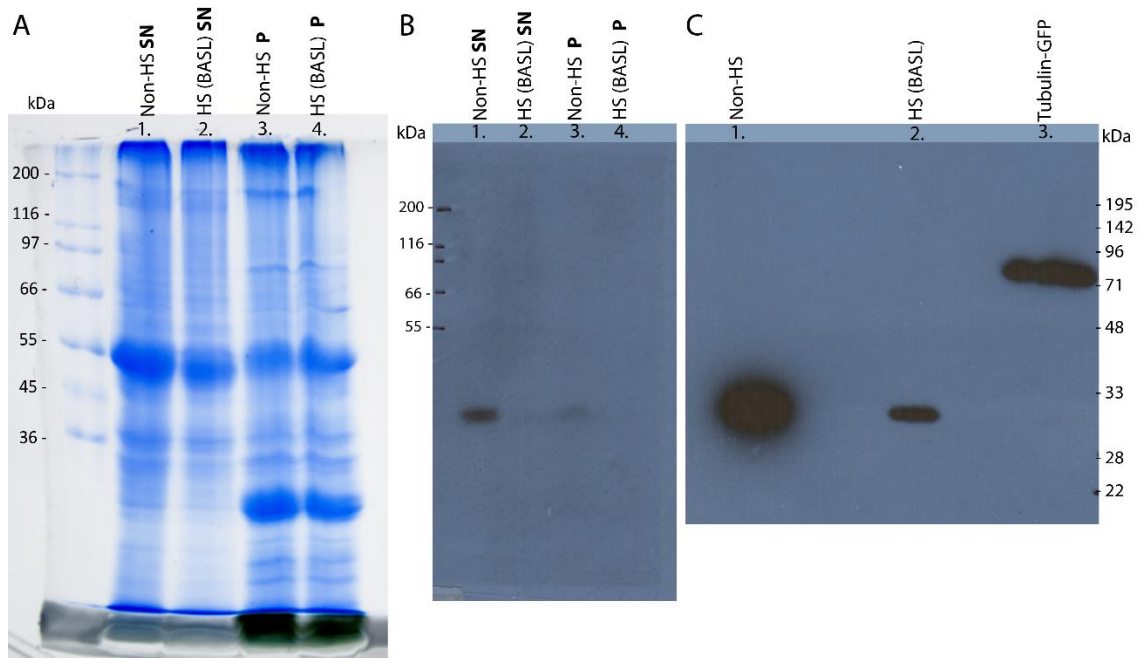


Figure 4.4 Total protein extraction in *A. thaliana* did not extract GFP-BASL.

(A) SDS-page gel from total protein extraction in *A. thaliana* leaves. 1.5 g of raw material was collected 4 days after heat-shock and total protein extracted, run as supernatant and pellet fraction. Lane 1 is the non-heat shocked supernatant (SN) sample, lane 2 is the heat-shocked *35S::GFP-BASL* (GFP-1) supernatant sample, lane 3 is the non-heat shocked pellet (P) sample and lane 4 is the heat-shocked *35S::GFP-BASL* pellet sample. (B) Western blot from the gel in A, with the same samples used. (C) Western blot for total protein extraction in *A. thaliana* using a more sensitive ECL kit and tubulin-GFP control. Lane 1 is the non-heat shocked *35S::GFP-BASL* SN sample, lane 2 is the heat-shocked *35S::GFP-BASL* SN sample and lane 3 is *35S::TUA6-GFP* SN sample. The SigmaMarker™ high range marker (Sigma) was used in A and B, and RunBlue™ prestained molecular weight marker (Expedeon) was used in C.

The lack of GFP-BASL in these total protein extractions could be accounted for by a number of reasons. It is possible that GFP was being cleaved from BASL in the extraction process, that GFP-BASL was degraded on harvesting the samples or during the extraction, that the BASL in the sample was at an undetectably low concentration, or that the antibodies were not recognising the GFP-1 variant used in the inducible *35S::GFP-BASL* line. In order to test the latter of these ideas, I repeated the western blotting with different anti-GFP antibodies to ensure the lack of GFP-BASL signal was not due to incompatibility between the GFP-1 variant and the antibody (data not shown, detailed in section 6.9.8.1). These iterations of experiments yielded the same patterns as those shown in Figure 4.4 and did not show any evidence of BASL extraction.

4.4.2 Total protein extraction in *N. benthamiana*

Given the challenges faced in extracting BASL from *A. thaliana*, I decided to try using *N. benthamiana* for total protein extraction. This transient system provides a much faster and easier way of generating larger amounts of material to use for optimising conditions for protein extraction. Whilst there are issues associated with the use of a different system for identifying novel components, it seemed like a useful and more efficient way to test extraction conditions before applying them to *A. thaliana*. The localisation of BASL to multiple lobes in pavement cells of *N. benthamiana* remains a key difference from the localisation in *A. thaliana*. However, given the similarities in localising to a distinct lobe domain, the molecular address targeting BASL may well be conserved between the two systems.

4.4.2.1 Ectopic BASL expression in *N. benthamiana*

I used construct 71253 (*35S::GFP-BASL*), which contains the same GFP-1 variant as the heat-shock inducible *35S::GFP-BASL* line in *A. thaliana*, and *35S::LYK5-eGFP* as a membrane-bound eGFP (referred to as GFP-2) positive control (construct kindly provided by Cecilia Cheval and Christine Faulkner). I infiltrated *N. benthamiana* leaves and imaged leaves two days later before confirming the localisation of the proteins using confocal microscopy (Figure 4.5). GFP-BASL localisation was observed in multiple lobes and in the nucleus of pavement cells, as described in section 4.3.1 (Figure 4.5 A), whilst LYK5-eGFP localised to the plasma membrane (Figure 4.5 B), as previously described (Cao et al., 2014).

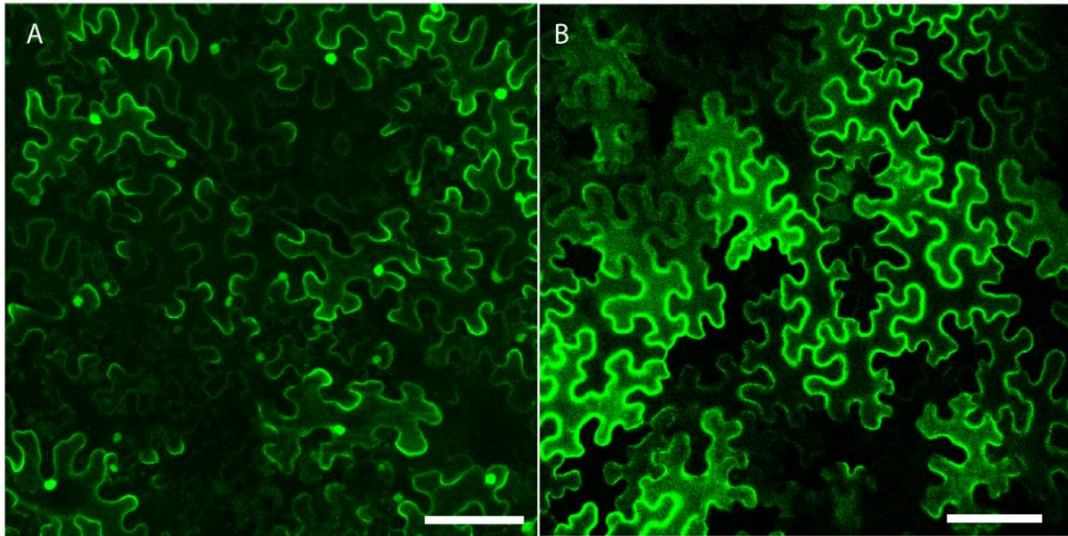


Figure 4.5 *35S::LYK5-eGFP* and *35S::GFP-BASL* transiently expressed in *N. benthamiana* provide a system for optimising protein extraction conditions.

(A) *35S::GFP-BASL* (construct 71253, GFP-1) and (B) *35S::LYK5-eGFP* (GFP-2) transiently expressed in leaves of *N. benthamiana* and imaged 2 days after infiltration. Scale bars 100 μm .

4.4.2.2 Optimising protein extraction in *N. benthamiana*

To initially test the total protein extraction method in *N. benthamiana*, I used leaves transiently expressing *35S::GFP-BASL* (71253, GFP-1) and used *35S::LYK5-eGFP* (GFP-2) and uninoculated leaves as positive and negative controls respectively. I harvested ~ 2.5 g of leaf tissue for each line 2 days after infiltration and used the same extraction conditions as described above (section 4.4.1) to extract total protein. I ran the supernatant and pellet fractions on a 10% SDS-page gel (Figure 4.6 A) and western blot (Figure 4.6 B).

I was able to see a band on the blot in the LYK5-eGFP samples ~ 100 kDa which is the expected molecular weight for this sample (the molecular weight of LYK5 is 72.5 kDa), and a faint band at ~ 27 kDa which is likely GFP-2 (Figure 4.6 B, lane 5). The LYK5-eGFP band was observed in both the supernatant and pellet fractions (Figure 4.6 B, lane 6). However, there were no bands in the BASL samples indicating that the BASL had not been extracted from the tissue, possibly due to the extraction buffer composition, degradation, or due to an undetectably low concentration of GFP-BASL in the samples (Figure 4.6 B).

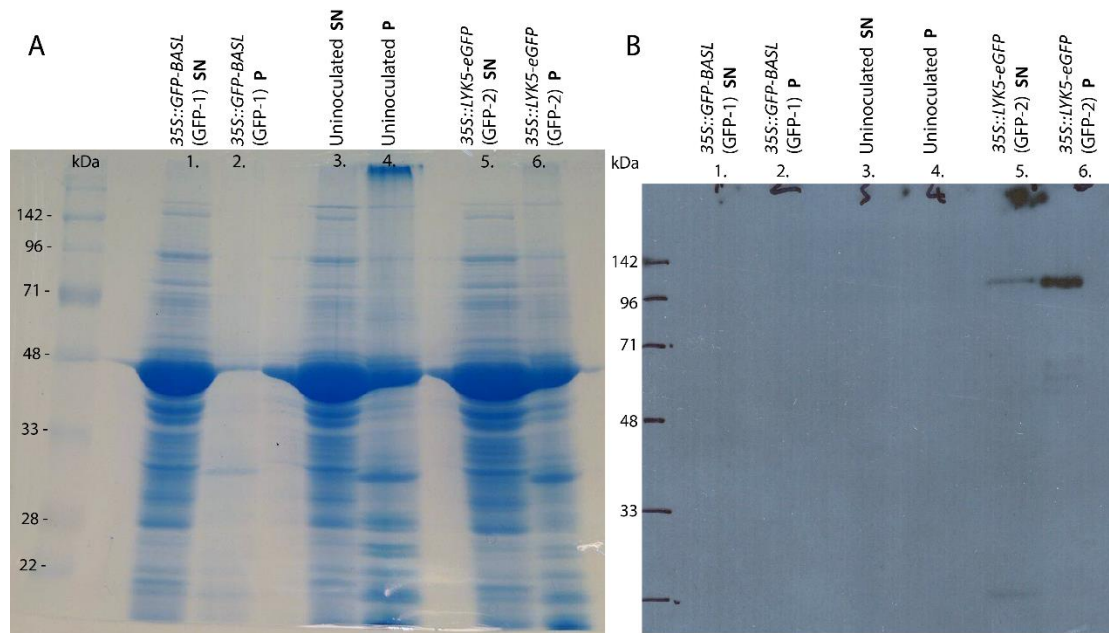


Figure 4.6 *N. benthamiana* total protein extraction did not extract GFP-BASL.

(A) SDS-page gel from total protein extraction in *N. benthamiana* leaves. 2.5 g of raw material was collected 2 days after infiltration into leaves. Lanes 1 and 2 are *35S::GFP-BASL* (GFP-1) supernatant (SN) and pellet (P) respectively, lanes 3 and 4 are uninoculated leaves SN and P respectively, lanes 5 and 6 are *35S::LYK5-eGFP* (GFP-2) SN and P respectively. (B) Western blot for the total protein extraction in *N. benthamiana* (from gel in A). Lanes are the same as in A. No bands are seen in the *35S::GFP-BASL* or uninoculated sample lanes for the SN or P fractions. A band between 96 and 142 kDa can be seen for LYK5-eGFP (GFP-2) in both the SN and P fractions.

To try and concentrate the samples and extract BASL I carried out multiple other extractions using *N. benthamiana* using the same lines described above (*35S::GFP-BASL* (GFP-1), *35S::LYK5-eGFP* (GFP-2) and uninoculated leaves). I carried out a total-protein extraction using a high-salt extraction buffer (see section 6.9.3.2 for details) and concentrated the samples using an acetone precipitation (see section 6.9.3.3 for details). In addition, I tried adding an additional protease inhibitor (Pefabloc, which is a PMSF alternative) to the extraction buffer to reduce possible degradation of BASL in the samples. Neither the high-salt buffer, the acetone precipitation, nor the addition of Pefabloc yielded any different results to those shown in Figure 4.6. Bands were consistently observed in the LYK5-eGFP fraction, but not in the uninoculated or GFP-BASL (GFP-1) samples (data not shown).

4.4.2.3 Total protein extraction using eGFP (GFP-2)

The GFP variant used to tag BASL in construct 71253 and the heat-shock inducible *35S::GFP-BASL* (GFP-1) was an older GFP variant, used in the generation of GFP-BASL by Dong et al.

(2009). One possible reason for not being able to successfully extract BASL is that this GFP variant may not be recognised by the GFP antibodies being used. *35S::LYK5-GFP* that I used as a positive control contained a standard eGFP variant (GFP-2) and was detectable on western blots. To check whether the reason BASL was not being extracted was due to the GFP-1, I generated a construct in which BASL was tagged using a standard eGFP variant (GFP-2, construct 71572). The protein sequences of these two GFP variants differ in six locations in the protein, and the GFP-1 variant also seems to have 8 extra amino acids at the C-terminal end (Figure 4.7). Both these GFP variants can be found in standard vectors. However, it is possible that the differences could result in differential interactions with GFP-antibodies.



Figure 4.7 The GFP-1 variant differs from standard eGFP (GFP-2) at multiple residues. Amino-acid sequences for the GFP-1 and GFP-2 variants used here are shown. GFP-2 (used in construct 71572) is a standard eGFP that was used in Golden Gate cloning in this project. GFP-1 (in the inducible BASL line and construct 71253) is an older variant that was used by Dong et al. (2009) to tag BASL. Residues where the amino acid sequences differ between the two variants are highlighted and coloured in red.

Exploring mechanisms of polarity coordination

I confirmed the localisation of BASL tagged with GFP-2 by transient expression and confocal imaging in *N. benthamiana* leaves (Figure 4.8 B). BASL localised predominantly to the lobes of pavement cells and to nuclei (Figure 4.8 Bi), as described for BASL tagged with GFP-1 (construct 71253, Figure 4.5 A). In addition to the GFP-BASL signal enrichment at lobes, I also observed signal along the plasma membrane which appeared to be brighter than that for GFP-1 tagged BASL (compare Figure 4.8 Bi with 4.5 A). Applying a Rainbow LUT to the images in Fiji indicated that the lobes were still enriched (Figure 4.8 Bii) and that this localisation remained distinctly different from that for the plasma membrane localised LYK5-GFP (Figure 4.8 A). This difference is likely due to improved brightness in newer variants of fluorescent proteins, such as GFP-2. The underlying pattern of GFP-BASL appears to be largely the same and thus this line may represent a useful tool in the biochemical analysis of BASL. It would be informative to also stably transform *A. thaliana* with this construct to compare BASL localisation in this context.

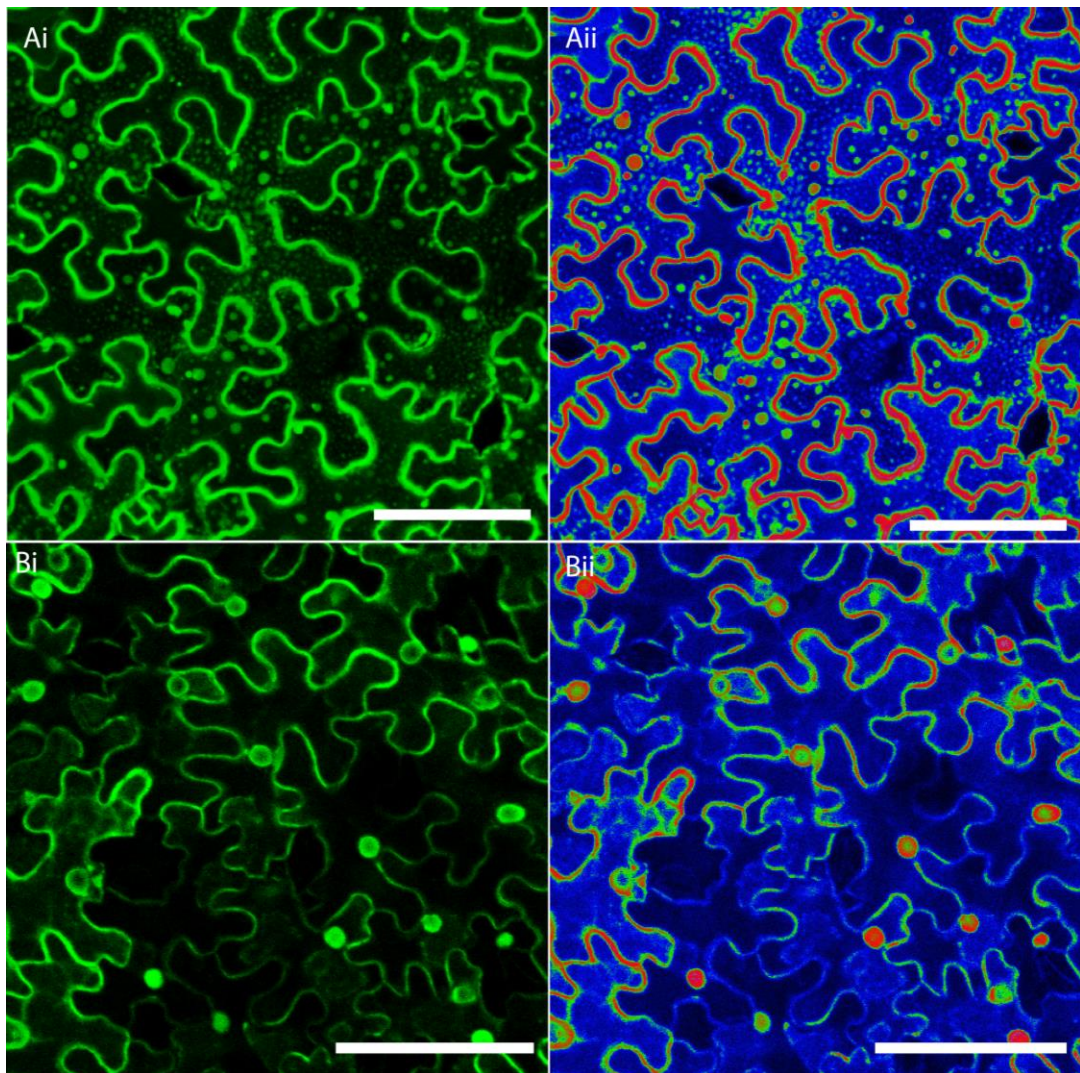


Figure 4.8 BASL tagged with GFP-2 localised to the lobes of pavement cells.

(Ai) *35S::LYK5-eGFP* (GFP-2) imaged two days after infiltration into *N. benthamiana* leaves; (Aii) shows the same image as in Ai with a rainbow LUT applied in Fiji to show the areas of highest signal intensity. (Bi) *35S::eGFP-BASL* (GFP-2, construct 71572) imaged two days after infiltration into *N. benthamiana* leaves; (Bii) shows the same image as in Bi with a rainbow LUT applied in Fiji indicating high signal intensity in the lobes and nuclei of cells. Scale bars are 100 μm .

I transiently expressed *35S::eGFP-BASL* (GFP-2, construct 71572) in *N. benthamiana* leaves and harvested 2.5 g of leaf tissue 2 days later. I used *35S::LYK5-eGFP* and uninoculated samples as positive and negative controls respectively. I used a similar protein extraction method as in section 4.4.1 and 4.4.2.2, using extraction buffer 2 (section 6.9.3.4) which contained 1% NP40, glycerol for increased protein solubility and stability, and pefabloc. I also compared the reducing agents DTT and β -mercaptoethanol for the BASL-containing samples to ensure that the proteins were not oligomerising and were properly reduced. The western

blot for this extraction indicated LYK5-eGFP had been extracted, as shown by a large mass of signal at ~ 100 kDa (Figure 4.9 B, lanes 1 and 2). These lanes also showed a strong band at ~ 28 kDa which may represent GFP-2 and faint bands of ~ 30 kDa which were also observed in all other lanes. These bands are likely to be due to non-specific binding as they were also observed in the negative controls (Figure 4.9 B, lanes 3 and 4) and the BASL samples (Figure 4.9 B, lanes 5-8). The supernatant fractions of the GFP-2 tagged BASL samples also contained very high bands >142 kDa which seem unusual and could indicate possible oligomerisation (Figure 4.9 B lanes 6 and 8). A faint shadow of band was also observed in the BASL samples between 48 and 71 kDa (white arrowhead in Figure 4.9 B). This suggestion of a band was very faint, and not easily observable on the blot but, if genuine, would represent a band of approximately the correct molecular weight for GFP-BASL.

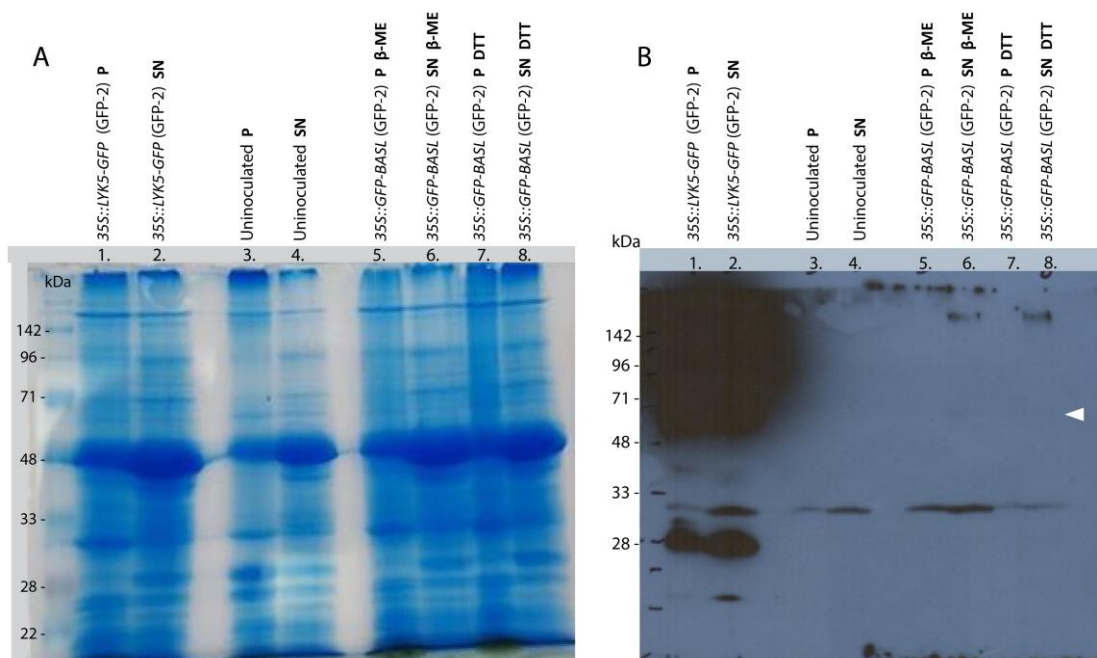


Figure 4.9 An alternative GFP variant and different reducing agents were tested in total protein extraction in *N. benthamiana*.

(A) SDS-page gel from total protein extraction in *N. benthamiana* leaves using GFP-2 and comparing DTT and β -mercaptoethanol as reducing agents. Lanes 1 and 2 are Lyk5-eGFP pellet (P) and supernatant (SN) respectively, lanes 3 and 4 are uninoculated leaves P and SN respectively, lanes 5 and 6 are *35S::eGFP-BASL* (GFP-2) P and SN respectively using β -mercaptoethanol as the reducing agent, lane 7 and 8 are *35S::eGFP-BASL* (GFP-2) P and SN respectively using DTT as the reducing agent. (B) Western blot for the total protein extraction in *N. benthamiana* using GFP-2 and comparing reducing agents (from gel in A). Lanes are the same as in A. Bands were observed both in the Lyk5-eGFP samples at ~ 28 kDa and a very strong, and a large mass of signal at ~ 100 kDa. Bands of ~ 30 kDa were observed in all lanes. A faint shadow was possibly present in lane 6 and 8 (white arrowhead).

Although the band specific to the BASL samples was very faint and difficult to detect, this total protein extraction using GFP-2 was the first indication of bands that may be specific to the BASL samples. It is possible that the bands were very difficult to detect due to the extraction conditions being unsuitable for BASL extraction, or that BASL was simply at a very low concentration in the tissue that could not be detected using total protein extraction methods.

4.4.3 Immunoprecipitation in *N. benthamiana*

Given that I had not been able to clearly detect GFP-BASL on a western blot using total protein extraction, despite conducting extractions under many different conditions, I decided to try to concentrate the samples by carrying out an immunoprecipitation (IP). Some proteins that have low expression in tissues cannot be observed using western blotting unless an IP has been carried out (Qüesta et al., 2016).

I harvested 10 g of leaf material from *N. benthamiana* transiently expressing *35S::eGFP-BASL* (GFP-2, construct 71572) and *35S::Lyk5-eGFP*, as well as uninoculated leaves for negative controls. The higher amount of starting material was used to increase the overall amount of BASL protein in the samples. I used a protocol adapted from Qüesta et al. (2016) and described in detail in section 6.9.4. After grinding and addition of extraction buffer, samples were centrifuged and filtered before being incubated with GFP-Trap®_MA beads (Chromotek). Protein samples were eluted from the magnetic beads and run on a 10 % SDS-page gel, alongside the samples without IP (Figure 4.10 A). Unfortunately, this gel did not run evenly, making the sizes of the bands difficult to interpret. After the immunoprecipitation, Lyk5-GFP showed a band of ~100 kDa (Figure 4.10 A, lane 2) indicating that it had been successfully isolated by the IP; a similar band was not visible for GFP-BASL (Figure 4.10 A, lane 4).

The western blot for these samples had a mass of bands for the immunoprecipitation of Lyk5-eGFP which could not be distinguished and indicated very high amounts of extracted protein in these samples (Figure 4.10, lane 2). No clear bands were observed in the negative control samples (Figure 4.10 B, lanes 3 and 4) or in the BASL sample without IP (Figure 4.10 B, lane 5). Where an IP had been carried out on the *35S::eGFP-BASL* samples, a band of between 48 and 71 kDa was observed (Figure 4.10 B, lane 6, white arrowhead). There was also some signal at a very high molecular weight or in the well, and some signals ~33 kDa which could represent GFP-2 (Figure 4.10 B, lane 6). To confirm the possible specific band and to observe

the bands more clearly for Lyk5-eGFP, I repeated this IP using new material and re-ran the samples from the previous attempt alongside (Figure 4.10 C).

In the new samples, I observed a similar pattern of signal on the blot. In the BASL overexpressor samples, there were bands at ~28 kDa and ~33 kDa that could be GFP-2, possibly also with some fragment attached, and also a band between 48 and 71 kDa that could be GFP-BASL (Figure 4.10 C, lane 2). The re-blotted BASL samples only contained the band between 48 and 71 kDa which could be a result of degradation during storage (Figure 4.10 C, lane 5). The Lyk5-eGFP IP samples (new samples and re-blotted samples) both showed a lot of signal, particularly ~100 kDa where Lyk5-eGFP would be expected (Figure 4.10 C, lanes 3 and 6). A faint band was observed in the re-blotted Lyk5-eGFP samples without IP (Figure 4.10 C, lane 9) and no bands were observed in the negative samples (Figure 4.10 C, lanes 1, 4 and 7).

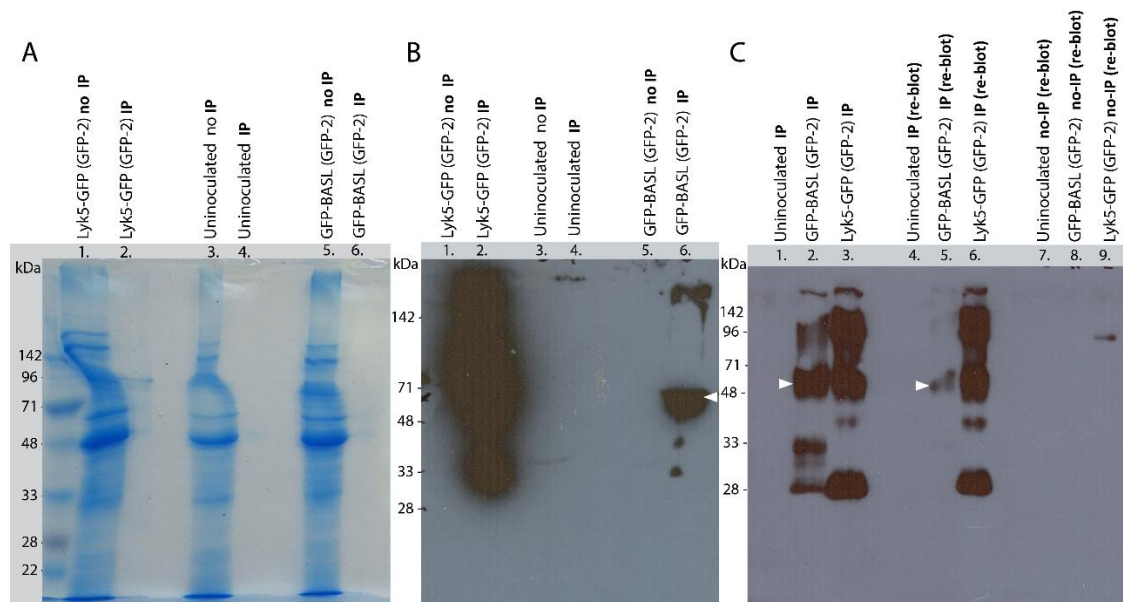


Figure 4.10 Gel and blots of immunoprecipitation in *N. benthamiana* indicated possible BASL extraction.

(A) SDS-page gel from *N. benthamiana* samples containing LYK5 and BASL tagged with GFP-2 and uninoculated leaves before and after immunoprecipitation (IP). Lanes 1 and 2 are 35S::LYK5-eGFP without IP and with IP respectively, lanes 3 and 4 are uninoculated leaves without IP and with IP respectively, lanes 5 and 6 are 35S::eGFP-BASL without and with IP respectively. (B) Western blot for the IP in *N. benthamiana* (from gel in A). Lanes are the same as in A. A band of between 48 and 71 kDa was observed in the 35S::eGFP-BASL sample (white arrowhead) that could correspond to GFP-BASL. (C) Western blot for the IP in *N. benthamiana* repeated with new samples (lanes 1-2) and re-running samples from the gel/blot shown in A/B, with diluted LYK5-eGFP samples. Bands were observed in both BASL IP samples, including a band at the correct molecular weight for GFP-BASL (white arrowheads, lanes 2 and 5).

This immunoprecipitation indicated that GFP-BASL may have been extracted. Ideally, I would hope to see individual bands on the SDS-gel corresponding to BASL and any interacting partners; multiple clear bands were not observed on this gel (Figure 4.10 A). However, GFP-BASL is the same molecular weight as Rubisco, which may obscure any GFP-BASL signal on a Coomassie-stained gel. Additionally, the Coomassie stain is not very sensitive and other staining techniques, such as silver-staining, could be used to identify proteins on the SDS-gel with increased sensitivity.

4.4.4 Immunoprecipitation in *A. thaliana*

4.4.4.1 IP in collaboration with Weijers lab, Wageningen University

Having some indication of BASL extraction following immunoprecipitation in *N. benthamiana* (Figure 4.10), I aimed to use *A. thaliana* to extract BASL and identify any potential interacting partners using mass-spectrometry (mass-spec). Having had useful discussions regarding the successful use of IP with mass-spec analysis for the recently identified SOK polar proteins (Dolf Weijers, personal communication), I collaborated with Maritza van Dop in the Weijers lab in Wageningen to conduct a co-immunoprecipitation (co-IP) followed by mass-spec to identify potential BASL interacting partners in *A. thaliana*. I used protocols that had been developed by the Weijers lab to identify SOK protein interactors (section 6.9.5.1).

I used *A. thaliana* expressing the heat-shock inducible *35S::GFP-BASL* (GFP-1) line, heat-shocked for 20 minutes 6 DAS, and a GFP control line (ER-tagged GFP-2, construct 71028). Ideally, the GFP-2 variant would have been used for tagging BASL, but an *A. thaliana* line with this GFP variant was not available. Likewise, a *35S::GFP* line using GFP-1 was not available for use as a control. The difference in GFP variants used therefore represents a limitation of this experiment. I confirmed the GFP localisation in these lines using confocal microscopy (Figure 4.11) and then harvested tissue for protein extraction.

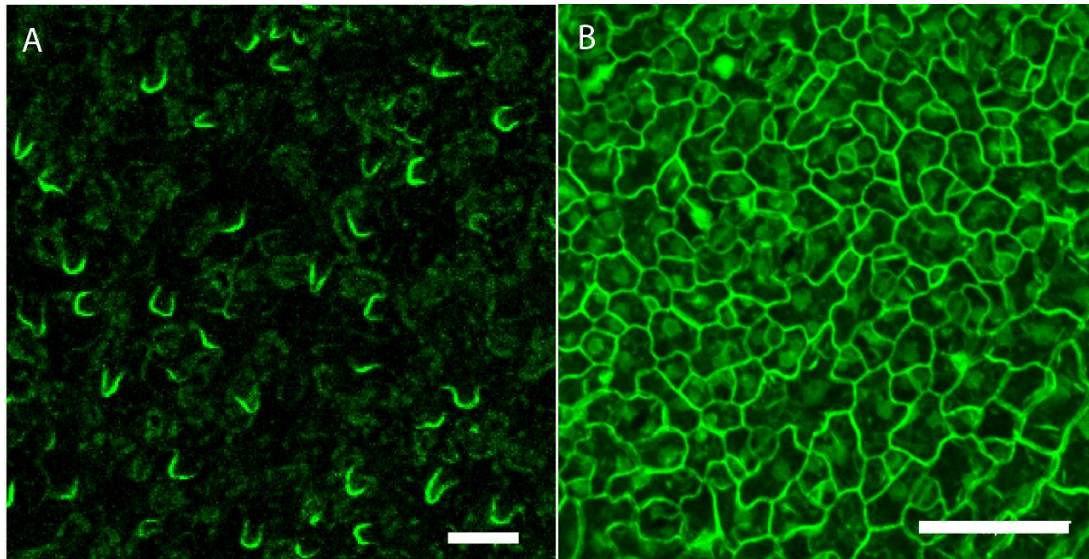


Figure 4.11 GFP localisations were confirmed in *A. thaliana* leaves before harvesting for co-IP.

(A) *A. thaliana* leaf expressing 35S::GFP-BASL (GFP-1) following heat-shock induction for 20 minutes at 39 °C, 6 DAS. As previously described, BASL is localised to the proximal end of cells. (B) *A. thaliana* leaf expressing a heat-shock inducible 35S::eGFP control (GFP-2, construct 71028, provided by Samantha Fox, Coen lab) following heat-shock induction for 20 minutes at 39 °C, 6 DAS. Scale bars are 50 µm.

I conducted the co-IP in Wageningen in collaboration with Maritza van Dop and according to the protocol outlined in section 6.9.5.1. I used three biological replicates for the GFP-BASL and GFP-control samples and, after immunoprecipitation, the samples were sent for mass-spectrometry analysis in Wageningen.

Unfortunately, the results for this analysis did not yield a clear list of potential BASL-interactors. After comparing the three control samples with the three BASL-containing samples, the only protein that had been significantly differentially identified was BASL (Figure 4.12 and Appendix C). However, there were only 7 counts of BASL peptides found, indicating that the reason no other interactors could be identified was due to the lack of BASL pulled down in this IP. This suggested that the IP did not successfully extract BASL from the samples.

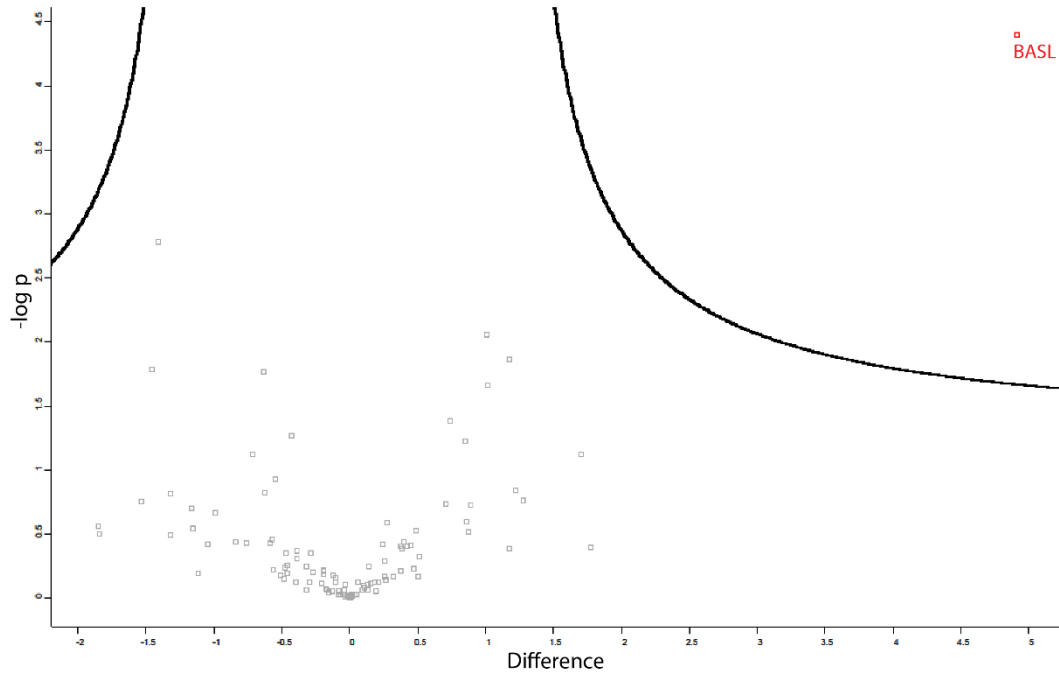


Figure 4.12 BASL-interacting partners were not identified from the IP-MS analysis in Wageningen.

Plot showing proteins found to be significantly differentially present between *35S::GFP-BASL* (GFP-1) samples and GFP-2 control samples. Statistically significant candidates lie above the black curved lines and only BASL is found in this region. All other proteins were not differentially present in the BASL and control samples (grey squares). Analysis for this plot was carried out by the mass-spectrometry facility and members of the Weijers lab, University of Wageningen.

The very low level of BASL peptides found in the samples meant that other proteins identified by the mass-spectrometry analysis could not be counted as putative BASL interactors. Multiple reasons could account for why the immunoprecipitation did not work. One possibility is that the slightly different extraction conditions used did not allow GFP-BASL to be isolated, possibly due to the sensitivity of BASL to specific extraction conditions. It is also possible that the GFP-1 variant used in the *A. thaliana* heat-shock inducible BASL overexpressor was not identified by the GFP beads used (notably, these were different from those I had used for the previously discussed IP experiments). An SDS-gel and western blot were not carried out with these samples as the whole sample volume was required for mass-spec in order to allow the maximum possible protein to be detected. However, running a gel and blot for these samples before and after IP might have helped understand why BASL was not successfully extracted.

4.4.4.2 Immunoprecipitation in *A. thaliana* using previously tested conditions

To test whether the extraction conditions used for the immunoprecipitation carried out in Wageningen may have been responsible for the lack of BASL found in the samples, I used the same samples as for the IP described above, using inducible ectopic BASL tagged with GFP-1 (section 4.4.4.1), but used the extraction conditions that I had used previously when I had been able to observe some possible GFP-BASL signal using *N. benthamiana* samples (section 4.4.3).

I conducted the immunoprecipitation and ran samples with IP, without IP, and a fraction from the supernatant leftover after IP (i.e. the fraction containing proteins that did not bind to the magnetic beads) on an SDS-gel (Figure 4.13 A) and western blot (Figure 4.13 B). No bands were visible for *35S::GFP-BASL* (GFP-1) on the gel (Figure 4.13 A, lane 1), but a band of ~29 kDa was observed in the GFP-2 control samples after IP (Figure 4.13 A, lane 4). This indicated that the IP had worked on the control samples, but not the BASL samples. This was confirmed by western blotting where a large mass of signal was observed, including between 28 and 33 kDa, for the GFP-2 control fractions (Figure 4.13 B, lane 4), but no clear signal was observed in the BASL IP fraction (Figure 4.13 B, lane 1). There were some hints of signals in the BASL IP samples, including possible signal between 28 and 33 kDa which could represent GFP, but the signal in this lane was very unclear and could not be confirmed (Figure 4.13 B, lane 1). Signal between 28 and 33 kDa was observed in the BASL fractions without IP and the leftovers from the IP (Figure 4.13 B, lanes 2 and 3). This seems unusual and could be due to the recognition of CyPET by the antibodies, or cleaved GFP in these samples.

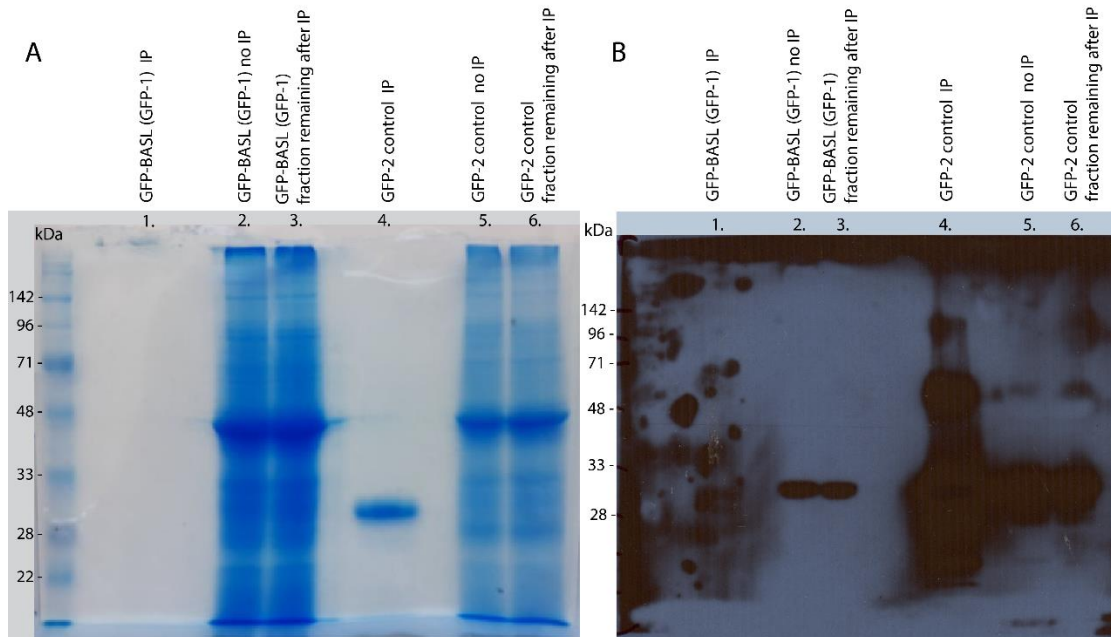


Figure 4.13 IP with inducible BASL in *A. thaliana* did not successfully extract GFP-BASL. (A) SDS-page gel from *A. thaliana* samples containing heat-shock inducible *35S::GFP-BASL* (GFP-1) and GFP-control (GFP-2, construct 71028) with IP, no IP, and the remaining fraction after IP. Lanes 1, 2 and 3 are *35S::GFP-BASL*, with IP, without IP, and remaining fraction after IP respectively. Lanes 4, 5 and 6 are GFP-control, with IP, without IP, and remaining fraction after IP respectively. (B) Western blot for the IP in *A. thaliana* (from gel in A). Lanes are the same as in A. A large mass of signal was observed in the GFP-control IP samples and a band of ~29 kDa was observed in the GFP-2 control samples without IP. A GFP-sized band was observed in the BASL non-IP fractions, and possibly the GFP-BASL IP sample.

4.4.5 Testing GFP sequence differences in *N. benthamiana*

The protein extractions and immunoprecipitation carried out thus far has indicated that a difference in GFP variants (shown in Figure 4.7) may be responsible for the differences in extraction success in both *A. thaliana* and *N. benthamiana*. This could also account for why the mass-spectrometry analysis carried out in Wageningen was not successful. In order to resolve this issue, I extracted protein from *35S::GFP-BASL* samples in *N. benthamiana* containing both GFP-1 and GFP-2 variants, and samples containing *35S::GFP-2* (construct 71223, Coen lab) as a positive control. Following IP, the samples were run on the same SDS-page gel (Figure 4.14 A) and western blot (Figure 4.14 B).

The results from this immunoblot indicate that BASL tagged with GFP-2 may have been extracted. The band observed for this sample on the western blot was the correct molecular weight for BASL tagged with GFP-2 (Figure 4.14 B, lane 4, white arrowhead) and is not observed in the negative controls, nor in the sample containing GFP-1 tagged BASL. No

specific bands were observed on the Coomassie-stained gel (Figure 4.14 A), but this may be due to the low sensitivity of the staining, and the fact that GFP-BASL is the same molecular weight as Rubisco. As expected, the positive *35S::GFP* (GFP-2) control showed a large band at the correct molecular weight for GFP following IP (Figure 4.14 B, lane 8). Interestingly, there was also a band of ~30 kDa in the GFP-BASL (GFP-1) IP samples which could be GFP (Figure 4.14 B, lane 2). This band is of a similar size to that shown in Figure 4.13 B in the non-IP samples in *A. thaliana*: the reason for this discrepancy remains unclear and the western blots should ideally be repeated in both systems to confirm this result. In the *N. benthamiana* IP, this band may indicate that GFP-1 could become cleaved from BASL during immunoprecipitation, and may suggest that GFP-1 variant can be recognised by the GFP antibodies used, but was not recognised when attached to BASL.

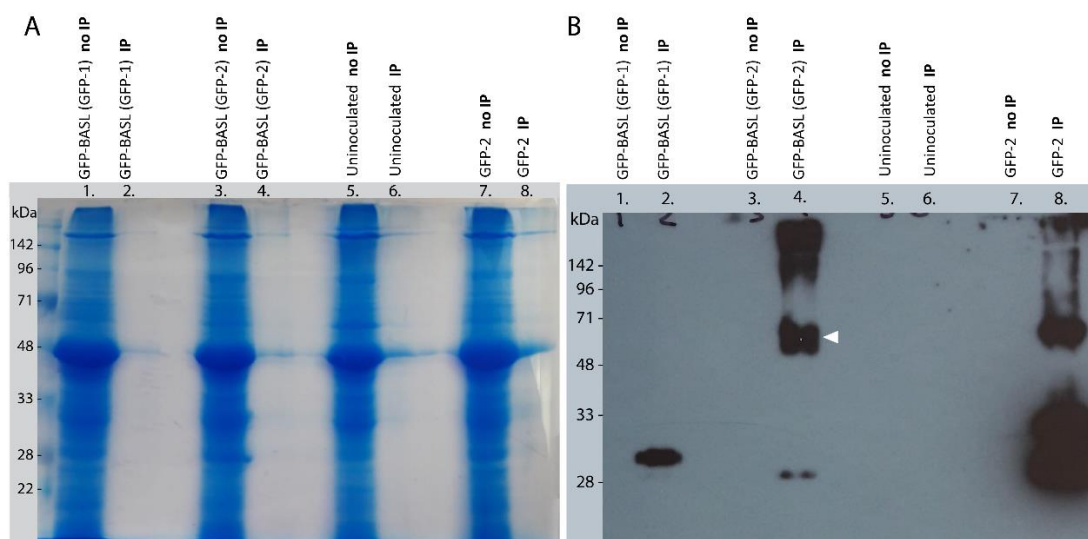


Figure 4.14 IP in *N. benthamiana* using GFP-2 indicated GFP-BASL extraction.

(A) SDS-page gel from *N. benthamiana* samples containing *35S::GFP-BASL* (GFP-1, construct 71253), *35S::eGFP-BASL* (GFP-2, construct 71572), uninoculated leaves and a *35S::eGFP* control (GFP-2, construct 71223) following IP. Lanes 1 and 2 are *35S::GFP-BASL* (GFP-1) without IP and with IP respectively. Lanes 3 and 4 are *35S::eGFP-BASL* (GFP-2) without IP and with IP respectively. Lanes 5 and 6 are uninoculated leaves without IP and with IP respectively. Lanes 7 and 8 are *35S::GFP* (GFP-2) without IP and with IP respectively. (B) Western blot for the IP in *N. benthamiana* (from gel in A). Lanes are the same as in A. A GFP-sized band was observed in the GFP-BASL (GFP-1) IP sample (lane 2) and a larger band in the control sample (lane 8). A band was observed between 48 and 71 kDa (white arrowhead) in the *35S::eGFP-BASL* (GFP-2) IP sample that could correspond to GFP-BASL.

The observation of a band in the region of the size expected for GFP-BASL was encouraging and would confirm the results from previous blots where there were indications of GFP-BASL when GFP-2 was used, but not when the alternative GFP-1 was used. However, a similar sized band was also observed in the GFP-2 control (Figure 4.14 B, lane 8) which could also indicate that this band is not specific. The reason for this band in the control sample remains unclear and thus this immunoprecipitation should be repeated. Ideally, this construct (construct 71572 containing BASL tagged with GFP-2) should be stably expressed in *A. thaliana* so that the IP can be repeated in this system to allow identification of possible BASL interactors by mass spectrometry. However, due to time constraints, I was not able to transform this line into *A. thaliana* and therefore decided to send the samples from the immunoprecipitation conducted in *N. benthamiana* (Figure 4.14) for proteomics analysis to identify possible putative BASL interactors in this system.

4.4.5.1 Immunoprecipitation with mass-spec analysis

I sent the samples extracted from *N. benthamiana* using GFP-2 (described above and shown in Figure 4.14) for mass-spec analysis at the proteomics facility at the John Innes Centre to identify the proteins in the samples and therefore potential BASL interacting partners. I prepared the samples for mass-spec (according to the protocol described in section 6.9.5.2) and trypsin digest was carried out by Gerhard Saalbach (JIC proteomics facility) before samples were run on an Orbitrap mass-spectrometer (section 6.9.5.2).

The peptide sequences obtained were searched against the *N. benthamiana* protein sequence database (section 6.9.6), identifying 393 proteins. Scaffold was used to analyse this list of protein candidates, with help from Paul Derbyshire (Proteomics, The Sainsbury Laboratory, Norwich, see section 6.9.6 for details of the analysis). Proteins with a minimum of 4 spectral counts and that were either unique to the GFP-BASL bait samples, or were enriched in the bait samples by at least 1.5-fold compared to the positive and negative controls, were selected as potential interactors. It remains possible that proteins with a lower spectral count could interact with BASL, but multiple replicates would need to be carried out to confirm this therefore, for this data, a cut-off of minimum 4 spectral counts was used to filter the data. The resulting list of 34 proteins that pass these criteria are shown in Appendix D.

BASL was detected at relatively high levels in the *35S::eGFP-BASL* samples and was found to be unique to this sample, as expected. The analysis showed a good coverage of the BASL protein (60%) from the mass-spec analysis (Figure 4.15 A) and the individual spectra for

Exploring mechanisms of polarity coordination

identified BASL peptides indicated that the peptide fragmented well at different sites (Figure 4.15 B).

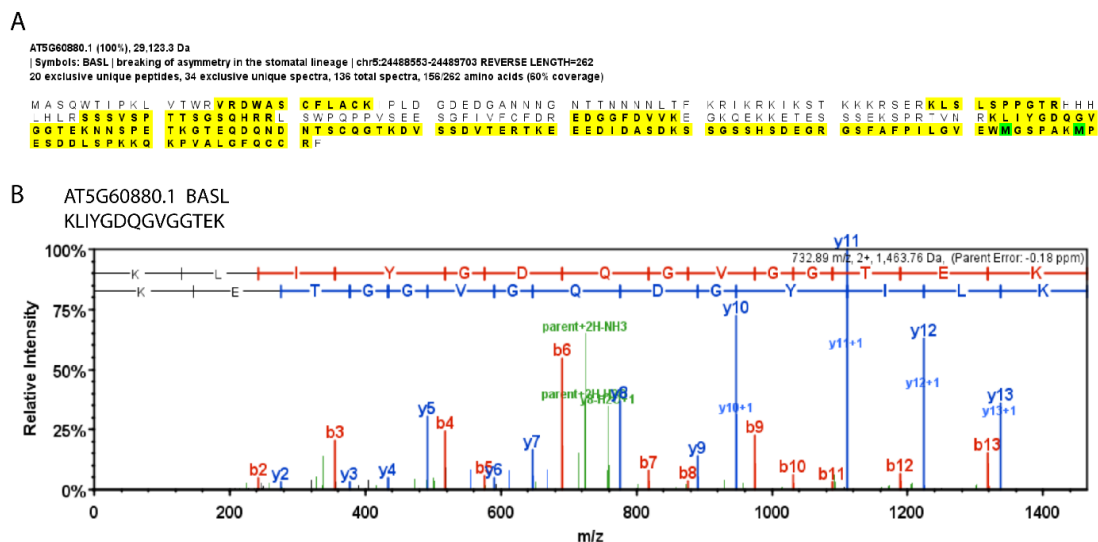


Figure 4.15 BASL was identified as a unique peptide with good coverage and fragmentation.

(A) BASL peptide sequence showing good coverage of this protein (60%) from the mass-spec analysis. Peptides detected are highlighted in yellow, and green highlights modified amino acids. (B) Example spectra from the detected BASL peptide with the highest Mascot ion score. The peptide sequence is indicated above in B and the spectrum shows that the peptide fragmented well at different sites.

The list of proteins differentially identified in the BASL-containing samples includes many metabolic enzymes and 14-3-3 proteins, as well as a calcium-sensing receptor (with homology to AT5G23060.1) and actin (Table 4.2). At present, these candidates cannot be confirmed due to the lack of replicates for this experiment. Some of the candidates identified in this list, such as actin, are often identified in IP datasets as ‘sticky’ proteins so would need further analysis and replicates before any conclusions can be drawn. However, this preliminary data suggests that the extraction of BASL was successful and that this approach might allow more conclusive identification of potential BASL interactors in the future.

Table 4.2 Short-list of five protein candidates, including BASL, identified by IP-MS.

List of 5 selected protein candidates, including their peptide count and uniqueness are shown. These proteins were selected from the complete list of filtered candidates shown in Appendix D as possible interesting candidates to test further. Their reference to the *N. benthamiana* database used is also shown.

Reference in database	Identified protein	Peptide count Un-infiltrated (negative)	Peptide count GFP-BASL (bait)	Peptide count GFP (positive)	Unique to bait?
-	GFP-BASL (GFP spectra removed to show only BASL)	0	13	0	✓
Niben101Scf03410g03002.1 sp P10987 ACT1_DROME	Actin-5C	0	9	0	✓
Niben101Scf03493g00020.1 sp P41113 ACT3_PODCA	Actin-3	0	8	0	✓
Niben101Scf10757g00001.1 sp Q6ZKC0 14333_ORYSJ	14-3-3-like protein, GF14-C	0	6	0	✓
Niben101Scf18639g00026.1 AT5G23060.1	Calcium sensing receptor	0	5	3	✗

4.5 Discussion

4.5.1 Putative BASL interactors from mb-SUS screen

I used the membrane interactome database based on a set of mb-SUS assays and conducted by Jones et al. (2014) to explore the localisation of some of the putative BASL interactors. Six candidates had been reported by Jones et al. (2014) as interacting with BASL in both primary screens and one out of two secondary screens. I was able to clone 5 of the 6 candidates and test their localisation when expressed transiently under a constitutive promoter. I found that three of the genes showed plasma membrane localisation in *N. benthamiana* (RLK: AT4G20790, construct 71332; VPS60.1: AT3G10640, construct 71335; and PAP3: AT1G14700, construct 71338) and therefore could potentially interact with BASL, though in this context, none of these candidates showed a polar localisation. It may also be useful to generate constructs tagging these proteins at both the N- and C-terminal to confirm their localisation. I also analysed the localisation of these three candidates in *A. thaliana* leaves, cotyledons and roots, but did not see any evidence of polar localisation.

I was unable to clone one of the candidate proteins (WAK3) due to recombination in *E.coli*. This candidate might be worth testing further, for example by expressing ectopic BASL in

wak3 mutants, as it is reported to have a role in membrane signalling and protein phosphorylation, both of which could be relevant to BASL function. Furthermore, whilst I did not identify any polar localisation of these candidates, it is possible that they do still interact with BASL but are not responsible for establishing a proximal address, or that these proteins function as BASL-interactors alongside other factors. Further testing, such as using FRET FLIM, bimolecular fluorescent complementation (BiFC) assays, and expressing candidates under their native promoters could indicate in planta BASL-interaction and any potential role in polarity establishment.

This work also tested the overexpression of BASL in *N. benthamiana*. I showed that *35S::GFP-BASL* in *N. benthamiana* is expressed in a polar manner localising to multiple lobes of pavement cells. This differs from the localisation pattern observed in *A. thaliana* pavement cells where ectopic BASL typically localises to a single lobe. One possible explanation for the localisation to multiple lobes in *N. benthamiana* is that the number of lobes could relate to cell size, as cells in *N. benthamiana* are larger than those in *A. thaliana*. Further analysis is required to test the differences in ectopic BASL expression between these two systems. In addition, the localisation pattern of BASL described here in *N. benthamiana* conflicts with that reported by Zhang et al., (2015) who show that overexpression of CFP-BASL in tobacco cells results in an apolar distribution at the plasma membrane unless co-expressed with the MAPK kinase kinase YODA (YDA). Given the subtle differences in BASL localisation that I observed using two different GFP variants, it is possible that this conflict is also a result of differences in fluorescent proteins.

4.5.2 Protein extraction and co-immunoprecipitation to identify BASL interactors

I used a biochemical approach to try and extract GFP-BASL from plant tissue. I initially carried out total protein extraction in *A. thaliana* and *N. benthamiana* testing various conditions. I was not able to observe BASL in these total protein extractions, possibly due to its low concentration in the total protein samples. I therefore carried out co-immunoprecipitation in *N. benthamiana* where there was some evidence of BASL extraction using an alternative GFP variant. I collaborated with the Weijers lab in Wageningen to carry out an immunoprecipitation and proteomics analysis using mass-spec in *A. thaliana*, using conditions similar to those used to identify novel interactors of the polar SOK proteins. Unfortunately, this IP did not identify any significant candidates for BASL interactors as BASL was extracted at very low levels.

Further analysis in *N. Benthamiana* indicated that this was likely to be due to the GFP variant used (GFP-1) not being recognised by the antibodies used, or potentially being cleaved from BASL. The antibodies used in the collaboration with Wageningen were not the same as those that I used in *N. Benthamiana* and it seemed that neither successfully recognised the GFP-1 variant. It may be useful to test a number of different antibodies, including polyclonal antibodies, to allow detection of this GFP-1 variant. It may also be worth exploring the possibility that the linker sequence used in the GFP-BASL (GFP-1) sequence initially developed by Dong et al. (2009), could contribute to the difficulties in detecting this GFP variant in IP. Ideally, future work would include stable transformation of *A. thaliana* with the construct containing the alternative GFP-2 variant (*35S::eGFP-BASL*) to allow IP and mass-spec analysis to be carried out in *A. thaliana*.

However, despite difficulties encountered with conducting IP in *A. thaliana*, I was able to use the *35S::eGFP-BASL* construct in *N. benthamiana* to identify potential BASL partners using mass-spec. At present, these results cannot be confirmed due to the lack of replicates. However, this list of candidates includes proteins that may be of interest in a developmental biology or signalling context (Table 7.3, Appendix D). For example, the CAS protein identified is homologous to an *A. thaliana* protein that has been reported to localise to the plasma membrane of HEK293 cells (Tang et al., 2007) and also to chloroplasts (Vainonen et al., 2008). Interestingly, this protein was also identified in the IP-MS I carried out in Wageningen and therefore, although both datasets are inconclusive, could warrant further investigation.

The identification of multiple 14-3-3 proteins could be an indication of stress responses, for example, from infiltration. 14-3-3 proteins are known to localise to different subcellular organelles, dependent on their isoform and interacting protein partners, and members of this protein family have been shown to regulate the subcellular redistribution of proteins between the nucleus and the cytoplasm (Paul et al., 2005). 14-3-3 proteins have also recently been implicated in hormone signalling and development, including a reported role in PIN polarity (Keicher et al., 2017), and therefore cannot be ruled out as potentially interesting candidates (Camoni et al., 2018). The IP-MS approach used here should be repeated, both in *N. benthamiana*, and also ideally in *A. thaliana*, to allow more conclusive identification of interacting partners of BASL in an ectopic context.

There does not appear to be any overlap between the candidates identified by Jones et al. (2014) using a mb-SUS approach, and those that I have identified using IP-MS. This may be due to the different approaches used, and highlights the need to use in planta methods, such

as FRET-FLIM analysis or Bimolecular fluorescence complementation (BiFC) to confirm any potential protein interactions identified.

4.5.3 Concluding remarks and future work

The work in this chapter aimed to identify and test putative interactors of BASL that may represent components of the hypothesised molecular address. The testing of previously identified candidates from a mb-SUS assay (Jones et al., 2014) did not yield clear results. However, the approach used to test these candidates, that included fluorescent tagging and transient expression in *N. benthamiana*, could be used to test candidates identified in the future and could be extended to include more detailed protein-interaction analysis (such as FRET-FLIM).

The biochemical analysis described here identified conditions in which BASL could be extracted from *N. benthamiana* tissue and led to the identification of putative interactor candidates by mass-spec. This work should be repeated in *N. benthamiana*, and ideally in *A. thaliana*, followed by in planta testing of candidates to identify components of the molecular address. The preliminary data could be of significant importance if candidates were confirmed to have polar localisations and could represent novel factors involved in polarity establishment.

5 Main discussion

5.1 Summary of this work

In this work, I have used inducible overexpression of the stomatal protein BASL to reveal a coordinated tissue cell polarity field across the *A. thaliana* leaf. I have characterised the polarity pattern revealed by BASL in detail using confocal microscopy and shown that BASL consistently localises to the proximal end of cells. I collaborated with computer scientists to develop software for quantifying polarity. I have shown that the polarity field revealed by BASL is present throughout the early stages of development of leaf 1, unlike known markers of polarity such as PIN1, which is expressed in the primordia, during serration formation and in the vasculature (Guenot et al., 2012; Hay et al., 2006; Scarpella et al., 2006). I also showed that the BASL polarity field is independent of the stomatal lineage by characterising the polarity pattern in the *speechless* mutant.

I have tested various predictions of a tissue-wide polarity field. I showed that the polarity field diverges at later stages of leaf development and that this occurs in near isotropic cells indicating that the divergent polarity pattern is not due to assigning polarity in relation to the cell centroid. I explored the behaviour of ectopic BASL in developmental contexts, including serrations, and found that ectopic BASL mirrors the convergence and divergence polarity points of PIN1 at serrations. I also expressed BASL in BY-2 cells and found that BASL can localise polarly in BY-2 cells, though is often not coordinated along a filament, and can remain polarised in BY-2 protoplasts. In addition, I used ectopic BASL to test possible mechanisms for the establishment and coordination of polarity, including testing the effects of NPA, oryzalin and mechanical stresses.

Finally, I used a biochemical approach to look for potential novel interactors of BASL, and tested previously described interactor candidates for polar localisation patterns to try to identify novel components involved in polarity establishment in plants.

5.2 Evidence for a polarity field in leaves present throughout development and independent of the stomatal lineage

Using ectopic BASL, I have characterised a polarity field that exists in the *A. thaliana* leaf, that possesses many different characteristics from previously reported polarity fields or polarised proteins in plant planar organs.

The polarity field revealed by ectopic BASL can be observed in the developing primordia and localises to the opposite end of cells to PIN1 (Benková et al., 2003; Scarpella et al., 2006). However, unlike PIN1, BASL polarity can be observed beyond the developmental stage at which PIN1 expression is no longer observed (~150 μm in width, Abley et al., 2016) and at all stages of leaf development analysed.

Other physical and molecular markers of polarity have been reported at later stages of leaf development but differ from the ectopic BASL polarity field. BRXL2 tends to localise at the proximal end of stomatal lineage cells showing coordinated polarity, albeit to a lesser extent than described in this work using ectopic BASL (Bringmann and Bergmann, 2017). In addition, trichomes also have a proximodistal polarity (Bouyer et al., 2001; Hülkamp and Schnittger, 1998; Hülkamp et al., 1994). Both trichome and stomatal lineage polarity fields are associated with only a subset of cells in the *A. thaliana* epidermis. The epidermis is thought to play a key role in growth and the development of a leaf shape (Fox et al., 2018). As such, a polarity field that exists in the majority of cells across the epidermis could be of significant importance. At early stages of leaf development there are only a few trichomes and stomata across the epidermis, meaning any coordinated polarity is not observable in a single primordium or leaf, limiting their usefulness as markers of polarity. By contrast, the polarity field described here is observable in a much larger proportion of the cells in the epidermis, allowing the polarity field to be visualised across a single leaf and in *A. thaliana* primordia.

Ectopic BASL expression was not observable in every cell despite using the 35S promoter and typically heat-shocking seedlings for long enough that the Cre-lox recombination reaction should have occurred in all cells. It is possible that the lack of signal in all cells is due to very low BASL expression that is not detectable in cells, or that the recombination reaction has not occurred in all cells. Alternatively, the level of BASL expression or protein may vary through the cell cycle, as is the case in its native context in the stomatal lineage (Robinson et al., 2011). It would be informative in future work to follow multiple cell divisions in live-

tracking of ectopic BASL to understand how BASL is inherited through cell divisions. The observation that ectopic BASL is often not seen in meristemoid cells of the stomatal lineage may also suggest that ectopic BASL levels can vary, perhaps through degradation. Mechanisms for BASL degradation have not been reported, but phosphorylation is known to be important in targeting BASL to the membrane and determining its polarity during stomatal development (Zhang et al., 2015; Zhang et al., 2016a).

BASL itself is unlikely to be involved in establishing the tissue-wide polarity. There are multiple reasons to support this idea. Firstly, in this work, BASL is being overexpressed in cells in which it would not be expressed in an endogenous context. Secondly, as shown in this work, BASL does not coalesce on a proximal point in a cell, but signal intensifies in a proximal location following BASL induction. In addition, I have induced BASL at later stages of leaf development. BASL would therefore have to quickly establish a polarity field in a mature tissue after induction and it is not clear how this could be achieved. Finally, BASL does not seem to be a protein well conserved across the plant kingdom and appears to have no detectable homologues outside of *A. thaliana* and a subset of related flowering plants. Some work has suggested there may be a BASL paralogue in *A. thaliana* that does have homologues in other multicellular plants and contains two well-conserved domains (Erich Schwarz, Joseph Cammarata and Adrienne Roeder, unpublished). Work to date characterising this paralogue has not shown any clear phenotypes (Joseph Cammarata, unpublished) and further work is needed to establish the functional relevance of this protein. This suggests that, if a polarity field is a common feature of cells and tissues, BASL does not play a role in establishing or maintaining this in other species. Instead, this work suggests a common underlying polarity coordinated across planar plant organs.

5.3 Polarity and growth

The polarity field described in this work represents evidence for a tissue-wide polarity field that exists throughout development and could coordinate anisotropic growth, as has been predicted through modelling (Coen and Rebocho, 2016; Coen et al., 2017; Kennaway et al., 2011). Anisotropic growth is known to be important for the growth and development of plant organs, as shown using clonal analysis in many species (Bencivenga et al., 2016; Eldridge et al., 2016; Green et al., 2010; Kuchen et al., 2012; Sauret-Güeto et al., 2013). In the absence

Main discussion

of conclusive links to growth, the existence of this polarity field cannot preclude other non-polarity-based models of development. However, the link between the ectopic BASL polarity field described here and PIN1 polarity indicates that the BASL polarity field is connected to systems known to play a role in the growth and development of plant shapes.

I have shown in this work that cell shape anisotropy can complicate interpretations of polarity due to the fact the cell polarity is assigned relative to points within a cell or leaf. This differs from a continuous polarity field in mathematical modelling, where polarity is understood to be a continuous vector field (Kennaway et al., 2011). This is an important difference which should be taken into account when comparing mathematical polarity fields, such as in Kuchen et al. (2012), with cell-based biological data. This also highlights the need to include cells in models of leaf growth, as has recently been implemented in Fox et al., (2018).

Previous studies have attempted to link cell polarity to cell shape or growth. Bringmann and Bergmann (2017), for example, track cell growth and BRXL2 polarity and illustrate that BRXL2 orientation correlates closely with the orientation of cell growth. This work concludes that BRXL2 is in the position to define growth orientations in meristemoid mother cells (Bringmann and Bergmann, 2017). In a similar manner, Kuchen et al. (2012) show a similarity between the growth directions in regions of the tissue and the polarity field predicted by their leaf model. In these studies, cell shape or growth seems to be correlated with polarity or predicted polarity. However, it remains difficult to experimentally link growth and polarity beyond correlation.

It would be informative to examine the ectopic BASL polarity field described in relation to tissue growth and analyse any correlations. To make more causative links between polarity and growth would ideally require experiments modulating either polarity or growth, which remains technically challenging, not least because the mechanisms underlying both are not fully understood. One possible way of conducting such experiments would be to induce sectors of proteins that have been proposed to modulate polarity and to use ectopic BASL as a marker to analyse any changes to the polarity field. Such proteins might include CUC2, known to play a role in polarity and outgrowth formation at serrations (Bilsborough et al., 2011) and *kanadi1kanadi2* outgrowths (Abley et al., 2016), though its precise role remains unclear (Bilsborough et al., 2011; Hasson et al., 2011; Rebocho et al., 2017a).

Plausible mechanisms have been suggested for how polarity and growth may be linked at the cellular level, such as preferential cell wall reinforcement through cellulose deposition (Baskin, 2005) guided by microtubules (Chan et al., 2010; Gutierrez et al., 2009; Peaucelle et al., 2015). Whilst links between the cytoskeleton, growth and polarity should be made with caution, recent work by Jordi Chan suggests that microtubules may be depleted in regions where BASL is localised (Jordi Chan, personal communication). This could represent a potential mechanism by which BASL could alter growth at the cellular level and could provide further evidence that BASL, or the polarity it reveals, are important factors in growth.

5.4 Mechanisms underlying polarity establishment and coordination

It can be useful to separate the polarity coordination mechanism and the partitioning mechanism, as is the case in intracellular-partitioning models of polarity (Abley et al., 2013).

5.4.1 Maintenance of polarity systems

The coordination of the proximodistal polarity field throughout the leaf epidermis could be accounted for by mechanical and/or chemical mechanisms (Abley et al., 2013; Bennett et al., 2014; Heisler et al., 2010; Hervieux et al., 2016; Sassi and Traas, 2015; Whitewoods and Coen, 2017). In the case of BRXL2 polarity, Bringmann and Bergmann (2017) report that mechanical stretching can deflect the polarity field, which indicates that tissue-wide mechanical forces could influence polarity. Preliminary results using ectopic BASL in similar experiments did not indicate any BASL polarity reorientation, but need to be conducted in more detail to be conclusive. The nature of polarity as a vector (with an arrowhead) means that tissue stress, which has axiality but not polarity, is not sufficient to establish the directional aspect of a vector field (Coen et al., 2017; Goriely, 2017; Hejnowicz and Romberger, 1984); thus, a stress gradient would be required (Heisler et al., 2010). Alternatively, a biochemical mechanism, such as flux sensing or cell-cell coupling, may underlie the coordination of the polarity field (Abley et al., 2013; Mitchison, 1980; Rolland-Lagan and Prusinkiewicz, 2005). Such a mechanism has the advantage of being uncoupled from the stresses generated through differential growth (Coen et al., 2017).

At present, the mechanisms underlying the coordination and maintenance of the ectopic BASL polarity field remain largely unknown. Other polarity proteins, such as the recently discovered SOK protein family are, like ectopic BASL, relatively insensitive to many hormones or drugs including those affecting membrane trafficking, cytoskeletal dynamics and protein degradation (Yoshida et al., 2019). SOK proteins were, however, found to be sensitive to cell wall degradation (Yoshida et al., 2019), unlike BASL in protoplasts. Future work could provide insights into the role of the cell wall in polarity and confirm the results shown here, for example, by staining protoplasts with calcofluor to ensure the entire cell wall has been degraded. In addition, mutants could be used to further test the mechanisms involved in BASL polarity coordination. Previous work has indicated that the rootward localisation of ectopic BASL polarity in roots can be slightly disrupted in the *kuq* mutant (Pietra et al., 2013), which is allelic to *SABRE* and thought to play a role in cell expansion and polarity (Aeschbacher et al., 1995). It would be interesting to test the ectopic BASL polarity field in the leaves of this mutant and other mutants reported to exhibit altered polarity, such as trichome mutants (Folkers et al., 1997).

Auxin is the best-known candidate involved in coordination of polarity in plants, and coordinates the polarity of PIN proteins (Feraru and Friml, 2008; Friml et al., 2003). The mechanisms underlying this coordination remain disputed and it is possible that multiple mechanisms exist simultaneously, coordinating PIN polarity in different contexts (Bennett et al., 2014). Auxin remains a possible candidate for the coordination of the BASL polarity field, particularly given the observed link to PIN1 polarity at serrations and despite the fact that experiments inhibiting polar auxin transport using NPA did not disrupt the ectopic BASL polarity field. It is worth noting that other auxin transport inhibitors, such as 2,3,5-triiodobenzoic acid (TIBA), could also be tested for a role in perturbing the polarity system. It also remains possible that an underlying polarity mechanism exists, in which establishment and coordination could be independent of auxin, and which polarity systems, such as PIN proteins and ectopic BASL, can respond to and interact with.

5.4.2 Establishment of polarity systems

It is possible that the unknown components of the molecular address with which BASL interacts are part of the partitioning mechanism involved in the establishment of polarity. To understand the mechanisms of polarity establishment and maintenance in more detail, experiments need to be conducted exploring the role of mechanical stresses, auxin and other unknown BASL interacting partners in ectopic BASL polarity. A key question is whether the

establishment of polarity can arise spontaneously in cells, or whether external cues are required to polarise cells.

Modelling has indicated that it is possible for both plant and animal cells to spontaneously polarise in the absence of external cues (Abley et al., 2013). In plants there is relatively little evidence of this, partly due to the experimental challenges of isolating single plant cells (notably, this has been done using plant xylem cells (Oda and Fukuda, 2012)). However, I have shown here that BY-2 protoplasts can be polarised using BASL. Further work will be necessary to test whether this polarity could arise spontaneously, or whether it is only observable in cells that previously possessed polarised BASL. In addition, it has been reported that BY-2 protoplasts are able to elongate anisotropically in response to a geometric cue (a rectangular microvessel), but without making contact with the walls of the vessel in an auxin dependent manner (Zaban et al., 2015). It would be interesting to conduct similar experiments using BASL-expressing protoplasts.

In other situations where individual cells from multicellular organisms are analysed, such as fish epidermal keratocytes, cells can also spontaneously polarise (Marée et al., 2006). In single-cell polarity models, such as yeast, polarity can arise spontaneously (Altschuler et al., 2008; Sohrmann and Peter, 2003; Wedlich-Soldner et al., 2004), or in response to external cues (O'shea and Herskowitz, 2000). By contrast, the zygote of the brown algae *Fucus*, which has long been studied as a paradigm of cell polarity, polarises in response to external factors (Goodner and Quatrano, 1993; Jaffe, 1956; Torode et al., 2016).

At present, one of the only factors known to disrupt BASL polarity at the cellular level is a chemical known as bubblin, which is a pyridine-thiazole derivative (Sakai et al., 2017). Bubblin was found from a library of small bioactive molecules. It is reported to disrupt BASL polarity and induces ectopic retention of the transcription factor SPEECHLESS, resulting in stomatal clustering (Sakai et al., 2017). It would be interesting to observe the effect on ectopic BASL polarity in the presence of this compound. However, despite representing a potential artificial way to alter polarity, this approach is limited in allowing understanding of the underlying mechanisms of plant polarity establishment and maintenance.

Elucidation of potential components of the molecular address may lead to an understanding of the signalling and biochemical mechanisms underlying the establishment of tissue-cell polarity in plants. Some of the candidates isolated in Chapter 4 of this work could represent interesting lines of evidence worth testing for roles in polarity. For example, the

identification of a calcium sensing receptor may be worth exploring in more detail to analyse its localisation and confirm any interaction with BASL.

Further experiments, including those identifying possible novel polarity components, and modelling will hopefully elucidate mechanisms involved in the establishment of polarity in plants. It would also be of great interest to compare polarity establishment mechanisms recently revealed with SOK proteins (Yoshida et al., 2019) to those that may be involved in BASL polarity, in order to understand whether conserved mechanisms underlie the polarisation of different polarity markers.

5.5 Evolution of a polarity field

5.5.1 The role of polarity in patterning the leaf epidermis

In addition to influencing growth, a common underlying polarity field in planar plant organs may also influence patterning and differentiation. For example, trichomes and stomatal patterning both have an element of proximodistal coordination (Bouyer et al., 2001; Bringmann and Bergmann, 2017; Hülkamp et al., 1994). Polarity is critical for stomatal spacing in *A. thaliana* (Lau and Bergmann, 2012; Robinson et al., 2011). However, it remains unclear why proximodistal coordination in both stomata and trichomes would be functionally important.

One hypothesis is that the coordination of these components of a leaf reflects evolutionary history rather than current function. Stomatal patterning mechanisms vary among plant species (Vatén and Bergmann, 2012). In *A. thaliana* and many other species, stomata are evenly spaced (Chater et al., 2017; Dong et al., 2009), however, in many monocots such as grasses, stomata are highly proximodistally oriented (Cartwright et al., 2009; Raissig et al., 2016; Rudall et al., 2017). A proximodistal polarity field could represent a highly conserved system for orienting tissue growth and transport (Meinhardt, 2007; Nelson, 2003; Strutt and Strutt, 2009). Perhaps various elements of the proximodistal polarity system were co-opted for stomatal patterning in different plant lineages. For the lineage leading to *A. thaliana*, co-option may have led to a polarity-switching mechanism and the evolution of BASL. This hypothesis would account for why BASL cross-reacts with the proximal address when ectopically expressed. Other plant lineages, such as grasses, which exhibit strong

proximodistal coordination in stomatal patterning (Facette and Smith, 2012; Raissig et al., 2016), might represent different ways of co-opting elements of a common underlying proximodistal field.

At present, this hypothesis remains difficult to test experimentally. Identification of the molecular components of the proximal address and analysis of BASL homologues in other species may provide insights into the evolutionary role of a proximodistal polarity field. In addition, it would also be interesting to analyse BASL localisation in the stomatal lineage in more detail, for example to distinguish whether the first divisions of meristemoid mother cells are proximodistally aligned, with future divisions then occurring in the polarity-switching spiral pattern (Robinson et al., 2011).

5.5.2 BASL polarity in other contexts

The lack of clear BASL homologues in other species (Dominique Bergmann, personal communication) raises the question of how other species with evenly spaced stomata undergo polarity switching. The localisation pattern observed when BASL is ectopically overexpressed in *A. thaliana* leaves has elements in common with that observed when BASL is expressed in *N. benthamiana*. There does not seem to be a clear BASL homologue in *N. benthamiana* which may provide further evidence that BASL is cross-reacting with a more common underlying polarity system in pavement cells. Whether or not BASL represents a useful polarity marker in other organs and tissues remains to be seen.

The observed polar localisation of ectopic BASL in BY-2 cells suggests that polarity can exist outside of a tissue context. This localisation differs from the axial localisation of PIN1 (i.e. to both the short ends of BY-2 cells) reported in BY-2 cells (Boutté et al., 2005). The polarisation of BASL in these cells and in protoplasts supports the intracellular partitioning model which predicted the ability of cells to spontaneously polarise in the absence of neighbours (Abley et al., 2013). This system also provides an experimental context in which to test hypotheses and predictions from this type of model, which is currently largely theoretical, in a way which has not been possible previously. For example, it may now be experimentally possible to apply auxin gradients to BY-2 cells and observe any response of BASL polarity to such conditions. BY-2 cells could also allow experiments involving the testing of mechanical stresses and other factors in the context of polarity. For example, experiments could be conducted, similar to those in Lynch and Lintilhac (1997) where mechanical stresses are

applied to protoplasts, or those in Zaban et al. (2015) in which protoplast regeneration is analysed.

5.5.3 Polarity in single-celled organisms and multicellularity

This work provides the first evidence for a tissue-wide polarity field in planar plant organs that exists throughout development, independent of the stomatal lineage. However, polarity systems have been identified and studied for many years in other multicellular systems. In single-celled systems, such as yeast (Johnson et al., 2011; Slaughter et al., 2009) and algae (Goodner and Quatrano, 1993; Torode et al., 2016), polarity is known to play a key role in chemotaxis (Marée et al., 2006; Wedlich-Soldner and Li, 2003). Coordinated polarity systems in multicellular organisms including *Drosophila* (Goodrich and Strutt, 2011; Thomas and Strutt, 2012), zebra-fish (Heisenberg et al., 2000), mice (Wang and Nathans, 2007) and human tissue (Butler and Wallingford, 2017) have also been described in detail.

The existence of polarity systems in a diverse range of single-celled and multicellular organisms indicates polarity is evolutionarily ancient. Arguably, the coordination of cell polarity is necessary in allowing coordination of signals in multicellular organisms, and ancient polarity establishment mechanisms may provide a basic building block for establishing tissue polarity (Meinhardt, 2007).

5.6 Tools for understanding polarity

5.6.1 Development of software

The development of software in this work to quantify a polarity field in a semi-automated manner was an important part of characterising the polarity field in a non-biased way. The rotation of each cell allowed polarity to be assigned to cells without prior knowledge of a cell's position or orientation within the leaf. This method of polarity quantification is unlike those used previously, where polarity has usually been assigned by hand, for example in quantification of BRXL2 polarity within the stomatal lineage (Bringmann and Bergmann, 2017). In some cases, particularly when assigning polarity to PIN proteins, it can be very difficult to confidently assign polarity in a cell and sometimes only an axiality can be assigned (Abley, 2014; Abley et al., 2016). BASL polarity is often easier to assign than PIN due to its preferential localisation to cell corners. The software for assigning polarity to a cell that was

developed as part of this work could therefore be a useful tool to the developmental biology community for quantifying the polarity of BASL or other markers.

At present, the quantification tools are coded in python, and the visualisation tools in Matlab, and require specific input image types and coding ability to adjust parameters. However, it would be possible to develop these tools further, perhaps allowing them to be integrated into other image analysis packages, such as Fiji (Schindelin et al., 2012) or MorphoGraphX (Barbier de Reuille et al., 2015) to allow them to be used more readily.

5.6.2 Development of a polarity marker

Adaptation of the Cre-lox heat-shock system (Gallois et al., 2002) to allow inducible ectopic expression of BASL across the leaf was initially developed by Jordi Chan. This has allowed the characterisation of the ectopic BASL polarity field in leaves, without the potential pleiotropic effects of overexpressing BASL in cells (Dong et al., 2009).

My work has focussed on the *A. thaliana* leaf as a planar plant organ used to characterise polarity. Coordinated tissue cell polarity has been predicted to be necessary for the development of many planar plant organs, using computational modelling. For example, the *A. thaliana* petal has been predicted to have a divergent polarity field that provides directionality for orienting anisotropic growth (Sauret-Güeto et al., 2013). In addition, the *Capsella rubella* silicle has also been modelled, predicting a polarity field which allows the heart-shape fruit to form (Eldridge et al., 2016). These examples where a tissue-wide polarity pattern has been predicted using GFtBox modelling (Kennaway et al., 2011) in *A. thaliana* and closely related species could potentially be easily tested using ectopic BASL. This would allow such models to be tested and refined accordingly. For example, more recent models of the leaf that include individual cells (Fox et al., 2018) could be refined with knowledge of the polarity patterns observed using BASL.

Ectopic BASL may also provide a tool for testing models and hypotheses regarding growth and shape formation in more complex shapes. For example, the 3D trap of *Utricularia gibba* has been modelled, and hypotheses have been generated regarding the role of anisotropic growth and polarity in the formation of this shape (Bushell, 2016; Whitewoods and Coen, 2017). The *U. gibba* bladder has quadrifid glands on its inside surface that have an asymmetry providing a physical marker of polarity in some cells across the bladder (Bushell, 2016), similar to trichomes in the *A. thaliana* leaf. Work is in progress to test ectopic BASL as a molecular marker of polarity in the bladder. This would not only provide useful insights into

the development of complex 3D shapes, but may also indicate that ectopic BASL could be used as a marker of polarity in more distantly related species.

5.6.3 Development of a biochemical assay for identifying potential polarity factors

In addition to collaborating to generate software tools as part of this project, and the inducible BASL system developed, one of the key elements of this work is the identification of possible components of the proximal address. I used a biochemical approach to try and identify potential BASL interactors.

During this project, I did not conclusively identify BASL interactors, but I have successfully conducted a co-immunoprecipitation with mass-spectrometry identification of potential BASL interactors in *N. benthamiana*. The list of potential BASL interactors represents a preliminary list of candidates that may warrant further testing, ideally in *A. thaliana* as well as *N. benthamiana*, to characterise their localisation and establish any role as BASL interactors. I have tested multiple conditions for BASL extraction which may pave the way for the identification of novel plant polarity factors in the future.

5.7 Future directions

5.7.1 Understanding the relationship between polarity and growth

This work has characterised a polarity pattern in the leaf epidermis which is reminiscent of the polarity field predicted through modelling the development of the *A. thaliana* leaf (Kuchen et al., 2012). Previous work has predicted that such a polarity field could be important in providing the directional information to guide anisotropic growth (Coen et al., 2017; Kennaway et al., 2011). I have provided evidence for a link between the ectopic BASL polarity field and that of PIN1, which is known to be involved in development and the generation of shape. Future work should be carried out to further explore the relationship between the tissue-wide polarity field and growth. This could include a more conclusive analysis of BASL and PIN in *kanadi1kanadi2* outgrowths, as well as analysis of the relationship between BASL and other members of the PIN family, or in different contexts, such as the root and vasculature.

Experiments conclusively linking polarity and growth are complicated by a number of factors including cell shape and anisotropy. In the future, it may be possible to experimentally modulate growth or polarity. At present, time lapse imaging, particularly using isotropic cells or cells whose growth axis is not aligned with the proximodistal axis of the leaf, could be used to unravel the complex relationship between polarity and the growth of a tissue.

In addition to tissue-level growth patterns, it is possible to explore the relationship between polarity (using ectopic BASL) and cellular level growth. I have showed that BASL can reveal a coordinated polarity pattern when microtubules have been destabilised using oryzalin. Several lines of evidence suggest that the cytoskeleton could interact with cell polarity: the cytoskeleton is known to play a role in the neck and lobe formation of pavement cells (Fu et al., 2002; Fu et al., 2005), microtubules may be depleted where BASL is localised (Jordi Chan, personal communication) and actin was highlighted as a possible interacting partner of BASL in the IP-MS work I conducted. Further work, for example using other cytoskeleton inhibiting drugs, cytoskeleton mutants, and observing BASL and microtubule dynamics in the same cells may elucidate any relationship between BASL polarity and cell growth.

5.7.2 Understanding the establishment of polarity

A key question is how cell polarity is established. Models have proposed how polarity may be established: polarity can arise as a response to external factors or neighbouring cells, or emerge spontaneously in the absence of external cues (Abley et al., 2013). A key challenge of future work, therefore, will be to test the mechanisms involved in the polarisation of BASL.

Given that there are likely to be BASL interacting partners involved in the establishment of polarity, further biochemical work confirming the interacting partners of BASL is necessary. This could use the preliminary results from the IP-MS conducted as part of this work, and may provide more conclusive evidence for some of the potential partners I have isolated, or elucidate novel interactors. Other polarity factors (SOK proteins) recently discovered in plants have been found to possess a DIX domain (Yoshida et al., 2019), known to be involved in polarity establishment in animals (Schwarz-Romond et al., 2007). It would be interesting to see if BASL and SOK polarity systems share common elements. Identification of the mechanisms underlying polarity formation in plant cells may also pave the way for testing of polarity models, such as the intracellular partitioning model (Abley et al., 2013).

The BY-2 BASL system that I developed as part of this work may also be a useful tool in elucidating mechanisms of polarity establishment. It is possible that regenerating BY-2

protoplasts, for example, could provide useful insights into how polarity is established de-novo. This system could also be used to analyse how polarity could arise in a single cell, and how polarity is inherited at cell division (Figure 3.42).

5.7.3 Understanding the polarity coordination mechanisms

In addition to the mechanisms involved in polarity establishment, the mechanisms involved in polarity coordination across a tissue remain unknown. Future work may build on the preliminary results I have presented in this work, including testing the role of mechanical stresses and auxin. In particular, it will be useful to further analyse the response of BASL polarity to mechanical stresses and to understand why the preliminary results presented here differ from those using native BRXL2 (Bringmann and Bergmann, 2017). The tool developed by Jamie Spooner in his undergraduate project work provides a useful but simple way to directly test BASL polarity in response to mechanical stresses. It would also be interesting to use more complex tools, such as an automated confocal micro-extensometer (ACME) (Robinson et al., 2017) to analyse BASL dynamics in response to mechanical stresses in a more controlled and detailed manner. Such experiments could lead to a better understanding of the respective roles of polarity and mechanical stresses during growth and development.

The identification of interacting partners of ectopic BASL may provide insights into polarity coordination mechanisms. For example, if lipid-domain proteins or receptors appeared to be interacting with BASL, this might provide clues as to the mechanisms to coordination. The identification of actin as a putative BASL interactor in the preliminary IP-MS in this work may suggest, for example, that latrunculin, which depolymerises actin filaments, could be used to disrupt the actin component of the cytoskeleton and see if this disrupted BASL polarity.

5.7.4 Exploring polarity in other systems

In this work, I have focussed on the characterisation of polarity in the development of the *A. thaliana* leaf. The tools developed in this work – both biological and technical – make it possible to test predictions of polarity patterns in other *A. thaliana* organs. For example, polarity predictions have been made in the petal and could be tested using BASL (Sauret-Güeto et al., 2013). The *A. thaliana* sepal might also provide an interesting organ in which to explore BASL polarity, as much work has been undertaken to understand its development (Hervieux et al., 2016; Hervieux et al., 2017; Tsugawa et al., 2017). Polarity could also be tested in the organs of other species, such as the *C. rubella* fruit (Eldridge et al., 2016), the

bladder of *U. gibba* (Coen lab, in preparation) and the thallus of *Marchantia polymorpha*, which is predicted to not require polarity to undergo its development (Solly et al., 2017). Thus, this work has provided the plant developmental biology community with tools to explore the role of polarity in the development of plant organs.

Whilst this work is conducted in plants, it may be of interest to the developmental biology communities in animals, where planar cell polarity has been characterised in detail (Goodrich and Strutt, 2011). Comparative analysis of polarity establishment, maintenance, and involvement with growth between plants and animals could provide novel insights into the importance of polarity more broadly and its evolution.

5.8 Concluding remarks

This work provides the first evidence of a coordinated tissue-wide polarity field that exists in *A. thaliana* leaves throughout development and is independent of the stomatal lineage. This polarity field is linked to the polarity of PIN proteins and possibly to the growth and development of plant organs. It is hoped that this work, particularly the preliminary biochemical analysis, will lead to a deeper understanding of how polarity is established and maintained in plant tissues. This work has contributed to the field of plant developmental biology by providing tools that may allow the testing of models of development and, in the future, will hopefully allow broader questions regarding the growth and development of plant shapes to be explored.

6 Materials and methods

6.1 Plant materials and growth conditions

6.1.1 *Arabidopsis thaliana* growth conditions

A. thaliana plants were grown on plates containing MS media (0.441% Murashige & Skoog including vitamins, 1% (w/v) glucose, 0.05% (w/v) MES, 1% Difco agar, pH to 5.7) and relevant antibiotic selection (BASTA, 15 mg/ml, kanamycin 50 mg/ml). Sterilised seeds were stratified in the dark at 4°C for 3 days, then grown at 20°C in controlled environment long day conditions (16 hours light and 8 hours dark). Leaves were typically taken from plants up to 9 days after stratification (DAS) for imaging and analysis.

For growing plants on soil (for example, for taking plants through generations), seeds were sown in John Innes Centre *Arabidopsis thaliana* Soil Mix (Levington F2 compost with Intercept and grit in a 6:1 ratio) and grown under long day conditions (16 hours light and 8 hours dark) at 20 °C.

Following dipping with *Agrobacterium tumefaciens*, plants were grown in a greenhouse supplemented with artificial light at approximately 22 °C.

6.1.2 Seed sterilisation

A. thaliana seeds were generally sterilised using gas (Cl₂ gas in desiccator overnight). When large volumes of seeds were sterilised at once (for example for immunoprecipitation experiments and the first generation of transgenic lines), surface sterilisation of seeds was used. Seeds were sterilised using 70% ethanol with 0.05% SDS for 5 minutes, followed by at least three washes in 100% ethanol. Seeds were then air-dried on sterile filter paper before being plated.

6.1.3 *Nicotiana benthamiana* growth conditions

Wild-type *N. benthamiana* plants were grown in soil in controlled environment rooms under long day conditions (16 hours light and 8 hours dark) at 22 °C.

6.1.4 Existing plant material used

A. thaliana lines used in this work that were generated previously are described below. This includes mutant and reporter lines, and well as the heat-shock inducible *35S::GFP-BASL* line generated by Jordi Chan. Lines that I generated are described in Section 6.2.

6.1.4.1 Mutants and fluorescent markers

The transgenic lines in the following table were used in this work. The *A. thaliana* accession and origin of the line are indicated.

Table 6.1 Mutant and reporter lines used from previously published sources.

Previously developed *A. thaliana* mutant lines and reporter lines used in this work are listed, indicating their ecotype and publication where lines are reported.

<i>Arabidopsis thaliana</i> line	Background	Origin
Heat shock inducible <i>35S::GFP-BASL</i>	Col-0	(Mansfield et al., 2018)
<i>BASL::GFP-BASL</i>	Col-0	(Dong et al., 2009)
RFP-plasma membrane (pm-rb)	Col-0	(Nelson et al., 2007)
<i>spch</i> mutant (<i>spch-1</i>)	Col-0	(MacAlister et al., 2007)
<i>HS::Cre</i>	Col-0	(Gallois et al., 2002)
<i>PIN1::PIN1-GFP</i>	Col-0	(Benková et al., 2003)
<i>35S::TUA6-GFP</i>	Col-0	(Ueda et al., 1999)
<i>35S::mCherry-TMCT</i> (TMCT)	Col-0	(Caillaud et al., 2014)
<i>kanadi1 kanadi2</i>	Ler	(Eshed et al., 2001)
<i>kanadi1 kanadi2</i> with <i>PIN1::PIN1-GFP</i>	Ler (<i>kan1kan2</i>), Col-0 (PIN1)	(Abley, 2014)
<i>phgap1 phgap2 (gap1gap2)</i>	Col-0	(Stöckle et al., 2016)
Heat-shock inducible <i>35S::ER-GFP</i> (71028)	Col-0	Coen lab

6.1.4.2 Generation of inducible *35S::GFP-BASL*

The inducible *35S::GFP-BASL* line was made by Jordi Chan according to the following protocol prior to the start of this project and is described in Mansfield et al., (2018). The generation of this line is described here for clarity and completeness.

Gateway cloning was used to construct the heat-shock inducible *35S::GFP-BASL* line which required a destination vector and an entry vector. A destination vector was made (referred to Active Blue destination vector) containing a 35S promoter in front of a CyPET-HDEL fluorescent marker and a Nos terminator flanked by lox sites. These lox sites allow heat-shock recombination to remove the fluorescent marker so that the 35S promoter drives the BASL gene following induction.

The Active Blue destination vector was made using a pre-existing Gateway vector, pB7WGC2 (Karimi et al., 2005) and the pBOB (Wachsman et al., 2011) vector in 2 steps. In the first step, a 1175 bp fragment containing lox-HDEL:CyPET:NOS-Terminator-lox was cloned from pBOB and flanked with SpeI and EcoRV sites using a 2-step PCR, involving the primers F_BOB_lox_speI and R_BOB_lox_N, then primers F_BOB_lox_speI and R3_BOB_lox_EcoRV (Table 6.2). The PCR product was then cloned into TOPO4 (Table 6.2). In the second step, the pB7WGC2 vector was digested with SpeI and BspEI, to excise a 1175 bp fragment containing ECFP, and replaced with the fragment cloned from pBOB vector (cut out from the TOPO4 vector using SpeI and BspEI) (Table 6.2). The ligation product was transformed into ccdB-resistant one-shot *E. coli*.

To introduce GFP-BASL into the destination vector (Table 6.2), an LR reaction (Invitrogen) was carried out using the Active Blue destination vector and an entry clone containing GFP-BASL (Dong et al., 2009). The construct was then transformed into *A. tumefaciens* strain GV3101 and floral dip method were used (Clough and Bent, 1998) to dip into *HS::Cre* (Gallois et al., 2002) containing plants. Three independent lines were obtained showing the same pattern. The line used here is a single copy, single insert line (iDNA Genetics, Norwich).

Table 6.2 Primers and vectors used in the generation of the heat-shock inducible BASL line. These primers, vectors and entry clone were used in the generation of the heat-shock inducible *35S::GFP-BASL* line, made by Jordi Chan prior to the start of this project. The origin of the DNA parts is indicated.

DNA	Sequence/Name	Origin
Primer	F_BOB_lox_speI (GGGACTAGTATCGCGCCGCTTCGAAA)	N/A
Primer	R_BOB_lox_N (CTATACGAAGTTATACGCGTCTGT)	N/A
Primer	R3_BOB_lox_EcoRV (GGGATATCATAACTTCG TATAAAGTATCCTATACGAAGTTATACGCGTCTG)	N/A
Vector	pBOB vector	(Wachsman et al., 2011)
Vector	TOPO4 vector	Invitrogen
Vector	pB7WGC2 vector	(Karimi et al., 2005) (VIB Gent)
Entry clone	GFP-BASL entry clone	(Dong et al., 2009)

6.1.5 Crossing

The inducible *35S::BASL-GFP* construct was introduced into mutant and fluorescent marker backgrounds by crossing. Where possible, the mutant line was used as the female and pollinated with the homozygous BASL line and then selected in the next generation using selective media and phenotyping. This was the case when crossing the inducible *35S::GFP-BASL* line to *gap1gap2* and TMCT lines. Where necessary, plants were taken through to the F2 generation and selected by phenotype and fluorescence.

The inducible *35S::BASL-GFP* line was crossed to the RFP-PM line (Nelson et al., 2007) and offspring containing RFP-PM and inducible *35S::BASL-GFP* were selected by growing on selective plates and screening for RFP (using BASTA for *35S::BASL-GFP*, and kanamycin for *HS::Cre*).

For crossing to *spch*, the inducible *35S::GFP-BASL* was crossed to the heterozygous *spch-1* mutant plants and offspring containing *spch-1* and inducible *35S::BASL-GFP* were selected by phenotype and growing on selective plates.

The *kanadi1kanadi2* (*kan1kan2*) double mutants are sterile. In order to generate a line with the inducible BASL line in the *kan1kan2* double mutant, I crossed the BASL line into the *kan1+/-kan2* background which is fertile and can be identified by an upward curled silique phenotype (Abley, 2014). The F1 offspring of this cross were then selfed and the F2 population was grown on selective media to select for *kan1+/-kan2* individuals with inducible *35S::GFP-BASL* and *HS::Cre*. Plants containing both constructs were grown on soil and *kan1+/-kan2* individuals were identified by their upwardly turned cotyledons (an intermediate phenotype between wild-type and *kan1kan2* double mutants, (Eshed et al., 2001). The offspring of these plants segregated for *kan1kan2* double mutants carrying the desired constructs which were selected for. The *kan1kan2* double mutant seedlings were identified for experiments based on their clear upwardly curled cotyledon phenotype.

6.1.6 Generation of new plant lines

Multiple *A. thaliana* lines were generated during this work using the Golden Gate cloning system (Table 6.3). A detailed description of the Golden Gate cloning methods used, and details of *A. thaliana* transformation can be found in section 6.2.

6.2 Cloning and *A. thaliana* transformation

6.2.1 Golden gate cloning

Goldengate cloning is a modular cloning system that was used to generate multiple *A. thaliana* lines in this work including the heat-shock inducible *35S::mCherry-BASL* line, fluorescent reporters for putative BASL candidates (from Jones et al., 2014) and *35S::GFP-BASL* lines for expression in *N. benthamiana*. Golden Gate cloning allows the generation of single binary transformation vectors through progressive stages of cloning and use of standardised parts. Synthesised level 0 (L0) components are combined to make level 1 (L1) transcriptional units, which can be combined to make level 2 (L2) multigene units that can be transformed into plants (Weber et al., 2011). Level 0 modules must be domesticated to remove BsaI, BpiI and DraIII restriction sites. This cloning method is based on the ability of bacterial type IIS endonuclease restriction enzymes (BsaI, BpiI and Esp3I) to cut downstream of a specific recognition site. By using specific 3' and 5' overhangs (fusion sites), fragments cut by the same type IIS endonuclease can then be linearly ligated by T4 ligase in a given order (Weber et al., 2011).

6.2.1.1 General Golden Gate protocols

For generating L1 modules, 100 ng of L1 vector backbone was combined with 100 ng of each L0 part, 1.5 µl of 10x BSA (New England Biolabs, NEB), 1.5 µl of 10 x T4 Buffer (NEB), 1 µl of BsaI enzyme (NEB), 1 µl of T4 ligase (NEB) and H₂O to a total volume of 15µl. For L1 constructs containing a *lox* component, the 1 µl of BsaI was replaced with a mixture of 0.5 µl of BsaI and 0.5 µl of Esp3I (NEB). The reaction was then incubated in a G-STORM® Thermocycler (GT40361) with the following program: 3 minutes at 37°C and 4 minutes at 16°C for 40 cycles followed by 1 cycle of 5 minutes at 50°C and 5 minutes at 80°C. The Thermocycler was then set to hold the temperature at 10 °C. The completed reaction was transformed into *E. Coli* and grown on selective media. Plasmids were then extracted using a miniprep kit (see below) and sequenced (Eurofins) to confirm correct positioning of components (Table 6.3).

For level 2 module cloning, 100 ng of L2 vector backbone was combined with 100 ng of each relevant L1 transcriptional unit and 1.5 µl of 10x BSA (NEB), 1.5 µl of 10 x T4 Buffer (NEB), 1 µl of BpiI enzyme (NEB), 1 µl of T4 ligase (NEB) and H₂O to a total volume of 15µl. The reaction was then incubated in a G-STORM® Thermocycler with the same program described above. The completed reaction was transformed into *E. Coli* and grown on selective media. Plasmids

Materials and methods

were then extracted using a miniprep kit (see below) and sequenced (Eurofins) to ensure correct positioning of components (Table 6.3).

6.2.1.2 Generation of mCherry-tagged putative BASL interactors

To generate the mCherry-tagged putative BASL interactor constructs (from Jones et al., 2014), I used Golden Gate cloning to drive these reporters under the 35S promoter. An outline of the constructs indicating the individual components is shown in Figure 6.1 and detailed below.

The L2 backbone containing a bacterial kanamycin resistance cassette was used. In position 1, a module conferring BASTA plant resistance was used. The standard parts (i.e. those not containing the MIND gene candidates) were obtained from The Sainsbury Laboratory (TSL) (<http://synbio.tsl.ac.uk/>) or ENSA (John Innes Centre, Norwich). The L2 position contained the putative BASL interactors (synthesised synthetically and domesticated to remove BsaI, Bpil and DraIII restriction sites), tagged with mCherry at the N or C terminal and driven by the 35S promoter, with a 35S terminator (Figure 6.1). In position 3, a module containing CyPET-tagged RC12A (membrane marker) under the Ub10 promoter was used, although this was not used for subsequent imaging, and an ELE end linker was used (ENSA, JIC, Norwich). The L1 modules were assembled using 'P, U, S, C, T' L0 parts, according to the protocol described in Weber et al., (2011). These constructs were then used in transient transformations in *N. benthamiana*, and stable transformation by floral dipping in *A. thaliana*. The plasmid maps for the L1 modules I generated for these 5 constructs generated can be found in Appendix A.

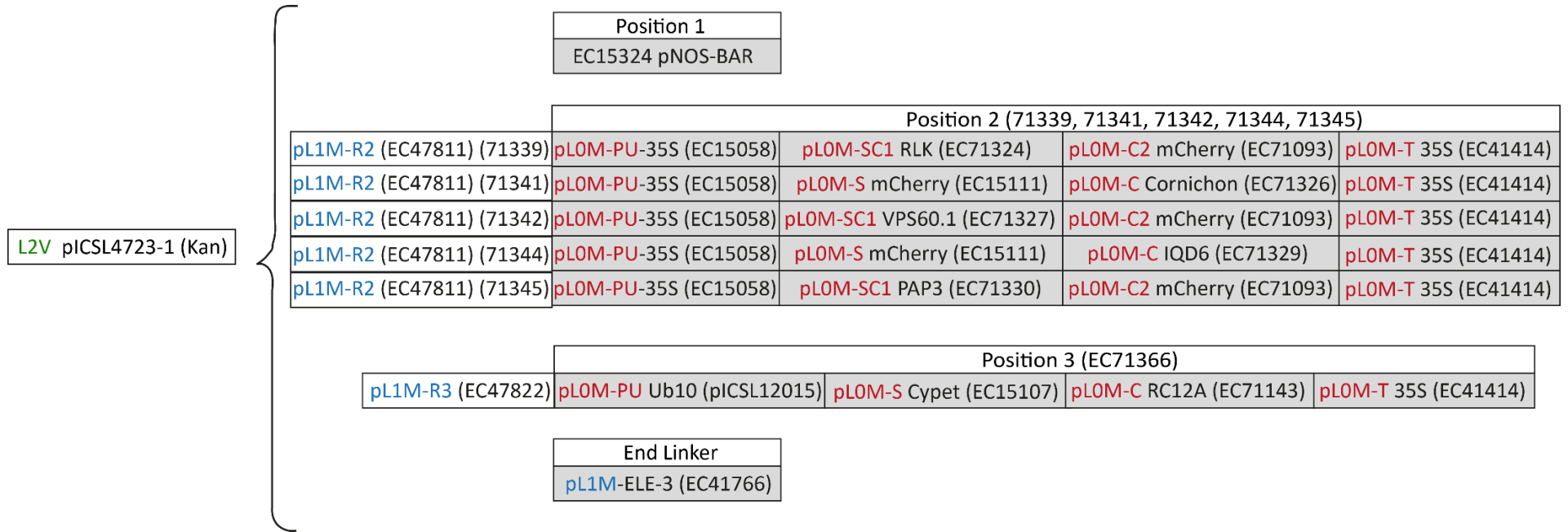


Figure 6.1 MIND gene construct outlines generated using Golden Gate cloning.

The pICSL4723 backbone vector was used to generate five MIND constructs, comprising of mCherry-tagged putative BASL interactors, under the 35S promoter. Components that make up the final level 2 (L2) construct (green) are indicated. Positions 1-3 and the end linker are L1 modules (blue), assembled from L0 parts (red) on individual backbone vectors. Position 2 varies depending on the gene of interest. The ‘P, U, S, C, T’ nomenclature refers to that explained in Weber et al. (2011).

6.2.1.3 Generation of 35S::GFP-BASL constructs

I generated two constructs containing BASL, tagged with 2 different versions of GFP (a standard widely-used eGFP version in construct 71572 and the version used in the heat-shock inducible BASL line in 71273) under the control of the 35S promoter. These two constructs were used for transient expression in *N. benthamiana* and in biochemistry experiments. They were generated using Golden Gate cloning, according to the protocol in Weber et al., (2011), using the L2 backbone vector pICSL4723. In position 1, both constructs contained the pICSL11024 module which confers Kanamycin resistance in plants. Both constructs then had dummy modules in position 2 and 3 (due to the previously developed BASL module being a position 4 module). In position 4, the BASL-containing module was used, before an end linker (ELE-4-EC41780). Construct 71253 contained the L1 module EC71248. This L1 was made up of the L0 'PU' 35S (EC15058), GFP-BASL as an 'SC' component (EC71137) (using the GFP version found in the heat-shock inducible BASL line) and an Act-2 terminator (EC44300). Construct 71572 contained the L1 module EC71569. This L1 was made up of the L0 'PU' 35S (EC15058), eGFP as an 'S' component (EC15094), BASL as a 'C' component (EC71284) and a 35S Terminator (EC41414). The plasmid maps for both constructs can be found in Appendix A.

6.2.1.4 Generation of inducible 35S::mCherry-BASL construct

To make the line with inducible 35S::mCherry-BASL and *PIN1::PIN1-GFP*, I generated a construct containing inducible 35S::mCherry-BASL and *HS::Cre*. The construct (35S::loxmCherry-BASLloxCyPET-HSP18::CRE-35S::BASTA-35S::CyPET-RC12A and called inducible 35S::mCherry-BASL (EC71268) for simplicity) was created by Golden Gate cloning in the vector pAGM4723, according to the protocol in Weber et al., (2011) and described above (Figure 6.2). The construct contained a module conferring BASTA resistance in position 1, the *HS::Cre* module in position 2, the lox-module flanking CyPET in position 3, a dummy position 4 and a membrane marker tagged with CyPET in position 5 (not used in subsequent imaging in this work). The L1 modules were comprised of L0 components from TSL (<http://synbio.tsl.ac.uk/>) or ENSA (John Innes Centre, Norwich), or synthetically synthesised parts that had been domesticated to remove BsaI, BpiI and DraIII recognition sites.

To generate the lox-flanked CyPET L1 module I adapted the standard Golden Gate protocol to incorporate an additional assembly step, termed Level 0.5 (L0.5), as developed by previous lab members (Annis Richardson, Samantha Fox). This allowed the heat-shock module, itself

composed of multiple parts, to be treated as a level 0 part. This was done using the vector backbone EC10161 which is opened by the enzyme Esp3I to allow the insertion of Level 0 modules cut by BsaI, just as for standard Level 1 cloning. This generates loxP flanked modules in the 'U' position suitable for use in subsequent Level 1 assembly (Figure 6.2). Sequences to be used in loxP-flanked modules were domesticated to remove Esp3I sites in addition to BsaI, Bpil and DraIII recognition sites. The plasmid maps for this construct can be found in Appendix A.

This construct was stably transformed into Col-0 containing *PIN1::PIN1-GFP* and *kanadi* mutants containing *PIN1::PIN1-GFP* (see section 6.2.7.1). The three independent lines used for imaging contain 1 or 2 copies (iDNA genetics).

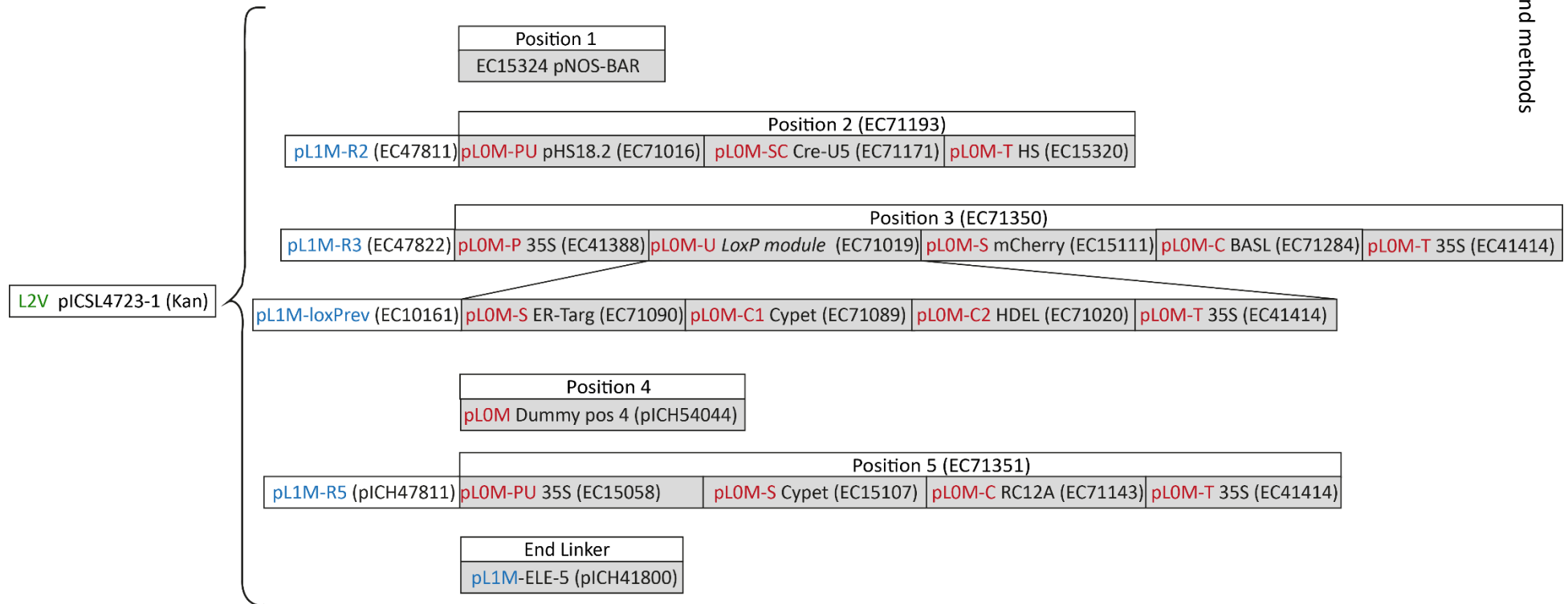


Figure 6.2 The heat-shock inducible *35S::mCherry-BASL* construct was generated using Golden Gate cloning.

The pICSL4723 backbone vector was used to generate construct EC71268, which contained heat-shock inducible *35S::mCherry-BASL* and *35S::CyPET-RC12A*. Components that make up the final level 2 (L2) construct (green) are indicated. Positions 1-5 and the end linker are L1 modules (blue), assembled from L0 parts (red) on individual backbone vectors. Position 3 has an additional layer comprising the lox module which is inserted using an additional cloning step. The 'P, U, S, C, T' nomenclature refers to that explained in Weber et al. (2011).

6.2.2 Transformation of *E. coli*

Transformation of *E. coli* was carried out by heat-shock using Library efficiency DH5 α chemically competent *E. coli* (Invitrogen Life Technologies) or Maximum Efficiency One Shot[®] OmniMAX[™] 2 T1 Phage-Resistant Chemically competent *E. coli* (Invitrogen Life Technologies). Competent cells were thawed on ice for 10 minutes and 1-5 μ l of ligation produce or plasmid DNA was added to cells and mixed gently. Cells were incubated on ice for 30 minutes and then heat shocked at 42 °C for 30 seconds, followed by 2 minutes on ice. 250 μ l of SOC medium (Invitrogen Life Technologies, 2% Tryptone, 0.5% Yeast Extract, 10 mM NaCl, 2.5 mM KCl, 10 mM MgCl₂, 10 mM MgSO₄, 20 mM glucose) was then added and cells were incubated at 37 °C with shaking for 1 hour for recovery. Cells were plated onto LB (lysogeny broth) plates with relevant antibiotic selection and incubated at 37 °C overnight.

6.2.3 Plasmid preparation

Plasmids from 6 ml of overnight *E. coli* cultures were purified using Quiagen Miniprep kits (Quiagen, 27106), according to the manufacturer's instructions. 50 μ l of sterile water was used for elution of DNA from spin columns. DNA concentration was measured using a NanoDrop 1000 Spectrophotometer (Thermo Scientific) according to the manufacturer's guidelines.

6.2.4 Sequencing

Sequencing reactions were carried out for L1 and L2 components using the primers shown in Table 6.3. Reactions were sent to Eurofins Genomics for sequencing.

Table 6.3 Primers used for confirming sequences during Golden Gate cloning.

The primers used for confirming L1 and L2 module sequences are shown below. The primer name and sequence, and a list of the L1 and L2 modules it was used for sequencing are given. Sequencing was carried out by Eurofins Genomics.

Primer Name	Sequence	Target	Constructs sequenced with this primer
GG3	CCCGCCAATATATCCTGTC	Vector backbone	71332, 71334, 71335, 71337, 71338, 71339, 71341, 71342, 71344, 71345, 71253, 71572, 71569, 71268, 71350, 71351, 71366
GG4	GCGGACGTTTTTAATGTA CTG	Vector backbone	71332, 71334, 71335, 71337, 71338, 71339, 71341, 71342, 71344, 71345, 71253, 71572, 71569, 71268, 71350, 71351, 71366
RC12A R	GAGAGGAAAGATAAATACCCC	RC12A	71268
RC12A F	GTTGGTTTGTACTTTGTGTGAAG	RC12A	71332, 71334, 71335, 71337, 71338, 71268
mCherry FP1	TGCAGAAGAAAACCATGGGC	mCherry	71332, 71334, 71335, 71337, 71338, 71344, 71350
mCherry R P1	CTTGGTCACCTTCAGCTTGG	mCherry	71350
mCherry R P2	GTCCTCGAAGTTCATCACGC	mCherry	71339, 71342, 71345
CyPET R	CCCAAGTCAGAGTAGTACTA	CyPET	71268, 71366
CyPET F	GCTGACCATTATCAACAAAATA	CyPET	71366
GCV F	TCAGGGTCAGCTTGCCGTA	GFP	71268
Act2T F P1	GCTACCTCCATCTCACTTGG	Act2 terminator	71253
35S Term F	TTCGCTCATGTGTTGAGCAT	35S terminator	71572
Cre Term F	CGCTGGAGTTTCAATACCGG	Cre terminator	71268
HS Cre R	CTTGCGAACCTCATCACTCG	Cre Recombinase	71268
pNOS R	CGTACTCCCTTAATTCTCC	NOS promoter	71334, 71337, 71253

6.2.5 Copy number analysis

Copy number analysis was performed by iDNA genetics, Norwich. The BASTA or kanamycin resistance genes (depending on the construct resistance) were used to determine the number of transgene copies in T1 plants (i.e. offspring of dipped plants) of all newly transformed lines. Single copy lines were used where possible, but in some instances, lines with 2 or more copies were also used for imaging, ensuring that they had the same phenotypes and localisation patterns as single copy lines.

6.2.6 Electroporation transformation of *Agrobacterium tumefaciens*

A. tumefaciens strain GV3101 was used for transformation. 40 µl of electro-competent cells were defrosted on ice for 10 minutes. ~100 ng of plasmid DNA was added to the cells and mixed gently before being transferred to pre-chilled cuvettes. For electroporation, cells were pulsed using the BioRad GenePulser[®] II (Voltage: 1800 V, Capacitance: 25 µF, Resistance: 400 Ω). 250 µl fresh, chilled SOC media was added to the cuvette and transferred to 1.5ml Eppendorf tubes. The cells were incubated for 1 hour at 28 °C before being plated on selective LB media with the appropriate antibiotics. Plates were incubated for 48 hours at 28 °C.

6.2.7 Stable transformation of *A. thaliana* by floral dipping

A. thaliana plants were transformed according to the protocol in Clough and Bent, (1998). Plants were sown and grown for 4-5 weeks in short day conditions and then moved to long day conditions for dipping when inflorescences are a few centimetres tall.

To prepare cultures for dipping, *A. tumefaciens* carrying the constructs of choice was grown on selective LB plates for 48 hours at 28 °C. A single colony was picked into 10 ml liquid LB with the relevant antibiotics and incubated with shaking overnight at 28 °C. 6ml of this overnight culture was transferred into 250 ml LB media and incubated for a further 24 hours at 28 °C. Bacterial cultures were spun down for 20 minutes at 3500 rpm at 4 °C and resuspended in 2 x 250 ml 5% sucrose solution with Silwet L-77.

For dipping of plants, any pre-formed siliques were removed and plants were dipped in *A. tumefaciens* solution for ~30 seconds – 1 minute. Plants were covered for 24 hours to maintain high humidity and seeds harvested once T0 seeds had dried.

6.2.7.1 Dipping into *kanadi1kanadi2* mutants

The *kanadi1kanadi2* (*kan1kan2*) double mutants are sterile and therefore cannot be used for floral dipping. Instead, to introduce constructs (for example 71268) into the *kan1kan2* double mutant, I used the *kan1+/-kan2* plants for dipping which can be identified by an upward curled silique phenotype (Abley, 2014). Floral dipping was carried out as described above and the T1 offspring were selected on selective media as well as for the *kan1+/-kan2* upturned cotyledon phenotype and for the relevant fluorescence. T1 individuals carrying the desired construct were selfed and the *kan1+/-kan2* plants used to generate seed.

6.3 Heat-shock and imaging

6.3.1 Heat-shock of inducible transgenic lines

Seedlings were heat-shocked by placing sealed plates in water bath at 39 °C for desired length of time (20 minutes was used to induce BASL across the whole seedlings). Seedlings were grown in standard conditions after heat-shock for typically at least 2 days before imaging. Seedlings were heat-shocked at 4 DAS (days after stratification) for sectors and between 2 and 24 DAS for imaging BASL in leaf 1 (typically 2 - 7 DAS).

6.3.2 Propidium iodide staining

To stain leaves with propidium iodide, leaves were submerged in a 2.5 µg/ml propidium iodide solution (Sigma, P4170) for at least 15 minutes before imaging.

6.3.3 Confocal imaging

Plants were grown under standard conditions as described above. For confocal imaging of leaves, depending on leaf size and curvature, whole seedlings or a single leaf (removed using forceps) were placed on a microscope slide with water and flattened with a coverslip. Imaging was performed using a x10 or x20 dry lens, or x40 oil lens, on a Leica SP5 confocal microscope equipped with Leica HyD Hybrid detectors, or a Zeiss 780. For imaging GFP, argon ion (488 nm) excitation laser was used, collected at 495-530 nm. For PI, mCherry and RFP, 561 nm excitation was used, collected at 625-690 nm for PI, 575-630 for RFP and 600-620 nm for mCherry. For imaging CyPET, a 458 nm excitation was used, collected at 465-490 nm. For some imaging of BY-2 cells, a VisiTech spinning disc confocal microscope fitted with a 40×/1.3 NA oil objective lens used with GFP excited using the 488 nm line of an argon ion laser and emitted light filtered through a 500–550-nm band-pass filter.

Leaves were staged according to leaf width and were typically imaged 48-hours after heat-shock. When imaging induced *35S::GFP-BASL*, seedlings were typically heat-shocked for 20 minutes to induce BASL across the entire lamina, and 3 mins to induce sectors.

6.3.3.1 *Using the growth chamber/time lapse imaging*

Plants were grown under standard conditions as described above and placed in the imaging chamber described in Calder et al., (2015). Seedlings were imaged in the chamber using the

settings described above, and the chamber was returned to the growth room with standard conditions in between imaging.

6.3.3.2 *Time lapse imaging of BASL following induction*

To image *35S::GFP-BASL* appearing after induction, 7 day old seedlings were heat-shocked for 20 mins and placed in an imaging chamber with media as described in Chan et al., (2007). Leaves were imaged every hour using a Zeiss 780 confocal microscope, with the settings described above.

6.4 Drug treatments

6.4.1 Oryzalin treatment

Oryzalin (Sigma, 36182) was added to 6-day old seedlings (*35S::GFP-BASL* line described above and *35S::GFP-TUA6* as control line) at a concentration of 20 μM . Seedlings expressing *35S::TUA6-GFP* have previously been described (Ueda et al., 1999). *35S::TUA6-GFP* seedlings confirmed microtubules had depolymerised after 4 hours and seedlings were heat-shocked to induce BASL expression. Plants were imaged 48 hours after heat-shock and the *35S::GFP-TUA6* line was used to confirm the absence of microtubules.

6.4.2 NPA treatment

35S::GFP-BASL seedlings were grown on media containing 100 μM NPA (Chem Service, 12507), or an equivalent concentration of DMSO. Seedlings were heat-shocked 2 DAS and leaves imaged 3 days later. Propidium iodide staining (described above) was used to visualise cell outlines.

6.5 Leaf stretching

6.5.1 Developing leaf stretching device

Jamie Spooner developed a leaf-stretching device, based on that of Bringmann and Bergmann (2017), that also allowed leaves to be imaged on the confocal microscope whilst

being stretched. The device, pictured in section 3.37 A, used a small vice mechanism to which two bulldog clips were attached using glue (Gorilla Glue). The piece of elastomer strip (Sylgard 182) could then be attached between the clips and stretched using the vice mechanism to move the clips further away from each other. Seedlings were glued to the elastomer strip using medical adhesive (Hollister 7730) and both the elastomer strip and adhesive were the same as used by Bringmann and Bergmann (2017).

6.5.2 Leaf stretching and imaging

A. thaliana seedlings expressing inducible *35S::GFP-BASL* and RFP-PM were grown on plates in standard conditions (section 6.1.1) and heat-shocked before being adhered to the elastomer strip using medical adhesive and a fine paintbrush to prevent damage. Cotyledons were imaged using confocal microscopy after the seedling had been stuck to the membrane. The membrane was stretched a given amount (typically increased in length by 50%) and the seedling imaged again, and after 7 hours of stretching.

6.6 Software development

6.6.1 Developing software for assigning BASL vectors

6.6.1.1 *Cells-from-leaves and cells-from-leaves-tagger software*

Software for assigning BASL vectors semi-automatically was developed in collaboration with Tjelvar Olsson and Matthew Hartley (Scientific Computing, John Innes Centre). The software used for cell segmentation and random rotation of cells is called 'Cells-from-leaves' and the software used for visualisation of the cells and assigning of BASL vectors is 'Cells-from-leaves-tagger'. The Cells-from-leaves software is available at : <https://github.com/JIC-Image-Analysis/cells-from-leaves> and the 'Cells-from-leaves-tagger' software is available at : <https://github.com/JIC-Image-Analysis/cells-from-leaves-tagger>.

The 'Cells-from-leaves' software used the cell outline channel from confocal stacks to make a projection of the leaf surface that signal was then projected onto. The cell outline channel (either plasma-membrane marker or PI stain) then allowed segmentation by a watershed algorithm. Leaf-specific parameters allowed the surface and segmentation to be customised according to intensity and quality of image. The centroid for each cell was calculated by

averaging the x and y coordinates of the cell. BASL signal was projected onto the same surface.

To avoid bias in knowing the cell orientation and position in the leaf, each segmented cell was isolated and rotated in one of four random orientations (0, 90, 180, 270 degrees). Each cell is presented in turn to the user, in the visualisation software 'Cells-from-leaves-tagger', who clicks on the middle of any visible BASL crescent or can choose to skip a cell if there is a complication (the signal is not easy to identify, or the cell segmentation is wrong, etc). The tool produces a directory of JSON files and corresponding image files, recording the BASL orientation in separate files for each cell, along with an image of the cell segmentation. Lastly, BASL vectors are transformed back into the coordinate system of the whole leaf and written out to a CSV file along with the coordinates of each cell centroid.

6.6.1.2 MATLAB scripts to quantify the BASL vector field

Two Matlab scripts were developed in collaboration with Jake Newman: one to allow quantification of the BASL vector field (`CellLongAxisCorr7.m`) and one to visualise it in a more informative way (`SampleArrows8.m`).

6.6.1.2.1 SampleArrows8 software

One script developed, `SampleArrows8`, is for visualising BASL vectors on the leaf and downsampling them. This script uses a leaf image and .csv file of BASL vectors (produced by 'Cells from leaves'). The user identifies the leaf midline which is used to rotate the leaf image and BASL vectors to allow the image to be vertically oriented. The script contains various processing and display options, but it is frequently used to display the original BASL arrows on the leaf, coloured by orientation with respect to the leaf midvein. The colour of each arrow is determined by a colour map, where 0 degrees represents the proximodistal direction.

There can be a lot of BASL vectors on a leaf, with some areas having a very high density of points. BASL vectors can therefore be downsampled to reduce the total number of vectors displayed and to give a more even spread of BASL vectors across the leaf. Downsampling uses a triangular grid of points placed over the leaf. For each vertex of the grid, vectors within the distance `Maxdist` are averaged. A parameter, `neighbourThreshold`, ensures that downsampled BASL vectors are only displayed for samples that exceed the threshold number of BASL vectors.

This script can also be applied to cell orientations. This is achieved by gathering cell orientations within a certain radius, normalising and superimposing them onto the same axis, and then performing principle component analysis (PCA) on that cloud of points.

6.6.1.2.2 CellLongAxisCorr7 software

The script CellLongAxisCorr7 was developed in collaboration with Jake Newman to allow quantification of the BASL vector field. This script calculates various angles: orientation of cell axis, angle between BASL vector and its cell axis, and angle between BASL vector and leaf midvein axis. This script uses an image of the leaf and the directory of JSON files to rotate the cells back to their original orientation and cell masks are derived, allowing cell eccentricity (ratio of the distance between the foci of the ellipse fitted to a cell and its major axis length), centroid and orientation of the long axis of the cells to be determined.

For each cell, three angle measurements are made: the angle between the BASL vector (from the JSON files) and the cell long axis, angle between the BASL vector and the leaf midline axis (specified by the user), and the angle between the cell long axis and the leaf midline axis. Subsets of data can be selected by specifying lower and upper threshold values in the script parameters (for cell eccentricity and orientation relative to the leaf). This script displays the orientation information as histograms and also writes it out to CSV files for further analysis.

Both the SampleArrows8.m and CellLongAxisCorr7.m scripts are available from https://github.com/JIC-Image-Analysis/cells-from-leaves/tree/master/matlab_scripts.

These scripts also contain a detailed explanation of each of the input parameters.

6.7 Image analysis and statistics

6.7.1 BASL crescent and perimeter measurements

BASL crescent length and cell perimeter were calculated by clicking round the BASL signal and cell outline using the Fiji measure tool (Schindelin et al., 2012). Cells of different sizes from multiple different leaves of varying widths were measured.

6.7.2 Isotropic cell selection

To determine average BASL vector orientations for near isotropic cells in regions of the leaf, CellLongAxisCorr7 was used with a maximum eccentricity value of 0.6, and vectors were

visualised on the leaf using SampleArrows8. The leaf was then subdivided into 9 regions and vectors measured in each region measured using Fiji angle tool.

6.7.3 Statistics comparing coordination of vectors

Statistical comparison of BASL vector distributions between genotypes, was performed using chi-squared tests (df=1, p-values less than 0.01 were considered significant), comparing frequency of BASL vectors within or outside the range of -80° to 80°, in pairwise tests.

6.7.4 Figure preparation

Figures were assembled using Adobe Illustrator.

6.8 BY-2 cells

6.8.1 Stable transformation of BY-2 cells

Wild-type BY-2 cells were transformed with agrobacterium strain GV3101 containing *35S::GFP-BASL* (construct 71253 described above, section 6.2.1.3). *A. tumefaciens* containing the construct was grown in LB containing appropriate antibiotics (rifampicin 20 mg/ml, gentamycin 40 mg/ml and kanamycin 50 mg/ml) and grown to an optical density (OD) of 0.5 to 0.8 for about 24 hours at 25-28 °C. 100 µl of agrobacterium culture was then co-cultured with 4 ml of 3-day-old BY-2 cells in sealed deep petri dishes (100 x 20 mm, Falcon) and kept horizontal in the dark for 2 days at 25 °C without agitation.

The cultures were then washed by adding 8 ml BY-2 medium (Murashige & Skoog Medium without vitamins (Formedium) 4.6 g/l, pH 6.0 with NaOH, sucrose 30 g/l, Potassium Phosphate 0.2 g/l, Myo-inositol 0.1 g/l, thiamine 1 mg (1ml of 0.1g/100ml stock), and 2,4-D 0.2 mg (1 ml of 0.02 g/100ml stock)) and centrifuging at 1000 rpm for 1 minute. The washing step was repeated five times before resuspending the cells in 1-2 ml of media. The cells were spread onto deep petri dishes with phytigel containing BY-2 medium (liquid BY-2 recipe with 0.4% phytigel) and the appropriate antibiotics (as above).

Petri dishes were sealed with micropore tape and incubated in a horizontal position in the dark at 25 °C. After 2-3 weeks, transformed calli were visible. Transformed were grown to around 1cm in diameter and then transferred into a 50 ml flask of liquid BY-2 medium

Materials and methods

containing appropriate antibiotics. The flasks were incubated in the dark at 25 °C with shaking and grown until thick. When the culture was thick with cells, it was sub-cultured weekly, maintaining carbenicillin for numerous generations to ensure agrobacterium was completely eliminated.

6.8.2 Maintenance of BY-2 cell lines

BY-2 cells were sub-cultured weekly by inoculating 3-6 ml of 1 week old BY-2 cells in 100 ml of room temperature BY-2 medium. Cell cultures were maintained in constant dark, shaking at ~100 rpm at 25 °C.

6.8.3 Protoplasting of BY-2 cells

To generate protoplasts from BY-2 cells, cells in culture media were centrifuged for 3 minutes at 1000 rpm and resuspended in an enzyme solution composed of 0.4 M sorbitol (Sigma, S1876), 2% cellulase R-10 (Yakult pharmaceutical, L0012) and 0.05% pectolyase (P3026, Sigma). Cells in enzyme solution were incubated at room temperature with shaking for at least 5 hours. Protoplasts were imaged after this period and left longer in enzyme solution if necessary to ensure as much of the cell wall was removed as possible.

6.8.4 Regeneration of protoplasts

For regeneration, protoplasts (formed as described above) were washed by spinning at 1000 rpm for 2 minutes and resuspended in sterile FMS media (0.25 M sorbitol (Sigma, S1876), 10 g/l sucrose (Sigma, S0389), 4.3 g/l MS salts (Sigma, M5524), 100 mg/l myoinositol (Sigma, I5125), 0.5 mg/l nicotinic acid (Sigma, N4126), 0.5 mg/l pyroxidine HCl (Sigma, P9755), 0.1 mg/l thiamine HCl (Sigma, T4625). Washing was repeated three times to remove the enzyme solution. Once washed, the protoplasts were resuspended in FMS media supplemented with 0.1 mg/l NAA (Sigma, N0640) and 1 mg/l BAP (Sigma, B9395) to enhance longitudinal growth (Zaban et al., 2013). Droplets of cells in hormone-supplemented media were placed into sterile petri dishes, sealed, and incubated in the dark at 25 °C for 3 days.

6.8.5 Imaging of BY-2 cells

BY-2 cells and protoplasts were imaged on confocal microscopes using either a Leica SP5 equipped with Leica HyD Hybrid detectors, a Zeiss 780, or a VisiTech spinning disc using the settings described in Section 6.3.3. Cells or protoplasts were imaged by placing a droplet of

cells in media onto a microscope slide with a well and using a cover slip. *35S::GFP-BASL* was imaged using the settings described in section 6.3.3.

6.9 Biochemistry

6.9.1 *N. benthamiana* infiltration

For infiltration of *N. benthamiana*, *A. tumefaciens* carrying the construct of choice was grown at 28 °C with shaking for one night in LB media with rifampicin (50 µg/ml) and the plasmid selection antibiotic. 2 ml of cell cultures were spun at 6000 rpm for 10 minutes and cells were resuspended in 1 ml 10 mM MgCl₂. The *A. tumefaciens* solution was diluted to a final OD between 0.1 and 0.5 using 10 mM MgCl₂. Depending on the construct, *A. tumefaciens* solution containing the P19 silencing suppressor construct was added in 1/3 volume. For infiltration, a small hole was made in large *N. benthamiana* leaves and *A. tumefaciens* solution infiltrated in using a syringe. This was repeated across the leaf to saturate it with *A. tumefaciens*.

6.9.2 Sample preparation

Protein extraction experiments were carried out in *N. benthamiana*, stably transformed with *35S::GFP-BASL* constructs 71253 and 71572 and GFP controls (71223, see Appendix A), and *A. thaliana* with inducible *35S::GFP-BASL* and GFP controls (71028, see Appendix A).

6.9.2.1 Sample preparation for protein extraction using *N. benthamiana*

Infiltrated *N. benthamiana* leaves were imaged using a confocal microscope 2 days after infiltration to confirm localisation of the construct. Leaves were harvested, wrapped in foil and immersed immediately in liquid N₂. If being stored before protein extraction, samples were transferred to -80 °C.

6.9.2.2 Sample preparation for protein extraction using *A. thaliana*

For the total protein extraction in section 4.4.1, seedlings were grown on plates under standard conditions, and were heat-shocked for 20 minutes 7 DAS at 39 °C. To harvest, whole seedlings were collected from plates and frozen in liquid N₂. If being stored before protein extraction, samples were transferred to -80 °C.

6.9.3 Total protein extraction

For total protein extraction in both *N. benthamiana* and *A. thaliana*, tissue was ground in liquid N₂ using pre-cooled pestles and mortars. A minimal volume of pre-cooled extraction buffer was added (as little as possible to solubilise the plant material, usually 8-9 ml for 3 g of material). In experiments where Pefabloc® (Sigma) was used, a final concentration of 1 mM was added to the extraction buffer. The extraction buffers used are detailed below, and the version used is indicated in the results section of each extraction. Samples were then centrifuged for 10 minutes at 13000 rpm at 4 °C. Pellet and supernatant fractions were separated and 4 x LDS-buffer added (NuPAGE™, Invitrogen, NP0007) containing DTT or β-Mercaptoethanol as indicated before running on SDS-page gels and western blotting.

6.9.3.1 Extraction buffer 1

The extraction buffer used for total protein extraction in *A. thaliana* (section 4.4.1) and *N. benthamiana* (section 4.4.2.2) was as follows: 50 mM Tris-Cl pH 7.5, 150 mM NaCl, 0.5% NP40, 1% protease inhibitors.

6.9.3.2 High salt extraction buffer

The high salt extraction buffer used for total protein extraction in *N. benthamiana* in section 4.4.2.2 was as follows: 50 mM Tris-Cl pH 7.5, 1 M NaCl, 1% NP40, 1% protease inhibitors.

6.9.3.3 Acetone precipitation

For acetone precipitation of total protein samples from *N. benthamiana*, tissue was ground in liquid N₂ and a minimum volume of extraction buffer 1 (section 6.9.3.1) was added. After spinning at 4 °C at 13000 rpm for 10 minutes, the supernatant was used for acetone precipitation. 4 x volume of cold acetone was added and incubated at -20 °C for 1 hour to allow precipitation. Samples were centrifuged for 10 minutes at 10000 rpm at 4 °C and the supernatant was removed. The acetone was allowed to evaporate for ~15 minutes at room temperature before the pellet was resuspended in 200 µl of H₂O and sample buffer was added.

6.9.3.4 Extraction buffer 2

The extraction buffer used for total protein extraction in *N. benthamiana* (section 4.4.2.3) was as follows: 50 mM Tris-Cl pH 7.5, 150 mM NaCl, 1% NP40, 5% glycerol, 1% protease inhibitors, 1 mM Pefabloc® (Sigma).

6.9.4 Protein extraction for co-immunoprecipitation

Tissue was ground to a very fine powder in liquid N₂ using pre-cooled pestles and mortars. A minimal volume of pre-cooled extraction buffer was added (as little as possible to solubilise the plant material, usually 8-9 ml for 3 g of material). Extraction buffer was made up of 150 mM NaCl, 50 mM Tris-HCl pH 7.5, 5% glycerol, 1% NP40 and 1% protease inhibitors (Sigma). In experiments where Pefabloc® (Sigma) was used, a final concentration of 1 mM was added to the extraction buffer. Once extraction buffer was added, the tissue was ground further in extraction buffer and kept cool using liquid N₂. Material was transferred to a falcon tube and sonicated (amplitude 9, 10 seconds on, 20 seconds off) on ice for 2-3 cycles then incubated on ice for 15-30 minutes. Material was transferred to clean SS34 tubes and centrifuged at 13000 rpm for 30 minutes at 4 °C and transferred to a fresh tube before being filtered through 3-4 layers of Miracloth (Calbiochem®).

6.9.5 Immunoprecipitation

Following the protein extraction method outlined above, extracts were distributed across multiple Eppendorf tubes and incubated with GFP-Trap®_MA magnetic beads (Chromotek) for 4 hours at 4 °C with slow rotation. Beads were then washed in cold extraction buffer at least 3 times, with 5 minutes incubation at 4 °C between washes. The extracts were combined into a single Eppendorf for each line. After three washes, the extraction buffer was removed and the beads were resuspended in 2x LDS-buffer with 5% β-Mercaptoethanol and boiled for 15 minutes. Extracts were then run on an SDS-page gel or stored at -20 °C.

6.9.5.1 Co-Immunoprecipitation with mass-spectrometry (Wageningen collaboration)

A. thaliana seedlings were grown on selective media in square petri dishes with a layer of sterile membrane (Sefar Nitex 03-20/14) placed on top of the media to aid easy removal of seedlings from the plate. Seedlings were grown under standard conditions and heat-shocked for 20 minutes 6 DAS at 39 °C. Whole seedlings were harvested by scraping them from the membrane and grinding to a fine powder in liquid N₂. Samples were stored at -80 °C and transferred to the Weijers lab, University of Wageningen to carry out the IP-MS.

6.9.5.1.1 Immunoprecipitation with magnetic monoclonal anti-GFP beads (Miltenyi Biotec)

For the immunoprecipitation, a minimum volume of extraction buffer (50 mM Tris-HCl pH7.5, 150 mM NaCl, 1 % NP40, protease inhibitor mix cocktail (Sigma)) was added (8-9 ml for 3 g of material) and ground very thoroughly. Material was sonicated on ice 3 times (15

Materials and methods

seconds on, 15 seconds off) and incubated on ice for 30 minutes. The NP40 in the samples was diluted to 0.2% in the protein extract (using extraction buffer without NP40) and centrifuged for 15 minutes at 18000 rpm at 4 °C. The supernatant was transferred to a clean tube and centrifuges again using the same conditions before being filtered through a 40 µm cell strainer. 100 µl anti-GFP Microbeads (Miltenyi Biotec) was added to each sample and incubated with slow rotation for at least 2 hours at 4 °C. Columns were place in the MACS Separator (Miltenyi Biotec) and washed with extraction buffer with 0.1% NP40. The cell lysate was applied to the column and allowed to run through.

Once samples had run through, the columns were rinsed with 4 x 200 µl extraction buffer with 0.1% NP40 and rinsed with 2 x 500 µl 50 mM NH₄HCO₃. The beads were eluted from the columns into Low Bind Eppendorf tubes by adding 50 µl pre-heated (to ~95 °C) hot elution buffer (50 mM NH₄(CO₃)₂) to the column. Samples were stored at -20 °C.

6.9.5.1.2 Preparation of Immunoprecipitation samples for Mass Spectrometry

To reduce proteins in the samples, 10 mM DTT (dithiotreitol) in 50 mM NH₄HCO₃ pH8 was added to each IP sample and incubated for 1-2 hours at 60 °C. 15 mM iodocetamide in 50 mM NH₄HCO₃ pH8 was added to each IP sample and incubated at least 1 hour at room temperature in the dark. 1 µl 200 mM cysteine in 50 mM NH₄HCO₃ pH8 was added to each IP sample to stop the alkylation. For trypsin digestion, 1 µl trypsin was added to each IP sample and incubated overnight at 20°C with shaking. After a maximum of 16 hours incubation, 1.5 - 3 µl 10% Trifluoroacetic acid was added to each sample to adjust to pH 3. Samples were run through a homemade 'micro-column' (Weijers lab, Wageningen University). The columns were washed with 100 µl 0.1% formic acid, transferred to Low Bind Eppendorf tubes, and eluted using 50 µl 50% Acetonitrile + 50% 0.1% formic acid. Samples were dried on a Speed-Vac for 2 hours at 30-45 °C to reduce the Acetonitrile content. Sample volumes were adjusted to 50 µl with 0.1% formic acid and run on LCMS. Analysis of mass-spec results was carried out by members of the Weijers lab, Wageningen University.

6.9.5.2 Co-Immunoprecipitation with mass-spectrometry (*N. benthamiana*, JIC)

For the Co-IP with mass-spec analysis (carried out by Gerhard Saalbach, proteomics facility, JIC), *N. benthamiana* infiltrated as described in section 6.9.1 were used, and IP was conducted according to the protocol in section 6.9.4 and 6.9.5 using extraction buffer 2 (section 6.9.3.4). Samples were prepared for mass-spec by running for 5 minutes at 30 mAmp on a 10% SDS gel without a resolving gel.

Gel slices were prepared according to standard procedures adapted from Shevchenko et al., (2007). Gel slices were cut out and de-stained with 30% ethanol for 30 min at 65 °C. The slices were then washed in the following solutions; volumes were 1 ml and wash times 15 minutes unless otherwise stated. The slices were washed with 50 mM TEAB pH 8 (made from 1M stock from Sigma, T7408) in 50% acetonitrile followed by incubation with 10 mM DTT for 30 min at 55 °C. The DTT solution was removed and IAA solution added (30 mM Iodoacetamide in 50 mM TEAB). Samples were vortexed and incubated for 30 min at room temperature in the dark. The IAA solution was removed and samples washed with 50 mM TEAB in 50% acetonitrile. Samples were washed with 50 mM TEAB and then cut into 1x1 mm pieces and transferred to a fresh Low bind tube. Samples were washed again in 50nM TEAB in 50% acetonitrile and then 100% acetonitrile to dehydrate the gel slices. The acetonitrile was removed and a small hole was pierced in the lid of the tubes and dried for 30 minutes in a speed vac (Eppendorf Concentrator plus) with the lids closed. Samples were then sent to the JIC proteomics facility for trypsin digestion and mass-spec analysis by Gerhard Saalbach.

For trypsin digestion, the gels were soaked with 50 mM TEAB containing 10 ng/μl Sequencing Grade Trypsin (Promega) and incubated at 50 °C for 8 h. Peptides were extracted, and aliquots were analysed by nanoLC-MS/MS on an Orbitrap Fusion™ Tribrid™ Mass Spectrometer coupled to an UltiMate® 3000 RSLCnano LC system (Thermo Scientific). The samples were loaded and trapped using a pre-column which was then switched in-line to the analytical column for separation. Peptides were separated on a nanoEase M/Z column (HSS C18 T3, 100 Å, 1.8 μm; Waters, Wilmslow, UK) using a gradient of acetonitrile at a flow rate of 0.25 μl min⁻¹ with the following steps of solvents A (water, 0.1% formic acid) and B (80% acetonitrile, 0.15 formic acid): 0-4 min 3% B (trap only); 4-15 min increase B to 13%; 15-77 min increase B to 38%; 77-92 min increase B to 55%; followed by a ramp to 99% B and re-equilibration to 3% B.

Data dependent analysis was performed using parallel CID and HCD fragmentation with the following parameters: positive ion mode, orbitrap MS resolution = 60k, mass range (quadrupole) = 300-1800 m/z, MS2 top20 in ion trap, threshold 1.9e4, isolation window 1.6 Da, charge states 2-5, AGC target 1.9e4, max inject time 35 ms, dynamic exclusion 1 count, 15 s exclusion, exclusion mass window ±5 ppm. MS scans were saved in profile mode while MS2 scans were saved in centroid mode.

6.9.6 Analysis of mass-spectrometry data

Initial analysis of mass-spec data was done by Gerhard Saalbach (proteomics facility, JIC). Recalibrated peaklists were generated using MaxQuant 1.6.1.0 (Tyanova et al., 2016), using a database with *N. benthamiana* protein sequences downloaded from Uniprot (Oct 2015, 603 entries). The final database search was performed with the merged HCD and CID peaklists from MaxQuant using in-house Mascot Server 2.4.1 (Matrixscience, London, UK). The search was performed on the *N. benthamiana* protein sequence database downloaded from the Solgenomics project (https://solgenomics.net/organism/Nicotiana_benthamiana/genome, Sept 2018, 57160 entries) to which the sequence of the GFP-BASL construct was added. For the search, a precursor tolerance of 6 ppm and a fragment tolerance of 0.6 Da was used. The enzyme was set to trypsin/P with a maximum of 2 allowed missed cleavages. Oxidation (M) and deamidation (N/Q) were set as variable modifications and carbamidomethylation (CAM) of cysteine as fixed modification. The Mascot search results were imported into Scaffold 4.4.1.1 (www.proteomsoftware.com) using identification probabilities of 99% for proteins and 95% for peptides.

Once imported into Scaffold, the data from the mass-spec analysis was analysed with help from Paul Derbyshire (Proteomics, The Sainsbury Laboratory, Norwich). Data was exported into excel using a 99% protein threshold, minimum of 1 peptide, and 95% peptide threshold. The list of proteins was filtered to remove contaminants (e.g. keratin). Proteins were selected as possibly relevant interactors if they had a minimum of 4 spectral counts and were either unique to the GFP-BASL bait samples or were enriched in the bait samples by at least 1.5-fold compared to the positive and negative controls.

6.9.7 SDS-page gel

I used 10% home-made SDS-page gels composed of 3 ml Acrylamide (30% Acrylamide (w/v) Ratio 37.5:1, Severn Biotech, 20-2100-05), 2.25 ml 1.5 M Tris pH 8.8, 3.75 ml deionised water, 40 µl 10% ammonium persulfate (A3678, Sigma) solution, and 5 µl N,N,N',N'-Tetramethylethylenediamine (T9281, Sigma) for the resolving gel and 0.45 ml Acrylamide, 0.75 ml 0.5 M Tris pH 6.8, 1.8 ml deionised water, 10 µl 10% ammonium persulfate and 5 µl N,N,N',N'-Tetramethylethylenediamine for the stacking gel. Extracts were run on the 10% gel at 30 mA for 1 hour 45 minutes; typically 20 µl of extract was loaded onto the gel. I used the RunBlue™ prestained molecular weight marker (Expedeon) unless otherwise stated. Two

identical gels were usually run, and one was stained using InstantBlue™ Protein Stain (Expedeon) for at least one hour.

6.9.8 Western blotting

For immunoblots, proteins were run on a 10% gel (described in section 6.9.6) and transferred to a nitrocellulose membrane (GE Healthcare Life Sciences) by wet blotting in 25 mM Tris, 200 mM Glycine and 10% methanol for 1 hour 30 minutes at 200 V. Blots were stained with Ponceau S solution (P7170, Sigma) for 30 seconds and blocked for at least 1 hour in a 5% milk (Marvel) solution in Tris-Buffered Saline (TBS) solution. Unless otherwise stated, blots were incubated overnight at 4 °C with an anti-GFP antibody was used at 1:1000 dilution (Chromotek, 3H9), washed three times in TBS and incubated with an anti-rat IgG Peroxidase antibody (A5795, Sigma) for ~3 hours at room temperature. Chemiluminescence detection was performed with SuperSignal West Pico PLUS Chemiluminescent Substrate (ThermoFisher Scientific) following manufacturer instructions (unless otherwise stated). In the blot in Figure 4.4 B, the Amersham ECL Western blotting system was used (RPN2109, GE Healthcare) was used, and the SuperSignal West Femto Maximum Sensitivity Substrate (ThermoFisher Scientific) was used for the blot in Figure 4.4 C.

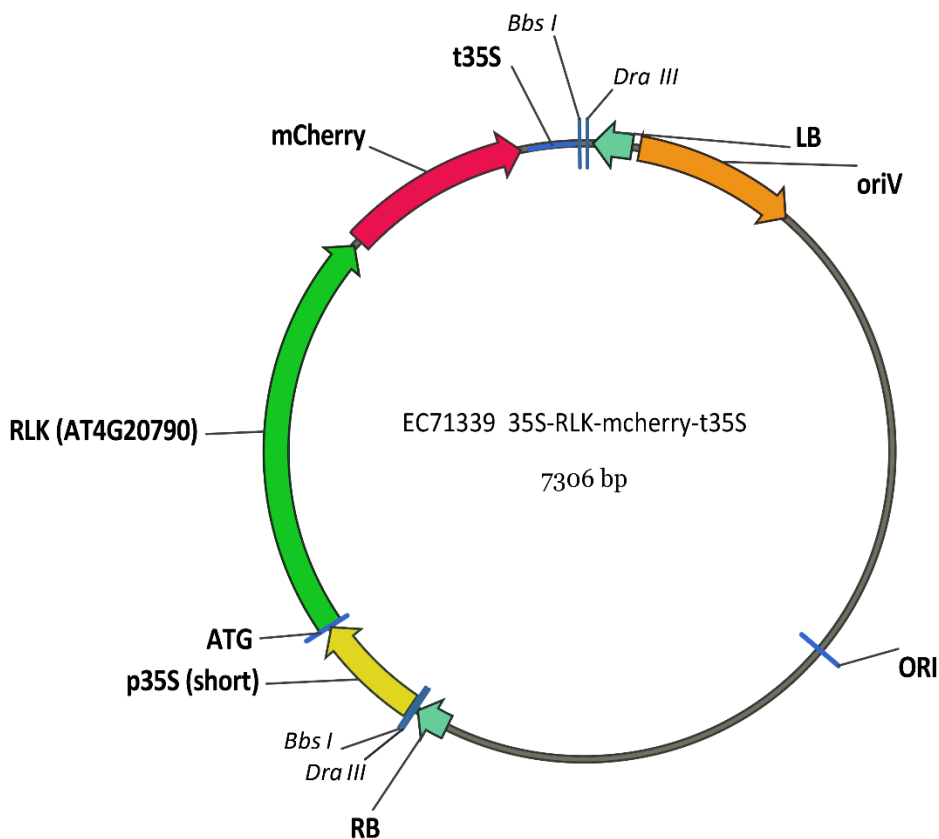
6.9.8.1 Testing antibodies in *A. thaliana* total protein extraction

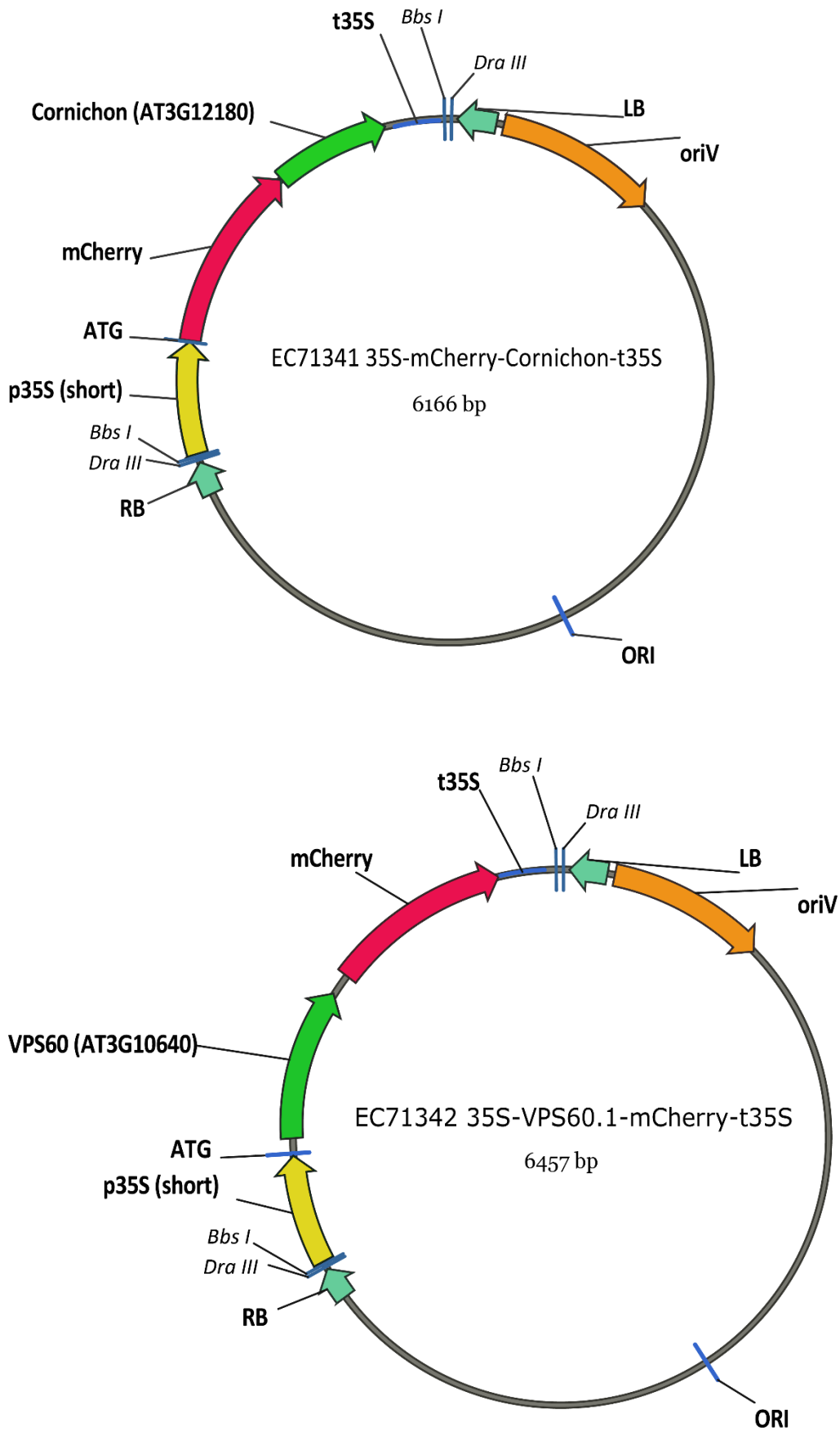
The antibodies tested in total protein extraction in *A. thaliana* were anti-GFP (ab6556, abcam), used at a 1:1500 dilution with anti-rabbit-HRP at 1:10000, anti-GFP (11814460001, Roche) used at a 1:1000 dilution with anti-mouse-HRP at 1:10000, and anti-GFP-HRP (130-091-833, Miltenyi Biotec) used at 1:20000 dilution.

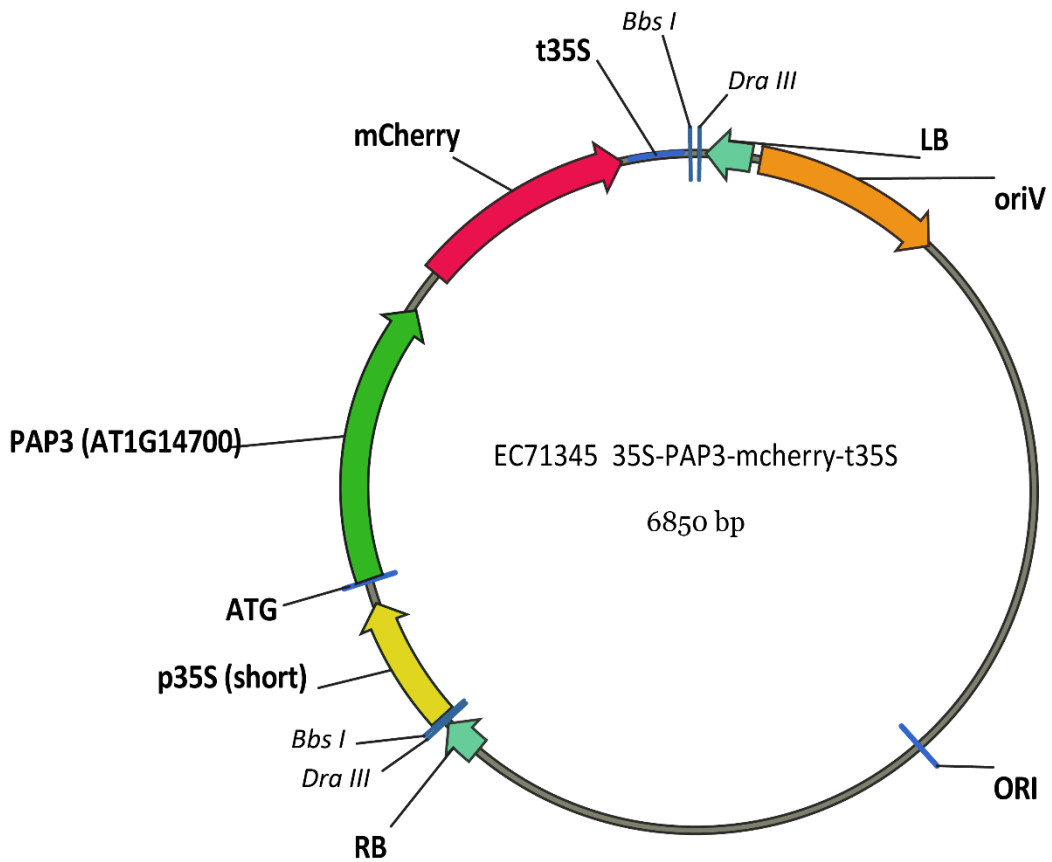
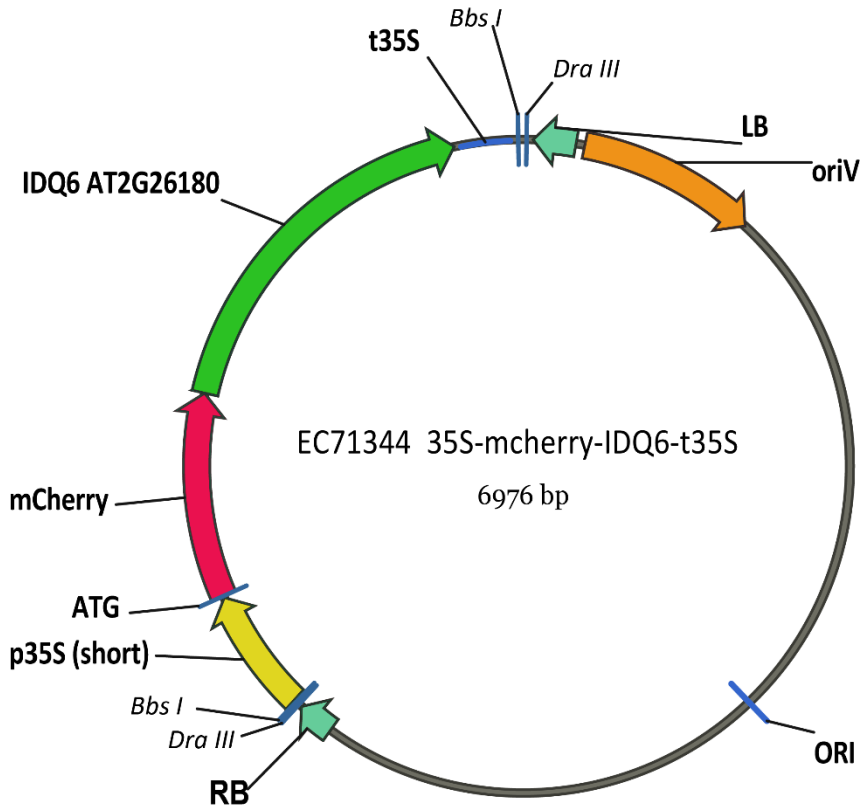
7 Appendices

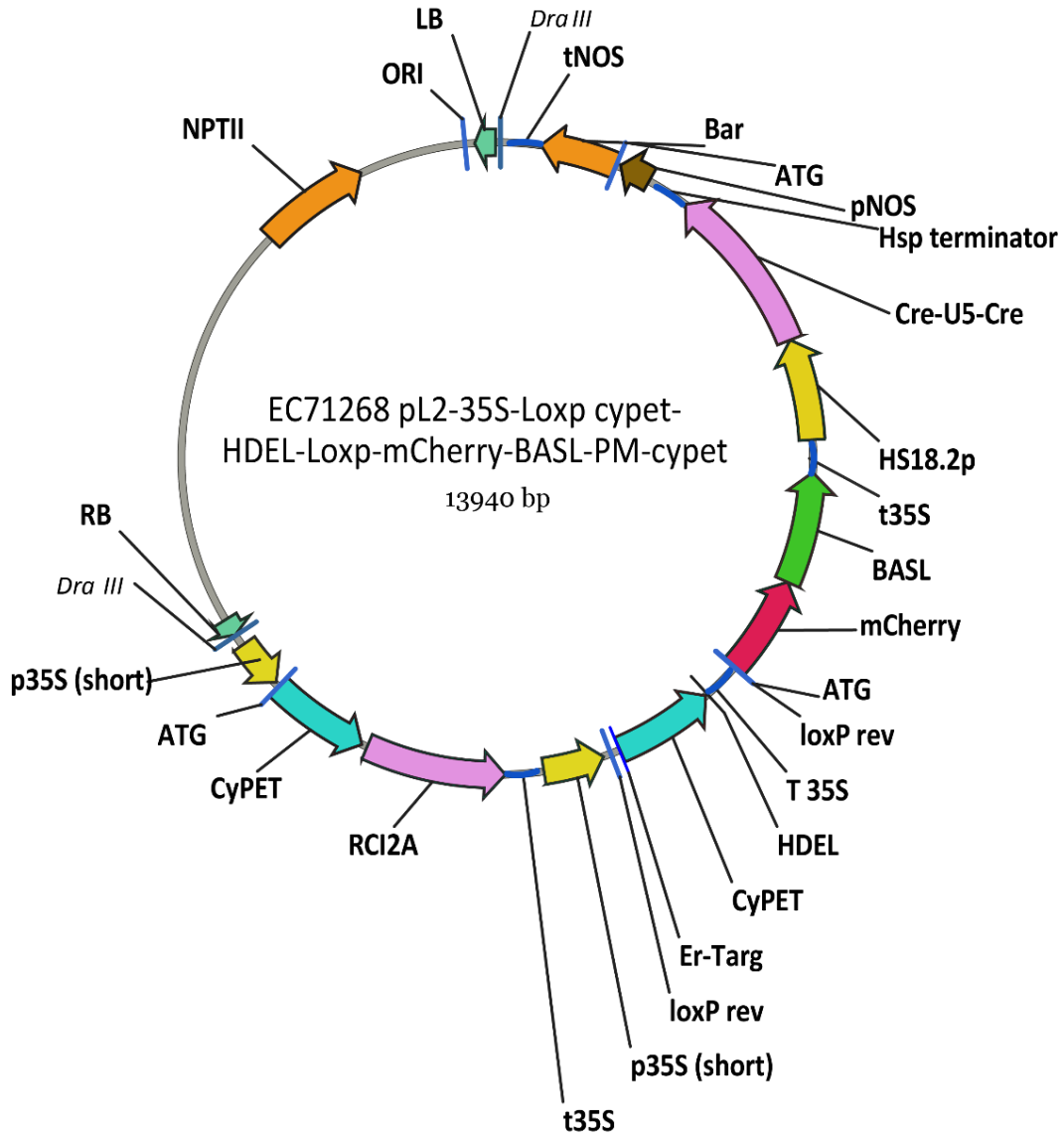
7.1 Appendix A: Constructs generated using Golden Gate

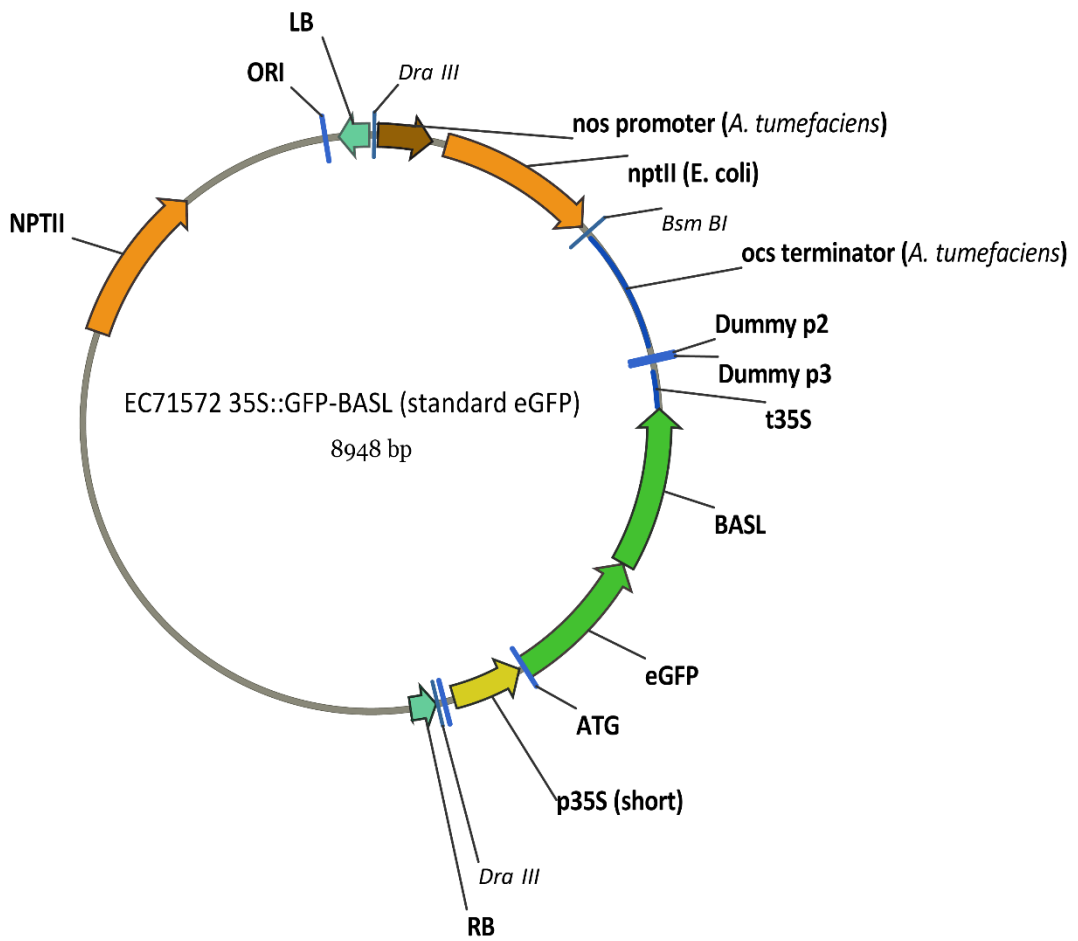
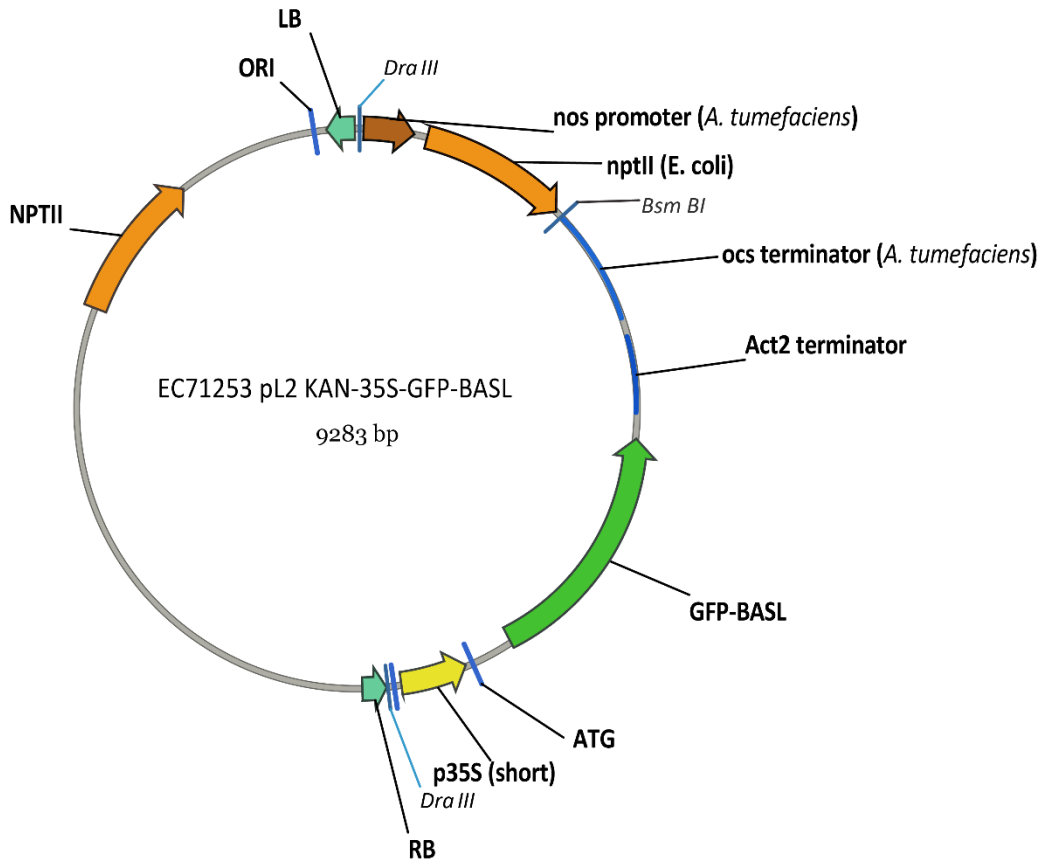
For reference, below are the plasmid maps for the L1 and L2 constructs that I generated using Golden Gate modular cloning during this work, and those generated by other members of the lab which were used as controls in biochemistry (L2 constructs 71223 and 71028). Each map is labelled with its plasmid number, and is referred to in the Materials and Methods section (Section 6.2). Each map has promoters, genes, fluorescent markers, terminators and *DraIII* restriction sites labelled and the size of each plasmid is indicated.

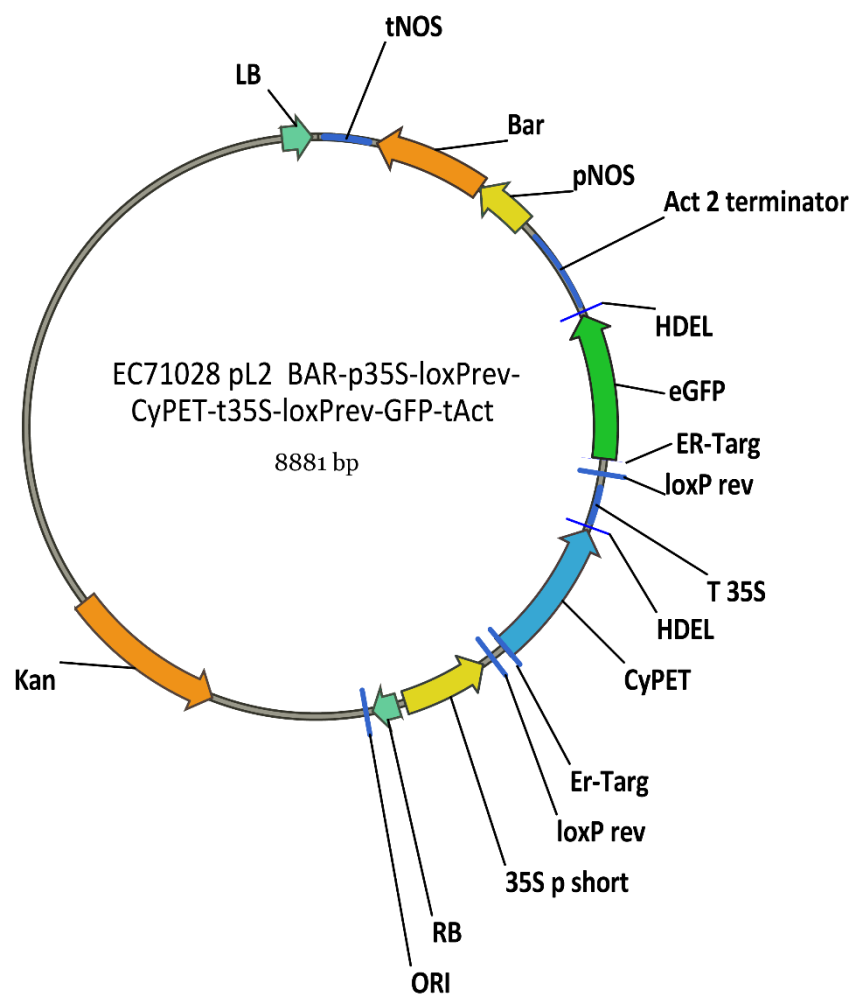
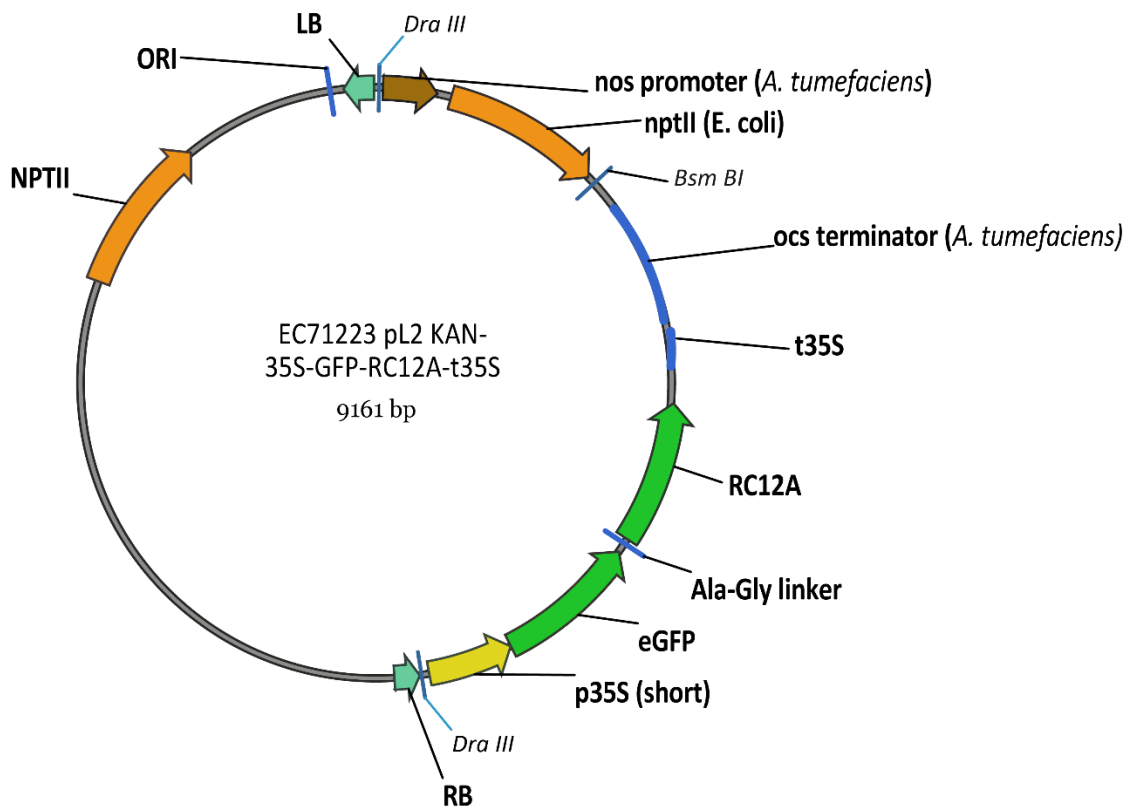












7.2 Appendix B: Membrane-linked Interactome Database results for BASL

Table 7.1 Result of membrane interactome screen by Jones et al. (2014) using BASL as a bait.

The number of positive interactions in the primary and secondary screen is shown in the last column. Proteins labelled +++- were positive in both the primary assays and one of two of the secondary assays and were candidates I focussed on.

Nub AGI	Nub gene	SUBAcon localisation	Cub AGI	Cub gene	SUBAcon localisation	Interaction Score
AT4G20790	Leucine-rich repeat protein kinase protein	P. membrane	AT5G60880	BASL	Nucleus	+++-
AT3G12180	Cornichon family protein	P. membrane	AT5G60880	BASL	Nucleus	+++-
AT3G10640	VPS60.1, SNF7 family protein	Nucleus	AT5G60880	BASL	Nucleus	+++-
AT1G21240	WAK3, wall associated kinase 3	P. membrane	AT5G60880	BASL	Nucleus	+++-
AT2G26180	IQD6, IQ-domain 6	Nucleus	AT5G60880	BASL	Nucleus	+++-
AT1G14700	PAP3, purple acid phosphatase 3	Extracellular	AT5G60880	BASL	Nucleus	+++-
AT5G60880	BASL	Nucleus	AT4G18195	ATPUP8, purine permease 8	P. membrane	+++-
AT5G60880	BASL	Nucleus	AT1G64900	CYP89, cytochrome P450, family 89A, peptide 2	E. Reticulum	+++-
AT5G59650	Leucine-rich repeat protein kinase protein	P. membrane	AT5G60880	BASL	Nucleus	+++-
AT5G60880	BASL	Nucleus	AT1G33080	MATE efflux family protein	P. membrane	+++
AT5G60880	BASL	Nucleus	AT5G01690	ATCHX27, CHX27, cation/H ⁺ exchanger 27	Vacuole	+++
AT5G60880	BASL	Nucleus	AT1G80910	Protein of unknown function (DUF1712)	Cytosol	+++
AT5G60880	BASL	Nucleus	AT1G68680	Unknown	Plastid	+++
AT5G52860	ABC-2 type transporter family protein	P. membrane	AT5G60880	BASL	Nucleus	+++
AT5G58270	STA1, ATM3, Mitochondrion ABC transporter 3	Mitochondrion	AT5G60880	BASL	Nucleus	+++
AT3G57650	LPAT2, lysophosphatidyl acyltransferase 2	E. Reticulum	AT5G60880	BASL	Nucleus	+++
AT4G38690	PLC-like phosphodiesterases superfamily protein	Cytosol	AT5G60880	BASL	Nucleus	+++
AT1G72470	EXO70D1, exocyst subunit exo70 family protein D1	Nucleus	AT5G60880	BASL	Nucleus	+++
AT1G21760	FBP7, F-box protein 7	Cytosol	AT5G60880	BASL	Nucleus	+++
AT4G32120	Galactosyltransferase family protein	P. membrane	AT5G60880	BASL	Nucleus	+++
AT5G44930	ARAD2, Exostosin family protein	Extracellular	AT5G60880	BASL	Nucleus	+++
AT1G19570	DHAR1, DHAR5, dehydroascorbate reductase	Cytosol	AT5G60880	BASL	Nucleus	+++
AT1G11000	MLO4, Seven transmembrane MLO family protein	P. membrane	AT5G60880	BASL	Nucleus	+++
AT2G24940	MAPR2, membrane-associated progesterone binding protein 2	Cytosol	AT5G60880	BASL	Nucleus	+++
AT1G08770	PRA1.E, prenylated RAB acceptor 1.E	P. membrane	AT5G60880	BASL	Nucleus	+++
AT4G35860	ATRAB2C, GB2, GTP-binding 2	Cytosol	AT5G60880	BASL	Nucleus	+++
AT4G14455	BET12, BS14B, Target SNARE coiled-coil domain	Golgi	AT5G60880	BASL	Nucleus	+++
AT5G42980	ATH3, TRXH3, TRX3, thioredoxin 3	Cytosol	AT5G60880	BASL	Nucleus	+++
AT1G45145	ATH5, LIV1, TRX5, thioredoxin H-type 5	Cytosol	AT5G60880	BASL	Nucleus	+++
AT3G62690	ATL5	P. membrane	AT5G60880	BASL	Nucleus	+++
AT2G45510	#N/A	E. Reticulum	AT5G60880	BASL	Nucleus	+++
AT4G17170	RAB GTPASE HOMOLOG B1C	E. Reticulum	AT5G60880	BASL	Nucleus	+++

7.3 Appendix C: Wageningen IP-MS results

Table 7.2 Wageningen IP-MS results (filtered).

The candidates identified in mass-spec analysis, carried out in Wageningen, are listed, along with their iBAQ (intensity-based absolute quantification) for each sample (3 BASL samples, 3 control samples), and significance, following analysis carried out by members of the Weijers lab, Wageningen University.

iBAQ						t-test Significant	Peptides	Unique peptides	Log t-test p value	t-test Difference	Protein IDs	Protein names	Gene names
BASL1	BASL2	BASL3	Control1	Control2	Control3								
2315300	2328600	4531700	557100	1772900	936120		3	3	0.12	-0.29	A8MR82;Q9FLD3		At5g05210
202240	488980	391330	104400	230450	150530		3	3	0.82	-1.32	A8MSE8;Q8W4H7;Q8GTY0;Q0WL56;PODH93;F4	Elongation factor 1-alpha 1-4	At5g60330;At1g07930
771070	5523500	22907000	511540	1624600	1284500		5	4	0.16	0.50	B3H5S2;P10738;P10797;F4KA76;P10796	Ribulose biphosphate carboxylase small chain	At5g38410;RBCS-3B;RBCS-2B
1511000	2180000	6337400	657910	3347900	550550		20	20	0.14	0.27	B6EUA3;B6EUA9-2	Pre-mRNA-processing protein 40A	PPP40A
1703100	2689300	2275900	149380	1351300	214740		4	4	1.12	1.70	F4I472;Q08112;Q9FY64;A8MQ96;Q9FIX6;Q9FY6	40S ribosomal protein S15-114	RPS15;RPS15A/D
4217200	5181100	10548000	2087900	4442600	1415600		12	12	0.73	0.71	Q92VW9;F4ILE0;F4ILE1		At2g16340
271540	744960	411660	183940	591150	88163		3	1	0.24	-0.48	F4IT48;P60039;Q9LHP1	60S ribosomal protein L7-3/4	At2g44120;RPL7C/D
1039700	1102900	1182000	165540	2383000	217940		7	7	0.08	0.11	F4IVZ7;P10896-2;P10896	Ribulose biphosphate carboxylase/oxygenase activase, chloroplastic	RCA
171440	449880	400650	106520	189540	93753		4	4	0.21	-0.19	F4JL11;Q96321	Importin subunit alpha-2	IMP2
2817100	7178700	5374100	1622100	7039000	1404400		8	8	0.31	-0.39	F4JQG2;Q23212;Q23212-2;Q23212-3	Splicing factor U2af large subunit A	ATU2AF65A;U2AF65A
661470	832920	458240	361090	851310	348420		2	2	1.76	-0.63	F4JQGG		At4g36700
5750400	9620600	3365000	1437100	7569100	1150900		5	5	0.32	0.51	F4JXC2		At5g53800
434170	704550	139940	101050	744330	80290		5	5	0.02	-0.07	F4K015;P42697;P42697-2	Dynamin-related protein 1A	DL1;DRP1A
1106000	1743700	832880	586960	5259200	507600		13	13	0.66	-0.99	F4K180;Q8L7S8-2;Q8L7S8	DEAD-box ATP-dependent RNA helicase 3, chloroplastic	emb1138;RH3
236790	242120	490910	140680	477250	82947		2	2	0.49	-1.32	F4K4Y5		At5g55660
2956500	4393900	1170500	585500	1848400	775070		5	5	0.03	0.06	F4K5C7;Q93VH9;Q8VYK6;P49204;F4IMI7	40S ribosomal protein S1-4	At5g07030;RPS4A;RPS4D;RPS4B
130330	214900	262300	48875	214460	58585		4	4	0.18	-0.19	F4KCE5;P22953;Q9C7X7;Q9LHA8;P22954;Q65	Probable mediator of RNA pol II subunit 37e;Heat shock 70 kDa protein 18	HSC70-1/3/18;MED37C/D/E
6968100	7779800	3216200	1900100	2309300	2919600		5	1	0.38	0.39	F4KGLU2;P51430	40S ribosomal protein S6-2	EMB3010;RPS6B
11600000	11958000	33562000	3670500	29853000	4143400		17	17	0.21	0.38	Q03042;P93292;F4INE2	Ribulose biphosphate carboxylase large chain	rbcl
144180	100560	226140	54407	139340	28241		9	9	0.02	0.02	Q04314-2;Q04314;Q04313	PYP10-binding protein 1/2	PBP1;PBP2
245880	582640	785930	69529	192800	141960		3	3	0.77	1.28	Q04603	50S ribosomal protein L5, chloroplastic	RPL5
1554600	1853900	2468500	567640	1775800	930970		12	11	0.10	1.00	Q04658	Probable nucleolar protein 5-1	NOP5-1
4001700	7515900	687710	798530	2482200	832450		11	11	0.05	-0.15	Q22607	WD-40 repeat-containing protein MSI4	MSI4
4713400	5784700	4904900	649880	4752000	2387900		3	3	0.12	0.06	Q9L2T0;Q9FFC0;	Histone H2B, 1-11	H2B
142450	214290	272920	53875	334900	51474		3	3	0.22	-0.56	Q9SRV5;Q50008	5-methyltetrahydropteroyltriglutamate--homocysteine methyltransferase 2	MS2;MS1
741540	426840	736760	194540	622360	243890		2	2	0.35	-0.47	Q2V4Q4;Q3EDH2;Q50061	50S ribosomal protein L4, chloroplastic	RPL4
15672000	16814000	10798000	8067500	8325000	4685900		4	4	0.02	0.04	Q04039	30S ribosomal protein S31, chloroplastic	RPS31
6085200	5157000	3430300	1560600	5324600	684250		3	3	0.39	1.18	Q9LD28;Q81826;Q9C681	Histone H2A, 1/2/3/6/Xb/Xa	RAT5
10683000	7320500	9560400	21144000	5726300	988050		5	2	0.05	0.20	Q39141;Q8V287;P0CJ48;P04778;Q39142	Chlorophyll a-b binding protein 1/2/3, chloroplastic	Lhb1B2;LHCB1.2;LHCB1.1
342020	244380	546450	0	254620	55157		4	3	0.00	0.01	P10795;F4HRR5	Ribulose biphosphate carboxylase small chain 1A, chloroplastic	RBCS-1A;RBCS1A
352120	375250	731630	93622	216460	217430		3	3	0.40	0.37	P16180	30S ribosomal protein S17, chloroplastic	RPS17
1663400	5977600	1923200	449410	764640	600240		4	4	0.84	1.22	P16181;P42733;Q65569	40S ribosomal protein S11-1/2/3	RPS11A;RPS11C;RPS11B
3223200	5854300	2108900	1064800	1412200	518970		8	8	1.86	1.18	P17094;A8MQQ1;P22738	60S ribosomal protein L3-1	ARP1;RP1
1172200	1257700	882260	430510	882300	417150		5	5	0.10	-0.03	P17745	Elongation factor Tu, chloroplastic	TUFA
1578200	1868900	2181700	326580	3265500	263280		13	12	0.11	0.16	P19366	ATP synthase subunit beta, chloroplastic	atpB
116510	33402	96316	25054	223920	26640		2	2	0.25	-0.46	Q9LJE4;P21240;C02361	Chaperonin 60 subunit beta 1/2/3, chloroplastic	CPN60B2;CPN60B1;CPN60B3
326950	732480	807240	183300	857930	114080		4	4	0.12	0.19	P25856;F4HNZ6;Q9LPW0-2;Q9LPW0	Glyceraldehyde-3-phosphate dehydrogenase GAP1/2, chloroplastic	GAP1;GAP2-2;GAP2
488220	569540	287280	244870	567950	194990		3	3	0.16	-0.11	P25857	Glyceraldehyde-3-phosphate dehydrogenase GAPB, chloroplastic	GAPB
1622800	1462900	936000	354600	2484300	357050		5	5	0.11	0.13	Q9FX54;P25858;F4HQT1	Glyceraldehyde-3-phosphate dehydrogenase GAPC1/2, cytosolic	GAPC2;GAPC1
938950	1168900	411150	202490	881230	176280		3	3	0.70	-1.16	P27521	Chlorophyll a-b binding protein 4, chloroplastic	LHCA4
5125800	5854100	2064500	3516200	3813900	1166000		5	5	0.02	0.02	P34788	40S ribosomal protein S18	RPS18A
5793600	13097000	4858100	4147900	5145300	3121800		3	3	0.07	-0.18	Q940B0;P42791	60S ribosomal protein L18-3;60S ribosomal protein L18-2	RPL18C;RPL18B
2802900	8322000	3706900	1179900	4085600	1029300		2	2	0.53	0.49	P42794-2;P42795;P42794	60S ribosomal protein L11-2;60S ribosomal protein L11-1	RPL11B;RPL11A
12239000	21701000	18473000	5585700	673660	4688400		4	4	0.39	1.77	Q9SF35;P493201	40S ribosomal protein S23-1;40S ribosomal protein S23-2	RPS23A;RPS23B
6816900	4423200	4435500	1404100	4424000	956540		4	4	1.38	0.74	Q8LBI1;P49227;F4J912	60S ribosomal protein L5-1;60S ribosomal protein L5-2	ATL5;RPL5B
2324800	1538000	1831600	646800	1511800	511270		2	2	0.01	0.01	Q9LR33;P49637	60S ribosomal protein L27a-2;60S ribosomal protein L27a-3	RPL27AB;RPL27AC
1303100	1073100	722280	418800	2584700	326480		6	3	0.43	-0.58	P49688;Q9SCM3	40S ribosomal protein S2-3;40S ribosomal protein S2-4	RPS2C;RPS2D
5063000	3133100	3076600	578530	1416600	1003600		3	3	0.73	0.89	P49693;Q9SRX2;Q9LUQ6	60S ribosomal protein L19-3;60S ribosomal protein L19-1	RPL19C;RPL19A
2940000	1228000	1851000	508430	3488600	566350		6	6	0.13	0.21	P56757	ATP synthase subunit alpha, chloroplastic	atpA
1150900	1023400	797950	366720	1512600	220410		3	3	0.37	-0.39	P56778	Photosystem II CP43 reaction center protein	psbC
506910	2598800	1462900	312220	947100	601450		3	3	0.05	-0.08	P56797	30S ribosomal protein S2, chloroplastic	rps2

iBAQ						t-test Significant	Peptides	Unique peptides	Log t-test p value	t-test Difference	Protein IDs	Protein names	Gene names
BASL1	BASL2	BASL3	Control1	Control2	Control3								
2282700	4943800	1945600	778840	2322900	651860		3	3	0.42	0.25	P56799	30S ribosomal protein S4, chloroplast	rps4
2631700	5898100	3576700	1129800	4463700	839180		3	3	0.55	-1.16	P56807	30S ribosomal protein S18, chloroplast	rps18
39764000	78234000	59306000	9753800	14617000	16942000		3	3	0.19	-1.11	P59233;P59232;P59271	Ubiquitin-40S ribosomal protein S27a-2/3	RPS27AC;RPS27AB
7195100	19194000	5981200	7087100	12132000	3513000		5	5	0.24	-0.32	P59259;A8MRV1	Histone H4	At1g07660
7065300	3251800	3794700	6158500	1295300	474610		3	1	0.50	-1.84	P61837;B9DFR3;A8MRW1;Q06611;Q39196	Aquaporin PIP1-1/2/4	PIP1-1;PIP1B;PIP1-2;PIP1.4
823280	985790	665170	400440	1395200	406940		3	3	1.27	-0.43	P93014	30S ribosomal protein S5, chloroplast	rps5
845450	968730	1074100	168260	3046700	280040		3	3	0.35	-0.29	Q03250;F4IHK3;Q03250-2	Glycine-rich RNA-binding protein 7	RBG7;CCR2
436540	1382000	13699000	375720	4929300	479590		39	30	0.06	-0.32	Q38882;P58766	Phospholipase D alpha 1	PLDALPHA1
228420	354690	263240	41322	203560	21616		5	5	0.44	0.40	Q9ASR0;Q56YW3;P23515;P29517	Tubulin beta-3 chain; Tubulin beta-2 chain; Tubulin beta-7 chain	TUBB3;TUBB2;TUBB7
4389000	5069600	5121100	0	0	0	+	7	7	4.40	4.91	Q5BPF3;Q5BPF3-2	Protein BREAKING OF ASYMMETRY IN THE STOMATAL LINEAGE	BASL
18084000	30784000	24350000	7736200	13450000	7042200		4	4	0.25	0.14	Q8GWY0	G patch domain-containing protein TGH	TGH
376650	1125600	584960	228540	643950	210350		4	4	0.29	0.26	Q9FN46;Q8GXN9	DEAD-box ATP-dependent RNA helicase 42	RH42
1615900	3392600	7271300	1166000	3997500	1650400		27	27	0.93	-0.55	Q8H0U8;Q8H0U8-2;Q9SF41	Splicing factor U2af large subunit B	U2AF65B
1190400	2424500	2697600	732870	3385500	675350		9	9	0.07	0.09	Q8L716;Q9C6C1	Transcription initiation factor TFIID subunit 2	TAF2
126310	643150	250650	35263	158610	35305		4	4	1.22	0.85	Q8LFP0-2;Q8LFP0	Putative HIACA ribonucleoprotein complex subunit 1-like protein 1	At1g76010
7382900	17871000	3972000	2277800	28324000	2841800		7	6	0.44	-0.84	Q8VZ70	40S ribosomal protein S8-1	RPS8A
57402	83421	306520	117990	1671700	172480		3	3	0.42	-1.04	Q93VA8	Mediator of RNA polymerase II transcription subunit 36a	MED36A
4337100	6260300	3087700	1368700	4928600	1402100		4	4	0.22	-0.19	Q93VG5	30S ribosomal protein S20, chloroplast	RPS20
2076900	1853500	1892000	1013500	6383200	1285800		10	3	1.78	-1.46	Q94AH9	40S ribosomal protein S7-1	RPS7A
5541700	9592000	7415400	2615800	6391700	2444600		5	5	0.17	-0.12	Q94JX8	60S ribosomal protein S14-2	RPS14B
10987000	13018000	3702400	5291300	1400300	5542100		6	6	0.12	-0.40	Q9ASV6	60S ribosomal protein S14-3	RPS14C
13305000	26095000	36872000	2800700	4814700	3905600		7	7	0.52	0.88	Q9C514	60S ribosomal protein L22-3	RPL22C
77806	137790	296340	0	7668.9	25398		5	5	1.66	1.01	Q9C7E7	Probable mediator of RNA polymerase II transcription subunit 36b	MED36B
1341300	1982700	361230	294590	476110	225430		3	3	0.02	0.02	Q9FZ76;Q9C9C6;Q9C9C5	50S ribosomal protein L23, chloroplast	RPL23
2918600	3901400	1197300	504560	1688400	600290		5	5	0.59	0.27	Q9CAV0;Q42262	50S ribosomal protein L27, chloroplast	RPL27
4076900	4325900	1959100	1619200	3215700	1362000		4	4	0.75	-1.53	Q9CAK6;Q9SIH0;P42036	Mediator of RNA polymerase II transcription subunit 19a	MED19A
27912000	42380000	74144000	10434000	36531000	14550000		10	2	0.01	0.01	Q9FE58	Calcium sensing receptor, chloroplast	CAS
1046800	1203200	1257100	63906	904510	571750		10	3	0.07	-0.17	Q9FEF8;Q9FEF8-2	50S ribosomal protein L29	RPL29
3002600	6382500	16387000	3864000	10441000	4200000		4	4	0.43	-0.76	Q9FJP3	50S ribosomal protein L31, chloroplast	RPL31
640760	488400	1759000	89763	338490	224700		2	2	0.40	0.42	Q9FLN4	Dynamin-related protein 1E	DRP1E
534570	570660	379230	214200	421480	341860		2	2	2.79	-1.41	Q9FMP0	Nucleolin 1	NUCL1
388870	456180	203790	45497	85718	51821		2	2	2.06	1.01	Q9FN48	50S ribosomal protein L31, chloroplast	RPL31
2062500	2218500	202620	715520	1482500	882080		17	17	0.15	-0.48	Q9FNE4;Q9LK91	50S ribosomal protein L31, chloroplast	RPL31
57638	137920	29964	23373	126710	11925		6	4	0.82	-0.62	Q9FNX5	Probable nucleolar protein 5-2	NOP5-2
711000	809520	442930	273070	6551700	378010		10	10	0.56	-1.85	Q9FVQ1	Splicing factor U2af small subunit A	U2AF35A;ATU2AF35A
518460	504330	609250	157950	311460	206260		2	2	0.06	-0.05	Q9FW54	60S ribosomal protein L4-1	RPL4A;At3g09630
3695900	10264000	535930	1271200	1876800	1241000		8	8	0.03	-0.08	Q9FXB5	60S ribosomal protein L14-2	RPL14B;RPL14A
20532000	41408000	7871500	6172000	36623000	5725900		43	43	0.02	-0.04	Q9LD90	Probable nucleolar protein 5-2	NOP5-2
1330700	1726400	2908200	885920	787660	708600		2	2	0.01	-0.01	Q9LER7	50S ribosomal protein L36-1/2/3	RPL36B;RPL36C;RPL36A
8514300	23887000	8883900	2922800	21750000	2443500		7	7	0.18	-0.50	Q9LEY9	50S ribosomal protein L36-1/2/3	RPL36B;RPL36C;RPL36A
913880	915880	3750100	215550	1636700	248290		5	5	0.17	0.33	Q9LFE0	HiACA ribonucleoprotein complex subunit 2-like protein	
2148300	2418300	3183900	988250	2047200	1315700		5	5	0.21	-0.27	Q9LJV8;Q9FKA5	SART-1 family protein DOT2	DOT2
369520	429630	101170	118680	559980	83802		8	4	0.01	-0.03	Q9LQ55	At3g23075	At3g23075
4310100	4764900	34803000	1803300	8084900	2675400		13	13	0.20	-0.46	Q9LU74	DRP2B	DRP2B
23865000	40111000	20407000	9141800	14685000	11347000		24	24	0.09	0.10	Q9LVH1	At5g57120	At5g57120
8055000	9477800	3017200	1942400	5286900	1765800		5	5	0.06	-0.13	Q9LXG1;B3H7J6;Q9FLF0	At5g60030	At5g60030
60884000	53602000	23925000	23071000	7355900	32318000		7	7	0.25	0.47	Q9M352-2;Q9M352;Q9LZ57;Q80929	40S ribosomal protein S9-1, 40S ribosomal protein S9-2	RPS9B;At5g15200;RPS9C
10287000	8005600	11237000	3018500	6797200	4773200		18	17	0.12	-0.11	Q9MAB3	60S ribosomal protein L36-1/2/3	RPL36B;RPL36C;RPL36A
418920	931390	1127800	240440	652400	158120		4	1	0.17	0.26	Q9S709;A8MRH1	Probable nucleolar protein 5-2	NOP5-2
472230	1250400	3355700	426740	1530700	780630		5	3	0.41	0.44	Q9SF40;Q2V3X4;F4KDU5	Splicing factor U2af small subunit A	U2AF35A;ATU2AF35A
2620800	3360000	3484700	1219300	6972600	1939500		15	15	1.12	-0.71	Q9SGT7;Q9LTV0	60S ribosomal protein L4-1	RPL4A;At3g09630
333810	759300	277250	169680	324480	203160		3	1	0.00	0.00	Q9SK22	T6H22.10	T6H22.10
3918200	4115500	12938000	1829700	2951000	2748100		6	6	0.02	-0.02	Q9SKX4	40S ribosomal protein S16-1	RPS16A
247570	775450	654750	50113	283930	88497		17	15	0.12	-0.21	Q9SR37	50S ribosomal protein L3-1, chloroplast	RPL3A
25650000	28657000	24311000	9831800	7889000	22014000		3	2	0.06	0.13	Q9SS17	Beta-glucosidase 23	BGLU23
670670	890400	490030	451310	1133900	232210		3	3	0.45	-0.57	Q9T043;Q9SIM4	40S ribosomal protein S24-1	RPS24A
503910	3790000	3796900	1677300	1061000	1160900		5	3	0.60	0.86	Q9ZU9	60S ribosomal protein L14-2; 60S ribosomal protein L14-1	RPL14B;RPL14A
												40S ribosomal protein S5-1	RPS5A

7.4 Appendix D: *N. benthamiana* IP-MS results

Table 7.3 Candidates identified from IP-MS in *N. benthamiana* (filtered).

The candidates identified by IP-MS, conducted using *N. benthamiana* leaves, that meet the filtering criteria described in section 6.9.6 are listed. Peptide counts are shown for the proteins in the un-infiltrated sample, GFP-BASL (GFP-2) sample, and the GFP-2 control. Peptides unique to the GFP-BASL (bait) sample are indicated. Proteins with a peptide count of <4, that were not unique to or enriched in the BASL sample by 1.5-fold are not shown. The reference to the *N. benthamiana* database used, and GO and InterPro (IPR) identifiers are also shown.

Reference in database	Identified protein	GO and IPR numbers	Peptide counts Un-infiltrated (negative)	Peptide counts GFP-BASL (bait)	Peptide counts GFP (positive)	Unique to bait?
-	GFP-BASL (GFP spectra removed to show only BASL)	-	0	13	0	✓
Niben101Scf01517g05010.1 sp C4ZXJ7 LLDD_ECOBW	L-lactate dehydrogenase	IPR012133, IPR013785	0	17	0	✓
Niben101Scf03410g03002.1 sp P10987 ACT1_DROME	Actin-5C	IPR004000	0	9	0	✓
Niben101Scf10278g01002.1 sp Q6ZKC0 14333_ORYSJ	14-3-3-like protein GF14-C	IPR000308, IPR023409, IPR023410, GO:0019904	0	8	0	✓
Niben101Scf03493g00020.1 sp P41113 ACT3_PODCA	Actin-3	IPR004000	0	8	0	✓
Niben101Scf02367g04001.1 sp Q6ZKC0 14333_ORYSJ	14-3-3-like protein GF14-C	IPR000308, IPR023409, IPR023410, GO:0019904	0	7	0	✓
Niben101Scf05959g01005.1 sp Q96300 14337_ARATH	14-3-3-like protein GF14 nu	IPR000308, IPR023409, IPR023410, GO:0019904	0	7	0	✓
Niben101Scf03628g14020.1 AT1G26480.1	General regulatory factor 12	IPR000308, IPR023409, IPR023410, GO:0019904	0	7	0	✓
Niben101Scf02461g00003.1 AT1G79550.1	Phosphoglycerate kinase	IPR001576, GO:0004618, GO:0006096	0	7	0	✓
Niben101Scf10757g00001.1 sp Q6ZKC0 14333_ORYSJ	14-3-3-like protein, GF14-C	IPR000308, IPR023409, IPR023410, GO:0019904	0	6	0	✓
Niben101Scf00477g00017.1 sp Q96299 14339_ARATH	14-3-3-like protein, GF14 mu	IPR000308, IPR023409, IPR023410, GO:0019904	0	6	0	✓
Niben101Scf06183g03009.1 AT2G42590.3	General regulatory factor 9	IPR000308, IPR023409, IPR023410, GO:0019904	0	6	0	✓
Niben101Scf02480g02012.1 sp Q4ZXH2 GCSP_PSEU2	Glycine dehydrogenase (decarboxylating)	IPR020581, GO:0003824, GO:0004375, GO:0006544, GO:0006546, GO:0030170, GO:0055114	0	5	0	✓

Reference in database	Identified protein	GO and IPR numbers	Peptide counts Un-infiltrated (negative)	Peptide counts GFP-BASL (bait)	Peptide counts GFP (positive)	Unique to bait?
Niben101Scf06516g04018.1 sp Q6ZKC0 14333_ORYSJ	14-3-3-like protein GF14-C	IPR000308, IPR023409, IPR023410, GO:0019904	0	5	0	✓
Niben101Scf02366g06014.1 sp Q96300 14337_ARATH	14-3-3-like protein GF14 nu	IPR000308, IPR023409, IPR023410, GO:0019904	0	5	0	✓
Niben101Scf04024g00009.1 AT4G38970.1	Fructose-bisphosphate aldolase 2	IPR000741, IPR013785, IPR029768, GO:0003824, GO:0004332, GO:0006096	0	5	0	✓
Niben101Scf02452g01003.1 sp A3CT12 RS8_METMJ	30S ribosomal protein S8	IPR000630, GO:0003735, GO:0005840, GO:0006412	0	4	0	✓
Niben101Scf03263g08013.1 sp P25141 ADH1_PETHY	Alcohol dehydrogenase 1	IPR002085, IPR011032, IPR016040, GO:0006069, GO:0008270, GO:0016491, GO:0051903, GO:0055114	0	4	0	✓
Niben101Scf02062g06004.1 AT5G13490.1	ADP/ATP carrier 2	IPR002067, IPR023395, GO:0005215, GO:0005743, GO:0006810, GO:0055085	0	4	0	✓
Niben101Scf06157g00010.1 sp O65202 ACO1_ARATH	Peroxisomal acyl-coenzyme A oxidase 1	IPR009075, IPR012258, IPR013786, GO:0003995, GO:0003997, GO:0005777, GO:0006631, GO:0006635, GO:0008152, GO:0016627, GO:0050660, GO:0055114	0	4	0	✓
Niben101Scf09304g00002.1 sp BOC431 RS11_ACAM1	30S ribosomal protein S11	IPR001971, GO:0003735, GO:0005840, GO:0006412	0	4	0	✓
Niben101Scf02842g00014.1 sp Q98AX9 CH603_RHILO	60 kDa chaperonin 3	IPR002423, IPR027409, IPR027413, GO:0005524, GO:0005737, GO:0006457, GO:0042026, GO:0044267	0	7	1	✗
Niben101Scf05349g01011.1 sp P04782 CB24_PETSP	Chlorophyll a-b binding protein 25	IPR022796, IPR023329, GO:0009765, GO:0016020	0	6	1	✗
Niben101Scf07381g02007.1 sp Q06967 14336_ORYSJ	14-3-3-like protein GF14-F	IPR000308, IPR023409, IPR023410, GO:0019904	0	8	2	✗
Niben101Scf06668g02002.1 sp Q9SWE7 VATE_CITLI	V-type proton ATPase subunit E	IPR002842, GO:0015991, GO:0033178, GO:0046961	0	4	1	✗
Niben101Scf04287g09002.1 ref WP_021018876.1	Dihydroxynaphthoic acid synthetase	IPR001753, IPR014748, IPR018376, IPR029045, GO:0003824, GO:0008152	0	4	1	✗
Niben101Scf05442g02007.1 sp Q9LZG0 ADK2_ARATH	Adenosine kinase 2	IPR001805, IPR029056, GO:0004001, GO:0006166, GO:0016773	0	4	1	✗
Niben101Scf04198g01002.1 sp P55038 GLTS_SYNY3	Ferredoxin-dependent glutamate synthase 2	IPR002489, IPR013785, GO:0003824, GO:0006537, GO:0008152, GO:0015930, GO:0016491, GO:0016638, GO:0055114	0	4	1	✗
Niben101Scf01517g08001.1 sp P27522 CB13_SOLLC	Chlorophyll a-b binding protein 8	IPR022796, IPR023329, GO:0009765, GO:0016020	0	4	2	✗

Reference in database	Identified protein	GO and IPR numbers	Peptide counts Un-infiltrated (negative)	Peptide counts GFP-BASL (bait)	Peptide counts GFP (positive)	Unique to bait?
Niben101Scf04187g00037.1 AT2G04030.1	Chaperone protein htpG family protein	IPR001404, GO:0005524, GO:0006457, GO:0006950, GO:0051082	0	4	2	✗
Niben101Scf08723g02015.1 sp P84981 FENR_POPEU	Ferredoxin--NADP reductase	IPR001433, IPR015701, IPR017938, GO:0016491, GO:0055114	0	5	3	✗
Niben101Scf18639g00026.1 AT5G23060.1	Calcium sensing receptor	IPR001763	0	5	3	✗
Niben101Scf13942g00028.1 sp C1B027 RL6_RHOOB	50S ribosomal protein L6	IPR000702, GO:0003735, GO:0005622, GO:0005840, GO:0006412, GO:0019843	4	7	2	✗
Niben101Scf21647g01003.1 sp Q1JDX0 VATA_STRPB	V-type ATP synthase alpha chain	IPR005725, IPR027417, GO:0005524, GO:0015991, GO:0015992, GO:0016820, GO:0033178, GO:0033180, GO:0046034, GO:0046961	5	8	4	✗

7.5 Appendix E: Manuscript

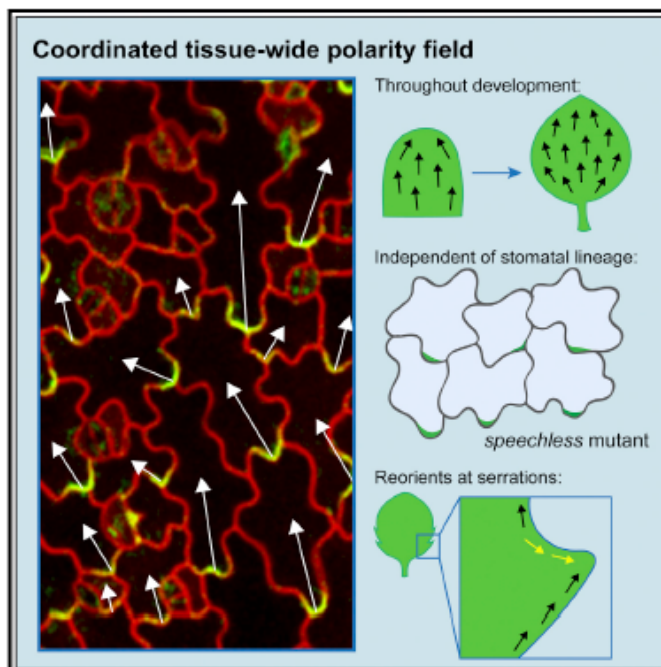
Below is a copy of the manuscript that was published in August 2018, and that is based on much of the work in Chapters 2 and 3 of this thesis. The supplementary information is available online.

Report

Current Biology

Ectopic BASL Reveals Tissue Cell Polarity throughout Leaf Development in *Arabidopsis thaliana*

Graphical Abstract



Authors

Catherine Mansfield,
Jacob L. Newman, Tjelvar S.G. Olsson,
Matthew Hartley, Jordi Chan,
Enrico Coen

Correspondence

jordi.chan@jic.ac.uk (J.C.),
enrico.coen@jic.ac.uk (E.C.)

In Brief

Mansfield et al. demonstrate a coordinated tissue cell polarity field in the *Arabidopsis* leaf epidermis revealed by ectopic expression of BASL. This polarity field is independent of the stomatal lineage and reorients around serrations, mirroring the polarity of PIN1.

Highlights

- Ectopic expression of BASL in *Arabidopsis* leaves reveals coordinated polarity
- The ectopic BASL polarity field is independent of the stomatal lineage
- The polarity field reorients around serrations, mirroring PIN1 polarity



Mansfield et al., 2018, *Current Biology* 28, 2638–2646
August 20, 2018 © 2018 The Author(s). Published by Elsevier Ltd.
<https://doi.org/10.1016/j.cub.2018.06.019>

CellPress

Ectopic BASL Reveals Tissue Cell Polarity throughout Leaf Development in *Arabidopsis thaliana*

Catherine Mansfield,¹ Jacob L. Newman,^{1,2} Tjelvar S.G. Olsson,¹ Matthew Hartley,¹ Jordi Chan,^{1,*} and Enrico Coen^{1,3,*}

¹John Innes Centre, Colney Lane, Norwich NR4 7UH, UK

²Present address: School of Computing Sciences, University of East Anglia, Norwich NR4 7TJ, UK

³Lead Contact

*Correspondence: jordi.chan@jic.ac.uk (J.C.), enrico.coen@jic.ac.uk (E.C.)

<https://doi.org/10.1016/j.cub.2018.06.019>

SUMMARY

Tissue-wide polarity fields, in which cell polarity is coordinated across the tissue, have been described for planar organs such as the *Drosophila* wing and are considered important for coordinating growth and differentiation [1]. In planar plant organs, such as leaves, polarity fields have been identified for subgroups of cells, such as stomatal lineages [2], trichomes [3, 4], serrations [5], or early developmental stages [6]. Here, we show that ectopic induction of the stomatal protein BASL (BREAKING OF ASYMMETRY IN THE STOMATAL LINEAGE) reveals a tissue-wide epidermal polarity field in leaves throughout development. Ectopic GFP-BASL is typically localized toward the proximal end of cells and to one lobe of mature pavement cells, revealing a polarity field that aligns with the proximodistal axis of the leaf (base to tip). The polarity field is largely parallel to the midline of the leaf but diverges in more lateral positions, particularly at later stages in development, suggesting it may be deformed during growth. The polarity field is observed in the *speechless* mutant, showing that it is independent of stomatal lineages, and is observed in isotropic cells, showing that cell shape anisotropy is not required for orienting polarity. Ectopic BASL forms convergence and divergence points at serrations, mirroring epidermal PIN polarity patterns, suggesting a common underlying polarity mechanism. Thus, we show that similar to the situation in animals, planar plant organs have a tissue-wide cell polarity field, and this may provide a general cellular mechanism for guiding growth and differentiation.

RESULTS AND DISCUSSION

Ectopic BASL Reveals a Polarity Field Independent of Stomatal Lineages

Asymmetries across individual cells (cell polarity) can be coordinated across a tissue to give tissue-wide polarity fields [7]. Polar-

ity fields have been invoked to account for patterns of oriented growth of planar organs, such as leaves [8]. Mathematically, a polarity field corresponds to each position in space having a vector (a vector field) [9]. In biological terms, these positions may correspond to individual cells. However, evidence for a tissue-wide polarity field maintained during planar plant organ development has been lacking.

Several proteins preferentially localized to one end of the cell (i.e., exhibiting cell polarity) have been described in plants, including PIN-FORMED (PIN) proteins, BASL (BREAKING OF ASYMMETRY IN THE STOMATAL LINEAGE), BRXL2 (BREVIS RADIX-LIKE 2), POLAR (POLAR LOCALIZATION DURING ASYMMETRIC DIVISION AND REDISTRIBUTION), OCTOPUS, BORs (BORON TRANSPORTERS 1), and NIPs (NODULIN26-LIKE INTRINSIC PROTEINS) [2, 10–14]. Some of these proteins, notably PIN1 and BRXL2, exhibit polarity coordination in the developing leaf epidermis. PIN1 is preferentially localized at the distal end of cells in leaf primordia, but this pattern disappears at later developmental stages [6, 15]. BRXL2 shows preferential localization to the proximal end of cells in the stomatal lineage [2], compounded by a spiral pattern of polarity switching involved in stomatal spacing [16].

Here, we use BASL to explore polarity patterns in developing leaves. BASL has a well-characterized polarity pattern that is similar to BRXL2, localizing to a crescent in stomatal lineage cells [2] [16]. Localized BASL domains have also been described in root cells ectopically expressing BASL [11].

To see if a polarity field could exist across the leaf independently of the stomatal pathway, we exploited the *speechless* (*spch*) mutant, which lacks stomatal lineages. We induced expression of *35S::GFP-BASL* using a heat-shock-inducible Cre-lox system [17] to avoid potentially pleiotropic effects of overexpressing BASL throughout development [11].

Ectopically induced BASL was asymmetrically localized in leaf epidermal cells of *spch* (Figure 1A). Signal typically spanned cell vertices (three-way junctions, Figure S1F), allowing assignment to individual cells. In pavement cells, signal was typically observed in a single lobe, toward the proximal end of the cell. To quantify the polarity pattern, we assigned cell unit vectors that pointed from the midpoint of the BASL crescent signal to the cell centroid (Figure 1B). To avoid subjective bias, we randomly rotated automatically segmented single cells before BASL signal was manually identified (Figures S1G–S1O). Processed cells were then returned to their original position and



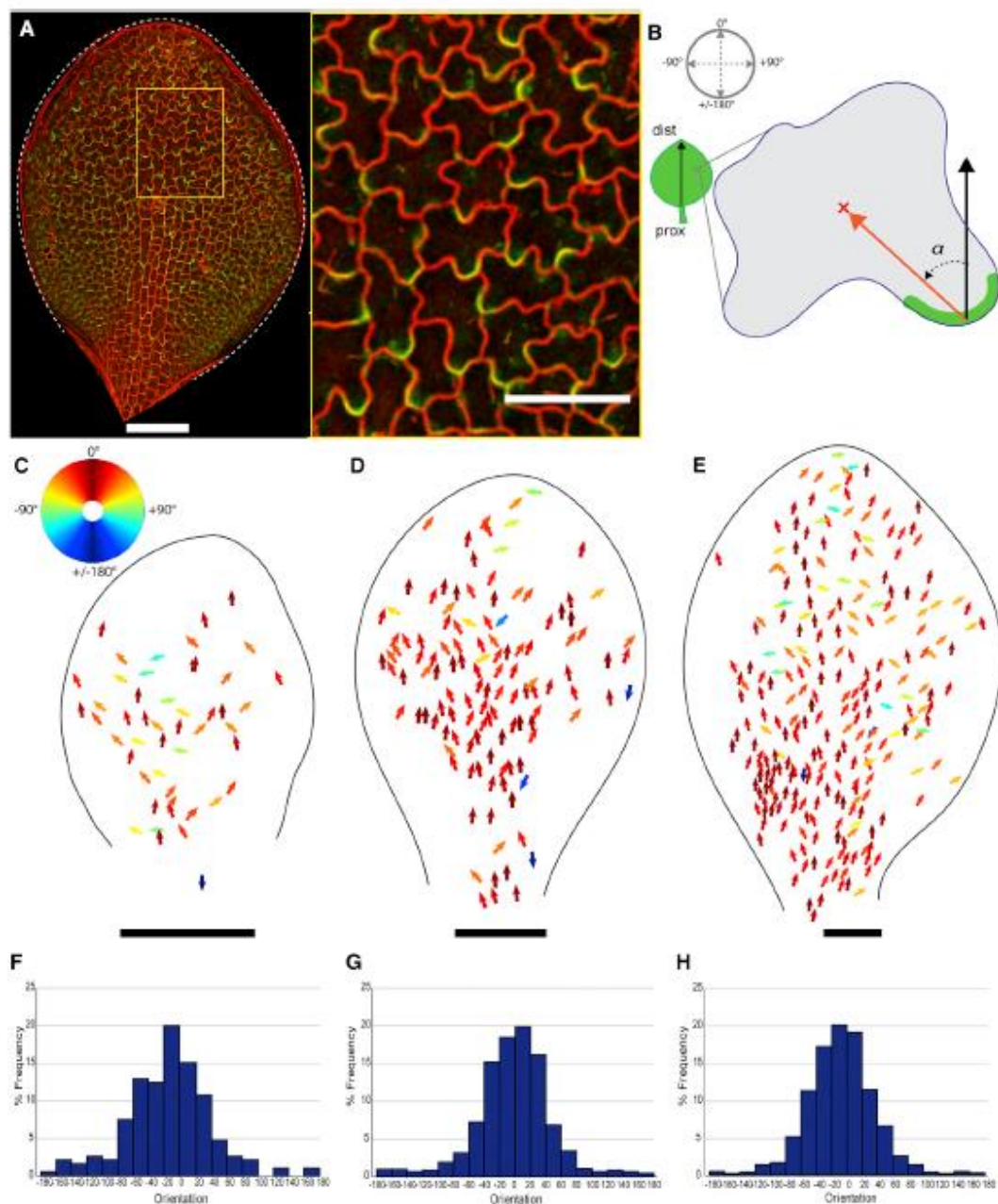


Figure 1. Ectopic BASL Reveals a Polarity Field Independent of Stomatal Lineages

(A) Induced 35S::GFP-BASL in *speechless* leaf stained with propidium iodide (PI). Scale bar is 50 μ m in right panel.

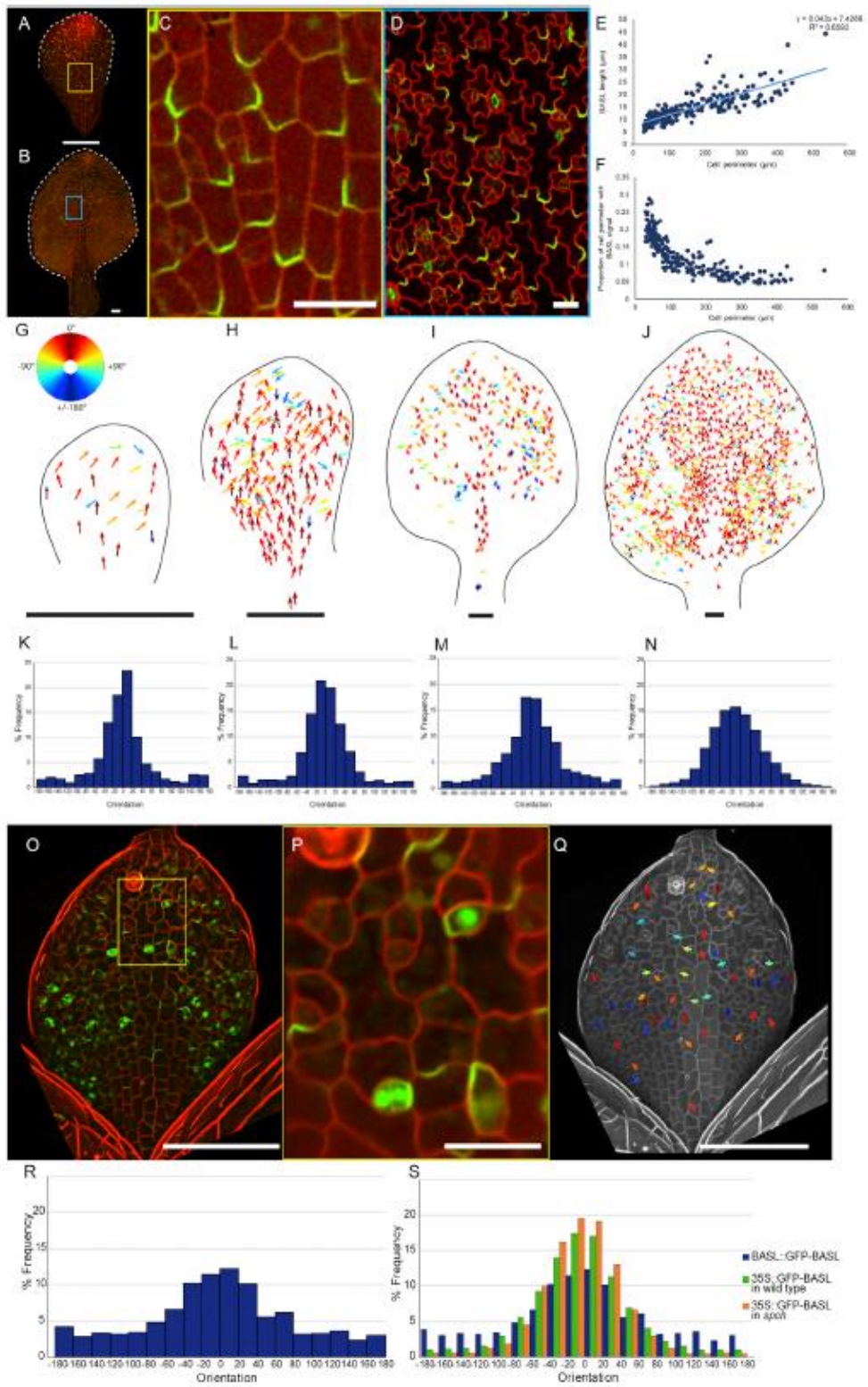
(B) BASL vectors (orange arrow) assigned from BASL crescent to cell centroid. α between midline vector (black arrow) and BASL vector.

(C-E) Ectopic BASL vectors colored according to color wheel (in C) indicating α orientation in *speechless* leaves of (C) 50–200 μ m, (D) 200–400 μ m, and (E) 400–800 μ m width categories. Leaf outlines shown.

(F–H) Vector orientation in *speechless* leaves pooled from widths (F) 50–200 μ m ($n = 185$ cells, 4 leaves, $\alpha = 55.34$), (G) 200–400 μ m ($n = 1199$ cells, 12 leaves, $\alpha = 49.43$), and (H) 400–800 μ m ($n = 2063$ cells, 9 leaves, $\alpha = 44.68$). 0° represents proximodistal vector. Scale bars are 100 μ m except for the right panel of (A). See also Figure S1.

orientation. The BASL vector orientation was calculated with respect to the proximodistal midline vector of the leaf (Figure 1B) and plotted according to a color map (Figure 1C). We refer to the resulting vector field as the ectopic BASL polarity field.

At all developmental stages analyzed, BASL vectors were largely proximodistally oriented in *spch* (i.e., BASL localized toward the proximal end of cells; red/orange arrows in Figures 1C–1E). Some vectors deviated from this proximodistal pattern,



(legend on next page)

particularly toward the leaf tip, though very few vectors pointed proximally (Figures 1C–1E). BASL vector orientations from multiple *spch* leaves were pooled according to leaf size and plotted in histograms (Figures 1F–1H). More than 90% of the BASL vectors were within the range of -80° to 80° . Thus, ectopic BASL reveals a strongly coordinated proximodistal polarity field across leaves of different sizes that is independent of stomatal lineages.

The Polarity Field Revealed by Ectopic BASL Is Present in Wild-Type Leaves

Given that ectopic BASL reveals a proximodistal polarity field in *spch*, we might expect a similar field to be present in the non-stomatal lineage cells of wild-type leaves. To test this hypothesis, 35S::GFP-BASL was induced in a wild-type background at different developmental stages (Figures 2A–2D). As in *spch*, ectopic BASL was predominantly observed at the proximal end of cells, often at cell corners (Figure 2C) or within single-pavement cell lobes (Figure 2D). These cells included those above the midvein, which do not develop stomatal lineages [18]. Proximal localization was confirmed from analysis of sectors of BASL expression (Figures S1A–S1E), and by polarity quantification (Figures 2G–2N).

BASL is not normally expressed outside stomatal lineage cells, suggesting that ectopic BASL expression either induces polarity or reveals a polarity field that does not itself depend on BASL function. If ectopic BASL induces polarity, we might expect signal to gradually coalesce on a proximal domain following induction. Time-lapse imaging leaves after heat-shock induction showed that, rather than coalescing, ectopic BASL appeared in its proximal location from approximately 12 hr after heat-shock induction and gradually intensified (Figure S2). This suggests that ectopic BASL does not itself induce cell polarity but rather marks a pre-existing polarity.

We hypothesize that ectopic BASL binds to interacting partners—for example, proteins or lipid domains—that are located proximally in each cell throughout development. We refer to these hypothetical interacting partners as providing a proximal molecular address. Localization of BASL to cell corners or to a single lobe of pavement cells may reflect a single address located at the proximal extrema of the cell. It is also possible that positioning of the proximal address is modulated by factors establishing lobe and neck formation [19–21] or located at cell corners.

The proximal address may be held at a fixed length or increase in length as the cell grows. To distinguish these possi-

bilities, we measured the length of the ectopic BASL domain at different developmental stages in a wild-type background. Domain length increased from $\sim 5 \mu\text{m}$ to $\sim 45 \mu\text{m}$ as cells increased in size, but at a rate lower than the rate of increase in cell perimeter (Figures 2E and 2F). This finding suggests that the proximal address does not have a fixed size but may be restricted through interactions with other factors in the cell, consistent with a model of polarity establishment involving intracellular partitioning [22].

The cytoskeleton has previously been associated with formation of cell polarity [23, 24]. To test if microtubules are required for positioning ectopic BASL, we destabilized microtubules with oryzalin before inducing BASL. In oryzalin-treated plants, ectopic BASL was still polarized (Figures S3A–S3G), suggesting that microtubules are not required for the polarization of BASL, similar to BRXL2 [2].

Wild-Type Exhibits a Combination of Stomatal and Non-stomatal Polarity Fields

For a comparable stage, the proportion of BASL vectors outside the range of -80° to 80° was significantly higher for wild-type than for *spch* (Table S1). To determine whether the lower level of proximodistal coordination in wild-type was caused by more variable BASL polarity orientation in stomatal lineage cells, we imaged leaves expressing BASL::GFP-BASL [11]. BASL was asymmetrically localized within individual cells, as well as expressed in the nucleus (Figures 2O and 2P), as previously described [11, 16]. Although not obvious from inspection of a single leaf (Figure 2Q), when multiple leaves were pooled, proximodistal coordination was observed for BASL vectors in BASL::GFP-BASL (Figure 2R), as reported for BRXL2 [2]. BASL polarity was significantly less coordinated than for ectopic BASL in *spch* (Table S1). Wild-type background showed an intermediate distribution (Figure 2S and Table S1), suggesting that it reflects a mixture of two patterns: a strongly coordinated proximodistal pattern in non-stomatal lineage cells and a weaker coordinated pattern in stomatal lineage cells.

Two hypotheses may account for the weaker polarity coordination of the stomatal lineage. One is that the proximodistal address becomes reoriented in stomatal lineage cells, and ectopic BASL follows this pattern. Alternatively, stomatal lineage cells contain two addresses (i.e., two regions with BASL-interacting factors) that compete for ectopic BASL: a proximal address and an address specific to stomatal lineages.

Figure 2. Ectopic BASL in a Wild-Type Background and BASL::GFP-BASL Show Coordinated Patterns throughout Development

(A–D) Induced 35S::GFP-BASL in (A) 50–200 μm and (B) >800 μm width leaves magnified in (C) and (D), respectively. Cell outlines shown using PI staining in C and RFP-PM in D.

(E) Length of BASL crescent against cell perimeter for leaves of various sizes.

(F) BASL crescent length as a proportion of cell perimeter.

(G–J) Ectopic BASL vectors colored according to color wheel (in G) in leaves of (G) 50–200 μm , (H) 200–400 μm , (I) 400–800 μm and (J) 800+ μm widths.

(K–N) Vector orientations pooled in leaves of (K) 50–200 μm ($n = 1042$ cells, 15 leaves, $\sigma = 64.76$), (L) 200–400 μm ($n = 1464$ cells, 9 leaves, $\sigma = 57.25$), (M) 400–800 μm ($n = 890$ cells, 4 leaves, $\sigma = 63.67$), and (N) 800+ μm ($n = 3642$ cells, 4 leaves, $\sigma = 52.71$) widths.

(O and P) (O) BASL::GFP-BASL leaf stained with PI and magnified in (P).

(Q) BASL vectors from leaf in (O) colored according to color wheel (shown in G).

(R) BASL vector orientations in BASL::GFP-BASL pooled from multiple leaves from 50–800 μm width ($n = 1319$ cells, 21 leaves, $\sigma = 82.3$).

(S) Percentage frequency of BASL vector orientations for induced 35S::GFP-BASL in WT and *speechless* background and BASL::GFP-BASL.

Each genotype pooled from at least 20 leaves from 50–800 μm . $p < 10^{-5}$ for each pairwise chi-squared comparison (Table S1). Scale bars are 100 μm in (A), (B), (G)–(I), (O), and (Q) and 20 μm in (C), (D), and (P). See also Figures S1 and S2.

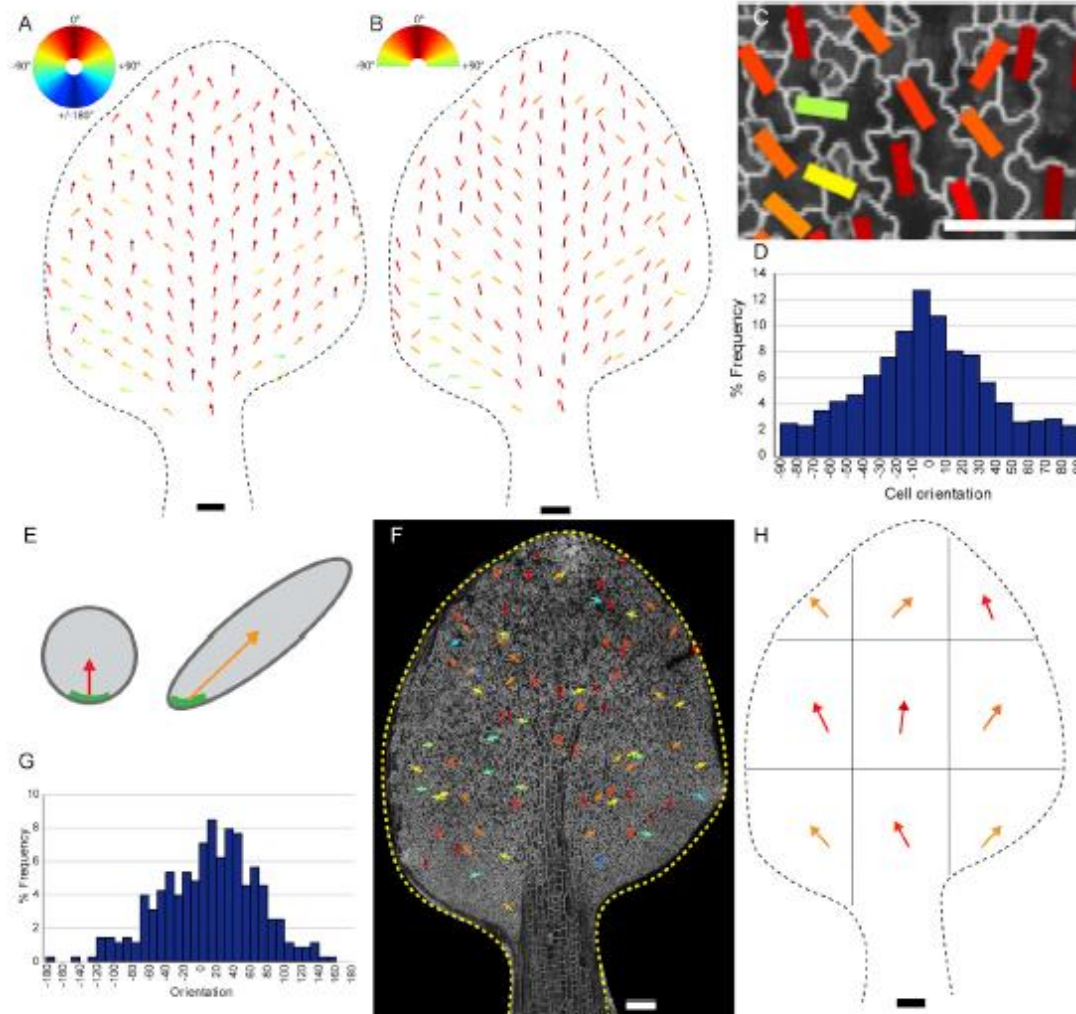


Figure 3. Ectopic BASL Polarity in a Wild-Type Background Becomes Divergent during Development and Is Present in Near-Isotropic Cells
 (A) Downsampled vectors in leaf of $>800\ \mu\text{m}$ width plotted according to color map.
 (B) Downsampled cell long axes for leaf in (A) plotted according to color map. Due to the long axes being tensors and not vectors, half of the color map is used.
 (C) Close-up of individual cell orientations for leaf in (B). Scale bar is $20\ \mu\text{m}$.
 (D) Orientation of cell long axis relative to leaf midline vector for leaf shown in (A) and (B). See also [Figure S4](#).
 (E) Schematic of an isotropic cell with BASL localized to the proximal end (left) and an anisotropic cell where BASL polarity vector has become deflected, even though BASL position is unchanged (right).
 (F) Leaf in (A) with BASL vectors for cells with eccentricity <0.6 plotted.
 (G) BASL vector orientation for near-isotropic cells relative to leaf midline vector. Data pooled from 4 leaves of $800+\ \mu\text{m}$ width.
 (H) Leaf in (A) divided into regions with average BASL vector orientations in each section shown and plotted according to color map in (A). See also [Table S2](#).
 Scale bars are $100\ \mu\text{m}$ except in (C).

The Polarity Field Becomes Divergent during Development

To visualize the ectopic BASL polarity pattern more easily, larger leaves were downsampled by averaging vector orientations using a grid ([Figure 3A](#)). This analysis showed that vectors in the midvein region were highly coordinated in a proximodistal orientation, while those in the proximal lamina diverged away from the midvein toward the margin ([Figure 3A](#)). The ectopic BASL polarity field shows striking similarities with a polarity field previously proposed to account for orientations of growth [8]. In both cases, the polarity field becomes divergent at later stages of develop-

ment. It has also been shown that the orientation of BRXL2 polarity is aligned with the orientation of subsequent growth [2]. These results suggest that polarity may provide orientation information to guide growth.

However, this interpretation is complicated because of the way polarity is assigned in relation to the centroid of the cell. For example, suppose BASL is proximal in a circular cell ([Figure 3E](#), left). If that cell becomes elongated diagonally (either through growth or diagonal division), polarity will also become diagonal, even though there has been no change in the positioning of the BASL signal ([Figure 3E](#), right).

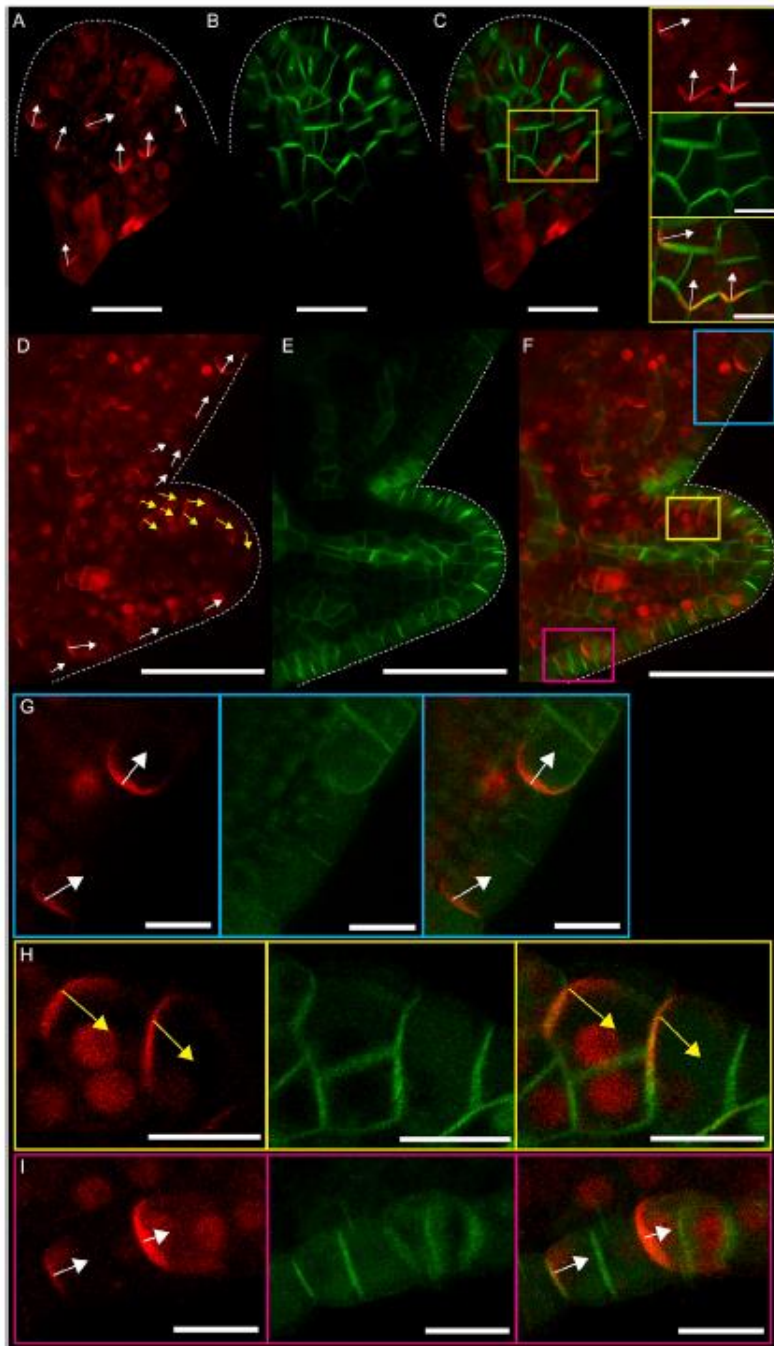


Figure 4. Ectopic mCherry-BASL Localizes to the Opposite End of Cells to PIN1 Mirroring Convergence and Divergence Points at Serrations

(A) Induced *35S::mCherry-BASL* in leaf primordium. Arrows indicate manually assigned BASL polarity based on curvature of the BASL crescent. (B) *PIN1::PIN1-GFP* in same primordium as (A). (C) *mCherry-BASL* and *PIN1-GFP* signals combined. Yellow box indicates magnified region of leaf. Scale bars are 20 μm in (A)–(C) and 10 μm in close-up regions of (C).

(D) Induced *35S::mCherry-BASL* at serration of leaf 5. Arrows are manually assigned, and yellow arrows highlight cells in which BASL is not proximally localized.

(E) *PIN1::PIN1-GFP* in same serration as shown in (D).

(F) *mCherry-BASL* and *PIN1-GFP* signals combined. Projections allow visualization of margin cells. Scale bars are 50 μm in (D)–(F).

(G–I) Magnified regions of serration in (F) in blue (G), yellow (H), and magenta (I) boxes, respectively. z slices were selected to allow visualization of cells due to curvature of serrations. *35S::mCherry-BASL* (left), *PIN1::PIN1-GFP* (middle), and combined signals (right). White dotted lines indicate leaf outline. Scale bars are 10 μm in (G)–(I).

See also Figure S3.

confirmed by calculating the angle between the BASL vector and the cell long axis (Figure S4D). Thus, the divergent pattern of the ectopic BASL polarity field could be a consequence of cell shape anisotropy and the way polarity is assigned to cells.

To test this possibility, we analyzed the subset of cells from the wild-type background, which had a nearly isotropic shape (Figure S4). Ectopic BASL vectors of these near-isotropic cells showed a preferential proximodistal orientation, including the splayed-out pattern in the proximal region of the lamina (Figures 3F and 3G). The leaf was subdivided into regions, and average vectors from the isotropic cells were calculated. This also showed the splaying out across the lamina (Figure 3H and Table S2). Thus, the observed divergent proximodistal polarity field is not dependent on cell shape anisotropy, consistent with cell polarity orientation

To evaluate the effect of such cell shape anisotropy on polarity measurements, we determined the orientation of the long axis of each cell (Figures 3B and 3C). This showed that, on average, cells were preferentially elongated in a divergent pattern like that of the axial component of the ectopic BASL polarity field (Figures 3B and 3D), and this correlation was also

being a guiding factor rather than consequence of oriented growth.

Ectopic BASL and PIN Mark a Common Polarity Field

The ectopic BASL polarity field resembles that for PIN1 localization at early stages of leaf development, except that whereas

BASL localizes proximally, PIN1 in epidermal cells localizes distally [25]. It is possible that both polarity markers are part of a common system, with PIN involved in early establishment of polarity and ectopic BASL revealing a polarity that is maintained through to later stages. To determine the relationship between PIN1 and BASL localization, we developed a line with inducible *35S::mCherry-BASL* also expressing *PIN1::PIN1-GFP* so that both polarity markers could be visualized in the same cells, though BASL signal was less uniform across the tissue than in the inducible *35S::GFP-BASL* line.

Induction of ectopic BASL in young leaf primordia showed that it localized to the proximal end of cells (Figure 4A) at a time when PIN1 was expressed. PIN1 had a broader distribution than ectopic BASL at this stage, making its polarity harder to assign (Figures 4B and 4C). Induction of ectopic BASL at later stages showed that co-expression with epidermal PIN1 expression was only observed in developing serrations (Figures 4D–4F). A region of reversed ectopic BASL polarity (yellow arrows) was seen at the distal edge of the serration, creating BASL convergence and divergence points (Figures 4D and 4F–4I). This BASL polarity pattern mirrors PIN1 convergence and divergence points previously described [5], with BASL localizing to the opposite end of the cell compared to that reported for PIN1. It has been shown that the PIN1 polarity pattern at serrations depends on a feedback loop involving auxin transport [5], suggesting that the polarity revealed by ectopic BASL is coupled to the same polarity-coordinating mechanism. To test the role of polar auxin transport in BASL localization, we grew seedlings on naphthylphthalamic acid (NPA), an auxin transport inhibitor, before inducing ectopic BASL. In NPA-treated seedlings, which exhibited root and leaf shape phenotypes [26, 27], ectopic BASL was still proximally localized (Figures S3H–S3M). The relationship between PIN, auxin, and ectopic BASL localization can vary, as ectopic BASL in roots has been shown to localize to the same end of cells as PIN or the opposite end, depending on the cell type and PIN family member [11].

Origin of the Polarity Field

The coordination of the proximodistal polarity field throughout the leaf epidermis could be accounted for by mechanical and/or chemical mechanisms [22, 24, 28–31]. The observation that mechanical stretching of a leaf can deflect the polarity field, as revealed by BRXL2 reorientation, indicates that tissue-wide mechanical forces can influence polarity [2]. However, the nature of polarity as a vector (with an arrow head) means that tissue stress, which has axially but not polarity, is not sufficient to establish the directional aspect of the vector field [32–34]; thus, a stress gradient would be required [24]. Alternatively, a biochemical mechanism, such as flux sensing or cell-cell coupling, may underlie the coordination of the polarity field [22, 35, 36]. Such a mechanism has the advantage of being uncoupled from the stresses generated through differential growth [34].

In addition to influencing growth, the polarity field may also influence patterning and differentiation (e.g., trichomes [3, 4], stomatal patterning [16]). Orientation of both BASL and BRXL2 in stomatal patterning exhibits proximodistal coordination, albeit much weaker than observed for the non-stomatal lineage cells in the *spch* mutant. Although polarity is critical for stomatal spacing in *Arabidopsis* [16, 37], it is unclear why proximodistal

coordination would be functionally important. It is possible that the coordination reflects evolutionary history rather than current function. Stomatal patterning mechanisms vary among plant species [11, 38–42]. By contrast, a proximodistal polarity field may be a highly conserved system for orienting tissue growth and transport [43–45]. Perhaps various elements of the proximodistal polarity system were co-opted for stomatal patterning in different plant lineages. For the lineage leading to *Arabidopsis*, co-option may have led to a polarity-switching mechanism and the evolution of BASL. This hypothesis would account for why BASL cross-reacts with the proximal address when ectopically expressed. Other plant lineages, such as grasses, which exhibit strong proximodistal coordination in stomatal patterning [38, 46], might represent different ways of co-opting elements of a fundamental proximodistal field.

Thus, the proximodistal field described here may have provided key elements that were co-opted during evolution for controlling patterns of differentiation and spacing. In addition, it may provide a conserved system for orienting growth in planar plant organs, similar to equivalent systems described for animal development [1].

STAR★METHODS

Detailed methods are provided in the online version of this paper and include the following:

- KEY RESOURCES TABLE
- CONTACT FOR REAGENT AND RESOURCE SHARING
- EXPERIMENTAL MODEL AND SUBJECT DETAILS
 - Growth conditions
 - Genetic material
- METHOD DETAILS
 - Construction of transgenic plants
 - Propidium iodide staining
 - Confocal microscopy
 - Oryzalin treatment
 - NPA treatment
- QUANTIFICATION AND STATISTICAL ANALYSIS
 - Cells-from-leaves and cells-from-leaves-tagger software
 - sampleArrows8 software and cellLongAxisCorr7 software
 - Additional image analysis
- DATA AND SOFTWARE AVAILABILITY
- ADDITIONAL RESOURCES

SUPPLEMENTAL INFORMATION

Supplemental Information includes four figures and two tables and can be found with this article online at <https://doi.org/10.1016/j.cub.2018.06.019>.

ACKNOWLEDGMENTS

We thank Desmond Bradley, Beatriz Gonçalves, Christopher Whitewoods, Anabel Whibley, and Karen Lee for helpful discussions and comments on the manuscript and Christine Faulkner for comments, suggestions, and support. Thanks to Dominique Bergmann for providing plant lines, vectors, and helpful comments on the manuscript. We thank Florent Pantin, Samantha Fox, Xana Rebocho, Tom Lawrenson, and Yoselin Benitez-Alfonso for help with making the heat shock destination vector. Thanks to JIC Bioimaging, particularly Grant

Calder, and horticultural services for technical support. This work was supported by BBSRC (BB/L008920/1, BB/J004588/1, BBS/E/J000PR9787, and BB/P013511/1) and the ERC grant Camomorph (ERC-2012-AdG-323028). C.M. was supported by a PhD studentship from the John Innes Foundation.

AUTHOR CONTRIBUTIONS

C.M., J.C., and E.C. conceived and designed the study. C.M. and J.C. acquired data and developed resources. C.M., J.L.N., and T.S.G.O. analyzed the data. C.M., J.L.N., J.C., and E.C. interpreted the data. J.L.N., T.S.G.O., and M.H. developed software. J.C. and E.C. provided supervision. C.M. and E.C. wrote the manuscript. All authors reviewed and revised the manuscript.

DECLARATION OF INTERESTS

The authors declare no competing interests.

Received: January 18, 2018

Revised: May 2, 2018

Accepted: June 11, 2018

Published: August 9, 2018

REFERENCES

- Goodrich, L.V., and Strutt, D. (2011). Principles of planar polarity in animal development. *Development* 138, 1877–1892.
- Bringmann, M., and Bergmann, D.C. (2017). Tissue-wide Mechanical Forces Influence the Polarity of Stomatal Stem Cells in Arabidopsis. *Curr. Biol.* 27, 877–883.
- Hülkamp, M., Misra, S., and Jürgens, G. (1994). Genetic dissection of trichome cell development in Arabidopsis. *Cell* 76, 555–566.
- Bouyer, D., Kirik, V., and Hülkamp, M. (2001). Cell polarity in Arabidopsis trichomes. *Semin. Cell Dev. Biol.* 12, 353–356.
- Bilsborough, G.D., Runions, A., Barkoulas, M., Jenkins, H.W., Hasson, A., Galinha, C., Laufs, P., Hay, A., Prusinkiewicz, P., and Tsaliantis, M. (2011). Model for the regulation of Arabidopsis thaliana leaf margin development. *Proc. Natl. Acad. Sci. USA* 108, 3424–3429.
- Guenot, B., Bayer, E., Kierzkowski, D., Smith, R.S., Mandel, T., Žádníková, P., Benková, E., and Kuhlemeier, C. (2012). Pin1-independent leaf initiation in Arabidopsis. *Plant Physiol.* 159, 1501–1510.
- Richardson, A.E., Rebocho, A.B., and Coen, E.S. (2016). Ectopic KNOX Expression Affects Plant Development by Altering Tissue Cell Polarity and Identity. *Plant Cell* 28, 2079–2096.
- Kuchen, E.E., Fox, S., de Reuille, P.B., Kennaway, R., Bensmihen, S., Avondo, J., Calder, G.M., Southam, P., Robinson, S., Bangham, A., and Coen, E. (2012). Generation of leaf shape through early patterns of growth and tissue polarity. *Science* 335, 1092–1096.
- Lawrence, P.A., Struhl, G., and Casal, J. (2007). Planar cell polarity: one or two pathways? *Nat. Rev. Genet.* 8, 555–563.
- Krecek, P., Skupa, P., Libus, J., Naramoto, S., Tejos, R., Friml, J., and Zazimalová, E. (2009). The PIN-FORMED (PIN) protein family of auxin transporters. *Genome Biol.* 10, 249.
- Dong, J., MacAlister, C.A., and Bergmann, D.C. (2009). BASL controls asymmetric cell division in Arabidopsis. *Cell* 137, 1320–1330.
- Pillitteri, L.J., Peterson, K.M., Horst, R.J., and Torii, K.U. (2011). Molecular profiling of stomatal meristemoids reveals new component of asymmetric cell division and commonalities among stem cell populations in Arabidopsis. *Plant Cell* 23, 3260–3275.
- Truemit, E., Bauby, H., Belcram, K., Barthémy, J., and Palauqui, J.-C. (2012). OCTOPUS, a polarly localised membrane-associated protein, regulates phloem differentiation entry in Arabidopsis thaliana. *Development* 139, 1306–1315.
- Shimotombo, A., Sotta, N., Sato, T., De Ruvo, M., Marée, A.F.M., Grieneisen, V.A., and Fujiwara, T. (2015). Mathematical modeling and experimental validation of the spatial distribution of boron in the root of Arabidopsis thaliana identify high boron accumulation in the tip and predict a distinct root tip uptake function. *Plant Cell Physiol.* 56, 620–630.
- Abley, K., Sauret-Güeto, S., Marée, A.F.M., and Coen, E. (2016). Formation of polarity convergences underlying shoot outgrowths. *eLife* 5, 1–60.
- Robinson, S., Barbier de Reuille, P., Chan, J., Bergmann, D., Prusinkiewicz, P., and Coen, E. (2011). Generation of spatial patterns through cell polarity switching. *Science* 333, 1436–1440.
- Gallois, J.L., Woodward, C., Reddy, G.V., and Sablowski, R. (2002). Combined SHOOT MERISTEMLESS and WUSCHEL trigger ectopic organogenesis in Arabidopsis. *Development* 129, 3207–3217.
- Pillitteri, L.J., Sloan, D.B., Bogenschutz, N.L., and Torii, K.U. (2007). Termination of asymmetric cell division and differentiation of stomata. *Nature* 445, 501–505.
- Fu, Y., Gu, Y., Zheng, Z., Wasteneys, G., and Yang, Z. (2005). Arabidopsis interdigitating cell growth requires two antagonistic pathways with opposing action on cell morphogenesis. *Cell* 120, 687–700.
- Armour, W.J., Barton, D.A., Law, A.M.K., and Overall, R.L. (2015). Differential Growth in Periclinal and Anticlinal Walls during Lobe Formation in Arabidopsis Cotyledon Pavement Cells. *Plant Cell* 27, 2484–2500.
- Chen, J., Wang, F., Zheng, S., Xu, T., and Yang, Z. (2015). Pavement cells: a model system for non-transcriptional auxin signalling and crosstalks. *J. Exp. Bot.* 66, 4957–4970.
- Abley, K., De Reuille, P.B., Strutt, D., Bangham, A., Prusinkiewicz, P., Marée, A.F.M., Grieneisen, V.A., and Coen, E. (2013). An intracellular partitioning-based framework for tissue cell polarity in plants and animals. *Development* 140, 2061–2074.
- Asnacios, A., and Hamant, O. (2012). The mechanics behind cell polarity. *Trends Cell Biol.* 22, 584–591.
- Heisler, M.G., Hamant, O., Krupinski, P., Uyttewaal, M., Ohno, C., Jönsson, H., Traas, J., and Meyerowitz, E.M. (2010). Alignment between PIN1 polarity and microtubule orientation in the shoot apical meristem reveals a tight coupling between morphogenesis and auxin transport. *PLoS Biol.* 8, e1000516.
- Scarpella, E., Marcos, D., Friml, J., and Berleth, T. (2006). Control of leaf vascular patterning by polar auxin transport. *Genes Dev.* 20, 1015–1027.
- Hay, A., Barkoulas, M., and Tsaliantis, M. (2006). ASYMMETRIC LEAVES1 and auxin activities converge to repress BREVIPEDICELLUS expression and promote leaf development in Arabidopsis. *Development* 133, 3955–3961.
- Casimiro, I., Marchant, A., Bhalerao, R.P., Beekman, T., Dhooge, S., Swarup, R., Graham, N., Inzé, D., Sandberg, G., Casero, P.J., and Bennett, M. (2001). Auxin transport promotes Arabidopsis lateral root initiation. *Plant Cell* 13, 843–852.
- Hervieux, N., Dumond, M., Sapala, A., Routier-Kierzkowska, A.-L., Kierzkowski, D., Roeder, A.H.K., Smith, R.S., Boudsoud, A., and Hamant, O. (2016). A Mechanical Feedback Restricts Sepal Growth and Shape in Arabidopsis. *Curr. Biol.* 26, 1–10.
- Sassi, M., and Traas, J. (2015). When biochemistry meets mechanics: a systems view of growth control in plants. *Curr. Opin. Plant Biol.* 28, 137–143.
- Whiteheads, C.D., and Coen, E. (2017). Growth and Development of Three-Dimensional Plant Form. *Curr. Biol.* 27, R910–R918.
- Bennett, T., Hines, G., and Leyser, O. (2014). Canalization: what the flux? *Trends Genet.* 30, 41–48.
- Goriely, A. (2017). *The Mathematics and Mechanics of Biological Growth* (New York, NY: Springer).
- Héjnowicz, Z., and Romberger, J.A. (1984). Growth tensor of plant organs. *J. Theor. Biol.* 110, 93–114.
- Coen, E., Kennaway, R., and Whiteheads, C. (2017). On genes and form. *Development* 144, 4203–4213.

35. Mitchison, G.J. (1980). A Model for Vein Formation in Higher Plants. *Proc. R. Soc. Lond. B Biol. Sci.* 207, 79–109.
36. Rolland-Lagan, A.-G., and Prusinkiewicz, P. (2005). Reviewing models of auxin canalization in the context of leaf vein pattern formation in *Arabidopsis*. *Plant J.* 44, 854–865.
37. Lau, O.S., and Bergmann, D.C. (2012). Stomatal development: a plant's perspective on cell polarity, cell fate transitions and intercellular communication. *Development* 139, 3683–3692.
38. Raissig, M.T., Abrash, E., Bettadapur, A., Vogel, J.P., and Bergmann, D.C. (2016). Grasses use an alternatively wired bHLH transcription factor network to establish stomatal identity. *Proc. Natl. Acad. Sci. USA* 113, 8326–8331.
39. Cartwright, H.N., Humphries, J.A., and Smith, L.G. (2009). PAN1: a receptor-like protein that promotes polarization of an asymmetric cell division in maize. *Science* 323, 649–651.
40. Vatén, A., and Bergmann, D.C. (2012). Mechanisms of stomatal development: an evolutionary view. *Evodevo* 3, 11.
41. Chater, C.C.C., Caine, R.S., Fleming, A.J., and Gray, J.E. (2017). Origins and Evolution of Stomatal Development. *Plant Physiol.* 174, 624–638.
42. Rudall, P.J., Chen, E.D., and Cullen, E. (2017). Evolution and development of monocot stomata. *Am. J. Bot.* 104, 1122–1141.
43. Nelson, W.J. (2003). Adaptation of core mechanisms to generate cell polarity. *Nature* 422, 766–774.
44. Strutt, H., and Strutt, D. (2009). Asymmetric localisation of planar polarity proteins: Mechanisms and consequences. *Semin. Cell Dev. Biol.* 20, 957–963.
45. Meinhardt, H. (2007). Computational modelling of epithelial patterning. *Curr. Opin. Genet. Dev.* 17, 272–280.
46. Facette, M.R., and Smith, L.G. (2012). Division polarity in developing stomata. *Curr. Opin. Plant Biol.* 15, 585–592.
47. Nelson, B.K., Cai, X., and Nebenführ, A. (2007). A multicolored set of in vivo organelle markers for co-localization studies in *Arabidopsis* and other plants. *Plant J.* 51, 1126–1136.
48. MacAlister, C.A., Ohashi-Ito, K., and Bergmann, D.C. (2007). Transcription factor control of asymmetric cell divisions that establish the stomatal lineage. *Nature* 445, 537–540.
49. Benková, E., Michniewicz, M., Sauer, M., Teichmann, T., Seifertová, D., Jürgens, G., and Friml, J. (2003). Local, efflux-dependent auxin gradients as a common module for plant organ formation. *Cell* 115, 591–602.
50. Ueda, K., Matsuyama, T., and Hashimoto, T. (1999). Visualization of microtubules in living cells of transgenic *Arabidopsis thaliana*. *Protoplasma* 206, 201–206.
51. Wachsmann, G., Heidstra, R., and Scheres, B. (2011). Distinct cell-autonomous functions of RETINOBLASTOMA-RELATED in *Arabidopsis* stem cells revealed by the Brother of Rainbow clonal analysis system. *Plant Cell* 23, 2581–2591.
52. Karimi, M., De Meyer, B., and Hilson, P. (2005). Modular cloning in plant cells. *Trends Plant Sci.* 10, 103–105.
53. Clough, S.J., and Bent, A.F. (1998). Floral dip: a simplified method for *Agrobacterium*-mediated transformation of *Arabidopsis thaliana*. *Plant J.* 16, 735–743.
54. Calder, G., Hindle, C., Chan, J., and Shaw, P. (2015). An optical imaging chamber for viewing living plant cells and tissues at high resolution for extended periods. *Plant Methods* 11, 22.
55. Chan, J., Calder, G., Fox, S., and Lloyd, C. (2007). Cortical microtubule arrays undergo rotary movements in *Arabidopsis* hypocotyl epidermal cells. *Nat. Cell Biol.* 9, 171–175.
56. Olsson, T.S.G., and Hartley, M. (2016). jicbioimage: a tool for automated and reproducible bioimage analysis. *PeerJ* 4, e2674.
57. Schindelin, J., Arganda-Carreras, I., Frise, E., Kaynig, V., Longair, M., Pietzsch, T., Preibisch, S., Rueden, C., Saalfeld, S., Schmid, B., et al. (2012). Fiji: an open-source platform for biological-image analysis. *Nat. Methods* 9, 676–682.

STAR★METHODS

KEY RESOURCES TABLE

REAGENT or RESOURCE	SOURCE	IDENTIFIER
Chemicals, Peptides, and Recombinant Proteins		
Propidium Iodide	Sigma-Aldrich	Cat# P4170
Spe I	Sigma-Aldrich	11008943001
BspEI	New England Biolabs	Cat# R0540S
codB-resistant one-shot <i>E. coli</i>	ThermoFisher Scientific	Cat# A10460
Difco agar	Becton & Dickinson	Cat# 214030
Oryzalin	Sigma-Aldrich	Cat# 36182
N-1-naphthylphthalamic acid (NPA)	ChemService	N-12507
Critical Commercial Assays		
iDNA genetics copy number analysis	iDNA genetics	N/A
Experimental Models: Organisms/Strains		
Heat-shock inducible BASL (35S::GFP-BASL)	This paper	N/A
BASL::GFP-BASL	[11]	N/A
RFP-plasma membrane (pm-rb)	[47]	CD3-1008
RFP-plasma membrane with inducible 35S::GFP-BASL	This paper	N/A
<i>spch</i> mutant (<i>spch-1</i>)	[48]	N/A
<i>spch</i> with inducible BASL (35S::GFP-BASL)	This paper	N/A
HS::Cre	[17]	N/A
PIN1::PIN1-GFP	[49]	N/A
Heat-shock inducible 35S::mCherry-BASL with PIN1::PIN1-GFP	This paper	N/A
35S::TUA6-GFP	[50]	N/A
Oligonucleotides		
F_BOB_lox_speI (GGGACTAGTATCGCGGCCGCTTCGAAA)	This paper	N/A
R_BOB_lox_N (CTATACGAAGTTATACGCGTCTGT)	This paper	N/A
R3_BOB_lox_EcoRV (GGGATATCATAAAGTTTGTATAAAGTATCCTATACGAAGTTATACGCGTCTG)	This paper	N/A
Recombinant DNA		
pBOB vector	[51]	N/A
TOPO4 vector	Invitrogen	N/A
pB7WGC2 vector	[52] (VIB Gent)	N/A
GFP-BASL entry clone	[11]	N/A
Destination vector with lox-HDEL: CyPET:NOS-Terminator-lox (Active blue destination vector)	This paper	N/A
Software and Algorithms		
cellfromleaves	This paper	GitHub; https://github.com/JIC-Image-Analysis/cells-from-leaves
cellsfromleaves tagger	This paper	GitHub; https://github.com/JIC-Image-Analysis/cells-from-leaves-tagger
sampleArrows8	This paper	GitHub; https://github.com/JIC-Image-Analysis/cells-from-leaves/tree/master/matlab_scripts
cellLongAxisCorr7	This paper	GitHub; https://github.com/JIC-Image-Analysis/cells-from-leaves/tree/master/matlab_scripts
VoViewer		http://cmpdartsvr3.cmp.uea.ac.uk/wiki/BanghamLab/index.php/Software#Viewing_and_measuring_volume_images:_VoViewer

CONTACT FOR REAGENT AND RESOURCE SHARING

Further information and requests for resources and reagents should be directed to and will be fulfilled by the Lead Contact, Enrico Coen (enrico.coen@jic.ac.uk).

EXPERIMENTAL MODEL AND SUBJECT DETAILS**Growth conditions**

Arabidopsis plants were grown on plates containing MS media (0.441% Murashige & Skoog including vitamins, 1% (w/v) glucose, 0.05% (w/v) MES, 1% Difco agar, pH to 5.7) and relevant antibiotic selection. Seeds were gas or surface sterilized and stratified in the dark at 4°C for 3 days, then grown at 20°C in long day conditions (16 hours light, 8 hours dark). Leaves were taken from plants up to 9 days after stratification for imaging and analysis.

Genetic material

The transgenic lines *spch-1* [48], *HS::Cre* [17], *BASL::BASL-GFP* [11], *RFP-PM* [47], *PIN1::PIN1-GFP* [49] and *35S::TUA6-GFP* [50] are in the Col-0 background.

METHOD DETAILS**Construction of transgenic plants**

We used Gateway cloning to construct heat-shock inducible *35S::GFP-BASL* line which required a destination vector and an entry vector. We made a destination vector (which we refer to Active Blue destination vector) containing a 35S promoter in front of a CyPET:HDEL fluorescent marker and a Nos terminator flanked by lox sites. These lox sites will later allow heat-shock recombination to remove the fluorescent marker so that the 35S promoter drives a downstream gene of interest.

The Active Blue destination vector was made using a pre-existing Gateway vector, pB7WGC [52] and the pBOB [51] vector. The procedure involved 2 steps. In the first step, a 1175 bp fragment containing lox-HDEL: CyPET: NOS-Terminator-lox was cloned from pBOB and flanked with SpeI and EcoRV sites using a 2-step PCR, involving the primers F_BOB_lox_speI and R_BOB_lox_N, then primers F_BOB_lox_speI and R3_BOB_lox_EcoRV. The PCR product was then cloned into TOPO4. In the second step, the pB7WGC2 vector was digested with SpeI and BspEI, to excise a 1175 bp fragment containing ECFP, and replaced with the fragment cloned from pBOB vector (cut out from the TOPO4 vector using SpeI and BspEI). The ligation product was transformed into *ccdB*-resistant one-shot *E. coli*.

To introduce GFP-BASL into the destination vector, an LR reaction (Invitrogen) was carried out using the Active Blue destination vector and an entry clone containing GFP-BASL [11].

For transformation of *Arabidopsis* plants, *Agrobacterium tumefaciens* strain GV3101 and floral dip method were used [53] to dip into *HS::Cre* [17] containing plants. Three independent lines were obtained showing the same pattern. The line used is a single copy, single insert line (iDNA genetics).

The inducible *35S::BASL-GFP* line was crossed to the heterozygous *spch-1* mutant plants and offspring containing *spch-1* and inducible *35S::BASL-GFP* were selected by phenotype and growing on selective plates (Basta for *35S::BASL-GFP*, Kanamycin for *HS::Cre*). The inducible *35S::BASL-GFP* line was crossed to the *RFP-PM* line [47] and offspring containing *RFP-PM* and inducible *35S::BASL-GFP* were selected by growing on selective plates and screening for RFP.

To make the line with inducible *35S::mCherry-BASL* and *PIN1::PIN1-GFP*, we generated a construct containing inducible *35S::mCherry-BASL* and *HS::Cre* using golden gate cloning and dipped [53] this into *PIN1::PIN1-GFP* [49] containing plants. The line used contains 2 copies (iDNA genetics). The *35S::loxmCherry-BASLloxCyPET-HSP18::CRE-35S::Basta-35S::CyPET-RC12A* (called inducible *35S::mCherry-BASL* for simplicity) construct was created by Golden Gate cloning in the vector pAGM4723 (Addgene #48015) as described by Weber et al. (2011). Level 0 modules were domesticated to remove BsaI, BpI and DraIII restriction sites and synthesized synthetically. To generate the lox-flanked mCherry Level 1 module we adapted the standard Golden Gate protocol to incorporate an additional assembly step, termed Level 0.5. Here the vector backbone EC10161 is opened by the enzyme Esp3I to allow the insertion of Level 0 modules cut by BsaI, just as for standard Level 1 cloning. This generates loxP flanked modules in the 'U' position suitable for use in subsequent Level 1 assembly. Sequences to be used in loxP-flanked modules were domesticated to be free of Esp3I sites in addition to BsaI, BpI and DraIII recognition sites. Plasmid maps are available on request.

Propidium iodide staining

To stain leaves with propidium iodide, leaves were submerged in a 2.5 µg/ml propidium iodide solution (PI - Sigma) for at least 15 minutes before imaging.

Confocal microscopy

For confocal imaging, leaves (typically first true leaf other than for serrations) were placed in water under a coverslip, or in the optical imaging chamber [54]. Imaging was performed using a x10 or x20 dry lens, or x40 oil lens, on a Leica SP5 confocal microscope equipped with Leica HyD Hybrid detectors, or a Zeiss 780. For imaging GFP, argon ion (488 nm) excitation laser was used, collected

at 495–530 nm. For PI, mCherry and RFP, 561 nm excitation was used, collected at 625–690 nm for PI, 575–630 for RFP and 600–620 nm for mCherry. Leaves were staged according to leaf width and were typically imaged 48-hours after heat-shock. Seedlings were typically heat-shocked for 20 minutes to induce BASL across the entire lamina, and 3 mins to induce sectors.

To image *35S::GFP-BASL* appearing after induction, 7 day old seedlings were heat-shocked for 20 mins and placed in an imaging chamber with media as described in [55]. Leaves were imaged every hour using a Zeiss 780 confocal microscope, with the settings described above.

Oryzalin treatment

Oryzalin was added to 6-day old seedlings (*35S::GFP-BASL* line described above and *35S::GFP-TUA6* as control line) at a concentration of 20 μ M. Seedlings expressing *35S::TUA6-GFP* have previously been described [50]. *35S::TUA6-GFP* seedlings confirmed microtubules had depolymerized after 4 hours and seedlings were heat-shocked to induce BASL expression. Plants were imaged 48 hours after heat-shock, with *35S::GFP-TUA6* confirming the absence of microtubules.

NPA treatment

35S::GFP-BASL seedlings were grown on media containing 100 μ M NPA, or an equivalent concentration of DMSO. Seedlings were heat-shocked 2DAS and leaves imaged 3 days later. Propidium iodide staining (described above) was used to visualize cell outlines.

QUANTIFICATION AND STATISTICAL ANALYSIS

Cells-from-leaves and cells-from-leaves-tagger software

For assigning BASL vectors, Python software was developed using *jicbioimage* [56]. It used the cell outline channel (either plasma-membrane marker or PI stain) from the confocal stack to make a projection of the leaf surface. The leaf surface projection was used to reduce noise by only extracting signal from the volume occupied by the leaf. The cell outline channel extracted from the leaf surface was then used as input to the watershed algorithm. Leaf-specific parameters allowed the surface and segmentation to be customized according to intensity and quality of image. The centroid for each cell was calculated. BASL signal was also extracted from the cell surface.

To avoid bias arising from knowledge of the orientation and position of a cell within the context of the whole leaf, each segmented cell was presented to the user in isolation, randomly rotated in one of four orientations (0, 90, 180, 270 degrees). For each cell the user then selected a point in the middle of any visible BASL crescent, or chose to skip a cell if there was a complication (i.e., if the signal was not easy to identify, or the cell segmentation was incorrect). For a sample leaf image, out of 162 cell assignments of BASL, 157 were based on three-way junctions, and 5 were based on concavity of the BASL signal. The tool produced a directory of JSON files and corresponding image files, recording the BASL orientation in separate files for each cell, along with an image of the cell segmentation. Lastly, BASL vectors were transformed back into the coordinate system of the whole leaf, and written out to a CSV file along with the coordinates of each cell centroid.

sampleArrows8 software and cellLongAxisCorr7 software

We developed two MATLAB scripts, one to allow us to quantify the BASL vector field (*cellLongAxisCorr7.m*) and one to visualize it in a more informative way (*sampleArrows8.m*).

One script developed, *sampleArrows8*, is for visualizing BASL vectors on the leaf, and down-sampling them. This script uses a leaf image and .csv file of BASL vectors (produced by 'cells from leaves'). The user identifies the leaf midline which is used to rotate the leaf image and BASL vectors to allow the image to be vertically oriented. The script contains various processing and display options, but it is frequently used to display the original BASL arrows on the leaf, colored by orientation with respect to the leaf midvein. The color of each arrow is determined by a color map, where 0 degrees represents the proximodistal orientation.

There can be a lot of BASL vectors on a leaf, with some areas having a very high density of points. BASL vectors can therefore be down-sampled to reduce the total number of vectors displayed and to give a more even spread of BASL vectors across the leaf. Down-sampling uses a triangular grid of points placed over the leaf. For each vertex of the grid, vectors within the distance *Maxdist* are averaged. A parameter, *neighborThreshold*, ensures that down-sampled BASL vectors are only displayed for samples that exceed the threshold number of BASL vectors.

This script can also be applied to cell orientations. This is achieved by gathering cell orientations within a certain radius, normalizing and superimposing them onto the same axis, and then performing principle component analysis (PCA) on that cloud of points.

We also developed a script named *cellLongAxisCorr7*, which quantifies the BASL vector field. This script calculates various angles: orientation of cell axis, angle between BASL vector and its cell axis, and angle between BASL vector and leaf midvein axis. This script uses an image of the leaf and the directory of JSON files to rotate the cells back to their original orientation and cell masks are derived, allowing cell eccentricity (ratio of the distance between the foci of the ellipse fitted to a cell and its major axis length), centroid and orientation of the long axis of the cells to be determined.

For each cell, three angle measurements are made: the angle between the BASL vector (from the JSON files) and the cell long axis, angle between the BASL vector and the leaf midline axis (specified by the user), and the angle between the cell long axis and the leaf midline axis. Subsets of data can be selected by specifying lower and upper threshold values in the script parameters (for cell eccentricity and orientation relative to the leaf). The script displays the orientation information as histograms and also writes it out to



CSV files for further analysis. To select the near-isotropic cells, we first calculated eccentricity of the segmented cells (cell eccentricity is the ratio of the distance between the foci of the ellipse fitted to a cell and its major axis length). Cells with an eccentricity of less than 0.6 were considered near-isotropic.

Further documentation is found in both `sampleArrows8.m` and `cellLongAxisCorr7.m`. These scripts also contain a detailed explanation of each of the input parameters.

Additional image analysis

BASL crescent length and cell perimeter were calculated by clicking round the BASL signal and cell outline using Fiji [57] measure tool for cells of different sizes. To determine average BASL vector orientations for near isotropic cells in regions of the leaf, `cellLongAxisCorr7` was used with a maximum eccentricity value of 0.6, and vectors were visualized on the leaf using `sampleArrows8`. The leaf was then subdivided into 9 regions and vectors measured in each region measured using Fiji angle tool.

Statistical comparison of BASL vector distributions between genotypes, was performed using chi-square tests (df = 1, p values less than 0.01 were considered significant), comparing frequency of BASL vectors within or outside the range of -80° to 80° , in pairwise tests.

For z stacks of leaves expressing *PIN1::PIN-GFP* and *35S::mCherry-BASL*, images were rendered in 3D using Volviewer. For serrations, Fiji was used to create maximum projections for visualization. Specific ranges of z-slices were used to allow visualization of specific cells.

DATA AND SOFTWARE AVAILABILITY

The custom code that implements the segmentation and random orientation pipeline (`cells-from-leaves`) is available at: <https://github.com/JIC-Image-Analysis/cells-from-leaves>.

The tool for visualizing cell segmentations and selection of BASL signal in the cell (`cells-from-leaves-tagger`) is available at: <https://github.com/JIC-Image-Analysis/cells-from-leaves-tagger>.

MATLAB software for visualization of vectors and angle calculation available at https://github.com/JIC-Image-Analysis/cells-from-leaves/tree/master/matlab_scripts.

VolViewer available for download from http://cmpdartsvr3.cmp.uea.ac.uk/wiki/BanghamLab/index.php/Software#Viewing_and_measuring_volume_images:_VolViewer.

ADDITIONAL RESOURCES

Plasmid maps for lines generated and raw data for leaf images available on request.

8 Abbreviations

BASL	BREAKING OF ASYMMETRY IN THE STOMATAL LINEAGE
BRXL2	BREVIS RADIX LIKE 2
BY-2	Bright Yellow 2
DAS	Days after stratification
DMSO	Dimethyl sulfoxide
DTT	Dithiothreitol
ENSA	Engineering Nitrogen Symbiosis for Africa
FMS	Fukuda, Murashige and Skoog
GFP	Green Fluorescent Protein
GPT Framework	Growing Polarised Tissue Framework
iBAQ	Intensity-based Absolute Quantification
IP	Immunoprecipitation
IP-MS	Immunoprecipitation with Mass-spectrometry
JIC	John Innes Centre
L0	Level 0
L1	Level 1
L2	Level 2
LB	Lysogeny broth
LYK	Lysin-motif RLK
mb-SUS	Mating-based Split Ubiquitin System
MIND	Membrane Interactome Database
MS	Murashige and Skoog
NPA	N-1-Naphthylphthalamic
OD	Optical Density
PI	Propidium iodide
PIN	PIN-FORMED
PM	Plasma membrane
PMSF	Phenylmethylsulfonyl fluoride
RLK	Receptor-like Kinase
ROP	Rho of Plants
SOC	Super Optimal broth with Catabolite
SOK	SOSEKI
WT	Wild-type

9 References

- Abas, L., Benjamins, R., Malenica, N., Paciorek, T., Wiśniewska, J., Moulinier–Anzola, J. C., Sieberer, T., Friml, J. and Luschnig, C. (2006). Intracellular trafficking and proteolysis of the *Arabidopsis* auxin-efflux facilitator PIN2 are involved in root gravitropism. *Nat. Cell Biol.* 8, 249–256.
- Abley, K. (2014). Cellular-level mechanisms of polarity and their role in plant growth. PhD thesis, University of East Anglia.
- Abley, K., De Reuille, P. B., Strutt, D., Bangham, A., Prusinkiewicz, P., Marée, A. F. M., Grieneisen, V. A. and Coen, E. (2013). An intracellular partitioning-based framework for tissue cell polarity in plants and animals. *Development* 140, 2061–2074.
- Abley, K., Sauret-Güeto, S., Marée, A. F. M. and Coen, E. (2016). Formation of polarity convergences underlying shoot outgrowths. *Elife* 5, 1–60.
- Aeschbacher, R. A., Hauser, M. T., Feldmann, K. A. and Benfey, P. N. (1995). The *SABRE* gene is required for normal cell expansion in *Arabidopsis*. *Genes Dev.* 9, 330–340.
- Altschuler, S. J., Angenent, S. B., Wang, Y. and Wu, L. F. (2008). On the spontaneous emergence of cell polarity. 454, 886–890.
- Ambrose, J. C. and Wasteneys, G. O. (2008). CLASP modulates microtubule-cortex interaction during self-organization of acentrosomal microtubules. *Mol. Biol. Cell* 19, 4730–4737.
- Ambrose, J. C., Shoji, T., Kotzer, A. M., Pighin, J. A. and Wasteneys, G. O. (2007). The *Arabidopsis* *CLASP* gene encodes a microtubule-associated protein involved in cell expansion and division. *Plant Cell* 19, 2763–2775.
- Andriankaja, M., Dhondt, S., De Bodt, S., Vanhaeren, H., Coppens, F., De Milde, L., Mühlenbock, P., Skirycz, A., Gonzalez, N., Beemster, G. T. S., et al. (2012). Exit from Proliferation during Leaf Development in *Arabidopsis thaliana*: A Not-So-Gradual Process. *Dev. Cell* 22, 64–78.
- Asnacios, A. and Hamant, O. (2012). The mechanics behind cell polarity. *Trends Cell Biol* 22, 584–591.

References

- Avila, J. R., Lee, J. S. and Torii, K. U. (2015). Co-Immunoprecipitation of Membrane-Bound Receptors. *Arab. B.* 13, e0180.
- Axelrod, J. D. and Bergmann, D. C. (2014). Coordinating cell polarity: heading in the right direction? *Development* 141, 3298–3302.
- Barbier de Reuille, P., Routier-Kierzkowska, A.-L., Kierzkowski, D., Bassel, G. W., Schüpbach, T., Tauriello, G., Bajpai, N., Strauss, S., Weber, A., Kiss, A., et al. (2015). MorphoGraphX: A platform for quantifying morphogenesis in 4D. *Elife* 4, e05864.
- Baskin, T. I. (2001). On the alignment of cellulose microfibrils by cortical microtubules: A review and a model. *Protoplasma* 215, 150–171.
- Baskin, T. I. (2005). Anisotropic expansion of the plant cell wall. *Annu. Rev. Cell Dev. Biol.* 21, 203–222.
- Basu, D. and Haswell, E. S. (2017). Plant mechanosensitive ion channels: an ocean of possibilities. *Curr. Opin. Plant Biol.* 40, 43–48.
- Bayer, E. M., Smith, R. S., Mandel, T., Nakayama, N., Sauer, M., Prusinkiewicz, P. and Kuhlemeier, C. (2009). Integration of transport-based models for phyllotaxis and midvein formation. *Genes Dev.* 23, 373–384.
- Bencivenga, S., Serrano-Mislata, A., Bush, M., Fox, S. and Sablowski, R. (2016). Control of oriented tissue growth through repression of organ boundary genes promotes stem morphogenesis. *Dev. Cell* 39, 198-208.
- Benková, E., Michniewicz, M., Sauer, M., Teichmann, T., Seifertová, D., Jürgens, G. and Friml, J. (2003). Local, efflux-dependent auxin gradients as a common module for plant organ formation. *Cell* 115, 591–602.
- Bennett, T., Hines, G. and Leyser, O. (2014). Canalization: what the flux? *Trends Genet.* 30, 41–48.
- Berens, P. (2009). CircStat : A *MATLAB* Toolbox for Circular Statistics. *J. Stat. Softw.* 31, 10.
- Bhatia, N., Bozorg, B., Larsson, A., Ohno, C., Jönsson, H. and Heisler, M. G. (2016). Auxin Acts through MONOPTEROS to Regulate Plant Cell Polarity and Pattern Phyllotaxis. *Curr. Biol.* 26, 3202–3208.

- Bichet, A., Desnos, T., Turner, S., Grandjean, O. and Höfte, H. (2001). *BOTERO1* is required for normal orientation of cortical microtubules and anisotropic cell expansion in *Arabidopsis*. *Plant J.* 25, 137–148.
- Bilsborough, G. D., Runions, A., Barkoulas, M., Jenkins, H. W., Hasson, A., Galinha, C., Laufs, P., Hay, A., Prusinkiewicz, P. and Tsiantis, M. (2011). Model for the regulation of *Arabidopsis thaliana* leaf margin development. *Proc. Natl. Acad. Sci. U. S. A.* 108, 3424–3429.
- Biot, E., Cortizo, M., Burguet, J., Kiss, A., Oughou, M., Maugarny-Calès, A., Gonçalves, B., Adroher, B., Andrey, P., Boudaoud, A., et al. (2016). Multiscale quantification of morphodynamics: MorphoLeaf, software for 2-D shape analysis. *Development* 143, 3417–3428.
- Bosch, M., Cheung, A. Y. and Hepler, P. K. (2005). Pectin methylesterase, a regulator of pollen tube growth. *Plant Physiol.* 138, 1334–1346.
- Boutté, Y., Crosnier, M.-T., Carraro, N., Traas, J. and Satiat-Jeunemaitre, B. (2005). The plasma membrane recycling pathway and cell polarity in plants: studies on PIN proteins. *J. Cell Sci.* 119, 1255–1265.
- Bouyer, D., Kirik, V. and Hülskamp, M. (2001). Cell polarity in *Arabidopsis* trichomes. *Semin. Cell Dev. Biol.* 12, 353–356.
- Bringmann, M. and Bergmann, D. C. (2017). Tissue-wide Mechanical Forces Influence the Polarity of Stomatal Stem Cells in *Arabidopsis*. *Curr. Biol.* 27, 877–883.
- Bürstenbinder, K., Möller, B., Plötner, R., Stamm, G., Hause, G., Mitra, D. and Abel, S. (2017). The IQD Family of Calmodulin-Binding Proteins Links Calcium Signaling to Microtubules, Membrane Subdomains, and the Nucleus. *Plant Physiol.* 173, 1692–1708.
- Bushell, C. (2016). Development of 3D leaf shape: *Utricularia gibba* as a model system. PhD thesis, University of East Anglia.
- Butler, M. T. and Wallingford, J. B. (2017). Planar cell polarity in development and disease. *Nat. Rev. Mol. Cell Biol.* 18, 375–388.
- Byrne, M. E. (2012). Making leaves. *Curr. Opin. Plant Biol.* 15, 24–30.

References

Byrne, M. E., Barley, R., Curtis, M., Arroyo, J. M., Dunham, M., Hudson, A. and Martienssen, R. A. (2000). *Asymmetric leaves1* mediates leaf patterning and stem cell function in *Arabidopsis*. *Nature* 408, 967–971.

Caggiano, M. P., Yu, X., Bhatia, N., Ram, H., Ohno, C. K., Sappl, P., Meyerowitz, E. M., Jönsson, H. and Heisler, M. G. (2017). Cell type boundaries organize plant development. *ELife* 6, e27421.

Caillaud, M.-C., Wirthmueller, L., Sklenar, J., Findlay, K., Piquerez, S. J. M., Jones, A. M. E., Robatzek, S., Jones, J. D. G. and Faulkner, C. (2014). The Plasmodesmal Protein PDL1 Localises to Haustoria-Associated Membranes during Downy Mildew Infection and Regulates Callose Deposition. *PLoS Pathog.* 10, e1004496.

Calder, G., Hindle, C., Chan, J. and Shaw, P. (2015). An optical imaging chamber for viewing living plant cells and tissues at high resolution for extended periods. *Plant Methods* 11, 22.

Camoni, L., Visconti, S., Aducci, P. and Marra, M. (2018). 14-3-3 Proteins in Plant Hormone Signaling: Doing Several Things at Once. *Front. Plant Sci.* 9, 297.

Cao, Y., Liang, Y., Tanaka, K., Nguyen, C. T., Jedrzejczak, R. P., Joachimiak, A. and Stacey, G. (2014). The kinase LYK5 is a major chitin receptor in *Arabidopsis* and forms a chitin-induced complex with related kinase CERK1. *Elife* 3, e03766.

Carter, R., Sánchez-Corrales, Y. E., Hartley, M., Grieneisen, V. A. and Marée, A. F. M. (2017). Pavement cells and the topology puzzle. *Development* 144, 4386–4397.

Cartwright, H. N., Humphries, J. A. and Smith, L. G. (2009). PAN1 : A Receptor-Like Protein Asymmetric Cell Division in Maize. *Science*. 323, 649–651.

Casimiro, I., Marchant, A., Bhalerao, R. P., Beeckman, T., Dhooge, S., Swarup, R., Graham, N., Inzé, D., Sandberg, G., Casero, P. J., et al. (2001). Auxin Transport Promotes *Arabidopsis* Lateral Root Initiation. *Plant Cell* 13, 843–852.

Chan, J., Calder, G., Fox, S. and Lloyd, C. (2007). Cortical microtubule arrays undergo rotary movements in *Arabidopsis* hypocotyl epidermal cells. *Nat. Cell Biol.* 9, 171–175.

Chan, J., Crowell, E., Eder, M., Calder, G., Bunnewell, S., Findlay, K., Vernhettes, S., Höfte, H. and Lloyd, C. (2010). The rotation of cellulose synthase trajectories is microtubule dependent and influences the texture of epidermal cell walls in *Arabidopsis* hypocotyls. *J. Cell Sci.* 123, 3490-3495.

- Chant, J. and Herskowitz, I. (1991). Genetic control of bud site selection in yeast by a set of gene products that constitute a morphogenetic pathway. *Cell* 65, 1203–1212.
- Chater, C. C. C., Caine, R. S., Fleming, A. J. and Gray, J. E. (2017). Origins and Evolution of Stomatal Development. *Plant Physiol.* 174, 624–638.
- Chen, J., Wang, F., Zheng, S., Xu, T. and Yang, Z. (2015). Pavement cells: a model system for non-transcriptional auxin signalling and crosstalks. *J Exp Bot* 66, 4957–4970.
- Cheval, C. and Faulkner, C. (2018). Plasmodesmal regulation during plant-pathogen interactions. *New Phytol.* 217, 62–67.
- Cieslak, M., Runions, A. and Prusinkiewicz, P. (2015). Auxin-driven patterning with unidirectional fluxes. *J. Exp. Bot.* 66, 5083–5102.
- Clough, S. J. and Bent, A. F. (1998). Floral dip: a simplified method for *Agrobacterium*-mediated transformation of *Arabidopsis thaliana*. *Plant J.* 16, 735–743.
- Coen, E. and Rebocho, A. B. (2016). Resolving Conflicts: Modeling Genetic Control of Plant Morphogenesis. *Dev. Cell* 38, 579–583.
- Coen, E., Kennaway, R. and Whitewoods, C. (2017). On genes and form. *Development* 144, 4203–4213.
- Cosgrove, D. J. (2000). Loosening of plant cell walls by expansins. *Nature* 407, 321–326.
- Cosgrove, D. J. (2005). Growth of the plant cell wall. *Nat. Rev. Mol. Cell Biol.* 6, 850–861.
- Cosgrove, D. J. (2016). Catalysts of plant cell wall loosening. *F1000Research* 5, 1–13.
- Cui, W. and Lee, J.-Y. (2016). *Arabidopsis* callose synthases CalS1/8 regulate plasmodesmal permeability during stress. *Nat. Plants* 2, 1-9.
- Das Gupta, M. and Nath, U. (2015). Divergence in Patterns of Leaf Growth Polarity Is Associated with the Expression Divergence of miR396. *Plant Cell* 27, 2785–2799.
- Devreotes, P. N. and Zigmond, S. H. (1988). Chemotaxis in Eukaryotic Cells: A Focus on Leukocytes and *Dictyostelium*. *Annu. Rev. Cell Biol.* 4, 649–686.
- Dong, J., MacAlister, C. A. and Bergmann, D. C. (2009). BASL Controls Asymmetric Cell Division in *Arabidopsis*. *Cell* 137, 1320–1330.

References

- Eldridge, T., Łangowski, Ł., Stacey, N., Jantzen, F., Moubayidin, L., Sicard, A., Southam, P., Kennaway, R., Lenhard, M., Coen, E. S., and Østergaard, L. (2016). Fruit shape diversity in the Brassicaceae is generated by varying patterns of anisotropy. *Development* 143, 3394–3406.
- Eshed, Y., Baum, S. F., Perea, J. V and Bowman, J. L. (2001). Establishment of polarity in lateral organs of plants. *Curr. Biol.* 11, 1251–1260.
- Eshed, Y., Izhaki, A., Baum, S. F., Floyd, S. K. and Bowman, J. L. (2004). Asymmetric leaf development and blade expansion in *Arabidopsis* are mediated by KANADI and YABBY activities. *Development* 131, 2997–3006.
- Etienne-Manneville, S. (2008). Polarity proteins in migration and invasion. *Oncogene* 27, 6970–6980.
- Fàbregas, N., Li, N., Boeren, S., Nash, T. E., Goshe, M. B., Clouse, S. D., de Vries, S. and Caño-Delgado, A. I. (2013). The BRASSINOSTEROID INSENSITIVE1-LIKE3 signalosome complex regulates *Arabidopsis* root development. *Plant Cell* 25, 3377–3388.
- Facette, M. R. and Smith, L. G. (2012). Division polarity in developing stomata. *Curr Opin Plant Biol* 15, 585–592.
- Feraru, E. and Friml, J. (2008). PIN Polar Targeting. *Plant Physiol.* 147, 1553–1559.
- Folkers, U., Berger, J. and Hülskamp, M. (1997). Cell morphogenesis of trichomes in *Arabidopsis*: differential control of primary and secondary branching by branch initiation regulators and cell growth. *Development* 124, 3779–3786.
- Fox, S., Southam, P., Pantin, F., Kennaway, R., Robinson, S., Castorina, G., Sánchez-Corrales, Y., Sablowski, R., Chan, J., Grieneisen, V., et al. (2018). Spatiotemporal coordination of cell division and growth during organ morphogenesis. *PLoS Biol.* 16, e2005952.
- Friml, J., Vieten, A., Sauer, M., Weijers, D., Schwarz, H., Hamann, T., Offringa, R. and Jürgens, G. (2003). Efflux-dependent auxin gradients establish the apical–basal axis of *Arabidopsis*. *Nature* 426, 147–153.
- Fu, Y., Li, H. and Yang, Z. (2002). The ROP2 GTPase Controls the Formation of Cortical Fine F-Actin and the Early Phase of Directional Cell Expansion during *Arabidopsis* Organogenesis. *Plant Cell* 14, 777–794.

- Fu, Y., Gu, Y., Zheng, Z., Wasteneys, G. and Yang, Z. (2005). *Arabidopsis* Interdigitating Cell Growth Requires Two Antagonistic Pathways with Opposing Action on Cell Morphogenesis. *Cell* 120, 687–700.
- Gallois, J. L., Woodward, C., Reddy, G. V and Sablowski, R. (2002). Combined SHOOT MERISTEMLESS and WUSCHEL trigger ectopic organogenesis in *Arabidopsis*. *Development* 129, 3207–3217.
- Gälweiler, L., Guan, C., Muller, A., Wisman, E., Mendgen, K., Yephremov, A. and Palme, K. (1998). Regulation of Polar Auxin Transport by AtPIN1 in *Arabidopsis* Vascular Tissue. *Science* 282, 2226–2230.
- Geldner, N., Friml, J., Stierhof, Y.-D., Jürgens, G. and Palme, K. (2001). Auxin transport inhibitors block PIN1 cycling and vesicle trafficking. *Nature* 413, 425–428.
- Gerhart, J., Danilchik, M., Doniach, T., Roberts, S., Rowning, B. and Stewart, R. (1989). Cortical rotation of the *Xenopus* egg: consequences for the anteroposterior pattern of embryonic dorsal development. *Development*, 37-51.
- Goldstein, B. and Macara, I. G. (2007). The PAR Proteins: Fundamental Players in Animal Cell Polarization. *Dev. Cell* 13, 609–622.
- Gomez, J. M., Chumakova, L., Bulgakova, N. A. and Brown, N. H. (2016). Microtubule organization is determined by the shape of epithelial cells. *Nat. Commun.* 7, 13172.
- Goodner, B. and Quatrano, R. S. (1993). *Fucus* Embryogenesis: A Model to Study the Establishment of Polarity. *Plant Cell* 5, 1471-1481.
- Goodrich, L. V and Strutt, D. (2011). Principles of planar polarity in animal development. *Development* 138, 1877–1892.
- Goriely, A. (2017). *The Mathematics and Mechanics of Biological Growth*. New York, NY: Springer.
- Grebe, M. (2004). Ups and downs of tissue and planar polarity in plants. *BioEssays* 26, 719–729.
- Grebe, M., Friml, J., Swarup, R., Ljung, K., Sandberg, G., Terlou, M., Palme, K., Bennett, M. J. and Scheres, B. (2002). Cell Polarity Signaling in *Arabidopsis* Involves a BFA-Sensitive Auxin Influx Pathway. *Curr. Biol.* 12, 329–334.

References

- Greeff, C., Roux, M., Mundy, J. and Petersen, M. (2012). Receptor-like kinase complexes in plant innate immunity. *Front. Plant Sci.* 3, 209.
- Green, A. A., Kennaway, J. R., Hanna, A. I., Bangham, J. A. and Coen, E. (2010). Genetic Control of Organ Shape and Tissue Polarity. *PLoS Biol.* 8, e1000537.
- Guenot, B., Bayer, E., Kierzkowski, D., Smith, R. S., Mandel, T., Zadnikova, P., Benkova, E. and Kuhlemeier, C. (2012). PIN1-Independent Leaf Initiation in *Arabidopsis*. *Plant Physiol.* 159, 1501–1510.
- Gutierrez, R., Lindeboom, J. J., Paredes, A. R., Emons, A. M. C. and Ehrhardt, D. W. (2009). *Arabidopsis* cortical microtubules position cellulose synthase delivery to the plasma membrane and interact with cellulose synthase trafficking compartments. *Nat. Cell Biol.* 11, 797–806.
- Hamant, O., Heisler, M. G., Jönsson, H., Krupinski, P., Uyttewaal, M., Bokov, P., Corson, F., Sahlin, P., Boudaoud, A., Meyerowitz, E. M., et al. (2008). Developmental patterning by mechanical signals in *Arabidopsis*. *Science* 322, 1650–1655.
- Hara, K., Kajita, R., Torii, K. U., Bergmann, D. C. and Kakimoto, T. (2007). The secretory peptide gene EPF1 enforces the stomatal one-cell-spacing rule. *Genes Dev.* 21, 1720–1725.
- Hasezawa, S. and Syono, K. (1983). Hormonal Control of Elongation of Tobacco Cells Derived from Protoplasts. *Plant & Cell Physiol* 24, 127–132.
- Hasson, A., Plessis, A., Blein, T., Adroher, B., Grigg, S., Tsiantis, M., Boudaoud, A., Damerval, C. and Laufs, P. (2011). Evolution and diverse roles of the *CUP-SHAPED COTYLEDON* genes in *Arabidopsis* leaf development. *Plant Cell* 23, 54–68.
- Haswell, E. S., Peyronnet, R., Barbier-Brygoo, H., Meyerowitz, E. M. and Frachisse, J.-M. (2008). Two MscS Homologs Provide Mechanosensitive Channel Activities in the *Arabidopsis* Root. *Curr. Biol.* 18, 730–734.
- Hay, A., Barkoulas, M. and Tsiantis, M. (2006). ASYMMETRIC LEAVES1 and auxin activities converge to repress *BREVIPEDICELLUS* expression and promote leaf development in *Arabidopsis*. *Development* 133, 3955–3961.
- Heath, I. B. (1974). A unified hypothesis for the role of membrane bound enzyme complexes and microtubules in plant cell wall synthesis. *J. Theor. Biol.* 48, 445–449.

- Heisenberg, C.-P., Tada, M., Rauch, G.-J., Saúde, L., Concha, M. L., Geisler, R., Stemple, D. L., Smith, J. C. and Wilson, S. W. (2000). Silberblick/Wnt11 mediates convergent extension movements during zebrafish gastrulation. *Nature* 405, 76–81.
- Heisler, M. G., Ohno, C., Das, P., Sieber, P., Reddy, G. V, Long, J. A. and Meyerowitz, E. M. (2005). Patterns of auxin transport and gene expression during primordium development revealed by live imaging of the *Arabidopsis* inflorescence meristem. *Curr Biol* 15, 1899–1911.
- Heisler, M. G., Hamant, O., Krupinski, P., Uyttewaal, M., Ohno, C., Jönsson, H., Traas, J. and Meyerowitz, E. M. (2010). Alignment between PIN1 Polarity and Microtubule Orientation in the Shoot Apical Meristem Reveals a Tight Coupling between Morphogenesis and Auxin Transport. *PLoS Biol.* 8, e1000516.
- Hejnowicz, Z. and Romberger, J. A. (1984). Growth tensor of plant organs. *J. Theor. Biol.* 110, 93–114.
- Henderson, D. J., Long, D. A. and Dean, C. H. (2018). Planar cell polarity in organ formation. *Curr. Opin. Cell Biol.* 55, 96–103.
- Hervieux, N., Dumond, M., Sapala, A., Routier-Kierzkowska, A.-L., Kierzkowski, D., Roeder, A. H. K., Smith, R. S., Boudaoud, A. and Hamant, O. (2016). A Mechanical Feedback Restricts Sepal Growth and Shape in *Arabidopsis*. *Curr. Biol.* 26, 1–10.
- Hervieux, N., Tsugawa, S., Fruleux, A., Smith, R. S., Li, C.-B. and Correspondence, O. H. (2017). Mechanical Shielding of Rapidly Growing Cells Buffers Growth Heterogeneity and Contributes to Organ Shape Reproducibility. *Curr. Biol.* 27, 1-12.
- Hooper, C. M., Tanz, S. K., Castleden, I. R., Vacher, M. A., Small, I. D. and Millar, A. H. (2014). SUBAcon: a consensus algorithm for unifying the subcellular localization data of the *Arabidopsis* proteome. *Bioinformatics* 30, 3356–3364.
- Hülkamp, M. and Schnittger, A. (1998). Spatial regulation of trichome formation in *Arabidopsis thaliana*. *Semin. Cell Dev. Biol.* 9, 213–220.
- Hülkamp, M., Misera, S. and Jurgens, G. (1994). Genetic Dissection of Trichome Cell Development in *Arabidopsis*. *Cell* 76, 555–566.
- Jaffe, L. (1956). Effect of Polarized Light on Polarity of *Fucus*. *Science* 123, 1081–1082.

References

- Johnson, J. M., Jin, M. and Lew, D. J. (2011). Symmetry breaking and the establishment of cell polarity in budding yeast. *Curr. Opin. Genet. Dev.* 21, 740–746.
- Jones, C. and Chen, P. (2007). Planar cell polarity signaling in vertebrates. *BioEssays* 29, 120–132.
- Jones, A. M., Xuan, Y., Xu, M., Wang, R.-S., Ho, C.-H., Lalonde, S., You, C. H., Sardi, M. I., Parsa, S. A., Smith-Valle, E., et al. (2014). Border control--a membrane-linked interactome of *Arabidopsis*. *Science*. 344, 711–716.
- Jönsson, H., Heisler, M. G., Shapiro, B. E., Meyerowitz, E. M. and Mjolsness, E. (2006). An auxin-driven polarized transport model for phyllotaxis. *Proc Natl Acad Sci USA* 103, 1633–1638.
- Juniper, B. E., Robins, R. J. and Joel, D. M. (1989). *The carnivorous plants*. London, San Diego: Academic Press.
- Kadota, Y., Sklenar, J., Derbyshire, P., Stransfeld, L., Asai, S., Ntoukakis, V., Jones, J. D., Shirasu, K., Menke, F., Jones, A., et al. (2014). Direct Regulation of the NADPH Oxidase RBOHD by the PRR-Associated Kinase BIK1 during Plant Immunity. *Mol. Cell* 54, 43–55.
- Karimi, M., De Meyer, B. and Hilson, P. (2005). Modular cloning in plant cells. *Trends Plant Sci.* 10, 103–105.
- Kasprzewska, A., Carter, R., Swarup, R., Bennett, M., Monk, N., Hobbs, J. K. and Fleming, A. (2015). Auxin influx importers modulate serration along the leaf margin. *Plant J.* 83, 705-718.
- Keicher, J., Jaspert, N., Weckermann, K., Möller, C., Throm, C., Kintzi, A. and Oecking, C. (2017). *Arabidopsis* 14-3-3 epsilon members contribute to polarity of PIN auxin carrier and auxin transport-related development. *Elife* 6, e24336.
- Kennaway, R., Coen, E., Green, A. and Bangham, A. (2011). Generation of diverse biological forms through combinatorial interactions between tissue polarity and growth. *PLoS Comput. Biol.* 7, e1002071.
- Kerstetter, R., Bollman, K., Taylor, R., Bomblies, K. and Poethig, R. (2001). KANADI regulates organ polarity in *Arabidopsis*. *Nature* 411, 706–709.

- Kibar, Z., Torban, E., McDearmid, J. R., Reynolds, A., Berghout, J., Mathieu, M., Kirillova, I., De Marco, P., Merello, E., Hayes, J. M., et al. (2007). Mutations in *VANGL1* Associated with Neural-Tube Defects. *N. Engl. J. Med.* 356, 1432–1437.
- Kim, G.-T., Shoda, K., Tsuge, T., Cho, K.-H., Uchimiya, H., Yokoyama, R., Nishitani, K. and Tsukaya, H. (2002). The *ANGUSTIFOLIA* gene of *Arabidopsis*, a plant CtBP gene, regulates leaf-cell expansion, the arrangement of cortical microtubules in leaf cells and expression of a gene involved in cell-wall formation. *EMBO J.* 21, 1267–1279.
- Křeček, P., Skupa, P., Libus, J., Naramoto, S., Tejos, R., Friml, J. and Zazimalová, E. (2009). The PIN-FORMED (PIN) protein family of auxin transporters. *Genome Biol.* 10, 249.
- Kuchen, E. E. (2011). How organs organise their ontogeny: Modelling feedback between polarity, growth and geometry during *Arabidopsis* leaf development. PhD thesis, University of East Anglia.
- Kuchen, E. E., Fox, S., de Reuille, P. B., Kennaway, R., Bensmihen, S., Avondo, J., Calder, G. M., Southam, P., Robinson, S., Bangham, A., et al. (2012). Generation of leaf shape through early patterns of growth and tissue polarity. *Science* 335, 1092–1096.
- Lau, O. S. and Bergmann, D. C. (2012). Stomatal development: a plant's perspective on cell polarity, cell fate transitions and intercellular communication. *Development* 139, 3683–3692.
- Lawrence, P. A. (1966). Gradients in the insect segment: the orientation of hairs in the milkweed bug *Oncopeltus fasciatus*. *J. Exp. Biol* 44, 607-620.
- Lawrence, P. A., Struhl, G. and Casal, J. (2007). Planar cell polarity: one or two pathways? *Nat. Rev. Genet.* 8, 555–563.
- Lei, Y.-P., Zhang, T., Li, H., Wu, B.-L., Jin, L. and Wang, H.-Y. (2010). *VANGL2* Mutations in Human Cranial Neural-Tube Defects. *N. Engl. J. Med.* 362, 2232–2235.
- Li, J., Wen, J., Lease, K. A., Doke, J. T., Tax, F. E. and Walker, J. C. (2002). BAK1, an *Arabidopsis* LRR receptor-like protein kinase, interacts with BRI1 and modulates brassinosteroid signaling. *Cell* 110, 213–222.
- Li, R., Rodriguez-Furlan, C., Wang, J., van de Ven, W., Gao, T., Raikhel, N. V and Hicks, G. R. (2016). Different Endomembrane Trafficking Pathways Establish Apical and Basal Polarities. *Plant Cell* 29, 90-108.

References

- Lockhart, J. A. (1965). An analysis of irreversible plant cell elongation. *J. Theor. Biol.* 8, 264–275.
- Lucas, W. J. and Jung-Youn, L. (2004). Plasmodesmata as a supracellular control network in plants. *Nat. Rev. Mol. Cell Biol.* 5, 712–726.
- Lynch, T. M. and Lintilhac, P. M. (1997). Mechanical Signals in Plant Development: A New Method for Single Cell Studies. *Dev. Biol.* 181, 246–256.
- MacAlister, C. A., Ohashi-Ito, K. and Bergmann, D. C. (2007). Transcription factor control of asymmetric cell divisions that establish the stomatal lineage. *Nature* 445, 537–540.
- Macara, I. G. and Mili, S. (2008). Polarity and Differential Inheritance— Universal Attributes of Life? *Cell* 135, 801-812.
- Mansfield, C., Newman, J. L., Olsson, T. S. G., Hartley, M., Chan, J. and Coen, E. (2018). Ectopic BASL Reveals Tissue Cell Polarity throughout Leaf Development in *Arabidopsis thaliana*. *Curr. Biol.* 28, 2638-2646.
- Marée, A. F. M., Jilkine, A., Dawes, A., Grieneisen, V. A. and Edelstein-Keshet, L. (2006). Polarization and movement of keratocytes: a multiscale modelling approach. *Bull. Math. Biol.* 68, 1169–1211.
- Masucci, J. D. and Schiefelbein, J. W. (1994). The *rhd6* Mutation of *Arabidopsis thaliana* Alters Root-Hair Initiation through an Auxin and Ethylene-Associated Process. *Plant Physiol.* 106, 1335–1346.
- McQueen-Mason, S. J. and Cosgrove, D. J. (1995). Expansin mode of action on cell walls. *Plant Physiol.* 107, 87–100.
- Meinhardt, H. (2007). Computational modelling of epithelial patterning. *Curr. Opin. Genet. Dev* 17, 272–280.
- Menke, F. L. H. and Scheres, B. (2009). Plant Asymmetric Cell Division, Vive la Différence! *Cell* 137, 1189–1192.
- Mitchison, G. J. (1980). A Model for Vein Formation in Higher Plants. *Proc. R. Soc. B Biol. Sci.* 207, 79–109.

- Müller, A., Guan, C., Gälweiler, L., Tänzler, P., Huijser, P., Marchant, A., Parry, G., Bennett, M., Wisman, E. and Palme, K. (1998). *AtPIN2* defines a locus of *Arabidopsis* for root gravitropism control. *EMBO J.* 17, 6903–6911.
- Nagata, T., Nemoto, Y. and Hasezawa, S. (1992). Tobacco BY-2 Cell Line as the “HeLa” Cell in the Cell Biology of Higher Plants. *Int. Rev. Cytol.* 132, 1–30.
- Nelson, W. J. (2003). Adaptation of core mechanisms to generate cell polarity. *Nature* 422, 766–774.
- Nelson, B. K., Cai, X. and Nebenführ, A. (2007). A multicolored set of in vivo organelle markers for co-localization studies in *Arabidopsis* and other plants. *Plant J.* 51, 1126–1136.
- Nickerson, D. P., West, M., Henry, R. and Odorizzi, G. (2010). Regulators of Vps4 ATPase activity at endosomes differentially influence the size and rate of formation of intraluminal vesicles. *Mol. Biol. Cell* 21, 1023–1032.
- O’Connor, D. L., Runions, A., Sluis, A., Bragg, J., Vogel, J. P., Prusinkiewicz, P. and Hake, S. (2014). A division in PIN-mediated auxin patterning during organ initiation in grasses. *PLoS Comput. Biol.* 10, e1003447.
- O’Shea, E. K. and Herskowitz, I. (2000). The ins and outs of cell-polarity decisions. *Nat. Cell Biol.* 2, E39-41.
- Oda, Y. and Fukuda, H. (2012). Initiation of cell wall pattern by a Rho- and microtubule-driven symmetry breaking. *Science* 337, 1333–1336.
- Okada, K., Ueda, J., Komaki, M. K., Bell, C. J. and Shimura, Y. (1991). Requirement of the Auxin Polar Transport System in Early Stages of *Arabidopsis* Floral Bud Formation. *Plant Cell* 3, 677–684.
- Omelyanchuk, N. A., Kovrizhnykh, V. V., Oshchepkova, E. A., Pasternak, T., Palme, K. and Mironova, V. V. (2016). A detailed expression map of the PIN1 auxin transporter in *Arabidopsis thaliana* root. *BMC Plant Biol.* 16, 5.
- Ori, N., Eshed, Y., Chuck, G., Bowman, J. and Hake, S. (2000). Mechanisms that control *knox* gene expression in the *Arabidopsis* shoot. *Development* 127, 5523–5532.

References

- Osakabe, Y., Yamaguchi-Shinozaki, K., Shinozaki, K. and Tran, L.-S. P. (2013). Sensing the environment: key roles of membrane-localized kinases in plant perception and response to abiotic stress. *J. Exp. Bot.* 64, 445–458.
- Otsuga, D., DeGuzman, B., Prigge, M., Drews, G. and Clark, S. (2001). REVOLUTA regulates meristem initiation at lateral positions. *Plant J.* 25, 223–236.
- Paul, A.-L., Sehnke, P. C. and Ferl, R. J. (2005). Isoform-specific subcellular localization among 14-3-3 proteins in *Arabidopsis* seems to be driven by client interactions. *Mol. Biol. Cell* 16, 1735–1743.
- Peaucelle, A., Wightman, R. and Höfte, H. (2015). The Control of Growth Symmetry Breaking in the *Arabidopsis* Hypocotyl. *Curr. Biol.* 25, 1746–1752.
- Pietra, S., Gustavsson, A., Kiefer, C., Kalmbach, L., Hörstedt, P., Ikeda, Y., Stepanova, A. N., Alonso, J. M. and Grebe, M. (2013). *Arabidopsis* SABRE and CLASP interact to stabilize cell division plane orientation and planar polarity. *Nat. Commun.* 4, 2779.
- Pillitteri, L. J., Peterson, K. M., Horst, R. J. and Torii, K. U. (2011). Molecular profiling of stomatal meristemoids reveals new component of asymmetric cell division and commonalities among stem cell populations in *Arabidopsis*. *Plant Cell* 23, 3260–3275.
- Qüesta, J. I., Song, J., Geraldo, N., An, H. and Dean, C. (2016). *Arabidopsis* transcriptional repressor VAL1 triggers Polycomb silencing at *FLC* during vernalization. *Science* 353, 485–488.
- Raissig, M. T., Abrash, E., Bettadapur, A., Vogel, J. P. and Bergmann, D. C. (2016). Grasses use an alternatively wired bHLH transcription factor network to establish stomatal identity. *Proc. Natl. Acad. Sci. U. S. A.* 113, 8326–8331.
- Rangamani, P., Lipshtat, A., Azeloglu, E. U., Calizo, R. C., Hu, M., Ghassemi, S., Hone, J., Scarlata, S., Neves, S. R. and Iyengar, R. (2013). Decoding Information in Cell Shape. *Cell* 154, 1356–1369.
- Rebocho, A. B., Kennaway, J. R., Bangham, J. A. and Coen Correspondence, E. (2017a). Formation and Shaping of the *Antirrhinum* Flower through Modulation of the *CUP* Boundary Gene. *Curr. Biol.* 27, 1-13.

- Rebocho, A. B., Southam, P., Kennaway, J. R., Bangham, J. A., Coen, E., Paris, S., Gälweiler, L., Palme, K., Jürgens, G., Graner, F., et al. (2017b). Generation of shape complexity through tissue conflict resolution. *Elife* 6, 132–152.
- Reinhardt, D., Pesce, E.-R., Stieger, P., Mandel, T., Baltensperger, K., Bennett, M., Traas, J., Friml, J. and Kuhlemeier, C. (2003). Regulation of phyllotaxis by polar auxin transport. *Nature* 426, 255–260.
- Remmler, L. and Rolland-Lagan, A.-G. (2012). Computational Method for Quantifying Growth Patterns at the Adaxial Leaf Surface in Three Dimensions. *Plant Physiol.* 159, 27–39.
- Richardson, A. E., Rebocho, A. B. and Coen, E. S. (2016). Ectopic *KNOX* Expression Affects Plant Development by Altering Tissue Cell Polarity and Identity. *Plant Cell* 28, 2079–2096.
- Robinson, S. and Kuhlemeier, C. (2018). Global Compression Reorients Cortical Microtubules in *Arabidopsis* Hypocotyl Epidermis and Promotes Growth. *Curr. Biol.* 28, 1794–1802.
- Robinson, S., De Reuille, P. B., Chan, J., Bergmann, D. C., Prusinkiewicz, P. and Coen, E. (2011). Generation of Spatial Patterns Through Cell Polarity Switching. *Science* 333, 1436–1440.
- Robinson, S., Huflejt, M., Barbier de Reuille, P., Braybrook, S. A., Schorderet, M., Reinhardt, D. and Kuhlemeier, C. (2017). An Automated Confocal Micro-Extensometer Enables in Vivo Quantification of Mechanical Properties with Cellular Resolution. *Plant Cell* 29, 2959–2973.
- Rolland-Lagan, A.-G. and Prusinkiewicz, P. (2005). Reviewing models of auxin canalization in the context of leaf vein pattern formation in *Arabidopsis*. *Plant J.* 44, 854–865.
- Rosas-Santiago, P., Lagunas-Gómez, D., Barkla, B. J., Vera-Estrella, R., Lalonde, S., Jones, A., Frommer, W. B., Zimmermannova, O., Sychrová, H. and Pantoja, O. (2015). Identification of rice cornichon as a possible cargo receptor for the Golgi-localized sodium transporter OsHKT1;3. *J. Exp. Bot.* 66, 2733–2748.
- Rowe, M. (2013). A potential intrinsic mechanism for asymmetric cell division in the *Arabidopsis* stomatal lineage. PhD thesis, Stanford University.
- Rudall, P. J., Chen, E. D. and Cullen, E. (2017). Evolution and development of monocot stomata. *Am. J. Bot.* 104, 1122–1141.
- Runions, A., Tsiantis, M. and Prusinkiewicz, P. (2017). A common developmental program can produce diverse leaf shapes. *New Phytol.* 216, 401-418.

References

- Sakai, Y., Sugano, S. S., Kawase, T., Shirakawa, M., Imai, Y., Kawamoto, Y., Sugiyama, H., Nakagawa, T., Hara-Nishimura, I. and Shimada, T. (2017). Inhibition of cell polarity establishment in stomatal asymmetric cell division using the chemical compound bubblin. *Development* 144, 499–506.
- Sánchez-Corrales, Y. E., Hartley, M., van Rooij, J., Marée, A. F. M. and Grieneisen, V. A. (2018). Morphometrics of complex cell shapes: lobe contribution elliptic Fourier analysis (LOCO-EFA). *Development* 145, dev156778.
- Sassi, M. and Traas, J. (2015). When biochemistry meets mechanics: a systems view of growth control in plants. *Curr. Opin. Plant Biol.* 28, 137–143.
- Sauret-Güeto, S., Schiessl, K., Bangham, A., Sablowski, R. and Coen, E. (2013). *JAGGED* controls *Arabidopsis* petal growth and shape by interacting with a divergent polarity field. *PLoS Biol.* 11, e1001550.
- Scarpella, E., Marcos, D., Friml, J. and Berleth, T. (2006). Control of leaf vascular patterning by polar auxin transport. *Genes Dev.* 20, 1015–1027.
- Schindelin, J., Arganda-Carreras, I., Frise, E., Kaynig, V., Longair, M., Pietzsch, T., Preibisch, S., Rueden, C., Saalfeld, S., Schmid, B., et al. (2012). Fiji: an open-source platform for biological-image analysis. *Nat. Methods* 9, 676–682.
- Schwarz-Romond, T., Fiedler, M., Shibata, N., Butler, P. J. G., Kikuchi, A., Higuchi, Y. and Bienz, M. (2007). The DIX domain of Dishevelled confers Wnt signaling by dynamic polymerization. *Nat. Struct. Mol. Biol.* 14, 484–492.
- Sebbagh, M. and Borg, J.-P. (2014). Insight into planar cell polarity. *Exp. Cell Res.* 328, 284–295.
- Shevchenko, A., Tomas, H., Havlis, J., Olsen, J. V and Mann, M. (2007). In-gel digestion for mass spectrometric characterization of proteins and proteomes. *Nat. Protoc.* 1, 2856–2860.
- Shimotohno, A., Sotta, N., Sato, T., De Ruvo, M., Maree, A. F. M., Grieneisen, V. A. and Fujiwara, T. (2015). Mathematical Modeling and Experimental Validation of the Spatial Distribution of Boron in the Root of *Arabidopsis thaliana* Identify High Boron Accumulation in the Tip and Predict a Distinct Root Tip Uptake Function. *Plant Cell Physiol.* 56, 620–630.
- Shiu, S.-H. and Blecker, A. B. (2001). Plant Receptor-Like Kinase Gene Family: Diversity, Function, and Signaling. *Proc. Natl. Acad. Sci. USA* 98, 10763–10768.

- Singh, J. and Mlodzik, M. (2012). Planar Cell Polarity Signaling: Coordination of cellular orientation across tissues. *Wiley Interdiscip Rev Dev Biol* 1, 479–499.
- Slaughter, B. D., Smith, S. E. and Li, R. (2009). Symmetry breaking in the life cycle of the budding yeast. *Cold Spring Harb. Perspect. Biol.* 1, a003384.
- Smith, R. S., Guyomarc'h, S., Mandel, T., Reinhardt, D., Kuhlemeier, C. and Prusinkiewicz, P. (2006). A plausible model of phyllotaxis. *Proc. Natl. Acad. Sci. USA* 103, 1301–1306.
- Sohrmann, M. and Peter, M. (2003). Polarizing without a clue. *Trends Cell Biol.* 13, 526–533.
- Solly, J. E. (2015). Regulation of thallus shape in the liverwort *Marchantia polymorpha*. PhD thesis, University of Cambridge.
- Solly, J. E., Cunniffe, N. J. and Harrison, C. J. (2017). Regional Growth Rate Differences Specified by Apical Notch Activities Regulate Liverwort Thallus Shape. *Curr. Biol.* 27, 16–26.
- Steinmann, T., Geldner, N., Grebe, M., Mangold, S., Jackson, C. L., Paris, S., Galweiler, L., Palme, K. and Jurgens, G. (1999). Coordinated Polar Localization of Auxin Efflux Carrier PIN1 by GNOM ARF GEF. *Science* 286, 316–318.
- Stöckle, D., Herrmann, A., Lipka, E., Lauster, T., Gavidia, R., Zimmermann, S. and Müller, S. (2016). Putative RopGAPs impact division plane selection and interact with kinesin-12 POK1. *Nat. Plants* 2, 1–6.
- Stoma, S., Lucas, M., Chopard, J., Schaedel, M., Traas, J. and Godin, C. (2008). Flux-Based Transport Enhancement as a Plausible Unifying Mechanism for Auxin Transport in Meristem Development. *PLoS Comput. Biol.* 4, e1000207.
- Strutt, H. and Strutt, D. (2009). Asymmetric localisation of planar polarity proteins: Mechanisms and consequences. *Semin. Cell Dev. Biol.* 20, 957–963.
- Suzuki, A., Ishiyama, C., Hashiba, K., Shimizu, M., Ebnet, K. and Ohno, S. (2002). aPKC kinase activity is required for the asymmetric differentiation of the premature junctional complex during epithelial cell polarization. *J. Cell Sci.* 115, 3565–3573.
- Takano, J., Tanaka, M., Toyoda, A., Miwa, K., Kasai, K., Fuji, K., Onouchi, H., Naito, S. and Fujiwara, T. (2010). Polar localization and degradation of *Arabidopsis* boron transporters through distinct trafficking pathways. *Proc. Natl. Acad. Sci. USA.* 107, 5220–5225.

References

- Tanaka, H., Kitakura, S., Rakusova, H., Uemura, T., Feraru, M. I., De Rycke, R., Robert, S., Kakimoto, T. and Friml, J. (2013). Cell polarity and patterning by PIN trafficking through early endosomal compartments in *Arabidopsis thaliana*. *PLoS Genet* 9, e1003540.
- Tang, R.-H., Han, S., Zheng, H., Cook, C. W., Choi, C. S., Woerner, T. E., Jackson, R. B. and Pei, Z.-M. (2007). Coupling diurnal cytosolic Ca²⁺ oscillations to the CAS-IP3 pathway in *Arabidopsis*. *Science* 315, 1423–1426.
- Thomas, C. and Strutt, D. (2012). The roles of the cadherins Fat and Dachshous in planar polarity specification in *Drosophila*. *Dev. Dyn.* 241, 27–39.
- Thompson, D. W. (1942). *On Growth and Form*. 2nd Edition. Cambridge University Press, Cambridge.
- Tilsner, J., Nicolas, W., Rosado, A. and Bayer, E. M. (2016). Staying Tight: Plasmodesmal Membrane Contact Sites and the Control of Cell-to-Cell Connectivity in Plants. *Annu. Rev. Plant Biol.* 67, 337–364.
- Torode, T. A., Siméon, A., Marcus, S. E., Jam, M., Le Moigne, M.-A., Duffieux, D., Knox, J. P. and Hervé, C. (2016). Dynamics of cell wall assembly during early embryogenesis in the brown alga *Fucus*. *J. Exp. Bot.* 67, 6089–6100.
- Truernit, E., Bauby, H., Belcram, K., Barthelemy, J. and Palauqui, J.-C. (2012). OCTOPUS, a polarly localised membrane-associated protein, regulates phloem differentiation entry in *Arabidopsis thaliana*. *Development* 139, 1306–1315.
- Tsugawa, S., Hervieux, N., Kierzkowski, D., Routier-Kierzkowska, A.-L., Sapala, A., Hamant, O., Smith, R. S., Roeder, A. H. K., Boudaoud, A. and Li, C.-B. (2017). Clones of cells switch from reduction to enhancement of size variability in *Arabidopsis* sepals. *Development* 144, 4398–4405.
- Tsuge, T., Tsukaya, H. and Uchimiya, H. (1996). Two independent and polarized processes of cell elongation regulate leaf blade expansion in *Arabidopsis thaliana* (L.) Heynh. *Development* 122, 1589–1600.
- Tyanova, S., Temu, T. and Cox, J. (2016). The MaxQuant computational platform for mass spectrometry-based shotgun proteomics. *Nat. Protoc.* 11, 2301–2319.
- Ueda, K., Matsuyama, T. and Hashimoto, T. (1999). Visualization of microtubules in living cells of transgenic *Arabidopsis thaliana*. *Protoplasma* 206, 201–206.

- Uyttewaal, M., Burian, A., Alim, K., Landrein, B., Borowska-Wykręć, D., Dedieu, A., Peaucelle, A., Ludynia, M., Traas, J., Boudaoud, A., et al. (2012). Mechanical stress acts via katanin to amplify differences in growth rate between adjacent cells in *Arabidopsis*. *Cell* 149, 439–451.
- Vainonen, J. P., Sakuragi, Y., Stael, S., Tikkanen, M., Allahverdiyeva, Y., Paakkanen, V., Aro, E., Suorsa, M., Scheller, H. V, Vener, A. V, et al. (2008). Light regulation of CaS, a novel phosphoprotein in the thylakoid membrane of *Arabidopsis thaliana*. *FEBS J.* 275, 1767–1777.
- Vatén, A. and Bergmann, D. C. (2012). Mechanisms of stomatal development: an evolutionary view. *Evodevo* 3, 11.
- Vogel, S. and Martens, J. (2000). A survey of the function of the lethal kettle traps of *Arisaema* (Araceae), with records of pollinating fungus gnats from Nepal. *Bot. J. Linn. Soc.* 133, 61–100.
- Wachsman, G., Heidstra, R. and Scheres, B. (2011). Distinct Cell-Autonomous Functions of *RETINOBLASTOMA-RELATED* in *Arabidopsis* Stem Cells Revealed by the Brother of Rainbow Clonal Analysis System. *Plant Cell* 23, 2581–2591.
- Wang, Y. and Nathans, J. (2007). Tissue/planar cell polarity in vertebrates: new insights and new questions. *Development* 134, 647–658.
- Wang, W., Xu, B., Wang, H., Li, J., Huang, H. and Xu, L. (2011). YUCCA Genes Are Expressed in Response to Leaf Adaxial-Abaxial Juxtaposition and Are Required for Leaf Margin Development. *Plant Physiol.* 157, 1805–1819.
- Wang, Y., Chang, H., Rattner, A. and Nathans, J. (2016). Frizzled Receptors in Development and Disease. *Curr. Top. Dev. Biol.* 117, 113–139.
- Weber, E., Engler, C., Gruetzner, R., Werner, S. and Marillonnet, S. (2011). A Modular Cloning System for Standardized Assembly of Multigene Constructs. *PLoS One* 6, 11.
- Wedlich-Soldner, R. and Li, R. (2003). Spontaneous cell polarization: undermining determinism. *Nat. Cell Biol.* 5, 267–270.
- Wedlich-Soldner, R., Wai, S. C., Schmidt, T. and Li, R. (2004). Robust cell polarity is a dynamic state established by coupling transport and GTPase signaling. *J. Cell Biol.* 166, 889–900.
- Weis, C., Pfeilmeier, S., Glawischnig, E., Isono, E., Pachel, F., Hahne, H., Kuster, B., Eichmann, R. and Hückelhoven, R. (2013). Co-immunoprecipitation-based identification of putative BAX

References

INHIBITOR-1-interacting proteins involved in cell death regulation and plant-powdery mildew interactions. *Mol. Plant Pathol.* 14, 791–802.

Whitewoods, C. D. and Coen, E. (2017). Growth and Development of Three-Dimensional Plant Form. *Curr. Biol. Rev.* 27, R910–R918.

Whitney, H. M., Federle, W. and Glover, B. J. (2009). Grip and slip: Mechanical interactions between insects and the epidermis of flowers and flower stalks. *Commun. Integr. Biol.* 2, 505–508.

Williamson, R. (1990). Alignment of Cortical Microtubules by Anisotropic Wall Stresses. *Aust. J. Plant Physiol.* 17, 601.

Wisniewska, J., Xu, J., Seifertova, D., Brewer, P. B., Ruzicka, K., Blilou, I., Rouquie, D., Benkova, E., Scheres, B. and Friml, J. (2006). Polar PIN localization directs auxin flow in plants. *Science* 312, 883.

Wudick, M. M., Portes, M. T., Michard, E., Rosas-Santiago, P., Lizzio, M. A., Nunes, C. O., Campos, C., Santa Cruz Damineli, D., Carvalho, J. C., Lima, P. T., et al. (2018). CORNICHON sorting and regulation of GLR channels underlie pollen tube Ca²⁺ homeostasis. *Science* 360, 533–536.

Xu, T., Wen, M., Nagawa, S., Fu, Y., Chen, J.-G., Wu, M.-J., Perrot-Rechenmann, C., Friml, J., Jones, A. M. and Yang, Z. (2010). Cell surface- and rho GTPase-based auxin signaling controls cellular interdigitation in *Arabidopsis*. *Cell* 143, 99–110.

Yadav, S. R., Yan, D., Sevilem, I. and Helariutta, Y. (2014). Plasmodesmata-mediated intercellular signaling during plant growth and development. *Front. Plant Sci.* 5, 44.

Yang, Z. (2008). Cell polarity signaling in *Arabidopsis*. *Annu. Rev. Cell Dev. Biol.* 24, 551–575.

Yang, T., Jia, Z., Bryant-Pike, W., Chandrasekhar, A., Murray, J. C., Fritsch, B., Bassuk, A. G. and Alexander Bassuk, C. G. (2014). Analysis of PRICKLE1 in human cleft palate and mouse development demonstrates rare and common variants involved in human malformations. *Mol. Genet. Genomic Med.* 2, 138–151.

Yoshida, S., van der Schuren, A., van Dop, M., van Galen, L., Saiga, S., Adibi, M., Möller, B., Marhavy, P., Smith, R., Friml, J., et al. (2019). SOSEKI polarity determinants reveal mechanisms of supracellular polarity in *Arabidopsis*. *Nat. Plants* 5, 160–166.

- Zaban, B., Maisch, J. and Nick, P. (2013). Dynamic Actin Controls Polarity Induction de novo in Protoplasts. *J. Integr. Plant Biol.* 55, 142–159.
- Zaban, B., Liu, W., Jiang, X. and Nick, P. (2015). Plant Cells Use Auxin Efflux to Explore Geometry. *Sci. Rep.* 4, 5852.
- Zamani, K., Lohrasebi, T., Sabet, M. S., Malboobi, M. A. and Mousavi, A. (2014). Expression pattern and subcellular localization of *Arabidopsis* purple acid phosphatase *AtPAP9*. *Gene Expr. Patterns* 14, 9–18.
- Zhang, C., Halsey, L. E. and Szymanski, D. B. (2011). The development and geometry of shape change in *Arabidopsis thaliana* cotyledon pavement cells. *BMC Plant Biol.* 11, 27.
- Zhang, Y., Wang, P., Shao, W., Zhu, J. K. and Dong, J. (2015). The BASL polarity protein controls a MAPK signaling feedback loop in asymmetric cell division. *Dev Cell* 33, 136–149.
- Zhang, Y., Guo, X. and Dong, J. (2016a). Phosphorylation of the Polarity Protein BASL Differentiates Asymmetric Cell Fate through MAPKs and SPCH. *Curr. Bio.* 26, 2957-2965.
- Zhang, Y., Bergmann, D. C. and Dong, J. (2016b). Fine-scale dissection of the subdomains of polarity protein BASL in stomatal asymmetric cell division. *J. Exp. Bot.* 67, 5093–5103.